N73-13020
NASA CR-2135

NASA CONTRACTOR REPORT

NASA CR-2135

FLIGHT TESTS OF A ROTATING CYLINDER FLAP ON A NORTH AMERICAN ROCKWELL YOV-10 AIRCRAFT

by D. R. Cichy, J. W. Harris, and J. K. MacKay

Prepared by
NORTH AMERICAN ROCKWELL CORPORATION
COLUMBUS AIRCRAFT DIVISION
Columbus, Ohio
for Ames Research Center

NATIONAL AERONAUTICS AND SPACE ADMINISTRATION • WASHINGTON, D. C. • NOVEMBER 1972

1. Report No.	2. Government Accession No.	3. Recipient's Catalog No.
NASA CR-2135		

4. Title and Subtitle	5. Report Date
"Flight Tests of a Rotating Cylinder Flap on a North American Rockwell YOV-10 Aircraft"	November 1972
	6. Performing Organization Code
7. Author(s)	8. Performing Organization Report No.
	10. Work Unit No.
9. Performing Organization Name and Address North American Rockwell Corporation Aircraft Research and Engineering Columbus Aircraft Division	11. Contract or Grant No. NAS 2-5326
	13. Type of Report and Period Covered Contractor Report
12. Sponsoring Agency Name and Address National Aeronautics & Space Administration Washington, D.C.	14. Sponsoring Agency Code

15. Supplementary Notes

16. Abstract

Flight tests were conducted of a twin engine airplane modified to a STOL configuration with rotating cyl der flaps and interconnected propellers. The flight tests included verification of the functional operation of the rotating cylinder flap system and the determination of the low speed flying qualities and performance characteristics with emphasis on approach and landing.

17. Key Words (Suggested by Author(s))	18. Distribution Statement
Rotating Cylinder Flaps Deflected Slipstream STOL Interconnected Propellers	UNCLASSIFIED-UNLIMITED

19. Security Classif. (of this report)	20. Security Classif. (of this page)	21. No. of Pages	22. Price*
UNCLASSIFIED	UNCLASSIFIED	164	3.00

* For sale by the National Technical Information Service, Springfield, Virginia 22151

ABSTRACT

The initial flight testing of an YOV-10 airplane modified to a rotating cylinder flap configuration with two cross-shafted propellers powered by two Lycoming T-53 engines was carried out by the contractor for NASA Ames, Moffett Field, California, under contract NAS2-5326. The flight program was continued with further flight testing carried out by NASA in conjunction with the contractor. The flight tests included verification of the functional operation of the rotating cylinder system and the determination of low speed flying qualities and performance characteristics with the emphasis upon approach and landing. The flight characteristics are described based upon recorded data and pilot evaluation.

SUMMARY

The initial flight testing of an YOV-10 airplane modified to a rotating cylinder flap configuration with two cross-shafted propellers powered by Lycoming T-53-L-11 engines was performed to demonstrate the rotating cylinder flap concept proposed by Dr. Alvarez-Calderon. The low speed flying qualities and performance characteristics were evaluated with emphasis upon approach and landing flight phases.

A landing approach was made at 54.5 knots on a 6.3° glide path. Some approaches were made utilizing an 8° glide slope relative to the ground using a Bell radar system. The approach angles deduced from altitude and computed airspeed time histories indicated values of 6.5° to 7°. The difference can be attributed to light headwinds during the landing tests.

The airplane lift coefficients obtained in flight generally exceeded the initial estimates and values obtained in full scale tunnel tests. An unexpected shift in pitching moment characteristics, which required full nose-down control at low speeds, was not predicted from full scale wind tunnel testing. Downwash characteristics at the mid-span location of the horizontal tail were obtained in flight and compared to full scale wind tunnel test results and estimates. In general, the flight test downwash values showed fair agreement with estimates and were consistent with the lift results. The full scale wind tunnel test downwash values are lower than either the flight data or estimates.

Lateral-directional dynamic stability was dominated by an unstable spiral mode which was apparent in the low values of dihedral effect from the wind tunnel data. Dutch roll frequencies and damping were lower than estimated. Lateral control power available from ailerons and spoilers was satisfactory. A differential propeller blade angle system was flight tested also, and no significant roll response difference is indicated. However, adverse yaw reduction is apparent in the limited data available.

Climb performance was satisfactory and showed reasonable agreement with estimates.

The rotating cylinder and propeller cross-shafting operation were satisfactory. The failure of a cylinder drive system was simulated without any problem due to the long run-down time of the cylinders. An engine failure was also simulated satisfactorily.

TABLE OF CONTENTS

LIST OF FIGURES

LIST OF FIGURES (Concluded)

INTRODUCTION

As part of NASA Ames Research Center's STOL research vehicle program, North American Rockwell Corporation, Columbus Aircraft Division (NR-C), was contracted to design and implement a modification to a YOV-10 twin engine airplane (Figure 1) and perform initial flight tests. The modification consists of incorporation of the Alvarez-Calderon rotating cylinder flap system, installation of Lycoming T-53-L-11 engines and propeller cross-shafting for single engine safety, incorporation of a differential propeller blade angle system for lateral control power augmentation and an increase in horizontal tail incidence angle to lessen the possibility of tail stall. Reference (a) describes the modification design and the estimated aerodynamic characteristics.

The rotating cylinder concept is a boundary layer control device which, in conjunction with a propeller slipstream, produces lift and drag characteristics required by STOL vehicles for steep approaches and short landings. Wind tunnel testing carried out by NASA Ames on a twin boom model indicated the required aerodynamic characteristics could be achieved.

After the design and modification to the YOV-10 airplane was completed, the airplane was wind tunnel tested in the full scale (40 ft by 80 ft) NASA Ames tunnel. Based upon analysis of the wind tunnel data, Ames test 388, which indicated some aerodynamic characteristics to be different than estimated, it was agreed that the airplane could be safely flown. The initial flights were performed by the contractor and consisted of verification of functional operation of engines, power management system, cross-shafting, cylinder drive and flap deflection system, differential propeller blade angle and initial exploration of the flight characteristics at all flap deflections.

A total of 12 flights, one of which consisted of high speed taxi tests, were flown by North American Rockwell test pilot, Edward Gillespie. The flight program was continued by NASA and 22 additional flights were flown by NASA Ames Research Center test pilot, Robert Innis. The report includes data from contractor flights and NASA conducted flights.

NOTATION

SYMBOL	DEFINITION
C_D	$\frac{D}{qS_w}$ Drag coefficient
C_L	$\frac{L}{qS_w}$ Lift coefficient
C_M	$\frac{M}{qS_w C_w}$ Moment coefficient
C_{Ts}	$\frac{T_1}{T_1 + qS_p}$ Thrust coefficient based on propeller disk area
$\overline{C}_w$	Wing mean aerodynamic chord
N_Z	Vertical load factor
q	$\frac{1}{2}\rho V_T^2$ Dynamic pressure or pitch rate
r	Yaw rate
S_p	Propeller disk area
S_w	Wing area
T	Thrust, total
T_1	Thrust, one propeller
T_c'	T/qS_w Thrust coefficient based on wing area
V_i	Indicated airspeed
V_e	Equivalent airspeed
V_c	Calibrated airspeed
α	Angle of attack of fus. reference line
α_u	Recorded angle of attack, uncorrected
α_H	Angle of attack of horizontal tail reference chord
β	Sideslip angle

NOTATION (contd)

SYMBOL	DEFINITION
β_p	Propeller blade angle
δ_a	Aileron deflection
δ_e	Elevator deflection
δ_f	Flap deflection (shown as ___°/___°, forward flap/aft flap)
δ_r	Rudder deflection
ϵ	Downwash angle
ϵ'	$\alpha - \epsilon$
γ	Flight path angle
θ	Pitch angle
θ_u	Pitch angle, uncorrected
ϕ	Bank angle
ζ	Damping ratio
ω_N	Undamped airplane natural frequency

SUBSCRIPTS

$(\quad)_L$	Left
$(\quad)_R$	Right

AIRPLANE

The airplane is a twin boom prototype YOV-10 modified to a STOL configuration by installation of 1,100 horsepower engines and 9.4 ft diameter propellers, mechanical cross-shafting between propeller gear boxes and rotating cylinders at the leading edge of each flap segment. For compatibility with the high lift system, the horizontal tail incidence was increased +2 degrees for a total incidence with respect to the fuselage reference line of +4 degrees (leading-edge-up).

The airplane has an aspect ratio of 4.74 and a wing loading of 45 lbs/ft^2. The increased diameter propellers provide a thrust to weight ratio of .48 at 50 knots. The propeller slipstream covers 55 percent of the wing. The rotating cylinders extend over 61 percent of the wing span and are located in the propeller slipstream.

The control system is the same as the basic YOV-10 with the exception of modifications to the lateral system. The longitudinal system consists of a horizontal stabilizer and a tab boosted, mechanically dampened, overbalanced elevator. The tab system consists of geared and spring tabs.

The directional system consists of twin vertical stabilizers and twin rudders controlled by direct mechanical action through the rudder pedals.

The lateral system consists of spring and gear tab boosted ailerons augmented by spoilers. The spoilers are linked to the ailerons and rotate out of the wing when the trailing edge of the respective aileron is deflected upward by stick movement.

The lateral control system was modified by removal of the inboard spoiler segment (required for flap installation clearance) and the installation of a differential propeller blade angle system. The differential propeller blade angle system is actuated by commands from lateral stick deflection.

The power management system provides the pilot with the option of two methods of thrust control, beta or manual mode. When operating in the beta mode, the pilot controls the propeller blade angle and the system governor maintains RPM by controlling the fuel flow to the engines. This system provides rapid thrust response to the pilot's demand. When operating in the manual mode the pilot controls power by selecting a combination of propeller blade angle and throttle setting.

Cylinder operation, flap deflections, power management mode and differential blade angle operation are selected by the pilot. The landing gear is fixed down.

The cylinder speed is adjustable from 9,700 to 2,800 RPM at a propeller speed of 1,225 RPM. Data from NASA Ames test 388 indicate that a cylinder speed of 7,500 RPM will keep the flow attached to the flaps. Flight tests were conducted with this cylinder speed setting.

Figure 2 presents a three-view drawing of the aircraft and the aerodynamic dimensions of the flap. Tabulated dimensional data are summarized on page 20.

CORRECTIONS TO DATA

The airspeed calibration curves are shown in Figure 3 and are independent of flap deflection or power as shown in Figure 3b . The airspeed system calibration was performed with a trailing bomb hung below a Bell HU-1E helicopter used as the chase aircraft.

A pitch angle correction curve is shown in Figure 4 . All analyses using pitch angle were corrected by these data. Time histories showing pitch angle are labeled θ_u and are uncorrected.

In order to determine the validity of the airplane instrumented angle-of-attack data, a comparison was made with angle-of-attack determined from the relationship, $\gamma = \theta - \alpha$. Pitch angle, θ, was determined from the instrumented data and corrected. The flight path angle, γ, was obtained from the altitude rate of change and airspeed. The comparison is shown in Figure 5 and indicates the measured angle of attack data appear to be approximately 5° to 8° greater than the calculated data obtained by the method described above. Time history data where angle of attack is shown are labeled α_u and are uncorrected. All analyses using angle of attack are corrected as described above.

Measurements to determine downwash characteristics were made in the Ames wind tunnel tests and in flight by mounting a pressure measuring boom midspan and slightly below the horizontal tail leading edge. Figure 6 shows the location of the boom. Since measurements were made at only one spanwise station, no account of spanwise variation could be made. The spanwise variation was thought to be relatively small. However, the local angle error included on the boom by the presence of the horizontal tail was expected to be substantial. Consequently, theoretical calculations of local flow curvature at the boom location were made to allow corrections to be made to the measured data. The corrections were obtained as a function of tail angle of attack and elevator deflection. The method used in the computations is two-dimensional and was obtained from Reference (b). A comparison of pressure distribution data to computed data is shown in Figure 7 to illustrate the accuracy of the method. The correction applied to the measured data is shown in Figure 8 . Separate correction curves are shown for the Ames test 388 data and the flight data due to a slight difference in location of the pressure booms.

Throughout the report, data are presented as functions of two forms of thrust coefficient, one of which is used extensively by the contractor and the other by NASA Ames Research Center. The conversion curve is shown in Figure 9 .

DISCUSSION

LONGITUDINAL CHARACTERISTICS

Static Longitudinal Stability

Static longitudinal stability obtained in stabilized flight at constant power settings using power for level flight at the trim speed is shown in Figure 10 for all flap deflections flown. For 0°/0° flap deflection, stable stick-fixed stability is exhibited. Also shown in Figure 10 are flight test elevator deflection data for the unmodified YOV-10 airplane. Correcting these data for horizontal tail incidence difference, weight and center-of-gravity position, produces good correlation between the two airplanes as indicated in Figure 10a.

In Figure 10e, for 60°/30° flap deflection, a large change in the instability is shown due to cylinder operation. Figure 10e also shows a comparison to estimated data based on data from Ames Test 388. Although the estimate is for a more aft center-of-gravity location (27.6% m.a.c.) the effect of the center-of-gravity is to decrease the difference between the estimated data and the flight data. The large difference between the estimated and flight elevator deflections is discussed later under Downwash.

At a forward center-of-gravity the static longitudinal stability is stable for the airspeeds tested as shown in Figures 10f through 10i.

Longitudinal Control for Low Speed Steady Flight

Longitudinal control deflections for steady flight are affected by flap deflection, cylinder operation (running or stopped) and engine power. With approach power settings and cylinders operating, static longitudinal instability occurs and increases as speed is decreased as shown in Figure 11 . As flaps are lowered to larger deflections, the elevator deflections for steady flight increase in the trailing edge down (nose down) direction as shown in Figure 11 for a center of gravity of 24.6% $\bar{c}$, and minimum longitudinal control speeds of 43 and 52 KIAS occur for flaps 40°/20° to 50°/25° and 60°/30°, respectively.

As expected for a forward center-of-gravity, the elevator deflections are shifted in the trailing-edge-up direction, comparing the data of Figure 11a and Figure 11b. However, the minimum speed determined by full trailing-edge-down elevator deflection is not significantly affected.

While improved control margin is available above minimum control speed, the minimum control speeds are practically constant.

The effect of cylinder operation is presented in Figure 12 for two flap deflections and indicates a large shift in elevator deflection for the 60°/30° flap deflection. In addition, engine power effects produce significant shifts in elevator for steady flight. Figure 13 shows the effect of power and indicates increased power produces a shift in the trailing-edge-down elevator deflections. For the configuration of 40°/20° flap deflection and a forward center-of-gravity, the elevator shift is reasonable for power levels employed in an approach as shown in Figure 13b.

Downwash

Measurements to determine downwash characteristics were made in the Ames wind tunnel tests and in flight by mounting a pressure measuring boom mid-span and slightly below the horizontal tail leading edge, Figure 8. The data were corrected for the presence of the horizontal tail by the procedure described on page 6.

Comparisons were made of flight, Ames test 388, and the estimated downwash data. For 0° flap deflection, Figure 14a, the comparison does not show agreement. This is surprising because this configuration most closely resembles the unmodified YOV-10A airplane.

The 30°/15° flap deflection data of Figure 14b shows good agreement between flight and estimated data. The flight downwash values are larger than those measured in the 40 x 80 foot tunnel; this is consistent with the lift data shown in Figure 26a.

The 60°/30° flap deflection flight data of Figure 14c shows lower downwash values than estimated data. This trend agrees with the lift data, Figure 26b, which showed lower than estimated lift for this flap deflection.

It is noted that the downwash wind tunnel data of Ames test 388 produce lower downwash angles than the flight data. This is suspected to be due to wind tunnel wall effects. For high downwash fields resulting from high lift coefficients, tunnel wall effects become larger and more difficult to determine accurately.

Dynamic pressure ratio data obtained in flight are presented in Figure 15.

In order to determine the effect on elevator-to-trim due to the downwash difference between the wind tunnel and flight results, the following correlation was made. Using the corrected angle of attack and thrust levels from the flight data, an estimate of elevator-to-trim was obtained based upon the Ames test 388 aerodynamic data. The estimated elevator-to-trim data were then adjusted based upon the difference in downwash between wind tunnel and flight data. Horizontal tail characteristics of Reference (a) were used in the calculation. The elevator deflection estimates were also corrected for tab losses. Figure 16 shows the comparison. At 50 knots most of the pitching moment difference can be attributed to the downwash. At 77 knots, the downwash does not explain the difference. Therefore, it is possible that wind tunnel wall effects are distorting wing-body-nacelle pitching moments.

Maneuvering Control

Longitudinal control in a wind-up turn maneuver to maximum lift is shown in Figure 17. Satisfactory control is exhibited.

Longitudinal Control at Take-Off Rotation

Longitudinal control power is more than adequate to rotate the NASA STOL YOV-10 at any takeoff speed within its envelope. Takeoff rotation points of various flights are shown in Figure 18. Although these points do not represent attempts to achieve minimum lift-off speeds, the aircraft used only 30 percent of its maximum deflection at 68 knots with 0 degree flaps and cylinders off. Flap settings of 30°/15° do not appear to significantly increase the elevator required for rotation. The effect of cylinder operation is to decrease strongly the amount of aft stick required for rotation. This is due to the pitch-up at low speeds introduced by the rotating cylinders. From these data it can be concluded that the aircraft is able to rotate at speeds well below the lift-off speed over the center-of-gravity range tested of 21.9 percent m.a.c. to 25.4 percent m.a.c.

Longitudinal Control Response

In general, the pilot determined his approach speed based upon longitudinal control margin available and control response. Using 50°/25° flap deflections and approaching at 55 KOAS, the contractor pilot rated the longitudinal control as 4 on the Cooper scale, noting it as adequate but unsatisfactory. Data which illustrate the longitudinal control response characteristics with 40°/20° flaps are shown in Figures 19 and 20. Good agreement with estimates is evident.

A time history of a step change in elevator deflection is shown in Figure 21. A speed increase of 13 knots from 62 knots is effected in approximately 5 seconds. The pilot noted that longitudinal control response was satisfactory at this speed.

Trim Change Due to Power

At the airspeeds tested, the trim change characteristics appear to be satisfactory. The time history of a power change during an approach condition is shown in Figure 22. The aircraft was initially descending at a rate of 500 ft/min with a flap setting of 30°/15°. The tendency for the airplane to pitch up with power application to the EGT limit was easily controlled with approximately 3 degrees of trailing-edge-down elevator. As the increased engine torque level was reached, the airplane was gradually allowed to climb.

Stall Characteristics

Stall and/or minimum speed tests were conducted for 0°/0°, 30°/15°, 40°/20°, 50°/25° and 60°/30° flap deflections. Time histories of these tests are presented in Figures 23 and 24.

The 0°/0° flap deflection stalls were characterized by an abrupt yaw as seen in the data of Figure 23e through 23f. The direction of the yaw rate appeared to depend upon power since the power for level flight stall (Figure 23a and 23b) and the approach power stall (Figure 23c and 23d) was to the right while the flight idle stall (Figure 23e and 23f) was to the left. No significant pitching occurred and stall recovery was easily effected. The above yawing characteristics in stalls was not apparent on the YOV-10 airplane prior to the modification to the NASA STOL configuration.

With 30°/15° flaps for cylinders both operating and inoperative, stall characteristics consisted of mild random yaw motions and pitch motions. As shown in Figures 23g through 23l, the random motions occurred approximately 5 knots before stall. Recovery from the stalls with 30°/15° flap deflections was easily effected at all test conditions.

For flap deflections of 40°/20° and greater deflections, stall could not be produced due to the pitch-up characteristics of the airplane which

required full forward longitudinal control for an aft center-of-gravity. Figures 24a through 24h show approach to the minimum speed and the limiting condition for 40°/20°, 50°/25° and 60°/30° flap deflections. Mild random yawing and rolling motions occurred for the airspeeds shown. Recoveries from the minimum speeds were accomplished by power reduction which caused the airplane to pitch down and accelerate. The pitch-up characteristic is discussed in the longitudinal control section of this report.

With flaps deflected to 60°/30° and a forward center-of-gravity, the elevator was not limiting as seen in Figure 24i and j. The pilot terminated the attempt to stall in this case due to low directional stability, unstable pitch characteristics and lateral instability.

Maximum Lift

Flight data obtained from stalls and/or minimum longitudinal control speed were compared to Ames test 388 and estimated aerodynamics data of Reference (a). The maximum lift comparison is shown in Figure 25 . The Ames full scale test data and the estimated data are shown at the thrust coefficient of the flight data. For all flap deflections shown in Figure 25 , the flight data indicate angles of attack for stall or minimum speed which are higher than Ames test 388 or the estimated data.

For 30°/15° flap deflection, the maximum lift coefficient from flight data is substantially higher than the tunnel test or the estimated data as shown in Figure 25a. The 50°/25° flap deflection data show a modest increase over the estimated data and a greater increase over the wind tunnel data in Figure 25b. The 60°/30° flap deflection, however, shows a minimum speed lift value in Figure 25b which is less than the estimated data and slightly higher than the wind tunnel data maximum lift. The maximum lift or minimum speed lift coefficient data from flight tests are shown in another form (C_L versus T_C') in Figure 26 . Since the wind tunnel test was full scale and run at speeds very close to actual flight speeds, it is suspected that wind tunnel wall effects are responsible for the difference in lift noted above. Stall speed and/or minimum speeds obtained for the flight data above are presented in Figure 27 .

Landing Characteristics

Time histories of approaches and landings with flap deflections of 30°/15°, 40°/20° and 50°/25° are shown in Figure 28 . The pilots chose approach speeds based upon considerations of longitudinal control margin, longitudinal control response and stall margin.

The thrust used in the approach allows approach speeds to be less than the power-off stall speed. Figure 29 shows the thrust values employed

in the approach and landings. Included in Figure 29 are the thrust values at stall or minimum speed. Figure 30 shows the speed margin for the approach speeds used. For the 30°/15° flap deflection landing shown in Figure 30a, a substantial speed margin from stall existed. A minimum speed margin of approximately 9.5 knots was employed for one 50°/25° flap deflection landing as shown in Figure 30b. For the latter case, the margin is from minimum longitudinal control speed. In determining the approach speed stall margin, the variation in thrust with speed was included.

The approach angles obtained in the landings are shown in Figure 31 . The data for flights 10 to 12 in Figure 31 do not represent maximum approach angles. No approach angle aids were utilized and the pilot was investigating approach characteristics. Flight 25 employed a ground based approach aid (Bell radar system) and was conducted with 40°/20° flap deflection with a forward center-of-gravity which improved approach flying qualities.

Descent Angle Comparisons

Flight path angles were obtained from flight tests of steady descents, stalls and landing for 30°/15°, 40°/20°, 50°/25° and 60°/30° flap deflections. For comparison, flight envelopes based upon Ames test 388 data and estimated data are included with the flight data shown in Figure 32 .

As expected, the 30°/15° and 50°/25° flap deflection flight data in Figure 32a and 32c exceeds the stall portion of the estimated or wind tunnel test envelopes since higher lift coefficients occurred in flight. No wind tunnel test or estimated data were available for 40°/20° flap deflection. The data shown for 60°/30° flap deflection were obtained from steady descents and stall attempts. Although descent angles in the range of -8 to -12 degrees were achieved in the stall approaches for 30°/15° and 50°/25° flap deflection, those flight conditions could not necessarily be used to conduct actual approaches and landing. Flying qualities factors such as proximity to stall, control margin and response and airplane stability can be overriding characteristics in determining usable approach speeds.

The data from flight 25 shown in Figure 32b were obtained with a landing approach aid set for a glide slope of -8 degrees with respect to the ground. The data shown in Figure 32 were reduced from altitude and corrected airspeed time histories and as such are independent of wind velocity. The difference between an -8 degree glide slope and the data shown in Figure 32b is attributed to wind velocities components along the runway. This is corroborated by radar obtained ground speed.

The difficulty of obtaining a -8 degree flight path angle at speeds between 50 and 60 KEAS was examined from the standpoint of drag characteristics. For flap deflections of 30°/15° and 60°/30°, the thrust coefficient determined from flight test data was compared to the thrust coefficient based upon Ames test 388 data using flight test conditions (i.e., flight path angle, speed, etc.). This comparison is shown in Figure 33 and indicates that at the high descent angles (corresponding to high angle of attack) less thrust was required than estimated from Ames test 388.

LATERAL CHARACTERISTICS

Static Lateral Directional Stability

Static lateral-directional characteristics were obtained in constant heading sideslips. These data of Figure 34 show strong directional control power in the NASA STOL YOV-10. The aircraft is significantly more sensitive to rudder inputs than the 30 ft span OV-10A aircraft, as shown in the summary plot of Figure 35 . Also, within the range of flight data taken, the rudder effectiveness does not appear to be strongly influenced by flap deflection or rotating cylinder operation.

Flight data indicate that aileron control required is strongly affected by both cylinder operation and flap deflection. The effect of cylinder operation is to decrease the amount of aileron input required. At low flap deflections, the aileron input is in the same range as that of the 30 ft span OV-10A model and does not appear to be significantly affected by changes in flap settings.

The flight data at flap deflections of 60°/30° show a reversal in aileron input, as seen in Figure 34i. Data from Ames test 388 wind tunnel tests indicates that high flap deflections coupled with rotating cylinders cause a negative dihedral effect in the STOL YOV-10. In the summary plot of Figure 35 , the data for 60°/30° is therefore shown for two ranges of sideslip angle.

Roll Characteristics

Lateral control input in rate and magnitude varied considerably in roll characteristic tests. Full aileron input was not employed due to spiral instability and high lateral control power with cylinders operating. Roll time histories are shown in Figure 36. The pilot noted no noticeable gyroscopic effects due to cylinders operating in qualitative evaluations of normal turns.

These data are summarized in Figures 37 and 38 . To minimize the differences in control input the summary parameters of bank angle rate and peak-to-peak sideslip angle were normalized to aileron deflection.

The effect of the differential propeller beta system on roll response appears to be negligible as seen in Figure 37 . This could be due to the fact that small control inputs were used. Full scale airplane tunnel data (Ames test 388) indicate a 25 percent increase in roll control power with differential beta on.

The effect of the differential propeller beta system on sideslip angle occurring in rolls is apparent in the data of Figure 38b. The pilot also indicated that the differential propeller beta system improved the adverse yaw characteristics.

Turn Characteristics

Turn characteristics for 20° banked turns are shown in Figures 39 and 40 . The rudder fixed turns in Figure 39 indicate larger yaw rate, sideslip angle and bank angle deviations. Due to the high rudder control power and/or weak directional stability, very small rudder inputs were used in the coordinated turn data of Figure 40 . The calculated steady yaw rate for a 20° banked turn is 5.8°/sec at the airspeed employed in the flight tests.

Dynamic Lateral-Directional Stability

Lateral-directional dynamic stability tests were difficult to perform at low speeds. The maneuvers were initiated with rudders and due to airplane spiral instability and the low dutch roll natural frequency, the maneuvers were not held for a long enough time to record a sufficient number of cycles. The available data are shown in Figure 41 .

Lower frequencies and less damping is evident than estimated from static stability derivatives obtained from Ames test 388 and estimated rate derivatives. The destabilizing cylinder gyroscopic effects were included in the estimates and would not be expected to cause the difference from flight test results. The data scatter is believed due to inadvertent aileron and rudder inputs while the airplane motions were decaying after the disturbance input. Figures 41b and 41d show the bank to sideslip amplitude ratios from the dynamic stability tests. Due to the low frequencies and relatively short duration of the test maneuvers considerable scatter occurred.

Although no tests were performed to evaluate the degree of spiral instability, it was apparent to the pilots that spiral instability existed. The estimated dynamic stability calculations also predicted the instability and indicated that the divergence rates would be rapid, i.e., time to double amplitude of only several seconds.

Pilot reports indicated a coupling of lateral-directional dynamic motions with longitudinal modes. The coupling on pitch angle, angle of attack and airspeed can be seen in Figure 42 . The coupling may be initiated by the pitching moment due to sideslip angle. Inadvertent elevator and lateral control inputs are also evident in the data of Figure 42 which may be contributing to the longitudinal coupling.

CLIMB PERFORMANCE

Throughout the flight program, maximum power available was limited by an EGT limiting condition on the right-hand engine. For this reason, maximum rate-of-climb could not be established. Rate-of-climb data were obtained at less than rated maximum power and are shown in Figure 43 . These data are compared to estimated rate-of-climb based upon estimated engine thrust and Ames test 388 airplane aerodynamic data. Although small differences between propeller blade angle and propeller RPM between the test data and estimated data exist, the agreement appears good.

SIMULATED FAILURE CONDITIONS

Cylinder Drive System Failure

The effect of cylinder shutdown during approach was investigated by trimming the airplane at 68 KOAS 1,000 f.p.m. rate of descent with 300 ft-lbs/engine. After stabilizing for 1,000', the cylinders were manually shut off at 5,000' and the pilot held the approach speed. The cylinders slowed down slowly so that they were still turning 3,000 RPM at 3,500' Hp. There was no quantitative change in sink rate, and the only difference noted during the above tests was an increase in longitudinal force stability from neutral to weak positive as the cylinder rotation decreased below about 3,000 RPM.

The above characteristics indicate that failure of the cylinder drive system produces changes very slowly. Thus, a failure would not be critical if it occurred inadvertently and the pilot was aware the cylinders were running down.

Simulated Engine Failure

A simulated engine failure was performed by a slow power reduction to flight idle on the right-hand engine. Figure 44 shows a time history of the test. No significant airplane transients are noted in the data. The pilot also noted no abnormal vibration or other pecularities as the cross-shafting assumed the power transfer. Level flight was easily maintained on the left engine.

ENGINE CHARACTERISTICS

Power Lever Steps

Rapid propeller blade control lever inputs were evaluated and are shown in Figure 45 . The input is shown by the propeller blade time history. Throttle position changes shown in Figure 45 result from the throttle servo system driving them to adjust to the power demand. Engine torque response appears satisfactory.

CONCLUSIONS

The flight test data and comparisons to estimates and full scale wind tunnel test data result in the following conclusions:

1. The most significant difference between flight and estimated or wind tunnel results is in the airplane pitching moment. The unstable pitch-up is a strong function of flap deflection, cylinder operation, engine power and airspeed. At high power settings and flap deflections of 40°/20° and greater, minimum speeds resulted from full forward stick. Aerodynamic stalls occurred for 30°/15° or less flap deflection.

2. With flaps up and cylinders inoperative, the longitudinal stability and control are similar to the unmodified airplane.

3. Downwash characteristics generally agree with results on lift; i.e., where lift is higher than estimated, downwash is higher. Both estimated and flight downwash values are greater than wind tunnel values. Fair agreement between estimated and flight downwash exists except for the flaps up and cylinders inoperative case.

4. Control power for takeoff is satisfactory at all center-of-gravity positions tested.

5. For flap deflections of 50°/25° and lower, the actual lift obtained is higher than either the estimated or tunnel test lift.

6. High descent angles (8° to 12°) were obtained during approaches to stalls. In landing approaches, descent angles approaching 7° were achieved. This included landings performed with the Bell radar glide slope system which was set to an 8° slope. The difference is attributed to light headwinds which can be a large percentage of approach speed.

7. The aircraft has low lateral-directional stability in the approach flight condition. This is apparent in sideslip and dynamic stability tests by low control inputs to produce upsets, low oscillatory frequency and damping and high spiral divergence.

8. Roll control power appears to be satisfactory. Qualitatively, the pilots seemed to prefer use of the differential propeller roll augmentation. The data showed no clear improvement in roll control power but gave some indication of reduction in adverse yaw in rolling maneuvers. Longitudinal coupling occurred with the lateral-directional oscillation.

9. Climb performance showed reasonable agreement with estimates and was satisfactory.

10. Rotating cylinder and propeller cross-shafting operation was satisfactory.

11. Due to the long run-down time of the cylinders when turned off, failure of the cylinder drive system would not cause sudden aerodynamic changes.

REFERENCES

(a) ANON: "OV-10 STOL Research Vehicle Study Final Report - Phase 1," February 1969, North American Rockwell/Columbus Aircraft Division Report No. NR68H-863

(b) Giesing, Joseph P., "Extension of the Douglas Neumann Program to Problems of Lifting, Infinite Cascades," Douglas Aircraft Company, Long Beach Division, Report No. LB 31653, Revised 2 July 1964

TABULATED DIMENSIONAL DATA

Wing

S_w	Area (Square Feet)	244.0
b_w	Span (Feet)	34.0
AR_w	Aspect Ratio	4.74
c_w	Chord (Inches)	87.25
λ_w	Taper Ratio	1.0
Λ_w	Sweep Angle (Degrees)	0
i_w	Incidence Angle to FRL (Degrees)	3.0
$\bar{c}_w$	Mean Aerodynamic Chord (Inches)	87.25
Location of 25% MAC (FS/WP, Inches)		185/30.4
Airfoil Section		NACA 64_2A-315(MOD)

Flaps (Four Sections, 2 Per Side, Data for One Side)

S_f	Flap Area (Square Feet)	13.80
b_f	Flap Span (Inches)	98.00
c_f	Flap Chord (Inches)	20.30
Wing Stations of Inboard Flaps (Inches)		18.75-67.75
Wing Stations of Outboard Flaps (Inches)		95.25-144.25
$S_f/S_{w/2}$	Ratio of Flap Area to Wing Area	.113
$b_f/b_{w/2}$	Ratio of Flap Span to Wing Span	.544
c_f/c_w	Ratio of Flap Chord to Wing Chord	.253

Rotating Cylinders (Four Sections, 2 Per Side)

b_{cyl}	Cylinder Span Per Section (Inches)	62.00
d_{cyl}	Cylinder Diameter (Inches)	12.00
d_{disk}	Cylinder End Disk Diameter (Inches)	
	Outboard	16.8
	Inboard	14.4

Ailerons (Plain Balance, Data for One Aileron)

S_a	Aileron Area (Square Feet)	4.13
b_a	Aileron Span (Inches)	34.13
c_a/c_w	Aileron Chord Aft of Hinge Line (percent wing chord)	20.0
c_{a_b}/c_w	Aileron Balance Chord Forward of Hinge Line (percent wing chord)	6.1
Wing Stations of Ailerons (Inboard-Outboard, Inches)		144.750-178.875
$\delta_{A_{MAX}}$	Maximum Aileron Deflection (Up/Down, Degrees)	25/25

Aileron Tabs (Spring Tabs, Left and Right)

b_{t_a}	Aileron Tab Span (Inches)	34.13
c_{t_a}	Aileron Tab Chord (Inches)	4.0
Wing Stations of Aileron Tabs (Inboard-Outboard, Inches)		144.750-178.875
$\delta_{t_{a_{MAX}}}$	Maximum Deflection (Up/Down, Degrees)	20/20

Spoilers (Four Disc-Plate Type, Data for One Side)

b_S	Spoiler Span (Inches)	45.8
Wing Stations of Spoilers (Inboard-Outboard, Inches)		97.0-143.3
Chordwise Location (percent wing chord)		59.56
Maximum Projection (percent wing chord)		8.89
δ_S	Maximum Spoiler Deflection (Up, Degrees)	100

Horizontal Tail

S_H	Horizontal Tail Area (Square Feet)	70.0
b_H	Horizontal Tail Span (Inches)	163.0
AR_H	Aspect Ratio (Geometric)	2.6
c_H	Chord (Inches)	62.2
λ_H	Taper Ratio	1.0
$\Lambda_{L.E.}$	Leading Edge Sweep Angle to FRL (Degrees)	0

Horizontal Tail (Continued)

i_H	Incidence Angle to FRL (Degrees)	+4.0
Location of 25 Percent c_H	(FS/WP, Inches)	422.92/94.00
$l_{t_{H/C}}$	Tail Length (25 Percent $\bar{c}_w$ to 25 Percent $\bar{c}_H$)	2.73
Airfoil Section		Inverted 64_1A412(MOD)

Elevator

b_e	Elevator Span (Inches)	155.6
c_e/c_H	Elevator Chord Aft of Hinge Line (Percent of Horizontal Tail Chord)	28.0
c_{e_b}/c_H	Elevator Balance Chord Forward of Hinge Line (Percent of Horizontal Tail Chord)	4.3
$\delta_{e_{MAX}}$	Maximum Elevator Deflection (Up/Down, Degrees)	35/25

Elevator Tabs (Four Sections, Inboard Tabs Geared, Spring Tabs Outboard, No Trim)

$b_{t_{e\ INBOARD}}$	Inboard Elevator Tab Span (Inches)	42.2
$c_{t_{e\ INBOARD}}$	Inboard Elevator Tab Chord (Inches)	4.0
$b_{t_{e\ OUTBOARD}}$	Outboard Elevator Tab Span (Inches)	34.9
$c_{t_{e\ OUTBOARD}}$	Outboard Elevator Tab Chord (Inches)	4.0
Butt Planes of	Inboard Elevator Tabs (Inboard-Outboard, Inches)	0-42.92
Butt Planes of	Outboard Elevator Tabs (Inboard-Outboard, Inches)	42.92-77.81
$\delta_{t_{e_{MAX}}}$	Maximum Deflection of Inboard Geared Tabs (Up/Down, Degrees)	21/30
$\delta_{t_{e_{MAX}}}$	Maximum Deflection of Outboard Spring Tabs (Up/Down, Degrees)	12/28
δ_{t_e}/δ_e	Geared Elevator Tab Ratio	-.85

Vertical Tail (Data for One Side)

S_V	Vertical Tail Area (Square Feet)	35.69
b_V	Vertical Tail Span (Inches)	88.00
AR_V	Vertical Tail Aspect Ratio	1.507
c_V	Vertical Tail Chord (Inches)	58.40
λ_V	Vertical Tail Taper Ratio	1.0
$\Lambda_{V_{L.E.}}$	Leading Edge Sweepback Angle to FRL (Degrees)	32.0
Water Planes of Vertical Tail (Inches)		13-101
Location of 25 Percent $\bar{c}_V$ (FS/WP, Inches)		398.5/57.0
$l_{t_V}/\bar{c}_w$	Tail Length (25 Percent $\bar{c}_w$ to 25 Percent $\bar{c}_V$)	2.45
Airfoil Section		64_1A012

Rudder (Data for One Side)

b_r	Rudder Span (Inches)	72.17
c_r/c_V	Rudder Chord Aft of Hinge Line (Percent of Vertical Tail Chord, Streamwise)	30.0
c_{r_b}/c_V	Rudder Chord Forward of Hinge Line (Percent of Vertical Tail Chord, Streamwise)	10.0
Water Planes of Rudder (Inches)		13-85.17
$\delta_{r\ MAX}$	Maximum Streamwise Rudder Deflection	25/25

Fuselage (Basic Configuration)

L_F	Length (Overall, Inches)	300.0
h_F	Depth (Maximum, FS 117, Inches)	66.0
	(.25 L_F, Inches)	63.0
	(.75 L_F, Inches)	55.5
Water Plane of Maximum Depth, Inches		-20.0
W_F	Width (Maximum, FS 80-117, Inches)	66.0
	(.25 L_F, Inches)	42.0
	(.75 L_F, Inches)	37.0
S_F	Fuselage Surface Area (Net, including Canopy, Square Feet)	289.5

Nacelles

Thrust Line Angle to FRL (Degrees)	5°
Water Plane of Thrust Line at 25% c_w (Inches)	9.42
L_N Length (Overall, Inches) FS 142.2 to FS 416.5	274.80

Engines

Manufacturer	Lycoming
Model	T53-L-11
Sea Level Military Rating (SHP)	1100.00

Propeller (Four Blades)

Manufacturer	Curtiss Wright
Diameter (Feet, Inches)	9'5"
S_P Disk Area, Each Propeller (Square Feet)	69.7
Activity Factor/Blade	149.9

Typical Aircraft Weight

Aircraft Weight Empty + Ballast	10,279 lbs
Fuel	1,365 lbs
Pilot	200 lbs
T.O. Gross Weight	11,844 lbs

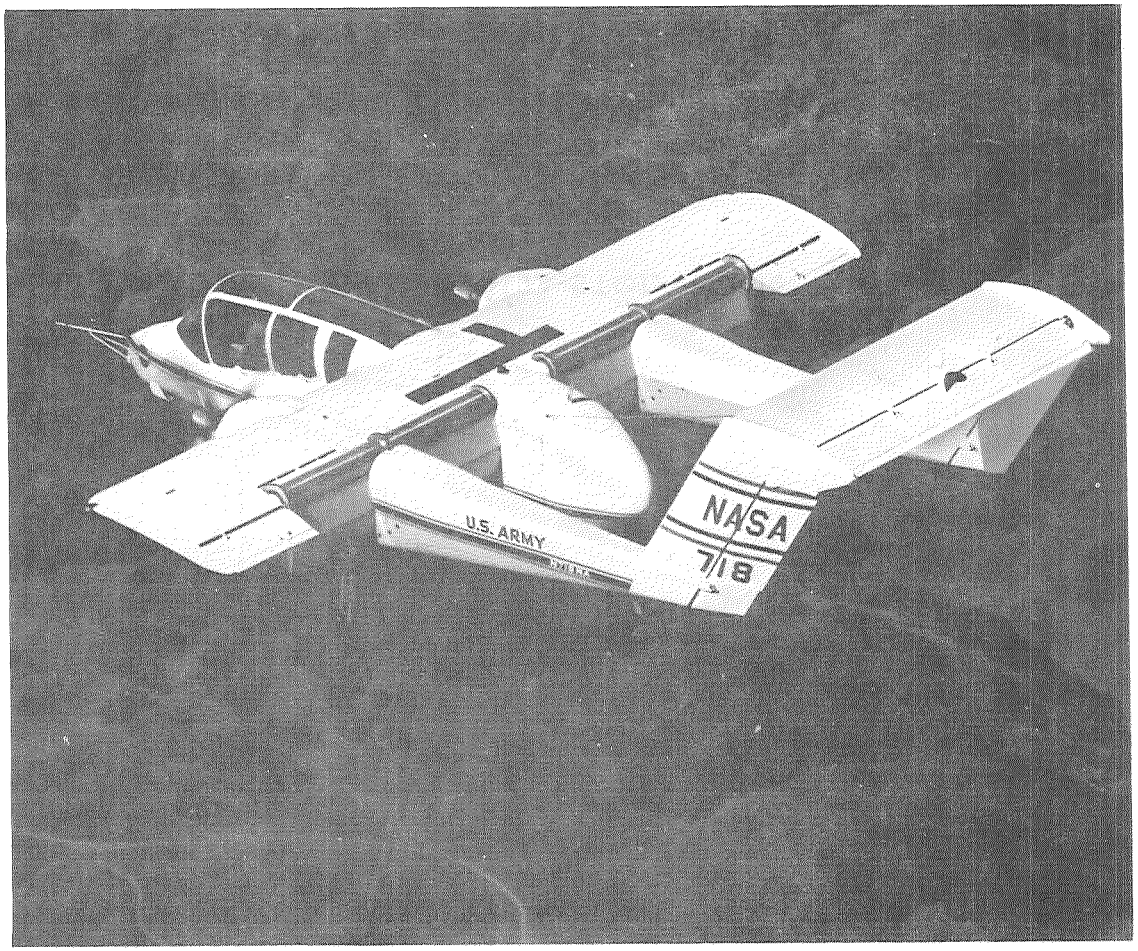

Figure 1.

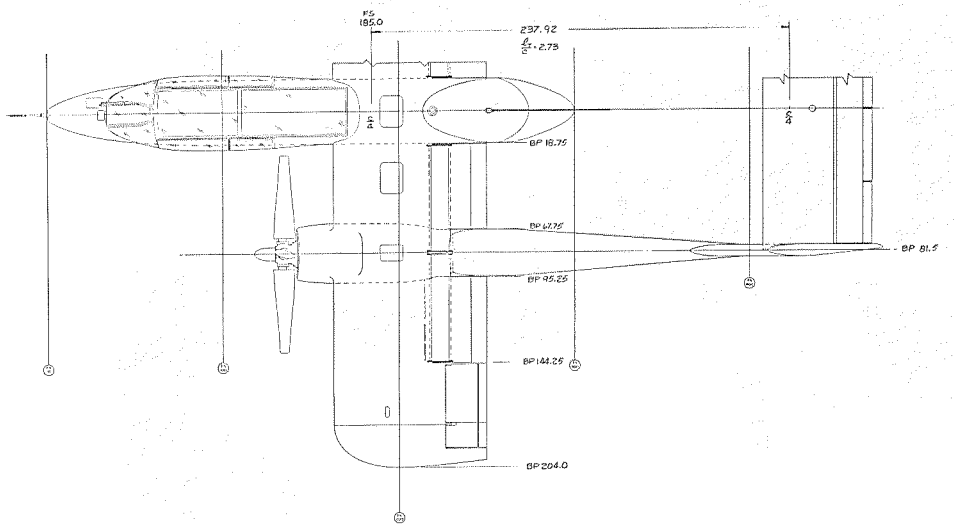

Figure 2(a). - Three view YOV-10A STOL vehicle.

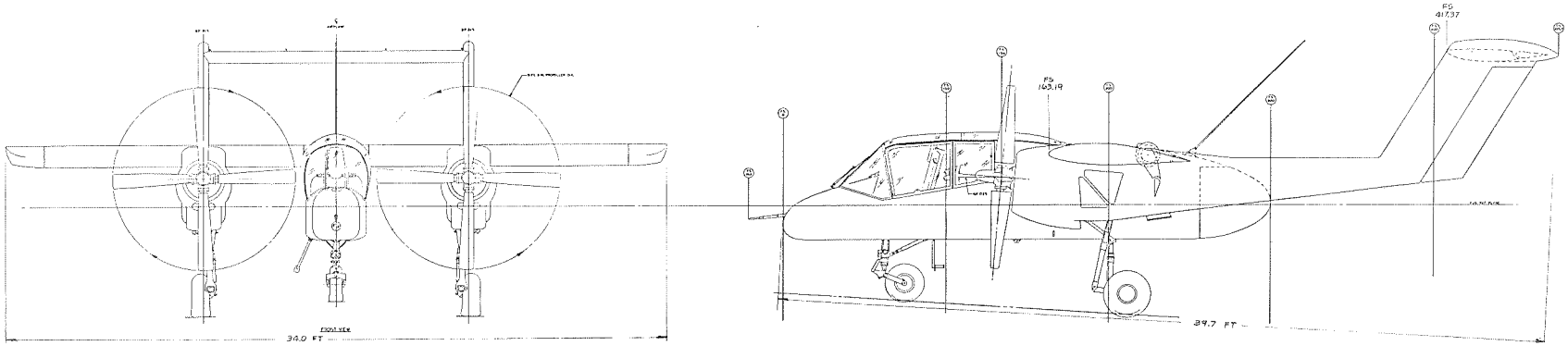

Figure 2(a). - Concluded.

FIGURE 2b

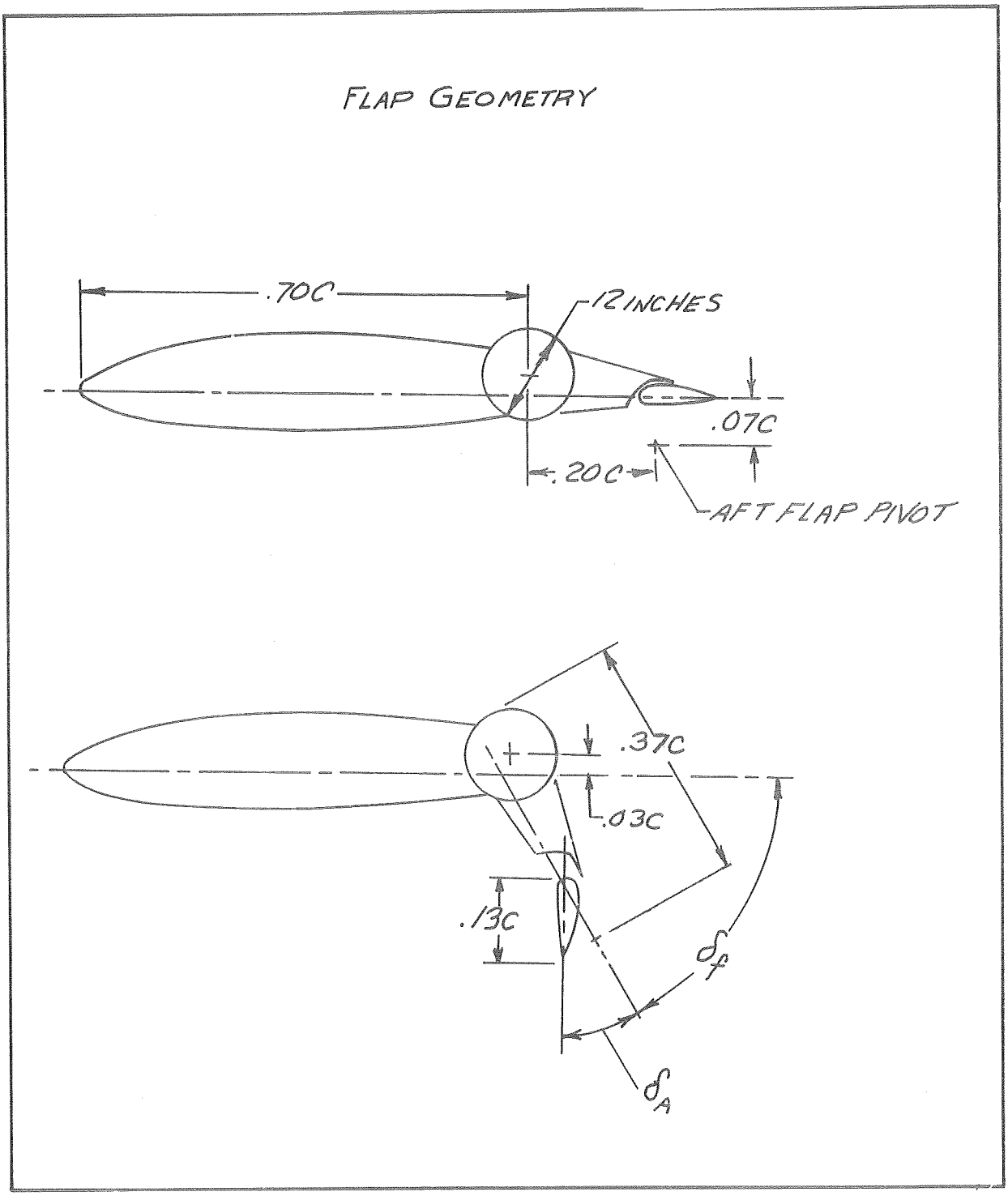
FLAP GEOMETRY
.70C
12 INCHES
.07C
.20C
AFT FLAP PIVOT
.37C
.03C
.13C
δ_f
δ_A

FIGURE 3z

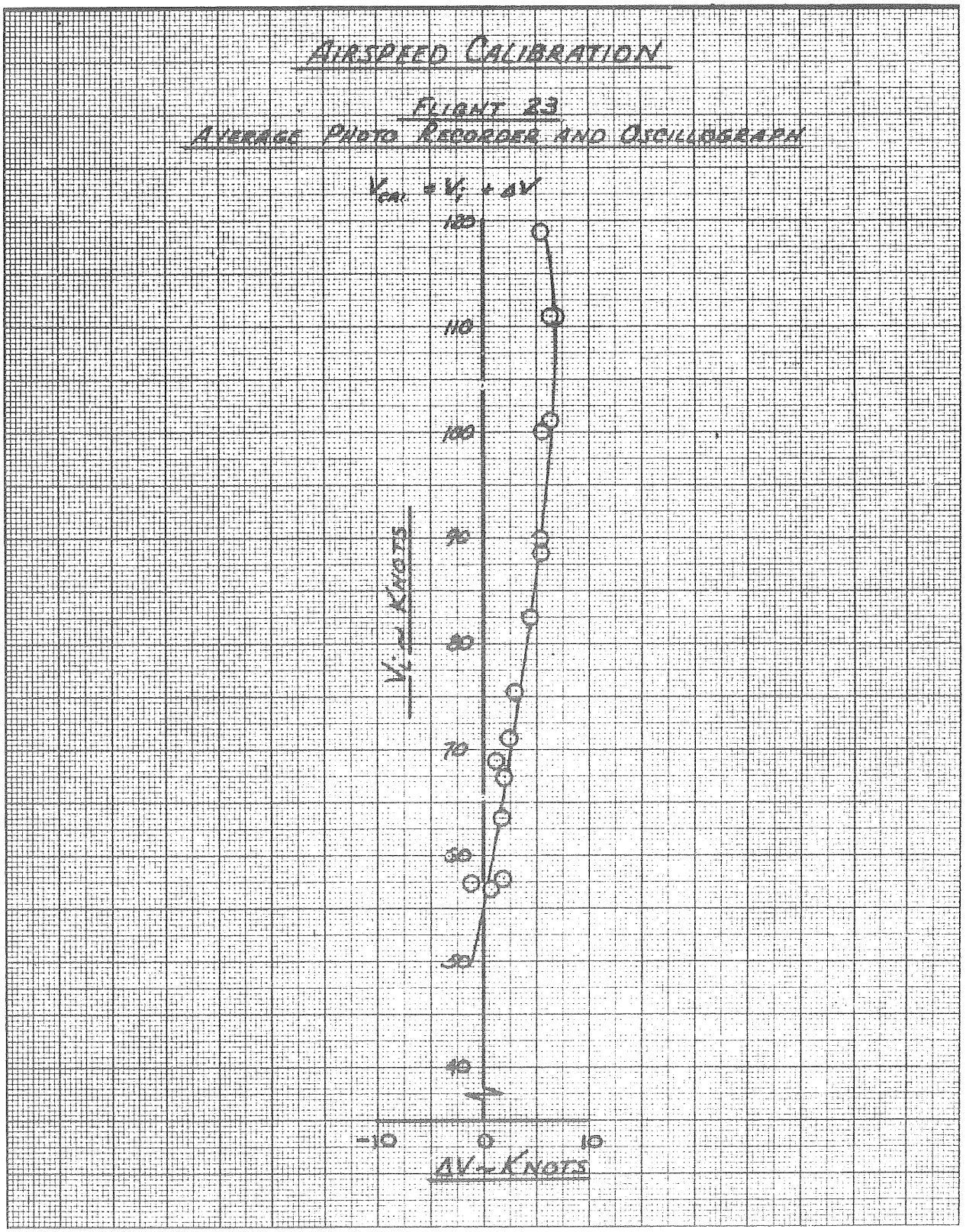
AIRSPEED CALIBRATION
FLIGHT 23
AVERAGE PHOTO RECORDER AND OSCILLOGRAPH
$V_{CAL.} = V_i + \Delta V$
120
110
100
90
80
70
60
50
40
V_i - KNOTS
-10
0
10
ΔV - KNOTS

FIGURE 3b

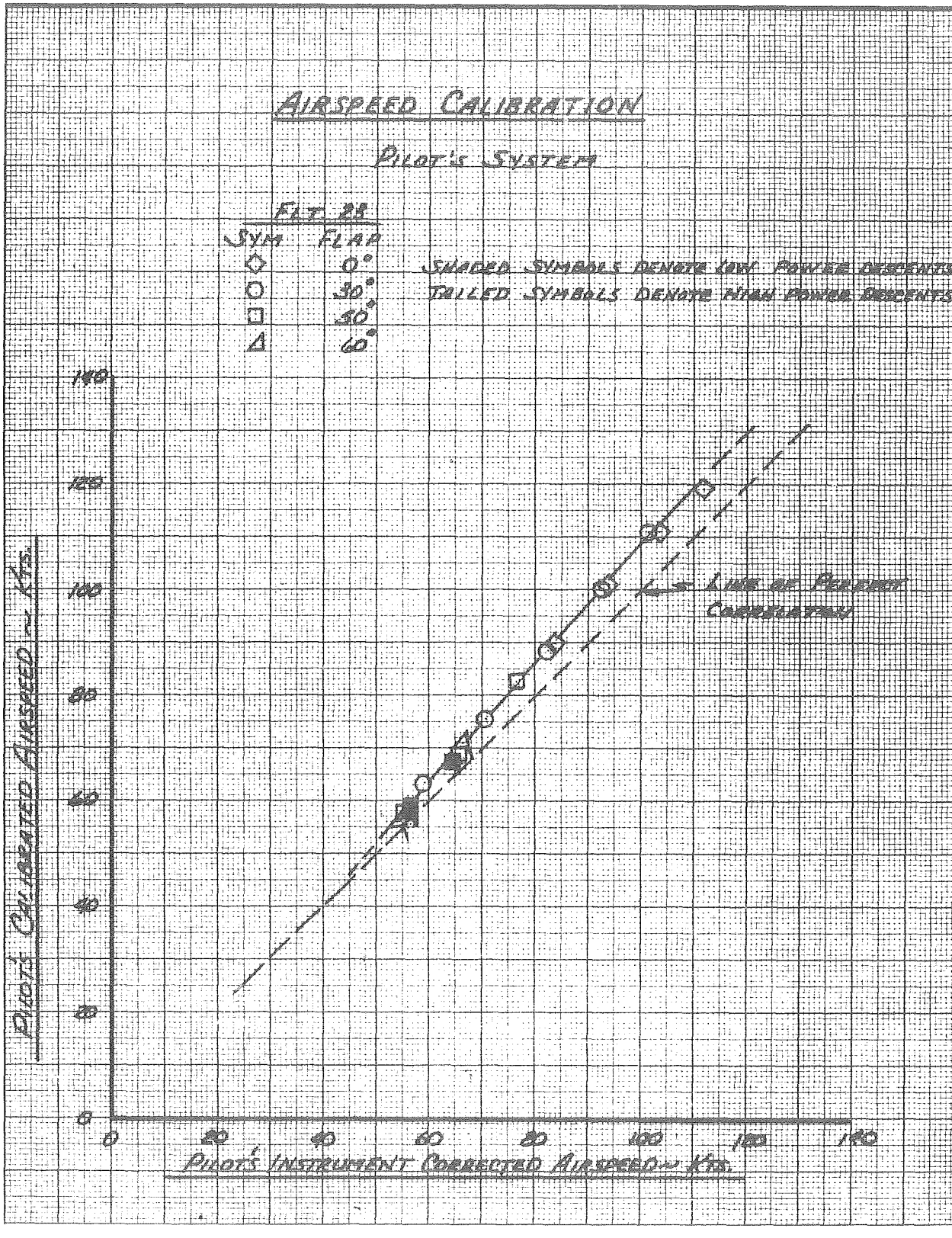
AIRSPEED CALIBRATION
PILOT'S SYSTEM
FLT. 25
SYM FLAP
0°
30°
30°
60°
SHADED SYMBOLS DENOTE LOW POWER DESCENTS
TRILED SYMBOLS DENOTE HIGH POWER DESCENTS
LINE OF PERFECT CORRELATION
PILOT'S CALIBRATED AIRSPEED - KTS.
PILOT'S INSTRUMENT CORRECTED AIRSPEED - KTS.
0
20
40
60
80
100
120
140

FIGURE 4

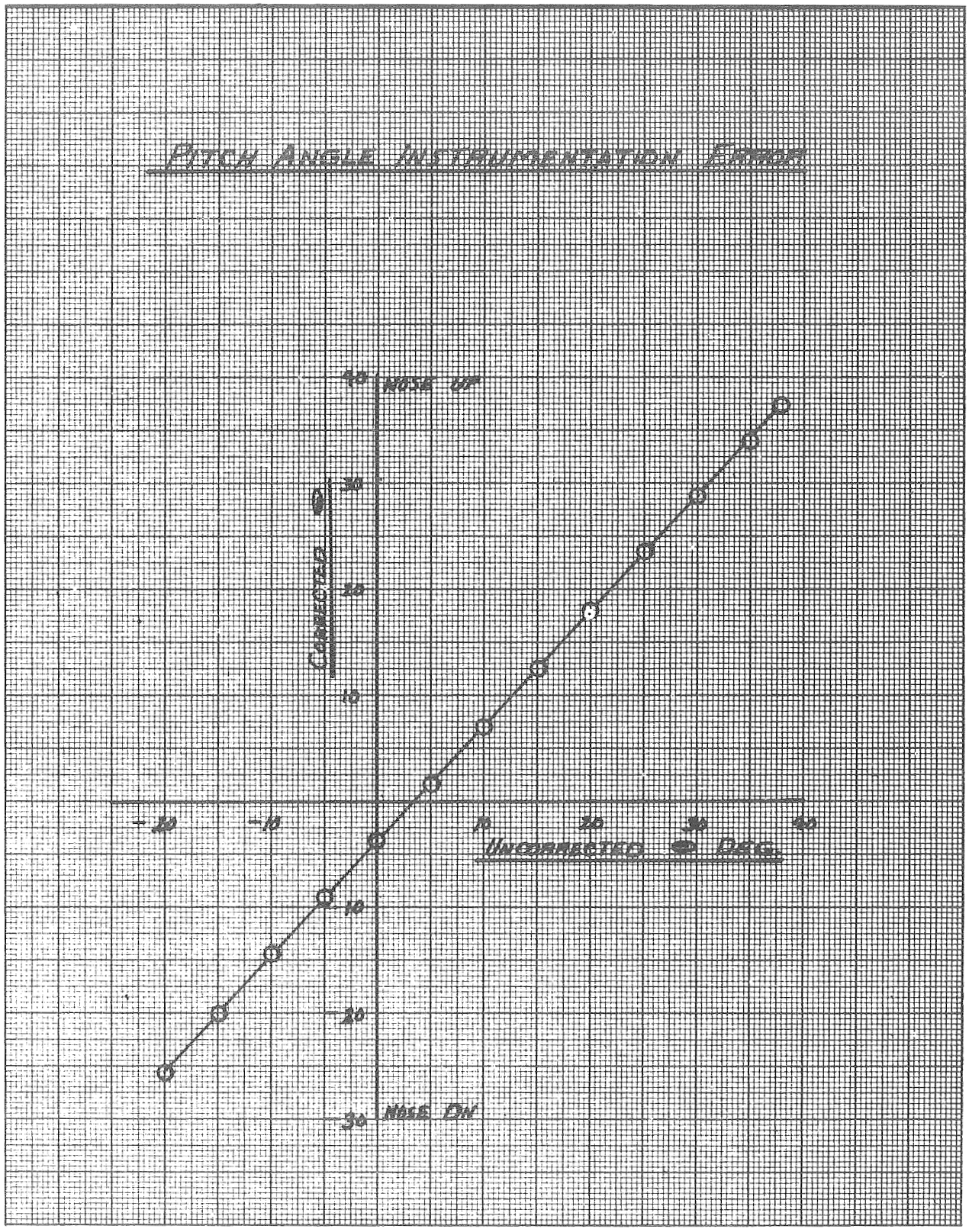
PITCH ANGLE INSTRUMENTATION ERROR
NOSE UP
NOSE DN
CORRECTED
UNCORRECTED
DEG.
40
30
20
10
-10
-20
-30

FIGURE 5a

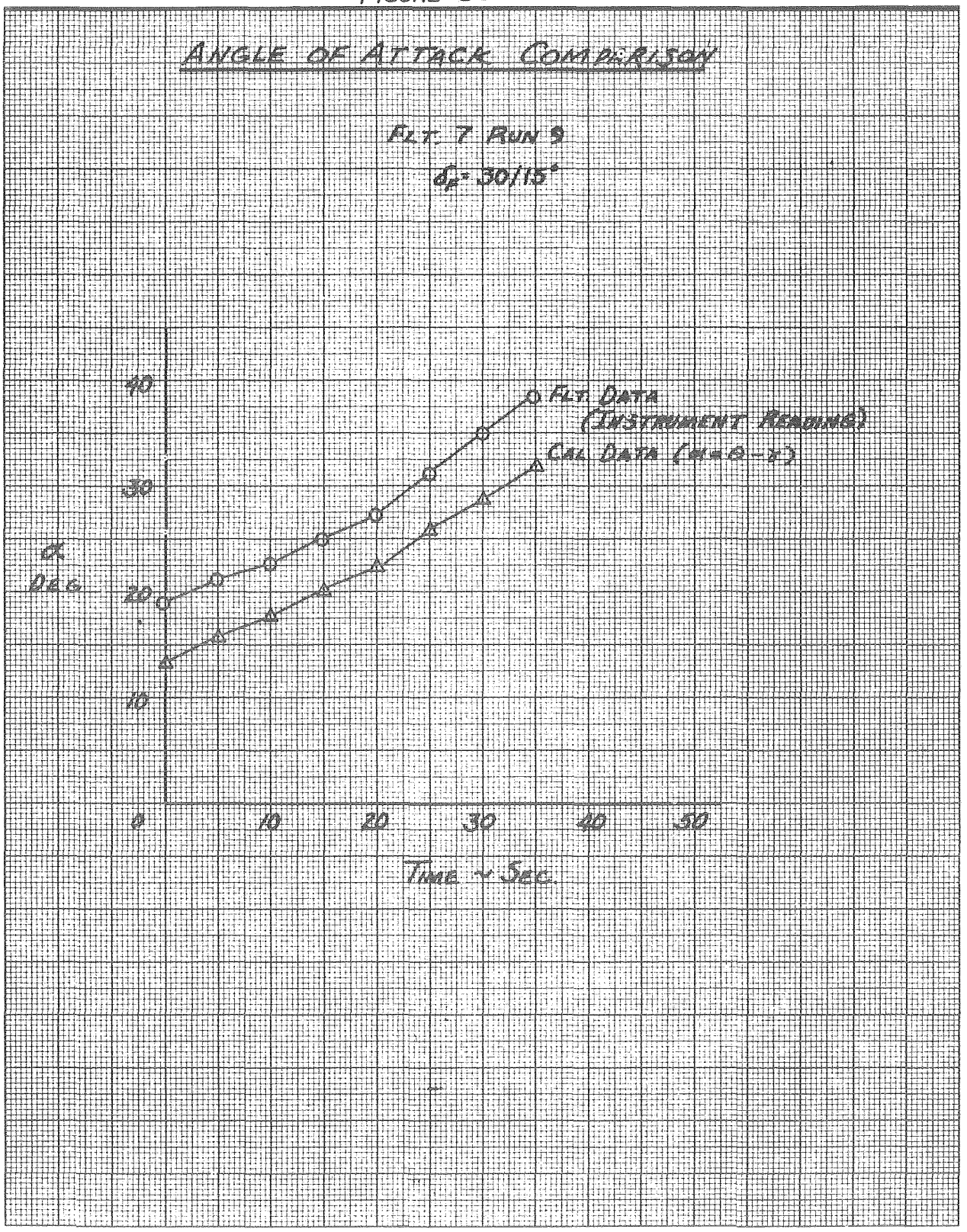
ANGLE OF ATTACK COMPARISON
FLT. 7 RUN 9
δ_e = 30/15°
40
30
20
10
0
α
DEG.
FLT. DATA
(INSTRUMENT READING)
CAL. DATA ($\alpha = \theta - \gamma$)
0
10
20
30
40
50
TIME ~ SEC.

FIGURE 5b

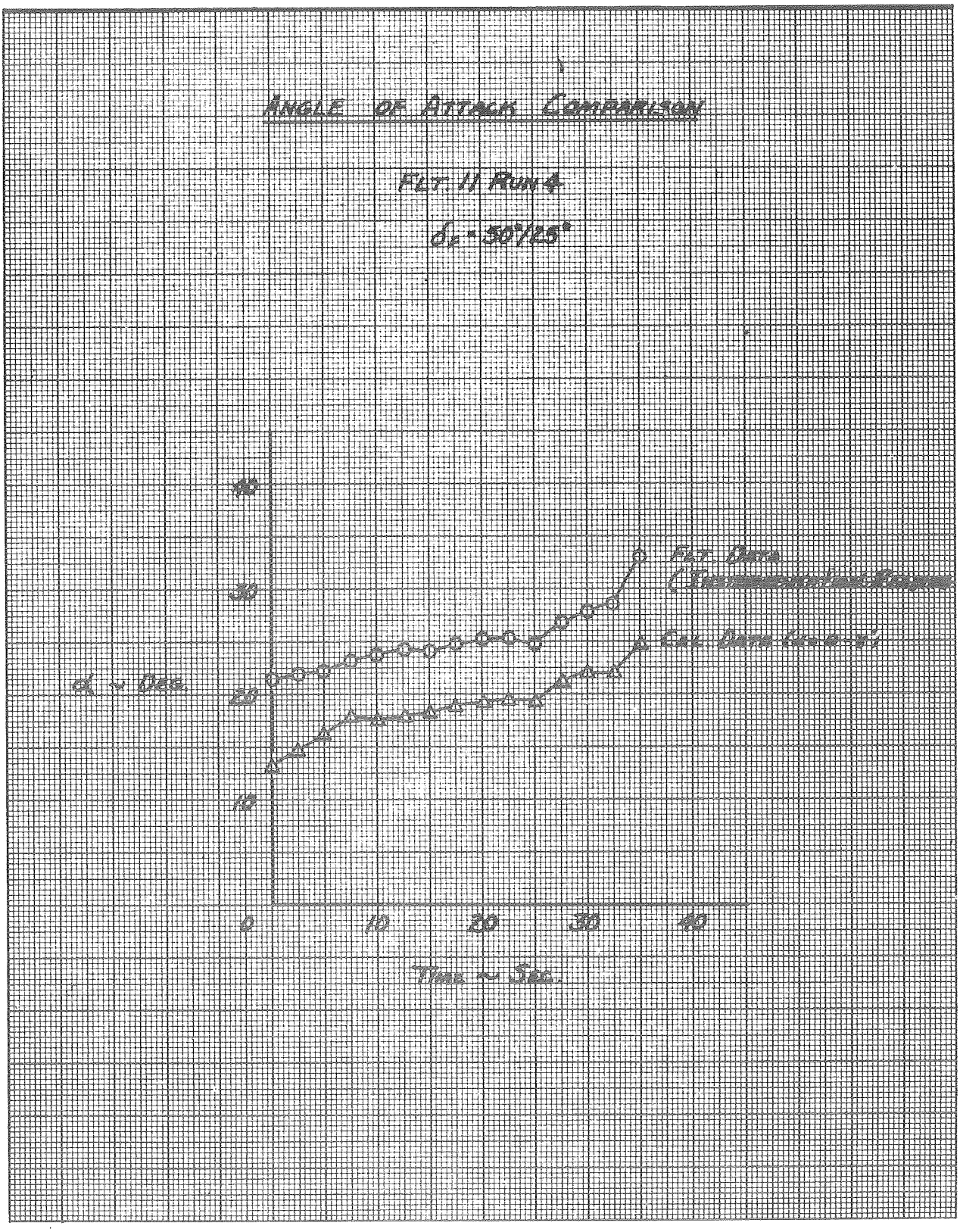
ANGLE OF ATTACK COMPARISON
FLT. 11 RUN 4
δ_E = 50°/25°
40
30
20
10
0
α ~ DEG.
FLT. DATA
CAL. DATA (W.B. G-E)
0
10
20
30
40
TIME ~ SEC.

FIGURE 6

HORIZONTAL TAIL LOCAL ANGLE MEASUREMENT

AMES TEST 388

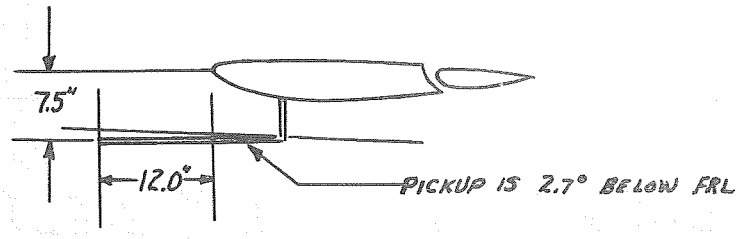

FLIGHT DATA

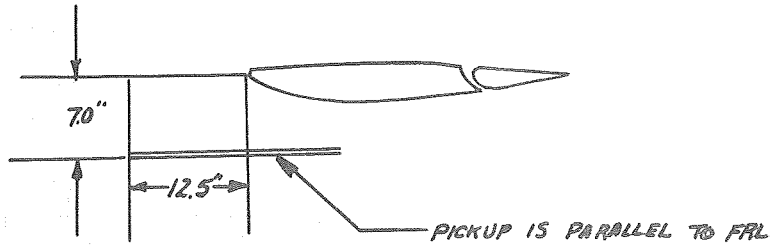

FIGURE 7

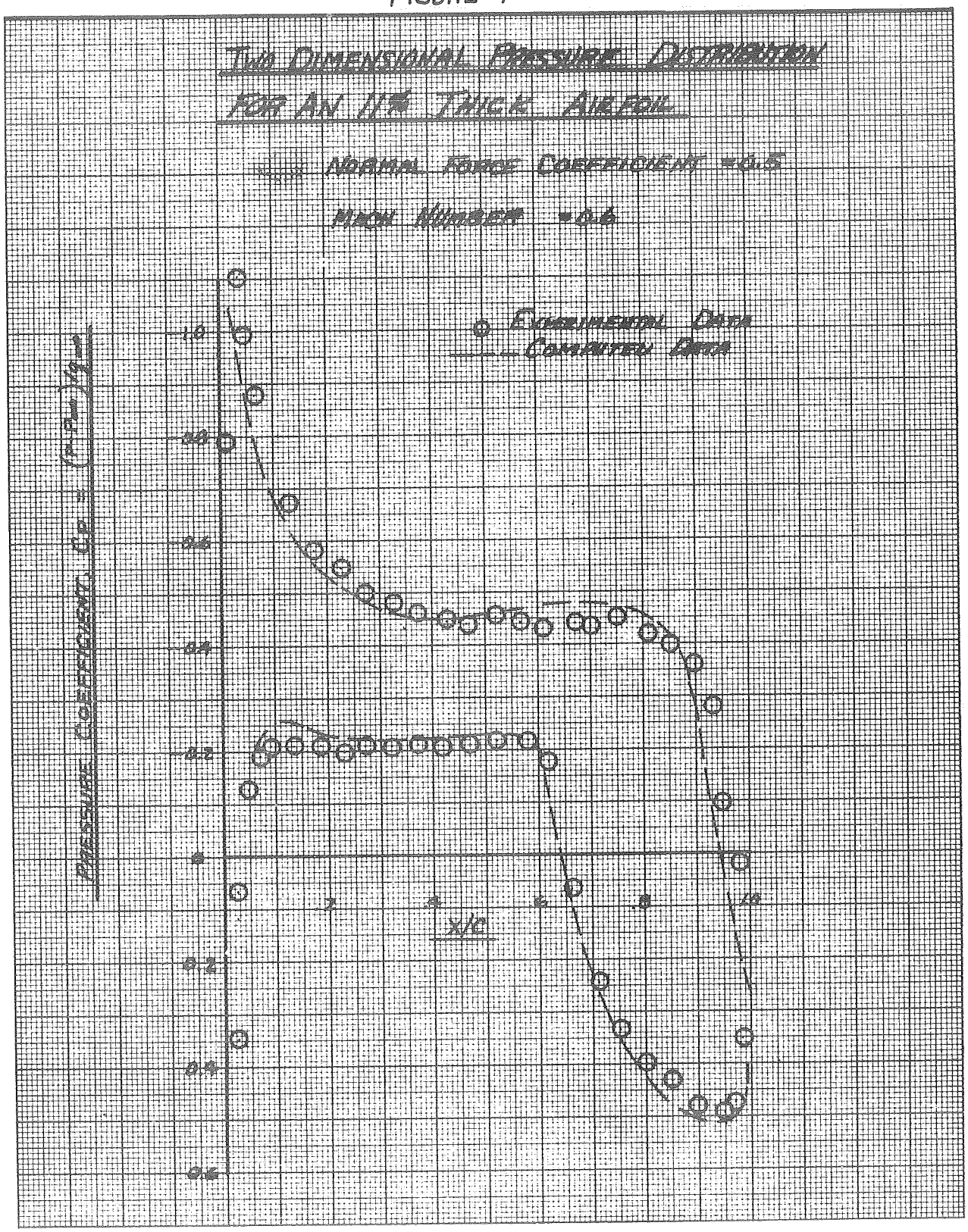
TWO DIMENSIONAL PRESSURE DISTRIBUTION
FOR AN 11% THICK AIRFOIL
NORMAL FORCE COEFFICIENT = 0.5
MACH NUMBER = 0.6
EXPERIMENTAL DATA
COMPUTED DATA
PRESSURE COEFFICIENT, Cp
x/c
1.0
0.8
0.6
0.4
0.2
0
0.2
0.4
0.6
0.8
1.0

FIGURE 8

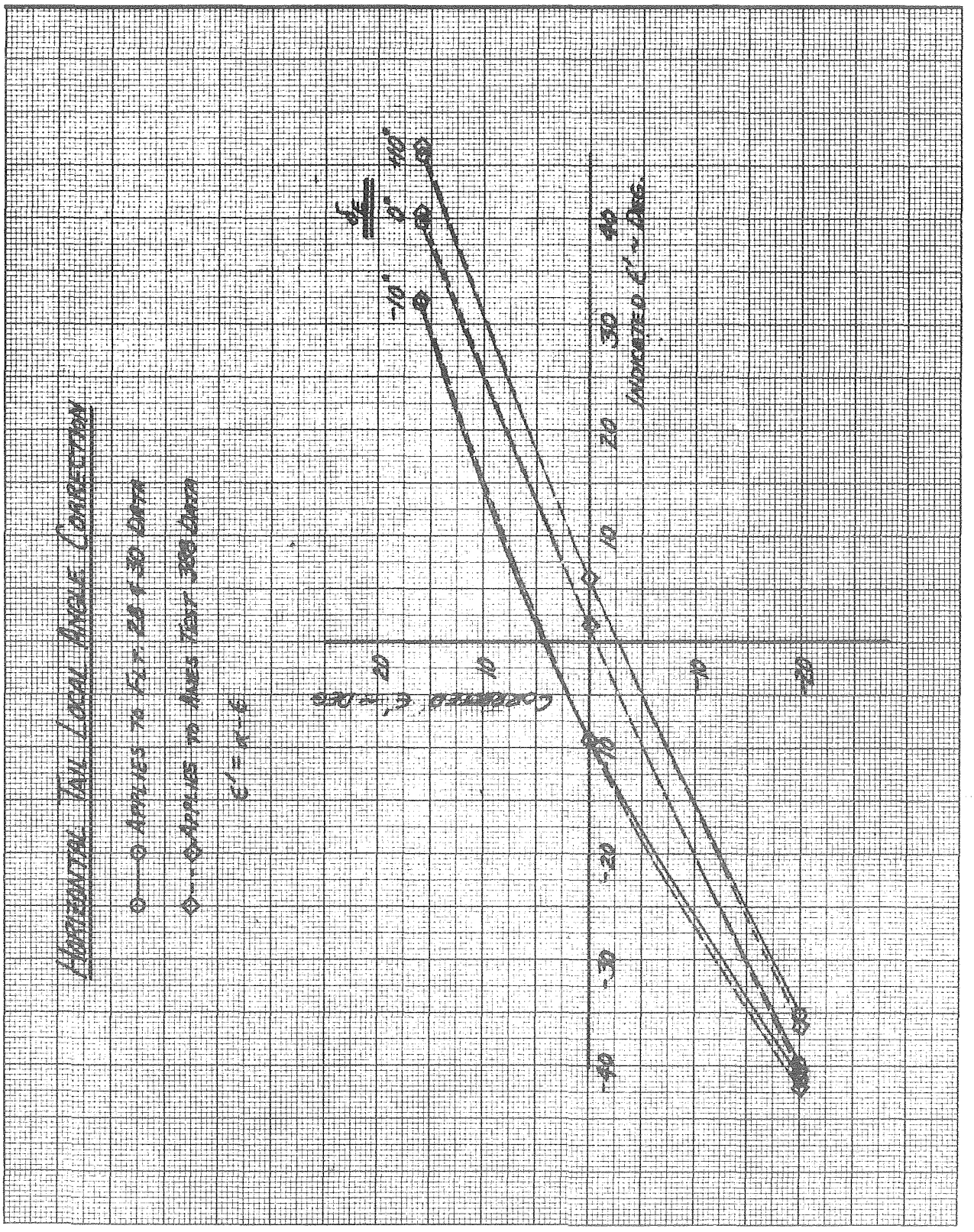
HORIZONTAL TAIL LOCAL ANGLE CORRECTION
Applies to $i_{H.T.}$ = 25 & 30 Data
Applies to Alpha Test 308 Data
$\epsilon' = K\alpha$
Corrected ϵ', Deg.
Indicated ϵ', Deg.
40
30
20
10
0
-10
-20
-30
-40
+10°
0°
-10°

FIGURE 9

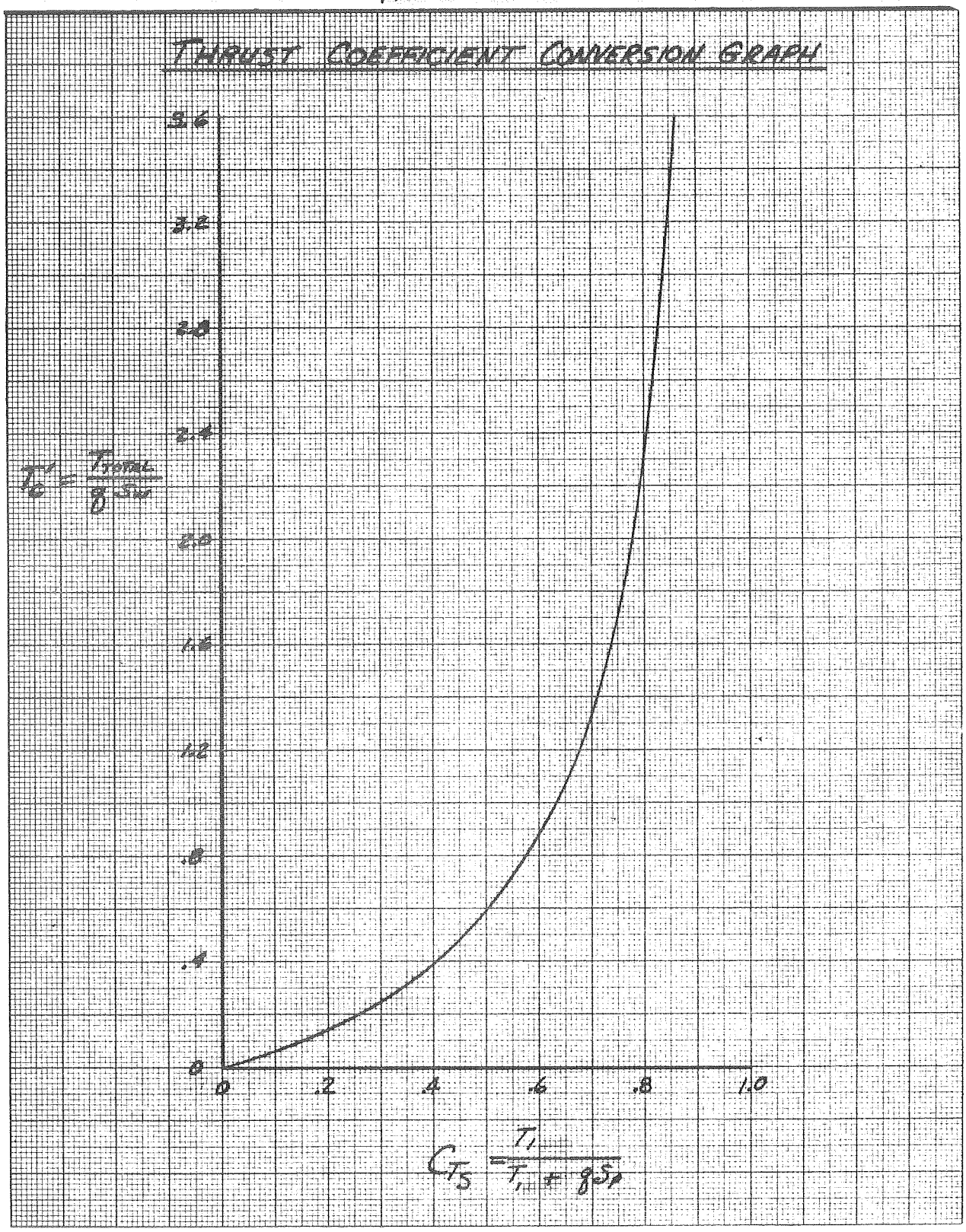
THRUST COEFFICIENT CONVERSION GRAPH
3.6
3.2
2.8
2.4
2.0
1.6
1.2
.8
.4
0
$T_c' = \frac{T_{TOTAL}}{\rho S_p}$
0
.2
.4
.6
.8
1.0
$C_{T_S} = \frac{T_{I_{max}}}{T_{I_{max}} + \rho S_p}$

FIGURE 102

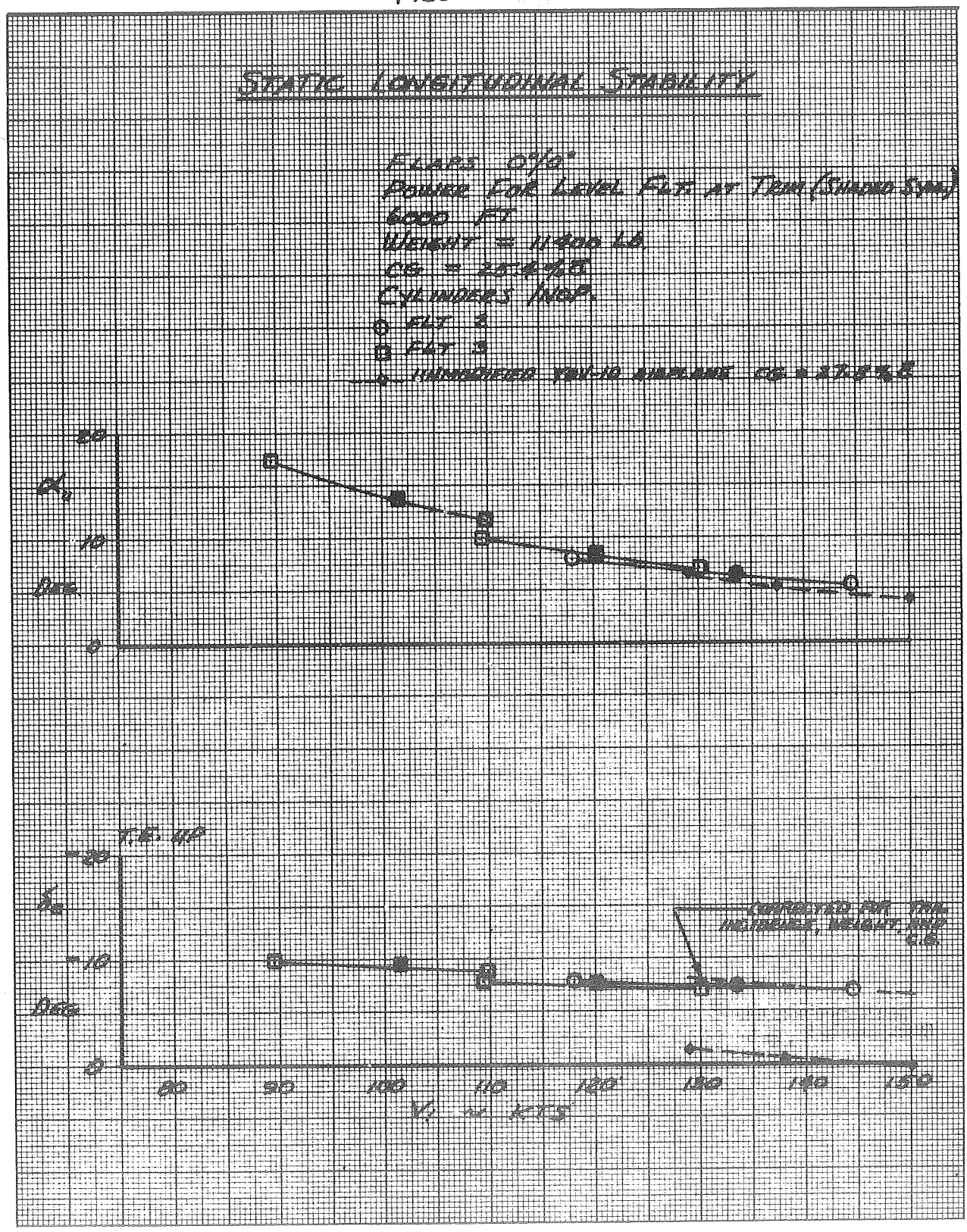
STATIC LONGITUDINAL STABILITY
FLAPS 0°/0°
POWER FOR LEVEL FLT AT TEST (SWEPT SYM)
6000 FT
WEIGHT = 11,400 LB
CG = 25.4 %E
CYLINDERS INOP.
FLT 2
FLT 3
HUMPHREYS TEST-10 AIRPLANE CG = 27.6 %E
20
10
0
DEG
-20
-10
0
T.E. UP
DEG
60
90
100
110
120
130
140
150
V_I = K-I.S.

FIGURE 10b

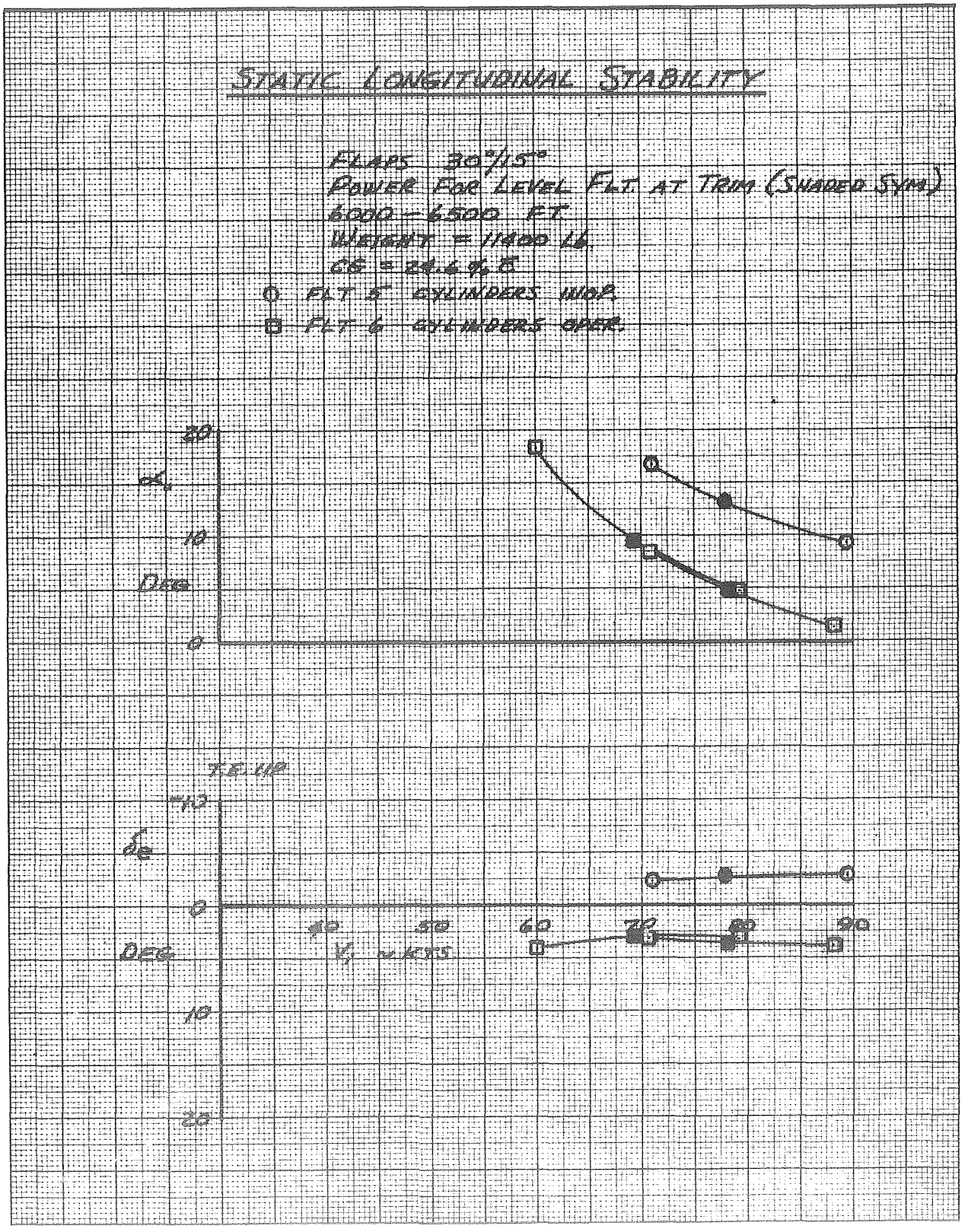
STATIC LONGITUDINAL STABILITY
FLAPS 30°/15°
POWER FOR LEVEL FLT. AT TRIM (SHADED SYM.)
6000 – 6500 FT.
WEIGHT = 11400 LB.
CG = 24.6 % c̄
FLT 5 CYLINDERS INOP.
FLT 6 CYLINDERS OPER.
20
10
DEG
0
T.E. UP
T.E. DN
0
10
20
40
50
60
70
80
90
V_I ~ KTS

FIGURE 10 C

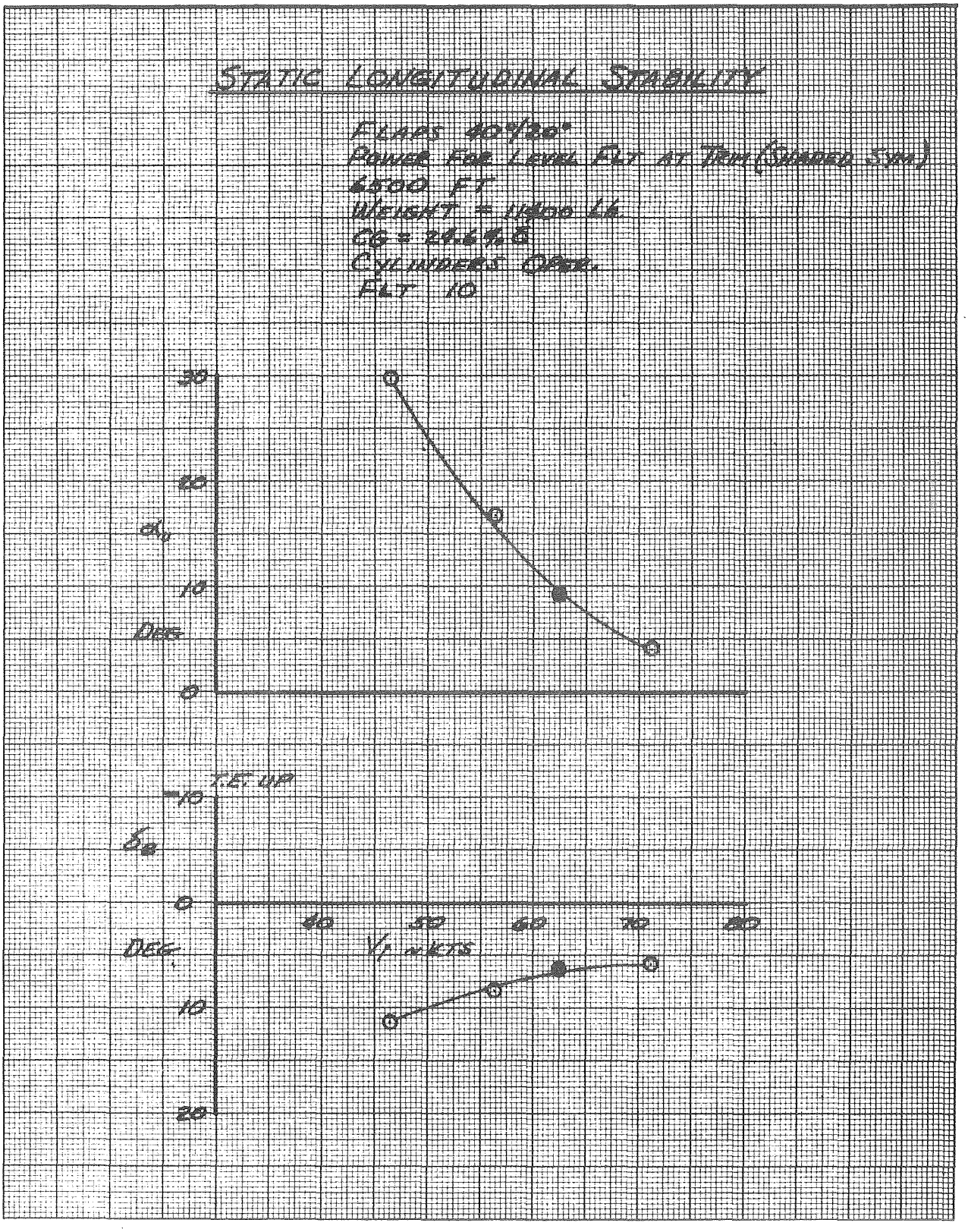
STATIC LONGITUDINAL STABILITY
FLAPS 40°/20°
POWER FOR LEVEL FLT AT TERM (SHADED SYM)
4500 FT
WEIGHT = 11000 LB.
CG = 24.6 %C̄
CYLINDERS OPER.
FLT 10
30
20
α_b
10
DEG
0
T.E. UP
-10
δ_e
0
40
50
60
70
80
V_i KTS
DEG.
10
20

FIGURE 10d

STATIC LONGITUDINAL STABILITY

FLAPS 50°/25°
POWER FOR LEVEL FLT. AT TRIM (SHADED SYM)
6500 FT
WEIGHT = 11400 LB.
CG = 24.6 % C
CYLINDERS OPERATING
FLT 11

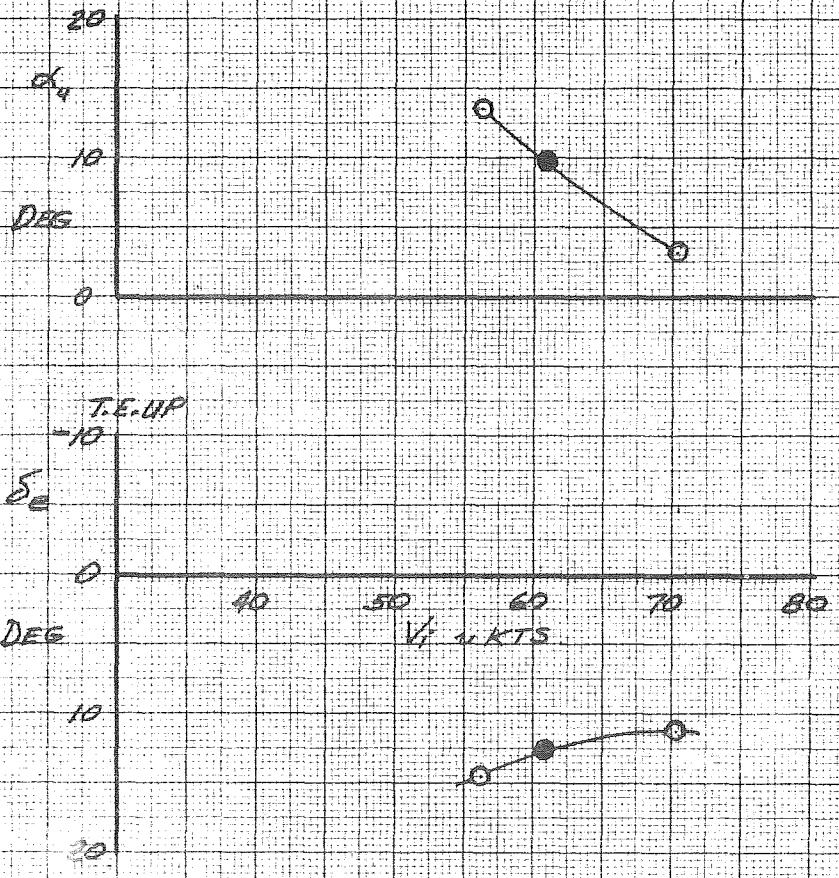

FIGURE 10a

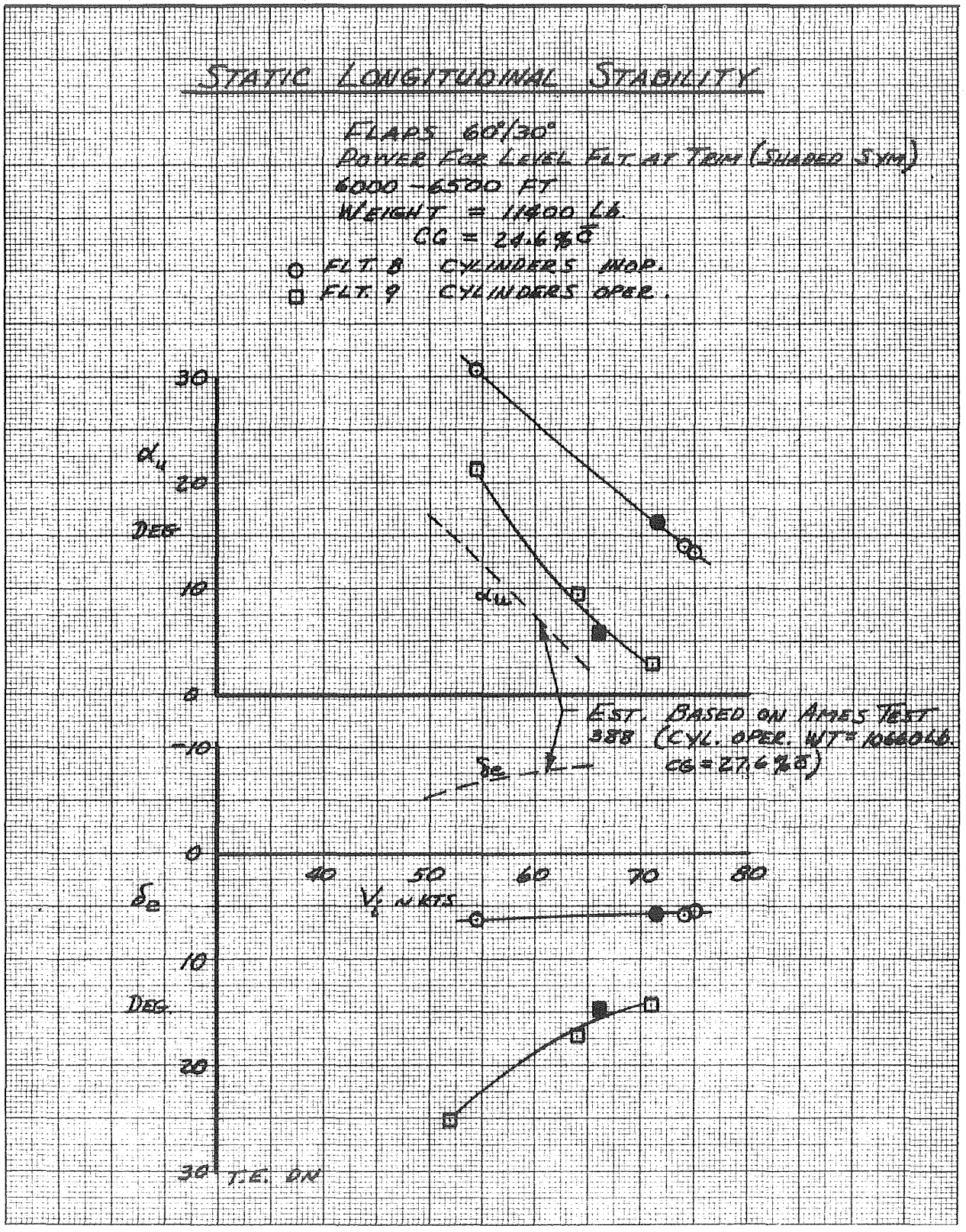
STATIC LONGITUDINAL STABILITY
FLAPS 60°/30°
POWER FOR LEVEL FLT. AT TRIM (SHADED SYM.)
6000 - 6500 FT
WEIGHT = 11400 LB.
CG = 24.6 %c̄
FLT. 8 CYLINDERS INOP.
FLT. 9 CYLINDERS OPER.
30
20
10
0
-10
α_4
DEG
α_w
EST. BASED ON AMES TEST 388 (CYL. OPER. WT = 10680 LB. CG = 27.6 %c̄)
δ_e
i_t
40
50
60
70
80
V_i KTS
δ_e
DEG.
10
20
30
T.E. DN

FIGURE 10 F

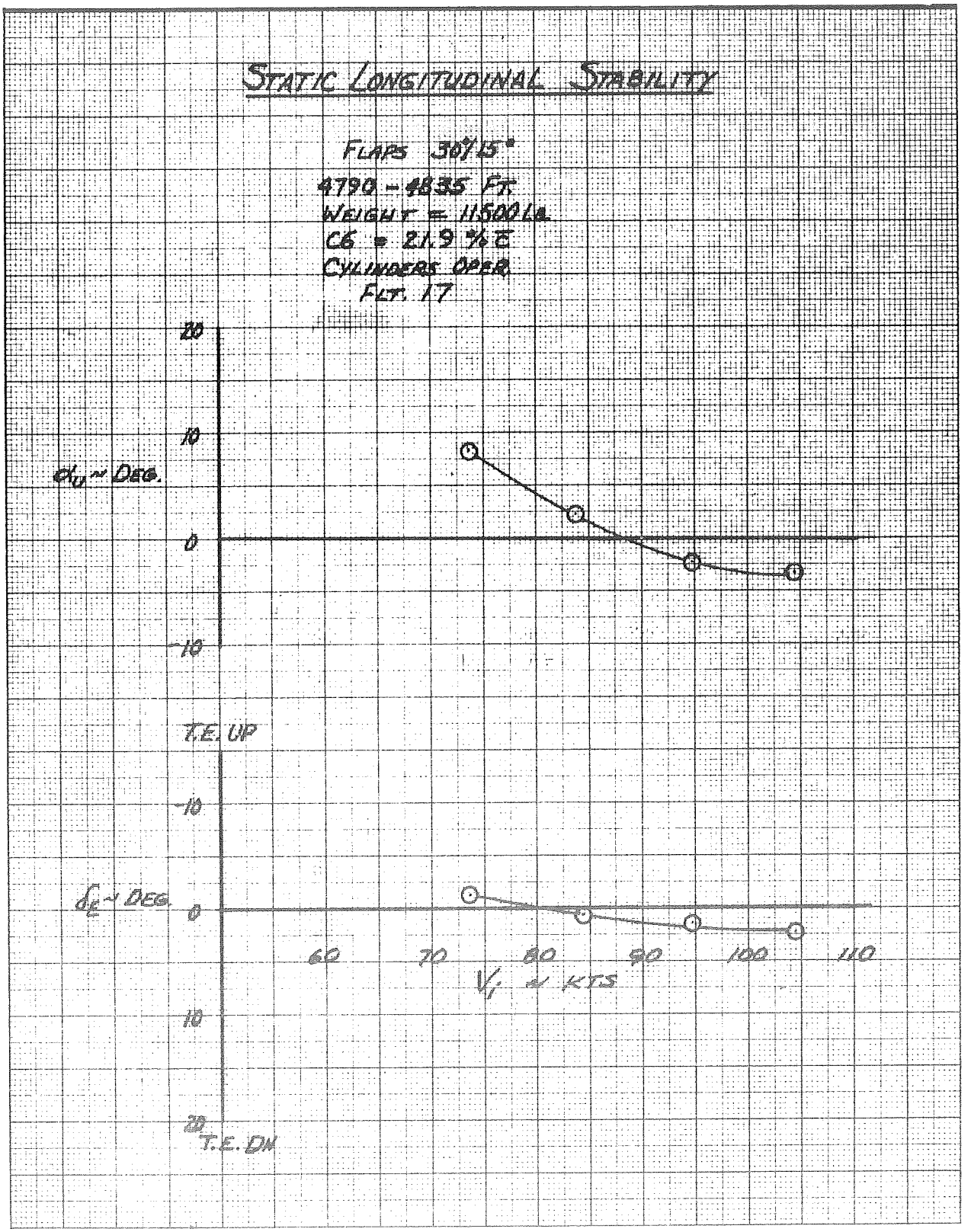
STATIC LONGITUDINAL STABILITY
FLAPS 30°/15°
4790 - 4835 FT.
WEIGHT = 11500 LB.
CG = 21.9 % C̄
CYLINDERS OPEB.
FLT. 17
20
10
0
-10
α_{H} ~ DEG.
T.E. UP
-10
0
δ_E ~ DEG.
10
20
T.E. DN
60
70
80
90
100
110
V_i ~ KTS

FIGURE 10 G

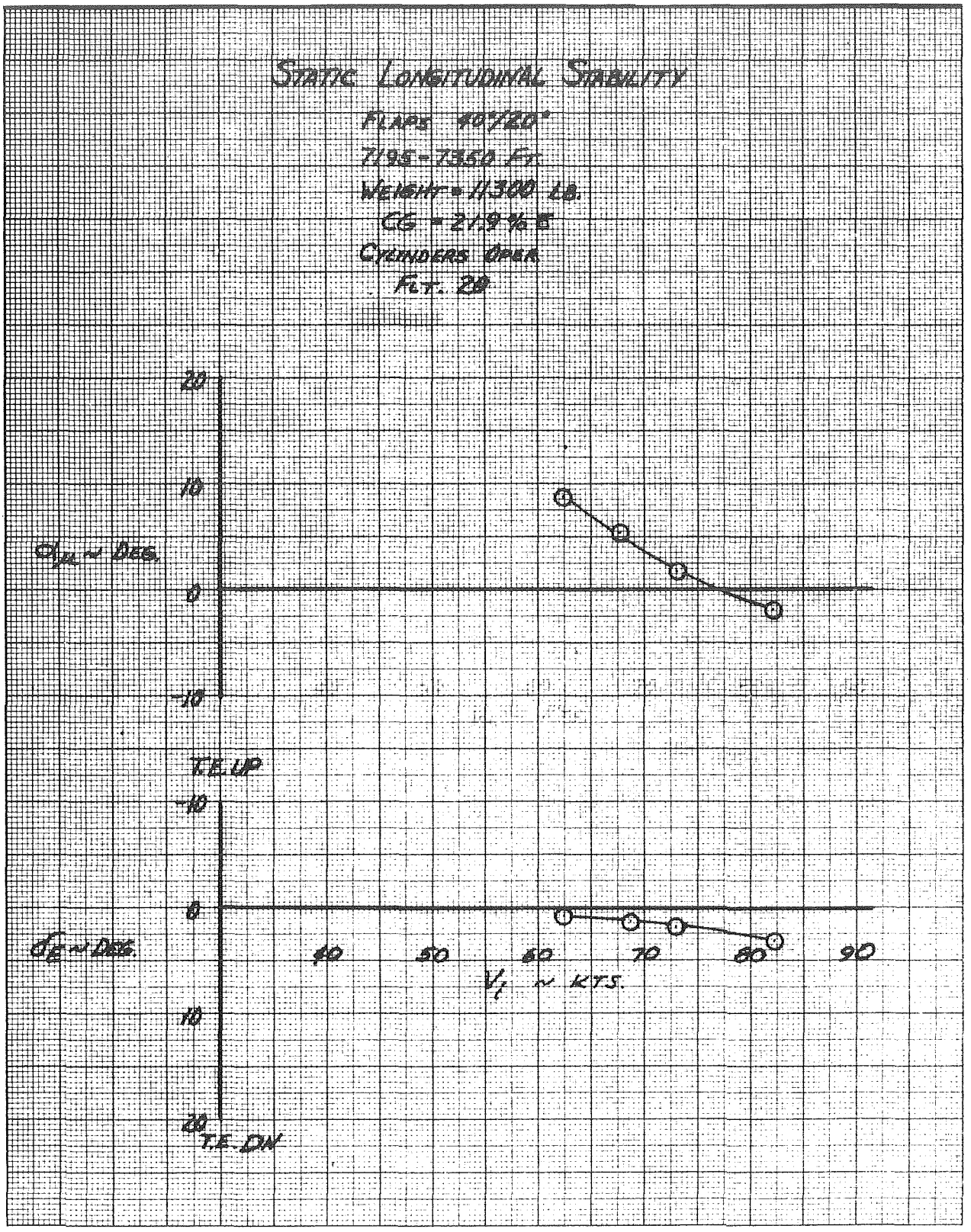
STATIC LONGITUDINAL STABILITY
FLAPS 40°/20°
7195 - 7350 FT.
WEIGHT = 11300 LB.
CG = 21.9 % E
CYLINDERS OPEN
ALT. 20
20
10
0
-10
α_{tu} ~ DEG.
T.E. UP
-10
0
δ_E ~ DEG.
10
20
T.E. DN
40
50
60
70
80
90
V_t ~ KTS.

FIGURE 10 h

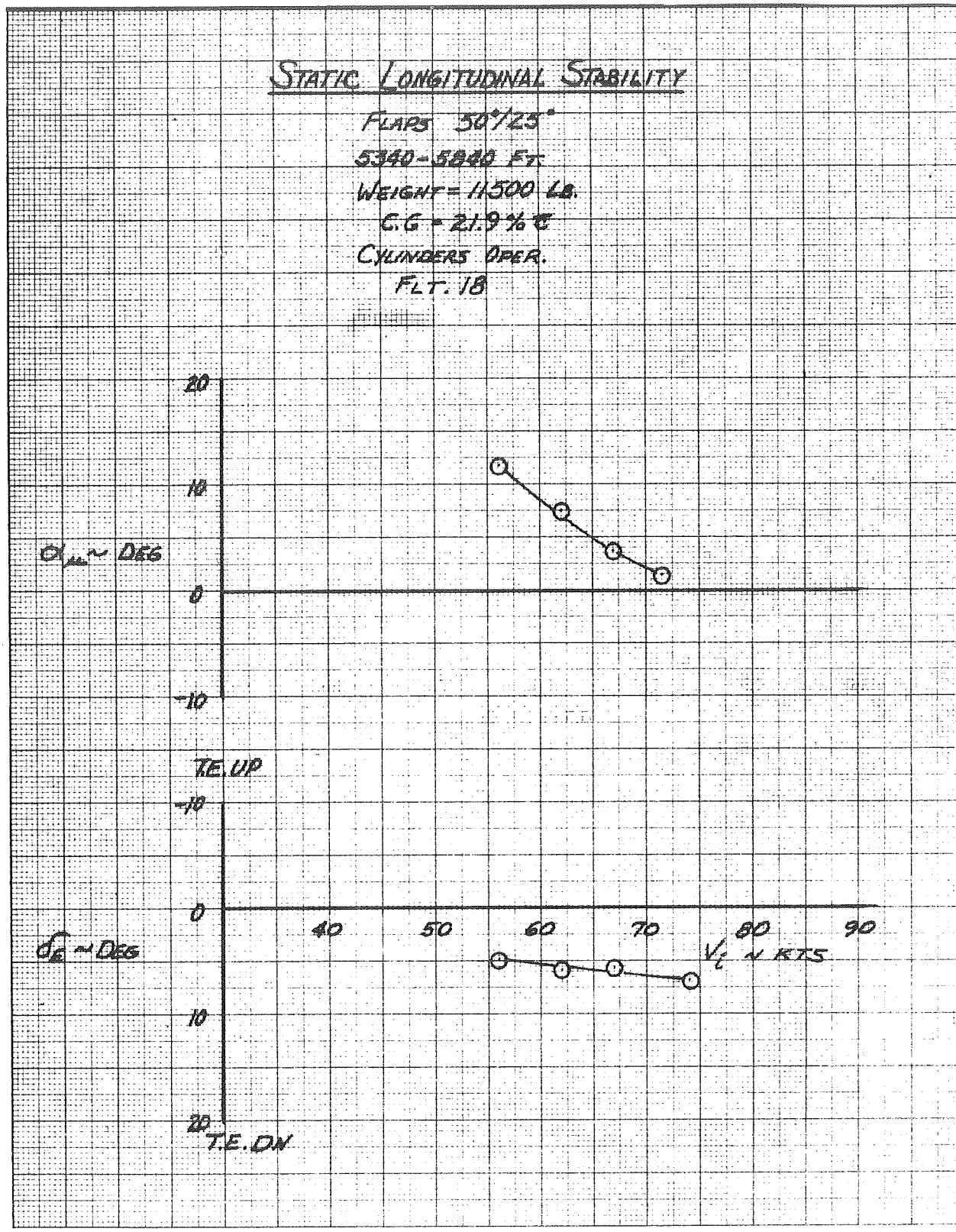
STATIC LONGITUDINAL STABILITY
FLAPS 50°/25°
5340 - 5840 FT
WEIGHT = 11500 LB.
C.G = 21.9 % C
CYLINDERS OPER.
FLT. 18
20
10
0
-10
α_{fus} ~ DEG
T.E. UP
-10
0
10
20
T.E. DN
δ_E ~ DEG
40
50
60
70
80
90
V_i ~ KTS

FIGURE 10 i

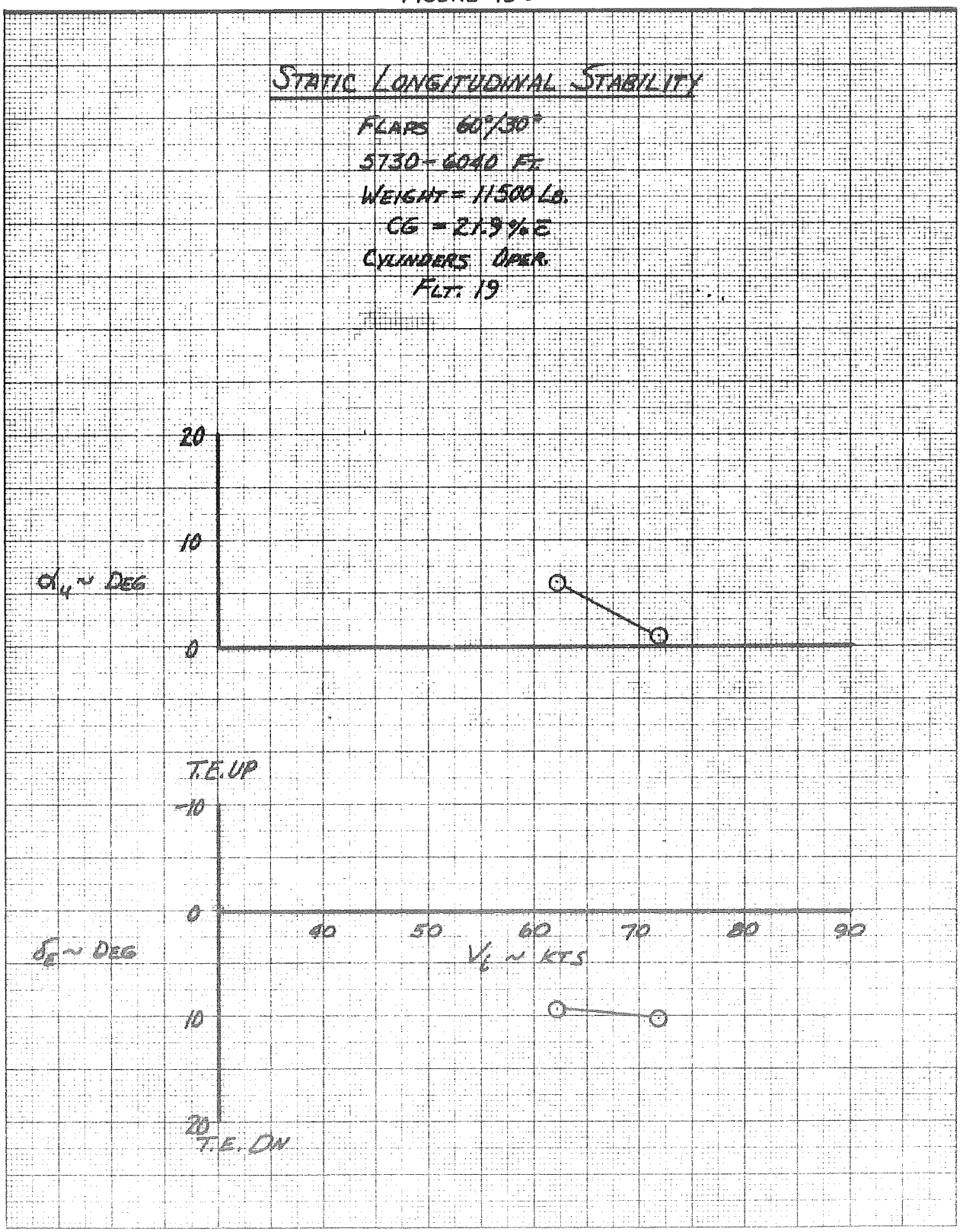
STATIC LONGITUDINAL STABILITY
FLAPS 60°/30°
5730 - 6040 FT.
WEIGHT = 11500 LB.
CG = 21.9 % E
CYLINDERS OPER.
FLT. 19
20
10
0
α_4 ~ DEG
T.E. UP
-10
0
40
50
60
70
80
90
V_t ~ KTS
δ_E ~ DEG
10
20
T.E. DN

FIGURE 11 a

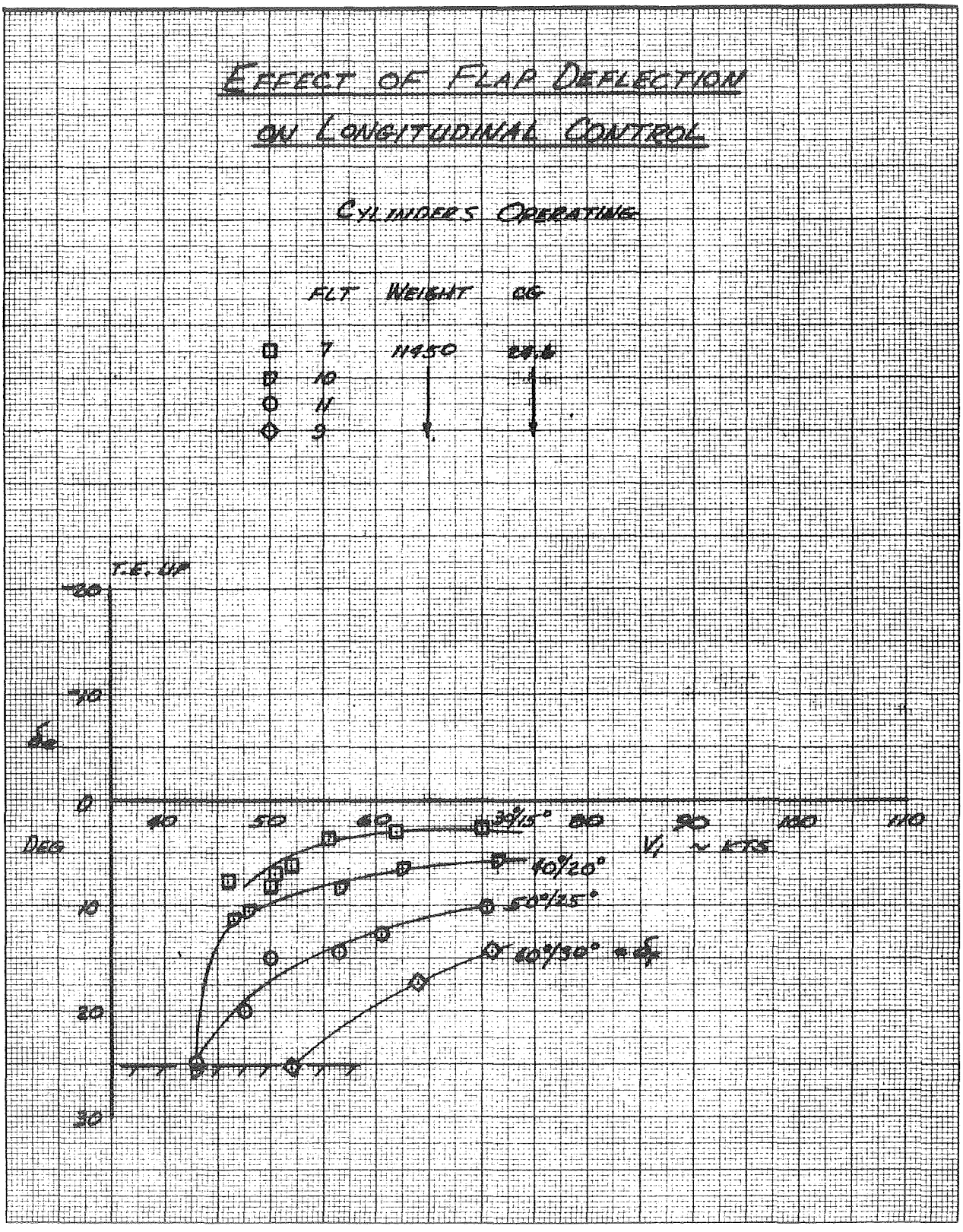
EFFECT OF FLAP DEFLECTION
ON LONGITUDINAL CONTROL
CYLINDERS OPERATING
FLT
WEIGHT
CG
7
10
11
9
11450
28.6
T.E. UP
-20
-10
δe
0
10
20
30
DEG
40
50
60
30°/15°
40°/20°
50°/25°
60°/30° = δf
80
90
100
110
V ~ KTS

FIGURE-11b

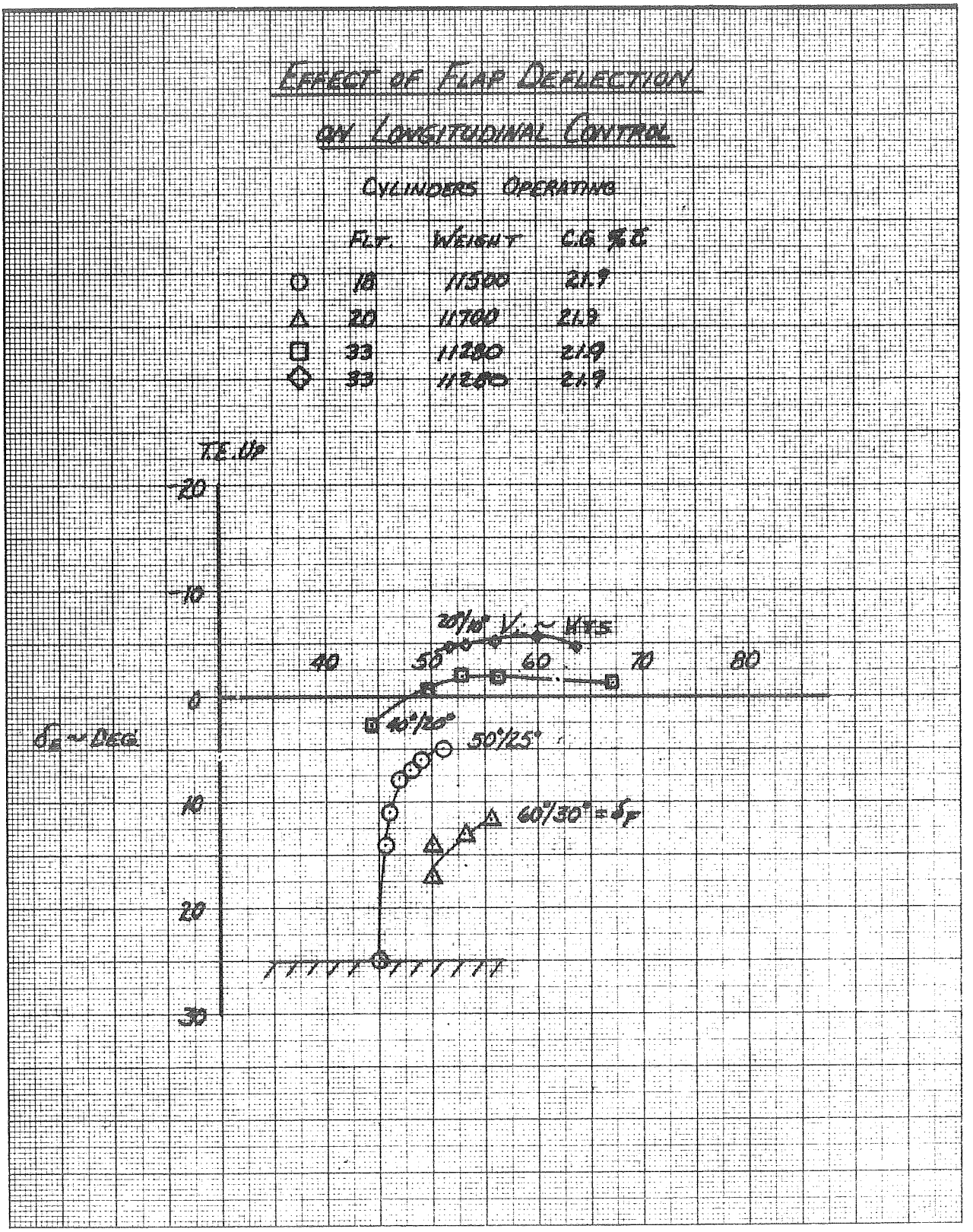
EFFECT OF FLAP DEFLECTION
ON LONGITUDINAL CONTROL
CYLINDERS OPERATING
FLT. WEIGHT C.G. %C
18 11500 21.9
20 11700 21.9
33 11280 21.9
33 11280 21.9
T.E. UP
-20
-10
0
10
20
30
40
50
60
70
80
20°/18° V. ~ KTS
40°/20°
50°/25°
60°/30° = δF
δE ~ DEG.

FIGURE 12

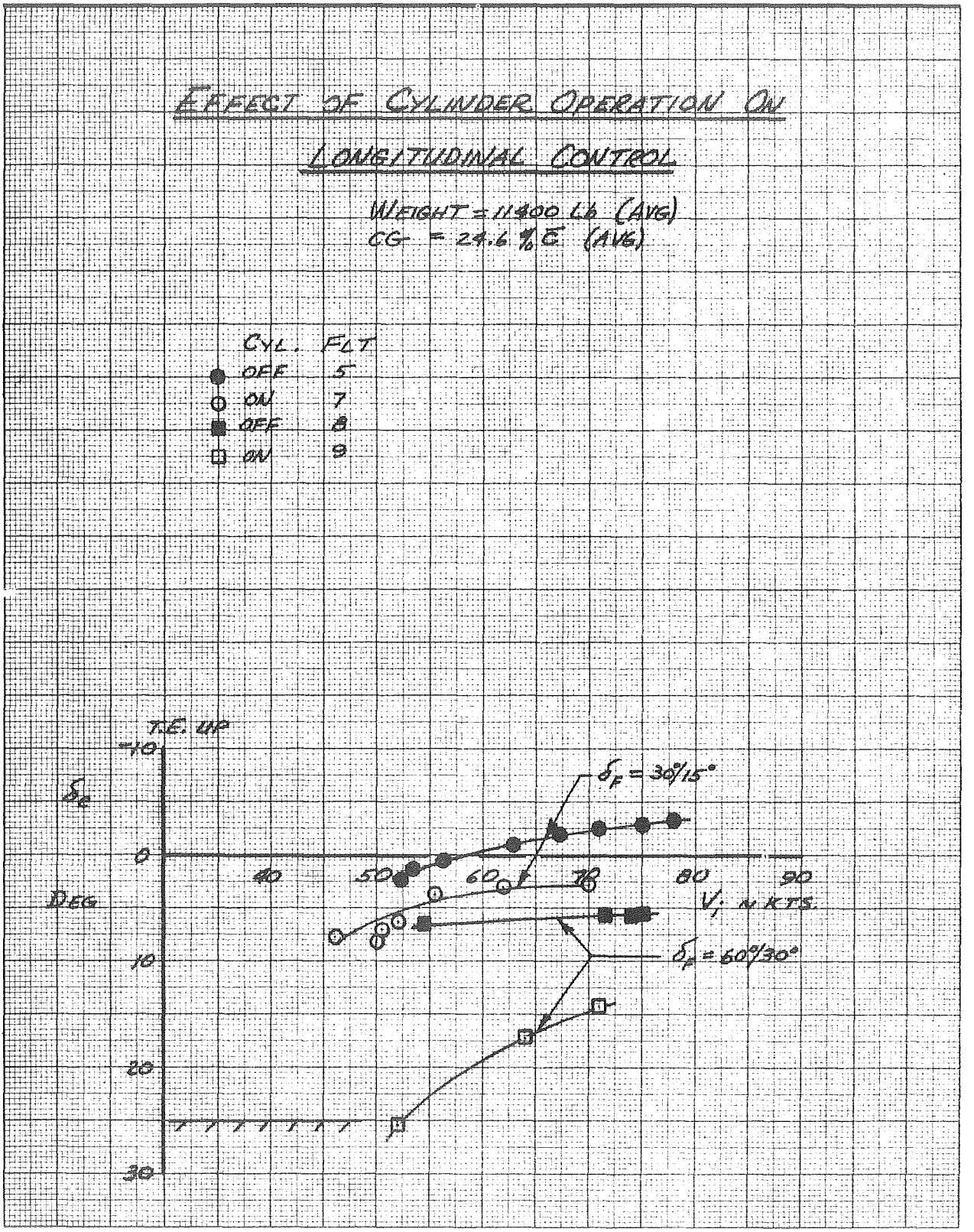
EFFECT OF CYLINDER OPERATION ON
LONGITUDINAL CONTROL
WEIGHT = 11400 Lb (AVG)
CG = 24.6 % C̄ (AVG)
CYL. FLT
OFF 5
ON 7
OFF 8
ON 9
T.E. UP
-10
0
10
20
30
δ_e
DEG
40
50
60
70
80
90
V_i KTS.
$\delta_F = 30°/15°$
$\delta_F = 60°/30°$

FIGURE 132

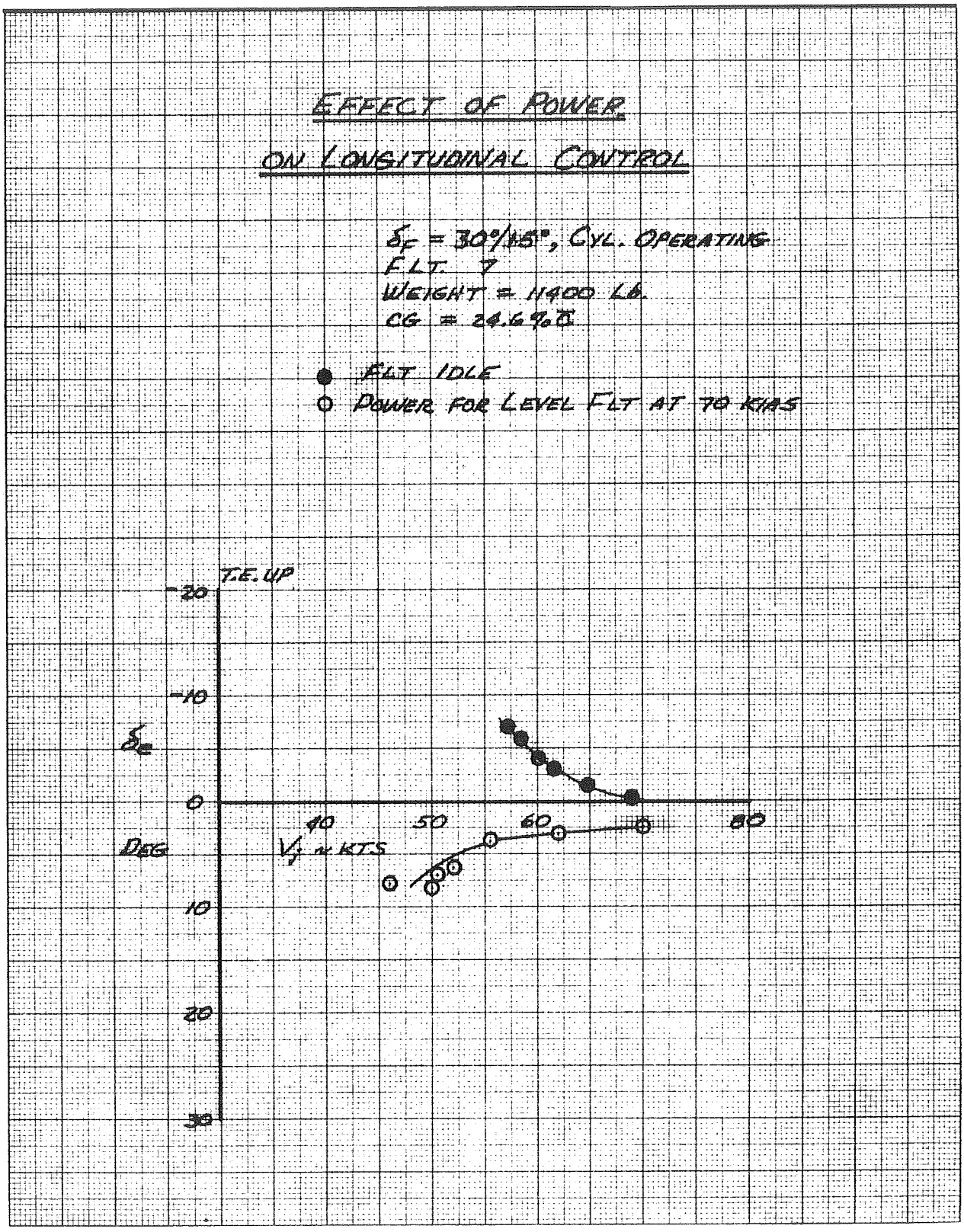
EFFECT OF POWER
ON LONGITUDINAL CONTROL
δ_F = 30°/15°, CYL. OPERATING
FLT. 7
WEIGHT = 11400 LB.
CG = 24.6 %$\bar{c}$
FLT IDLE
POWER FOR LEVEL FLT AT 70 KIAS
T.E. UP
-20
-10
0
10
20
30
δ_e
DEG
40
50
60
80
V_i IN KTS

FIGURE 13b

EFFECT OF POWER ON LONGITUDINAL CONTROL

δ_F = 40°/20° CYL OPER.
FLT. 33
WEIGHT = 11280 LB
CG = 21.9 %$\bar{c}$

○ POWER FOR 700 FT/MIN DESCENT AT V_i = 70 KTS
□ POWER FOR LEVEL FLIGHT AT V_i = 65 KTS

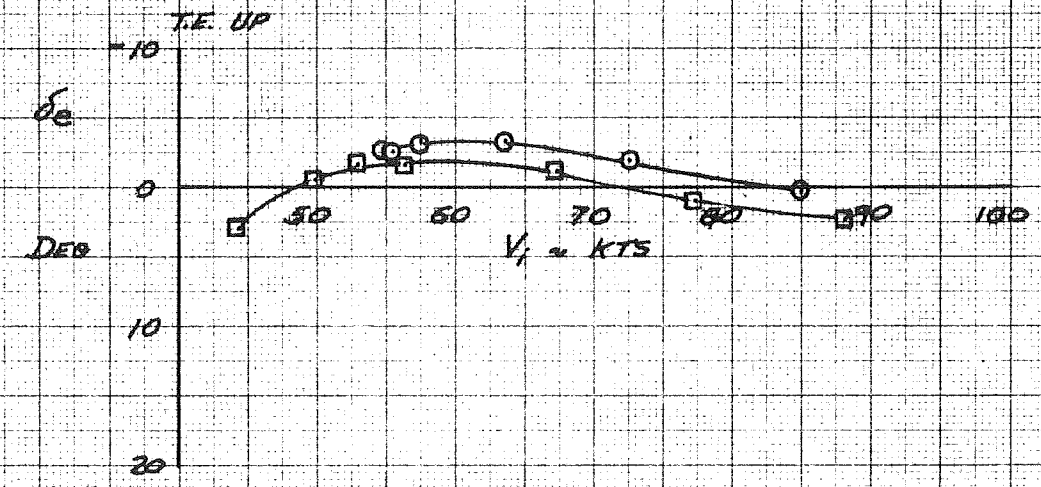

FIGURE 14a

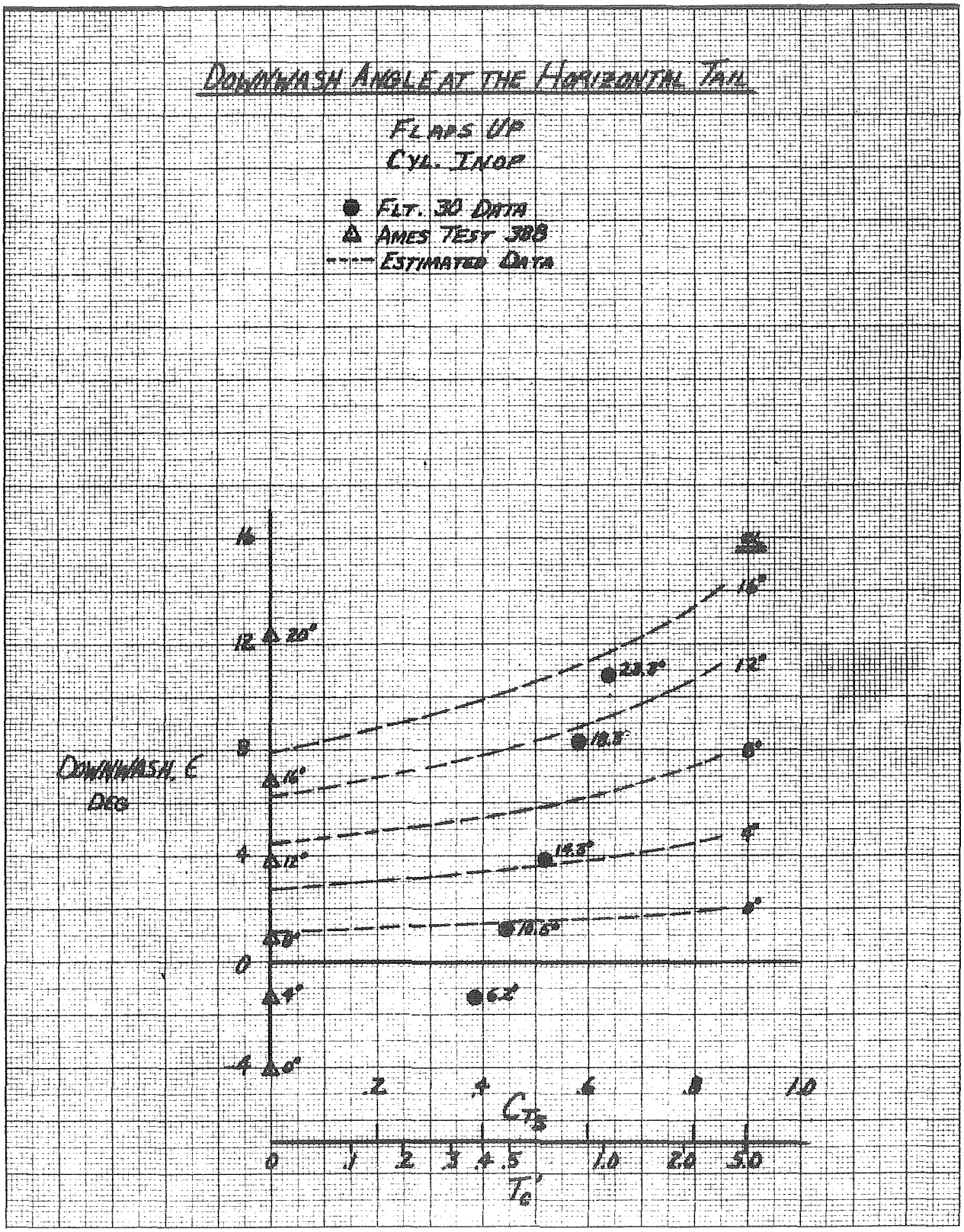
DOWNWASH ANGLE AT THE HORIZONTAL TAIL
FLAPS UP
CYL. INOP
FLT. 30 DATA
AMES TEST 388
ESTIMATED DATA
DOWNWASH, ε DEG
16
12
8
4
0
-4
20°
16°
12°
8°
4°
0°
-4°
28.3°
18.3°
14.3°
10.5°
6.2°
.2
.4
.6
.8
1.0
C_{T_S}
0
.1
.2
.3
.4
.5
1.0
2.0
5.0
T_c'

FIGURE 14 b

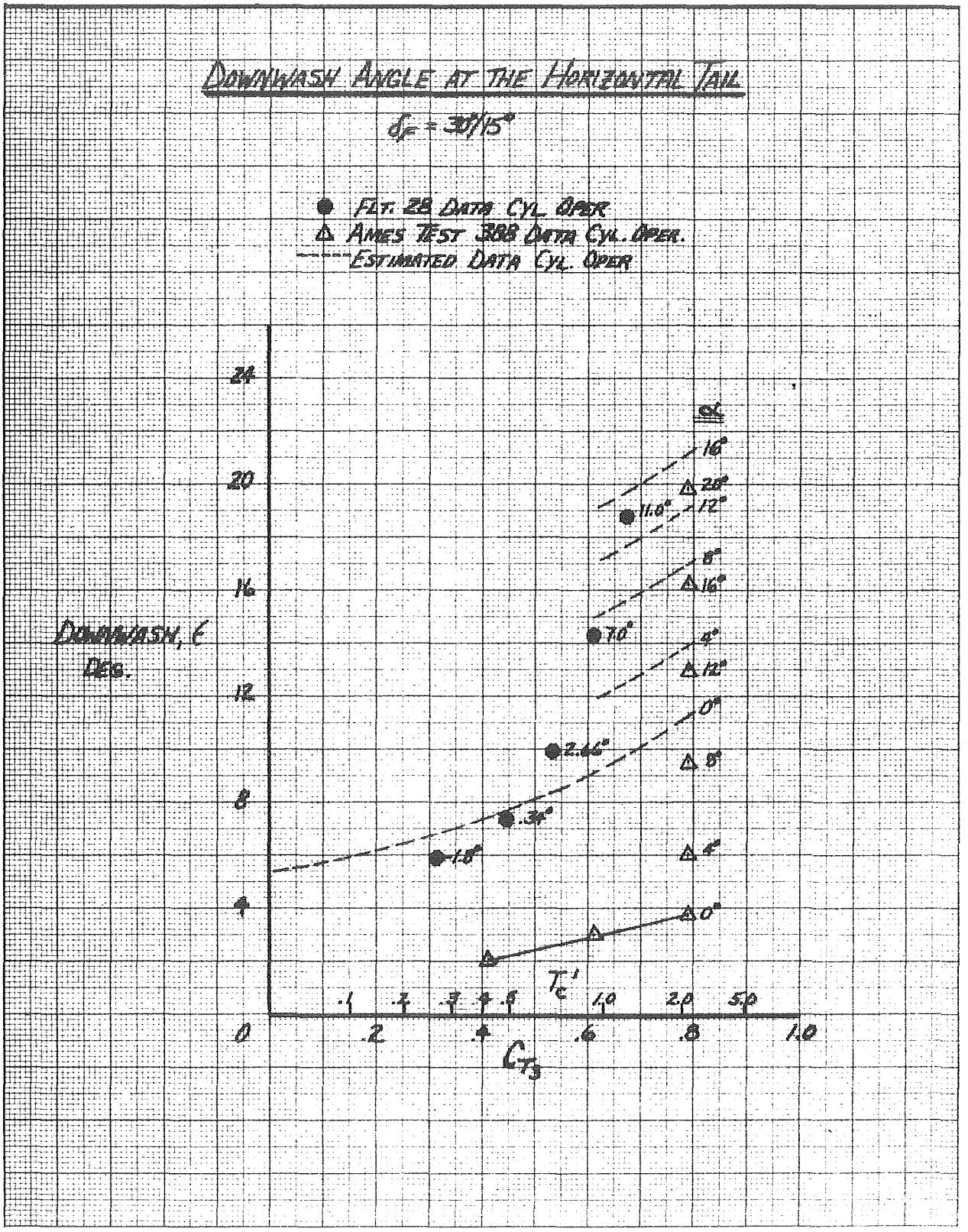
DOWNWASH ANGLE AT THE HORIZONTAL TAIL
δ_F = 30°/15°
● FLT. 28 DATA CYL. OPER.
△ AMES TEST 388 DATA CYL. OPER.
----- ESTIMATED DATA CYL. OPER
DOWNWASH, ε DEG.
24
20
16
12
8
4
0
α
16°
20°
12°
11.6°
8°
16°
7.0°
4°
12°
0°
2.46°
8°
.34°
4°
1.8°
0°
.1
.2
.3
.4
.5
T_c'
1.0
2.0
5.0
.2
.4
.6
.8
1.0
C_{T_3}

FIGURE 14C

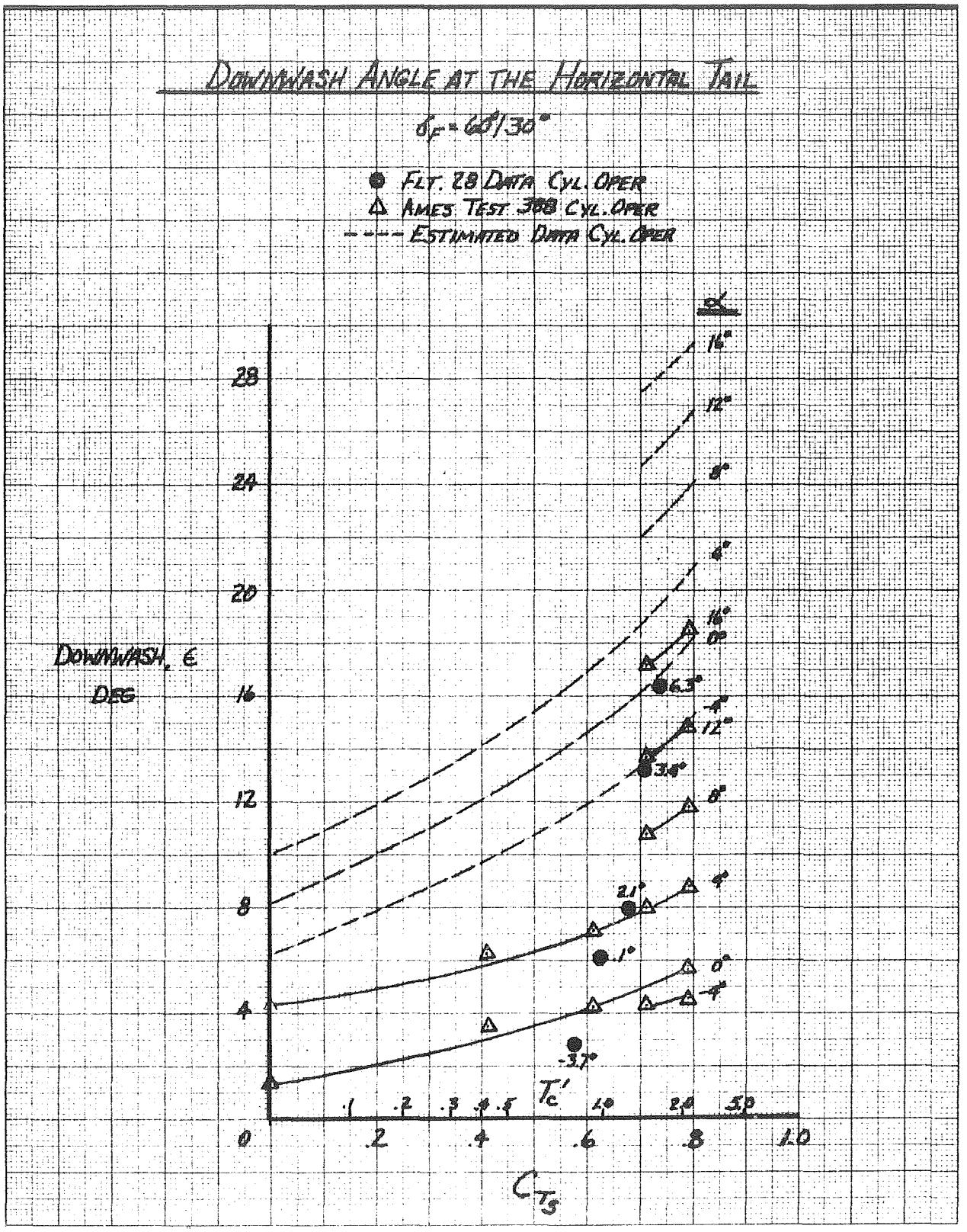
DOWNWASH ANGLE AT THE HORIZONTAL TAIL
δ_F = 60°/30°
FLT. 28 DATA CYL. OPER
AMES TEST 308 CYL. OPER
ESTIMATED DATA CYL. OPER
α
16°
12°
8°
4°
0°
-4°
6.3°
3.4°
2.1°
.1°
-3.7°
DOWNWASH, ε DEG
28
24
20
16
12
8
4
0
.1
.2
.3
.4
.5
T_c'
1.0
2.0
3.0
.2
.4
.6
.8
1.0
C_{T_S}

FIGURE 15

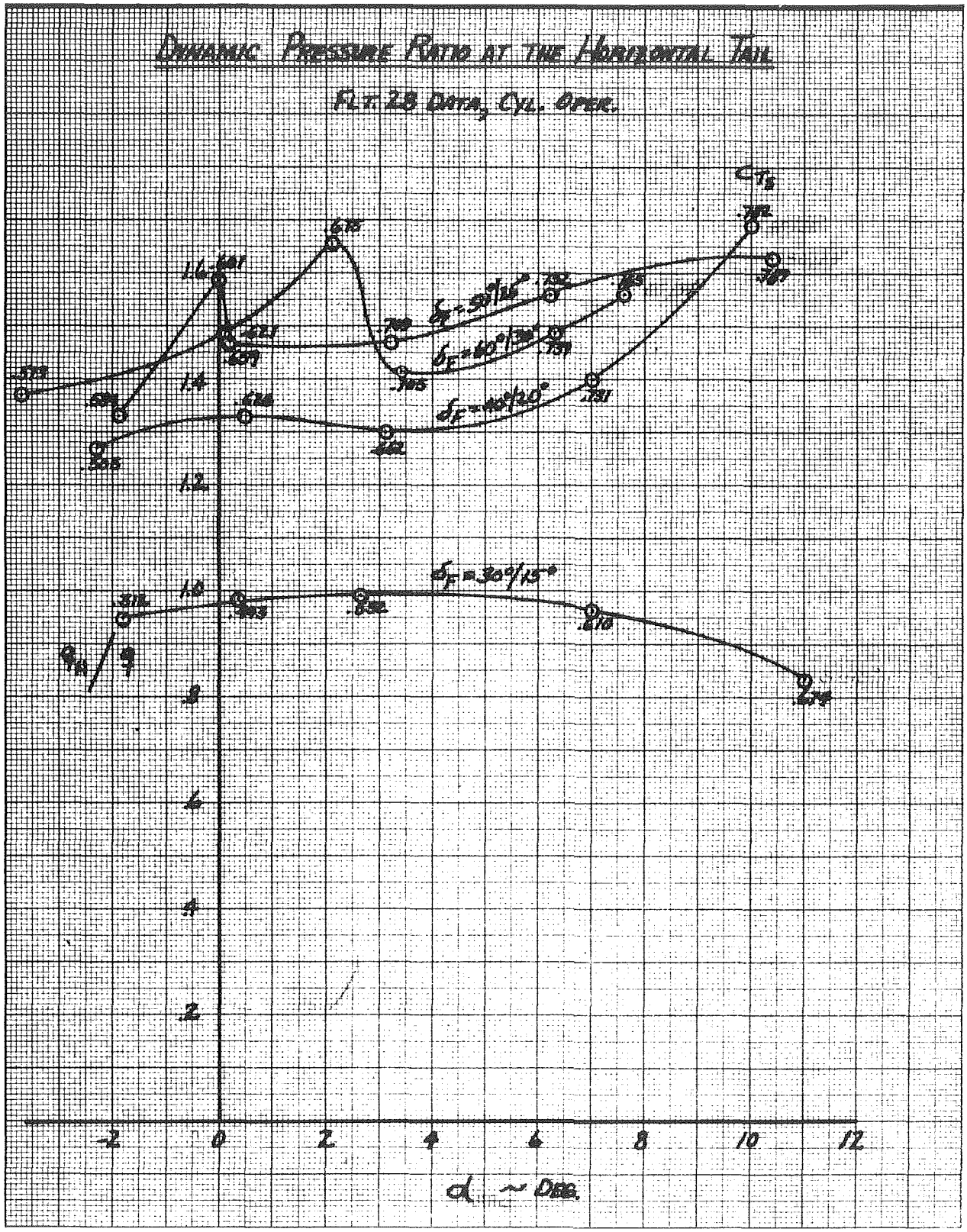
DYNAMIC PRESSURE RATIO AT THE HORIZONTAL TAIL
FLT. 28 DATA, CYL. OPER.
C_{T_S}
$\delta_F = 30°/15°$
$\delta_F = 40°/20°$
$\delta_F = 60°/30°$
$\delta_F = 30°/15°$
q_{H_t}/q
1.6
1.4
1.2
1.0
.8
.6
.4
.2
-2
0
2
4
6
8
10
12
α_{T_S} ~ DEG.

FIGURE 16

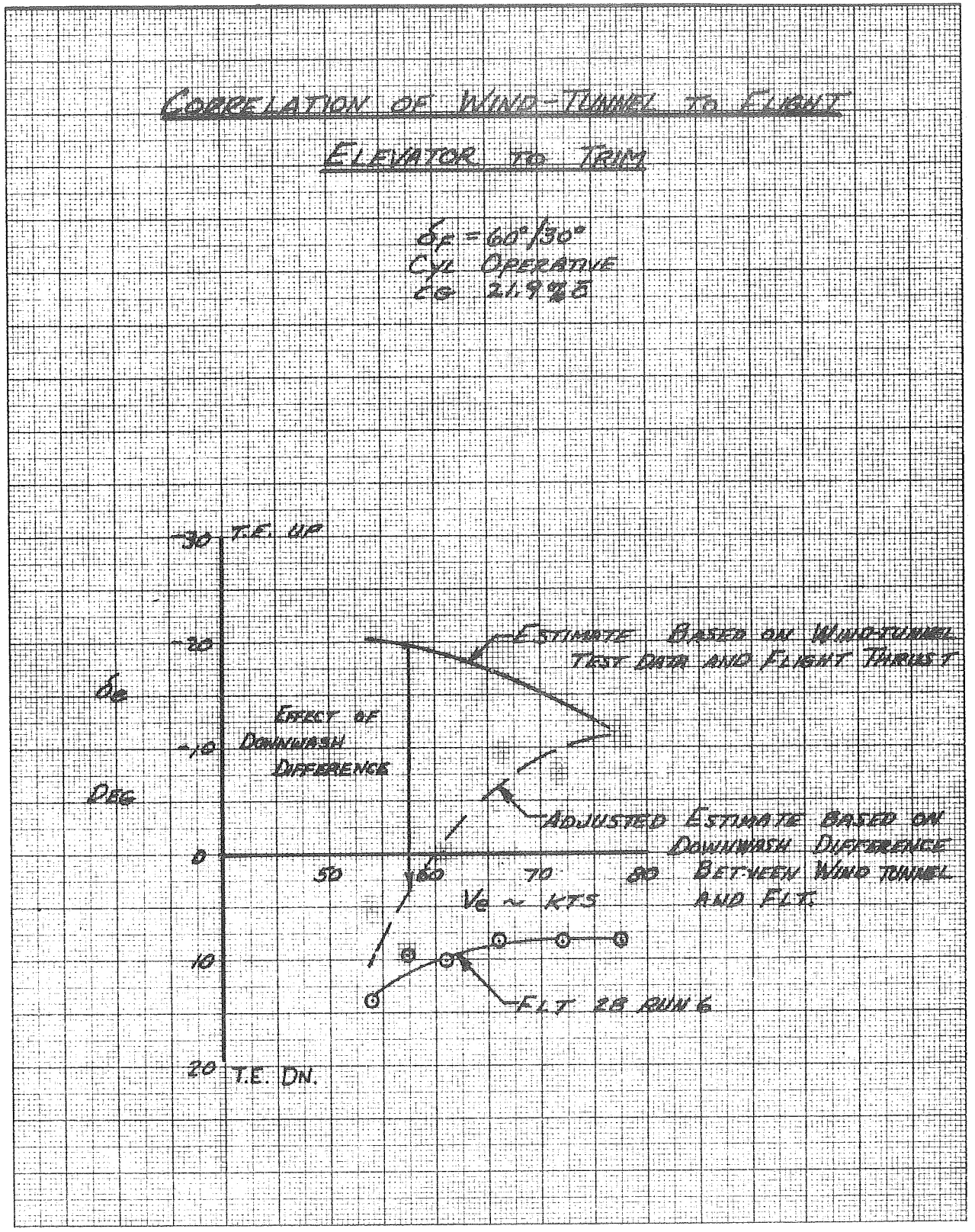
CORRELATION OF WIND-TUNNEL TO FLIGHT
ELEVATOR TO TRIM
δ_F = 60°/30°
Cyl OPERATIVE
C_Θ 21.9% $\bar{c}$
-30 T.E. UP
-20
-10
0
10
20 T.E. DN.
δ_e DEG
EFFECT OF DOWNWASH DIFFERENCE
ESTIMATE BASED ON WIND-TUNNEL TEST DATA AND FLIGHT THRUST
ADJUSTED ESTIMATE BASED ON DOWNWASH DIFFERENCE BETWEEN WIND TUNNEL AND FLT.
50
60
70
80
V_e ~ KTS
FLT 28 RUN 6

FIGURE 17

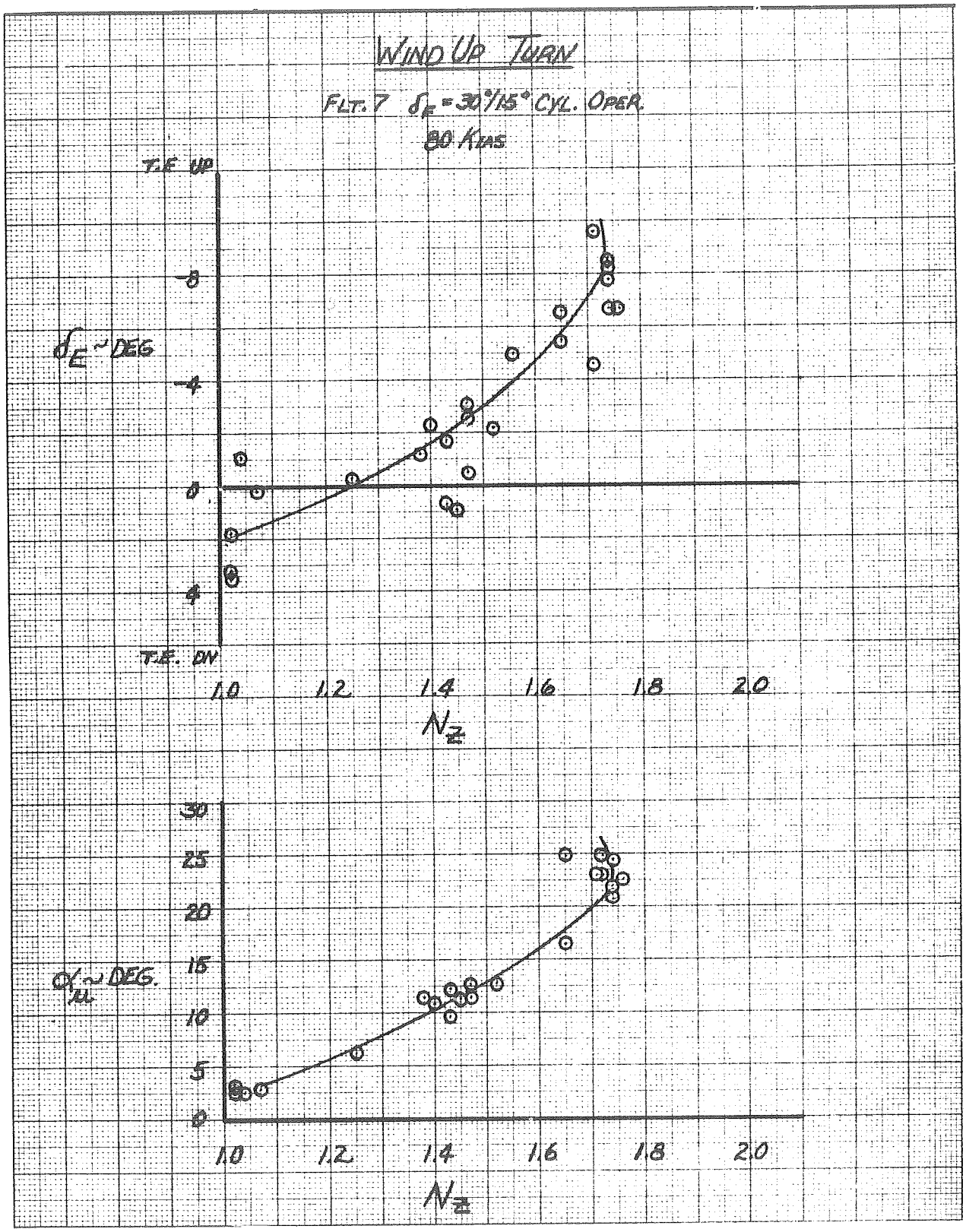
WIND UP TURN
FLT. 7 δ_E = 30°/15° CYL. OPER.
80 KTAS
T.E. UP
-8
-4
0
4
T.E. DN
δ_E ~ DEG
1.0
1.2
1.4
1.6
1.8
2.0
N_z
30
25
20
15
10
5
0
α_w ~ DEG.
1.0
1.2
1.4
1.6
1.8
2.0
N_z

FIGURE 18

LONGITUDINAL CONTROL FOR TAKE OFF

FLT.	δ_F	CYL.	C.G.	T.O. WEIGHT
2	0/0	INOP	25.4	11324
3	0/0	INOP	25.4	11324
4	0/0	INOP	25.4	11324
5	0/0	INOP	24.6	11374
6	30/15	INOP	24.6	11374
7	30/15	INOP	24.6	11374
8	30/15	OPER	24.6	11374
9	0/0	INOP	24.6	11374
10	0/0	INOP	24.6	11374
11	0/0	INOP	24.6	11374
12	0/0	INOP	24.6	11374
22	30/15	OPER	21.9	11849
33	20/10	OPER	21.9	11849

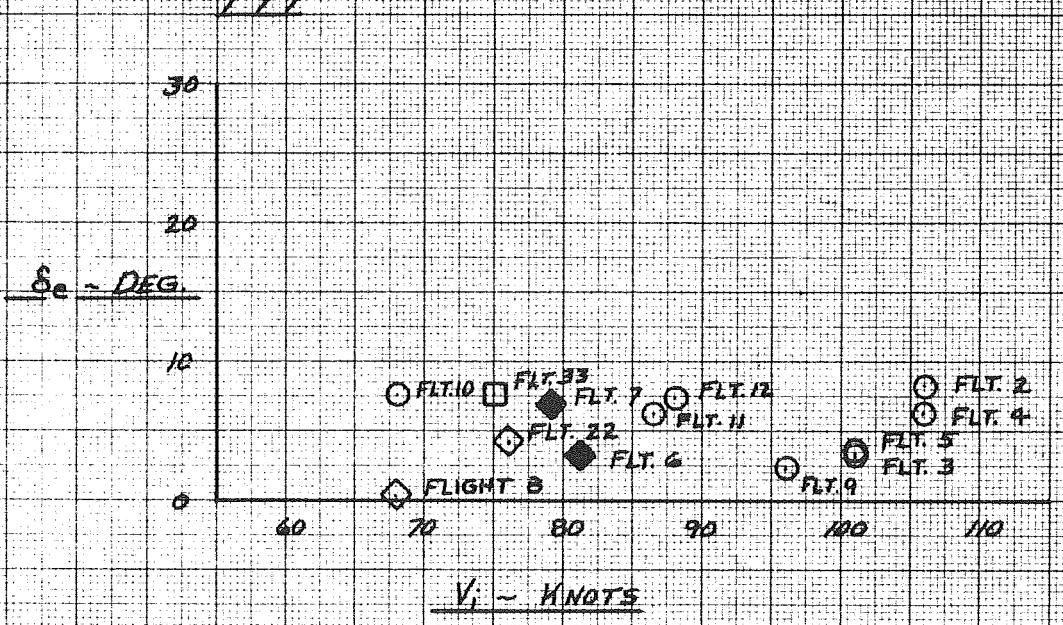

FIGURE 19

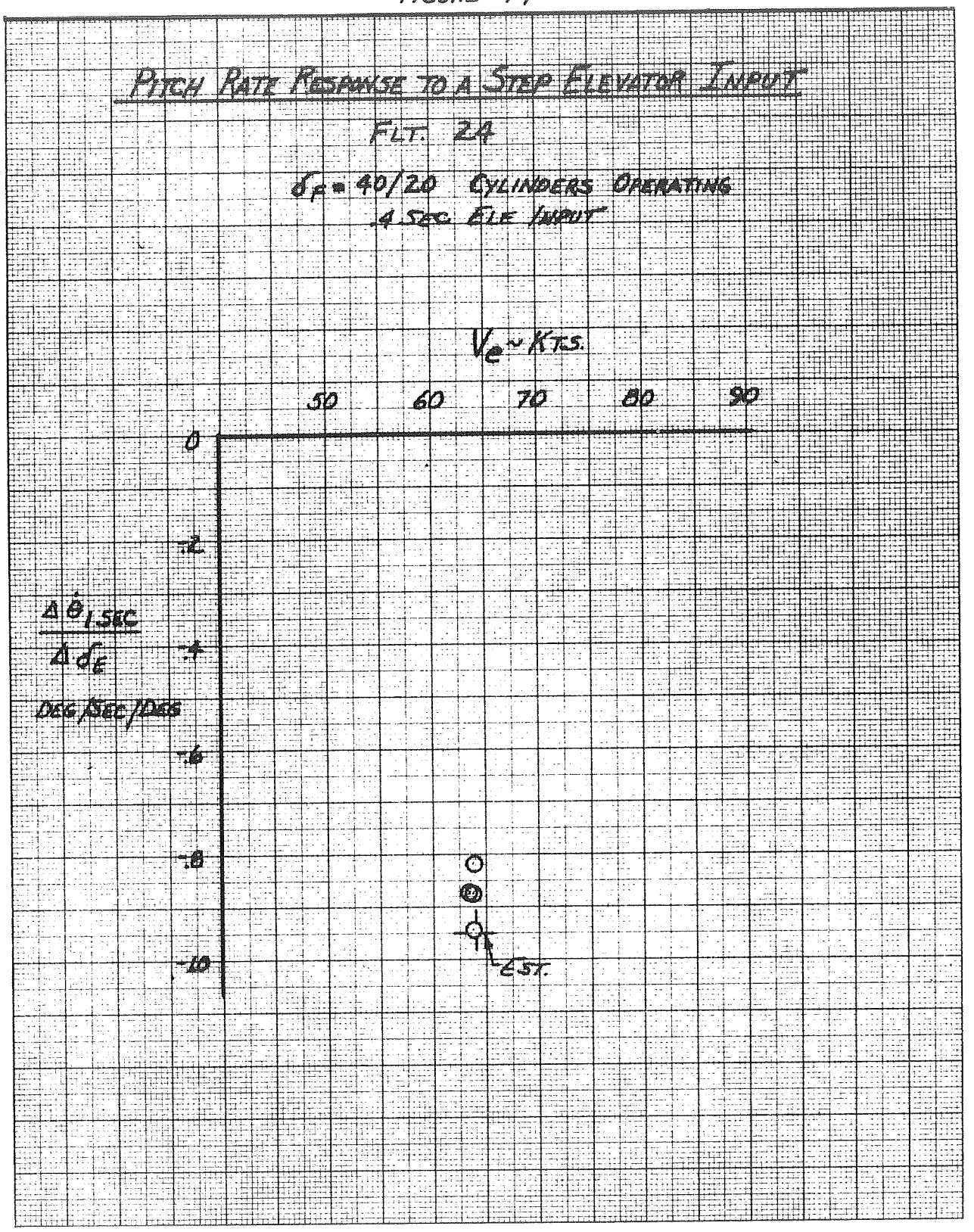
PITCH RATE RESPONSE TO A STEP ELEVATOR INPUT
FLT. 24
δ_E = 40/20 CYLINDERS OPERATING
.4 SEC. ELE INPUT
V_e ~ KTS.
50
60
70
80
90
0
-2
-4
-6
-8
-10
$\frac{\Delta \dot{\theta}_{1\,SEC}}{\Delta \delta_E}$
DEG/SEC/DEG
-2 ST.

FIGURE 20

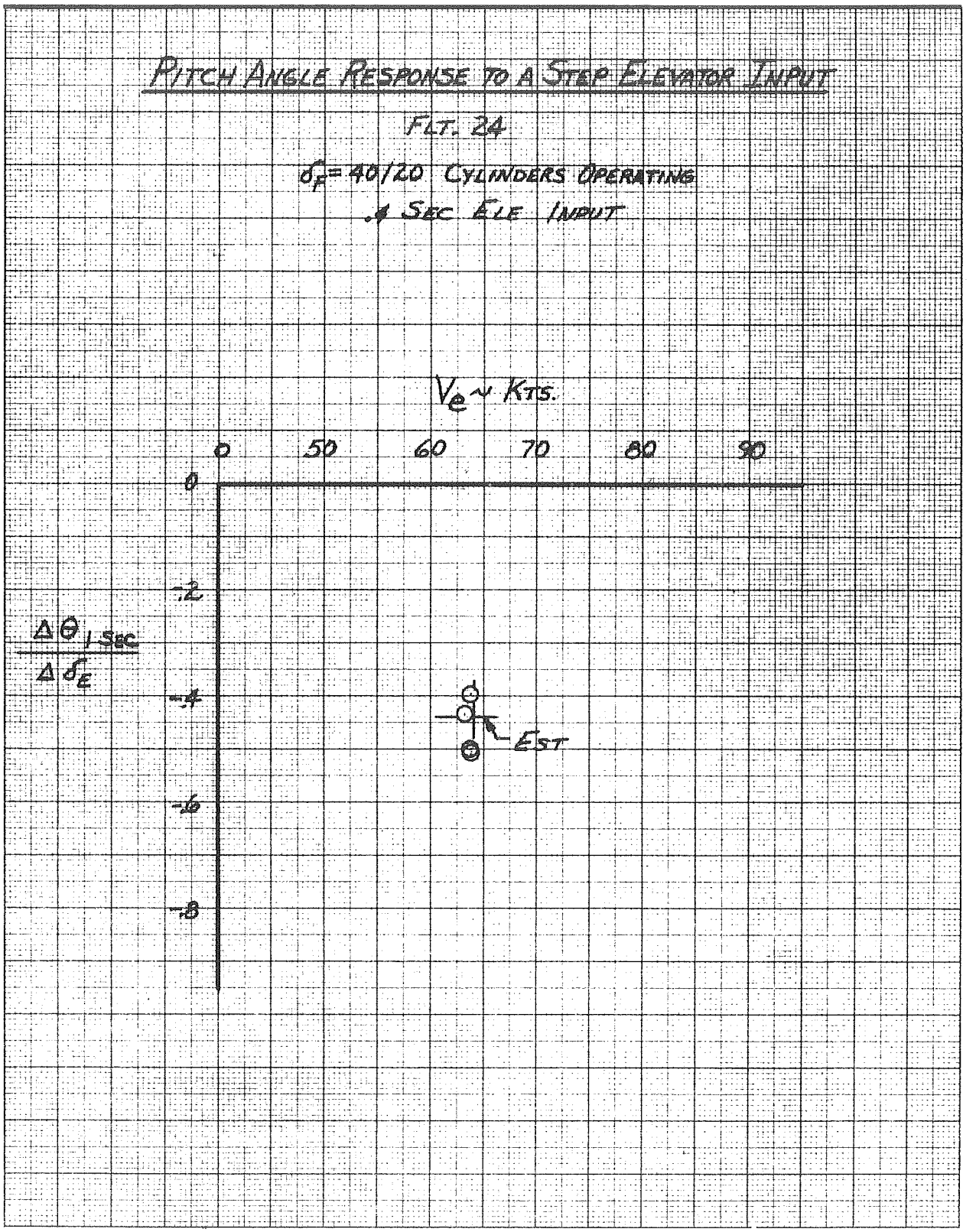
PITCH ANGLE RESPONSE TO A STEP ELEVATOR INPUT
FLT. 24
δ_F = 40/20 CYLINDERS OPERATING
.4 SEC ELE INPUT
V_e ~ KTS.
0
50
60
70
80
90
0
-.2
-.4
-.6
-.8
$\frac{\Delta\theta_{1\,SEC}}{\Delta\delta_E}$
EST

FIGURE 21

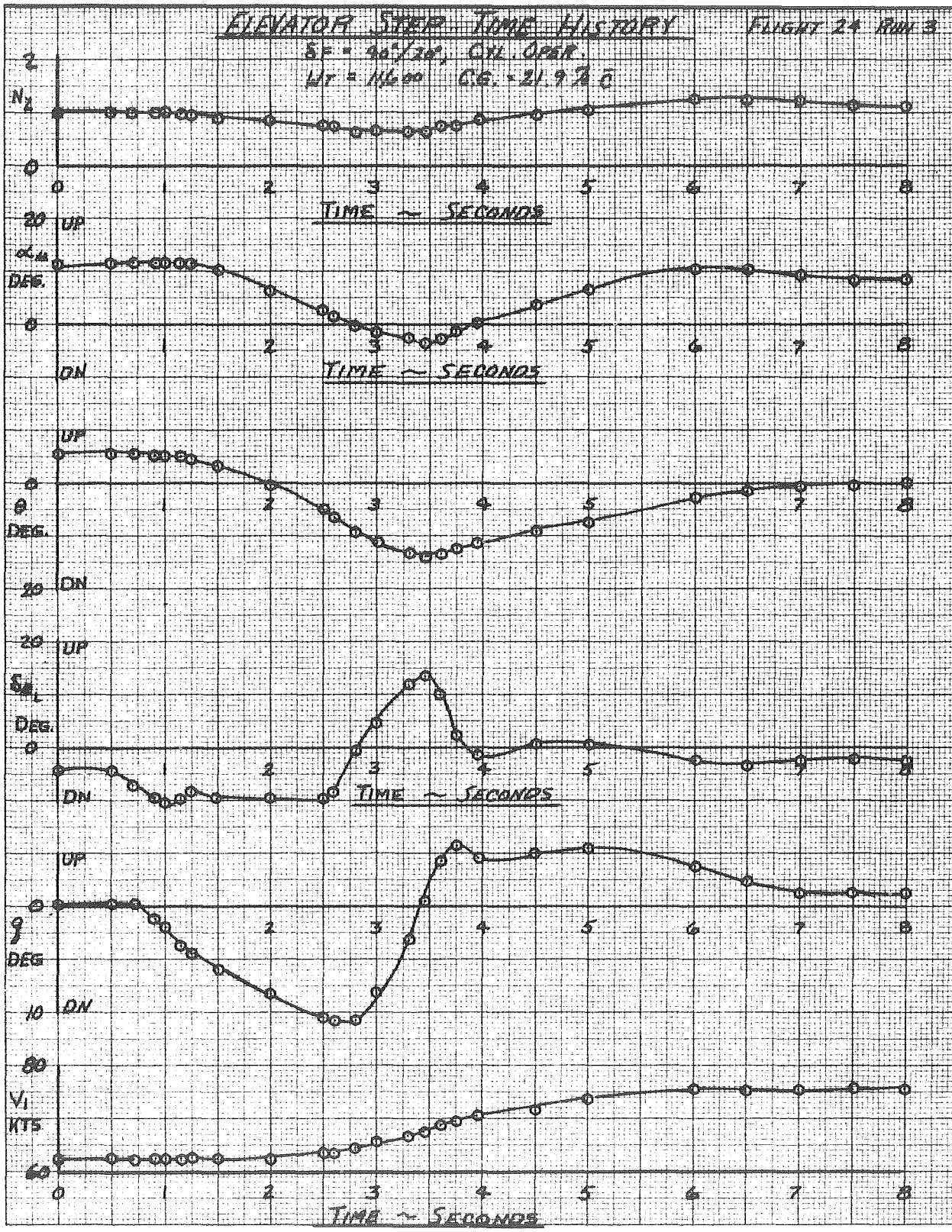
ELEVATOR STEP TIME HISTORY
FLIGHT 24 RUN 3
δE = 4.0°/20°, CYL. OPER.
Wt = 14,600 C.G. = 21.9 % c̄
n_z
TIME ~ SECONDS
UP
α_{ac}
DEG.
DN
θ
DEG.
δ_{SE_L}
DEG.
q
DEG
V_i
KTS

FIGURE 22a

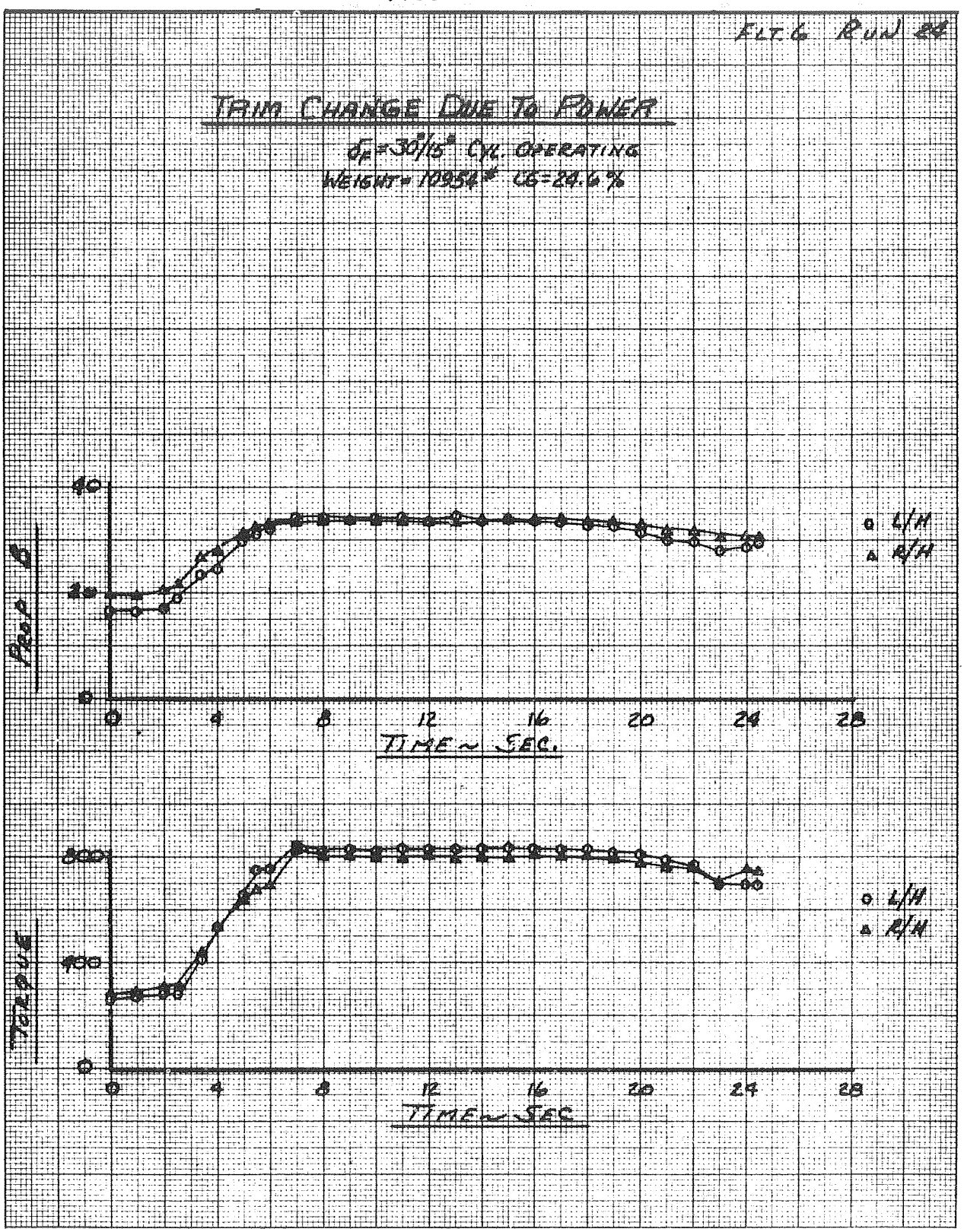
FLT 6 RUN 24
TRIM CHANGE DUE TO POWER
δ_F = 30°/15° CYL. OPERATING
WEIGHT = 10954# CG = 24.6 %
40
20
0
PROP. δ
0
4
8
12
16
20
24
28
TIME ~ SEC.
o L/H
Δ R/H
800
400
0
TORQUE
0
4
8
12
16
20
24
28
TIME ~ SEC.
o L/H
Δ R/H

FIGURE 22 b

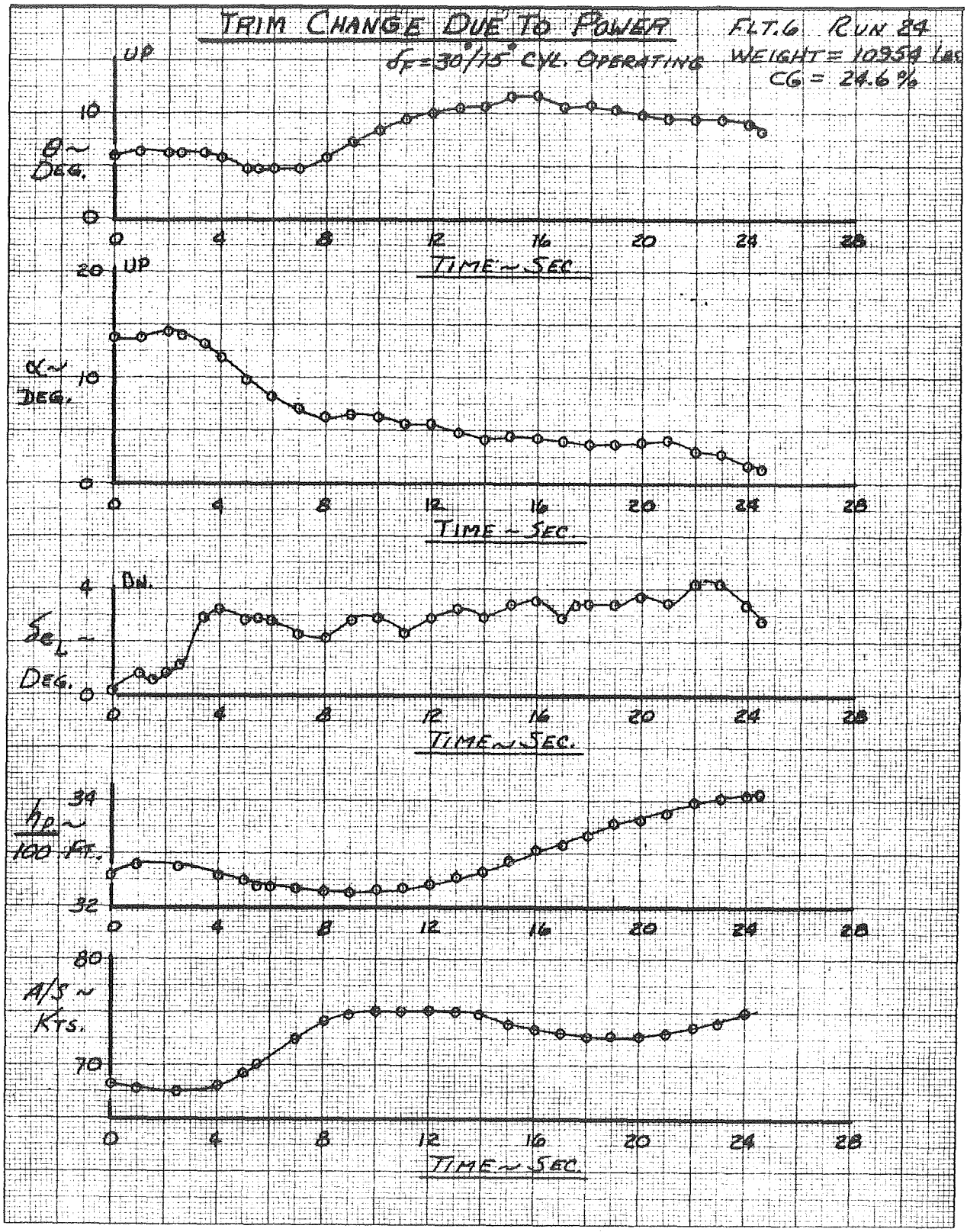
TRIM CHANGE DUE TO POWER
FLT. 6 RUN 24
δ_F = 30°/15° CYL. OPERATING
WEIGHT = 10954 Lbs
CG = 24.6 %
UP
θ ~ DEG.
10
0
0 4 8 12 16 20 24 28
TIME ~ SEC
20 UP
α ~ DEG.
10
0
TIME ~ SEC.
4 DN.
δ_{e_L} ~ DEG.
0
TIME ~ SEC.
h_p ~ 100 FT.
34
32
80
A/S ~ KTS.
70
TIME ~ SEC.

Time - Sec.
Time - Sec.
Time - Sec.
Time - Sec.
Time - Sec.
RT
LT
UP
DOWN
Pressure Rise Across Shock Wave - PSIA

FIGURE 232

FIGURE 236

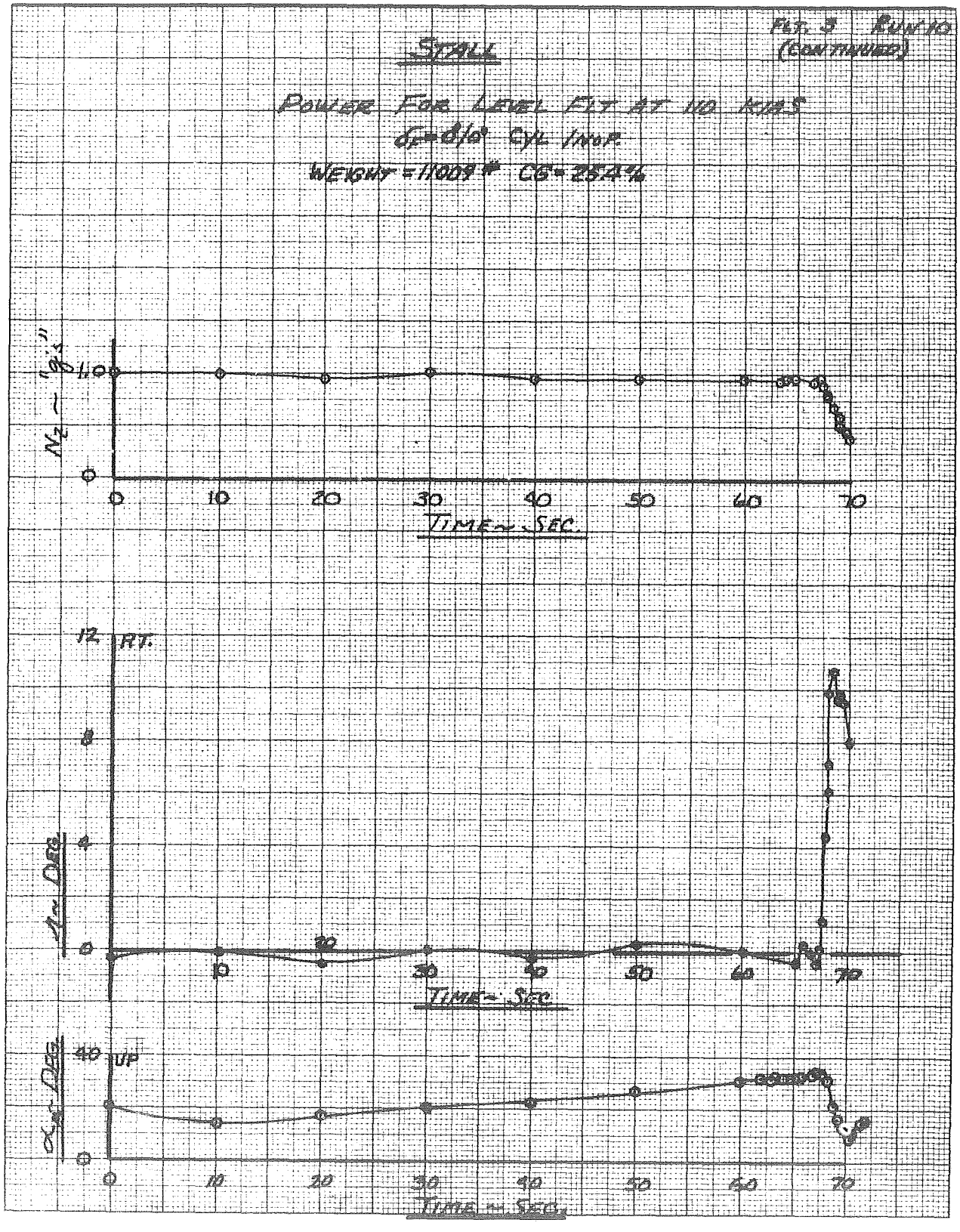
FLT. 3 RUN 10
(CONTINUED)
STALL
POWER FOR LEVEL FLT AT 110 KNOTS
δ_E = 0/0° CYL INOP.
WEIGHT = 11,009 LBS CG = 25.4%
N_z ~ "g's"
1.0
0
0 10 20 30 40 50 60 70
TIME ~ SEC.
12
8
4
0
RT.
α ~ DEG.
0 10 20 30 40 50 60 70
TIME ~ SEC.
40
0
UP
α ~ DEG.
0 10 20 30 40 50 60 70
TIME IN SEC.

STALL
Power Plant = 4 Piston Pump Model
Cyl. Pump = Cyl. Motor
Pressure = 1000 psi
Cg = 25%
Time ~ Sec.
Deg. ~ Deg.
Decrease ~ Volume
RT
LT
UP
DN

FIGURE 23C

FIGURE 23d

FLT. 3 RUN 11
(CONTINUED)

STALL

POWER FOR -4° FLIGHT PATH ANGLE
δ_e = 0°/0° CYL. TWR
WEIGHT = 10959# CG = 25.4 %

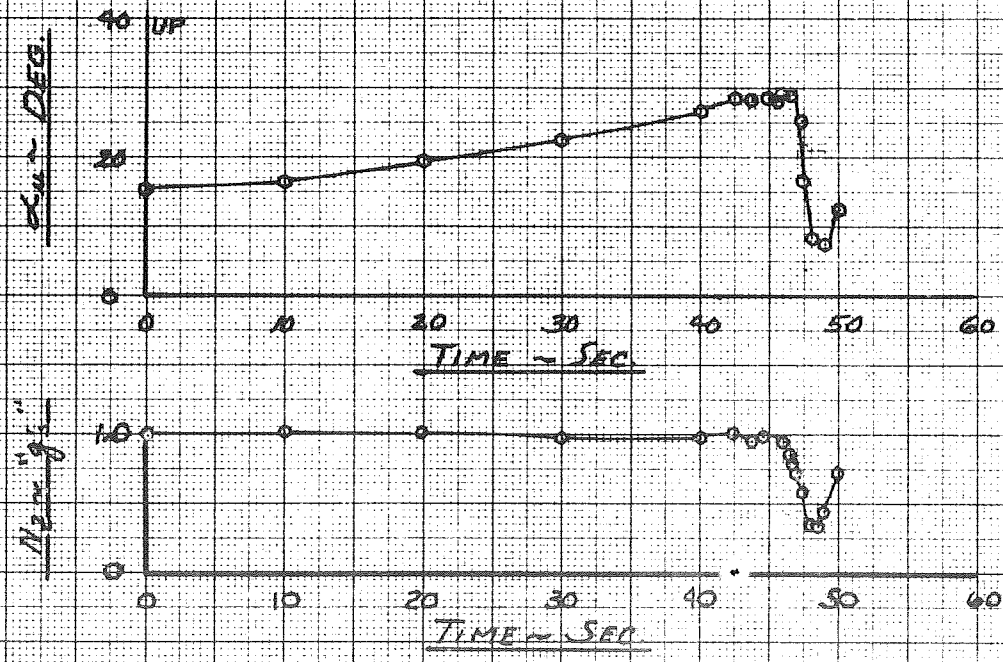

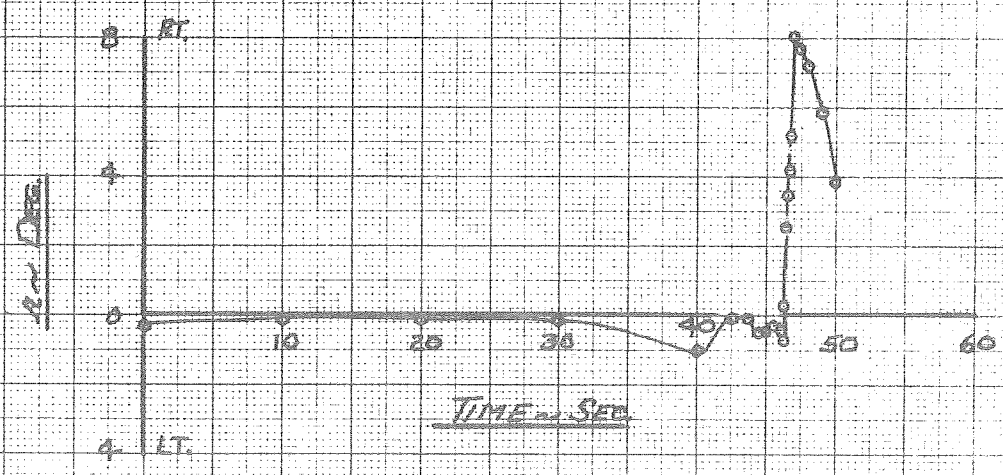

STALL
FLIGHT TAPE
CYL. MAP
WEIGHT = 10000 CG = 25%MAC
FIG. 9 REF. 18
δ_L ~ DEG.
10
0
FT.
0 10 20 30 40
TIME ~ SEC.
β ~ DEG.
8
4
0
LT.
0 10 20 30 40
TIME ~ SEC.
δ_E ~ DEG.
20
0
UP
DN
0 10 20 30 40
TIME ~ SEC.
ϕ ~ DEG.
0
10
20
LT.
0 10 20 30 40
TIME ~ SEC.
δ_L
20
0
UP
20
DN
0 10 20 30 40
TIME ~ SEC.
δ_{RUD}
20
0
UP
0 10 20 30 40
TIME ~ SEC.
AIRSPEED ~ KTS.
100
80
0 10 20 30 40
TIME ~ SEC.

FIGURE 23 E

FIGURE 23F

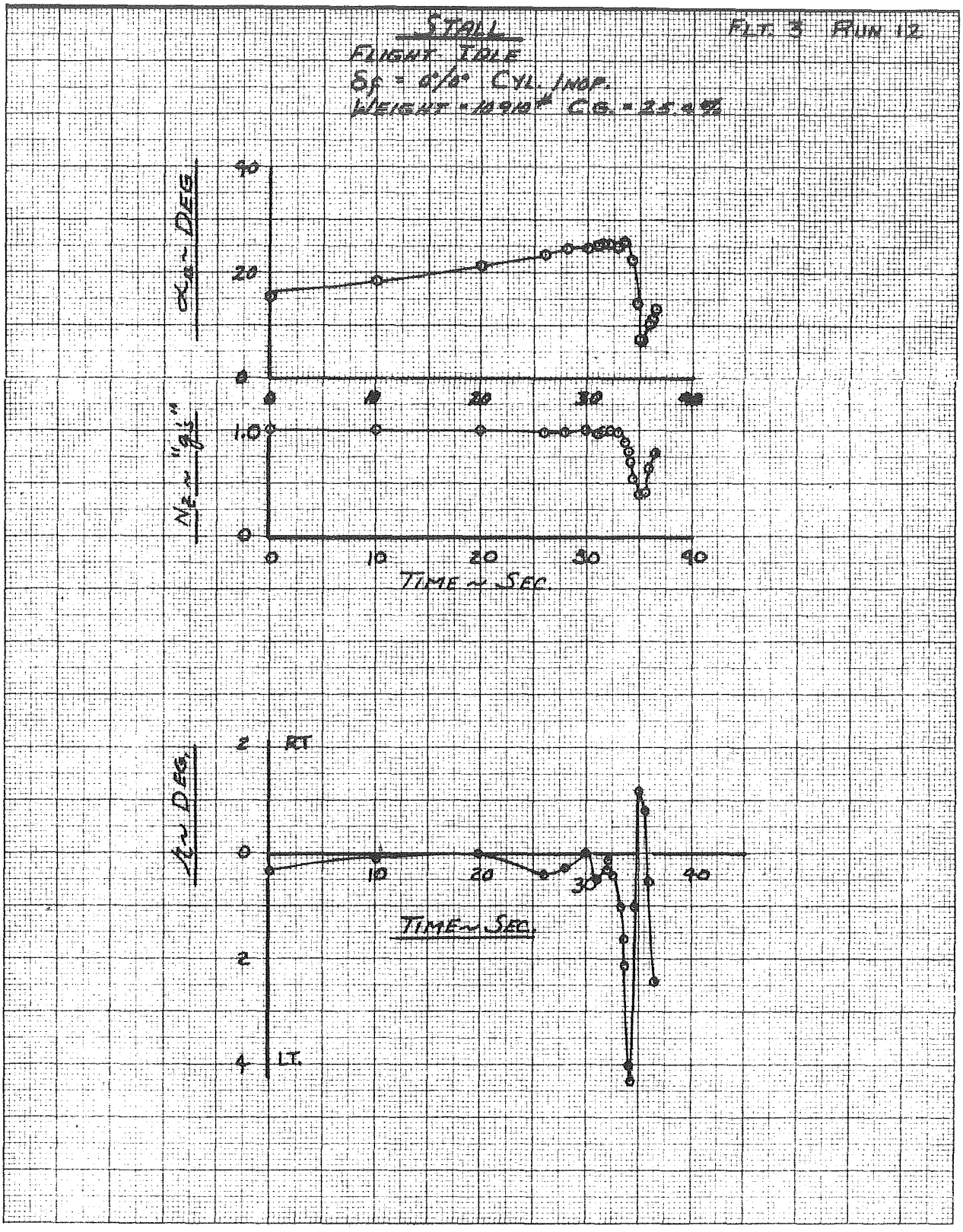
STALL
FLIGHT IDLE
δ_f = 0°/0° CYL. INDF.
WEIGHT = 11910# C.G. = 25.4%
FLT. 3 RUN 12
α_{cg} ~ DEG
40
20
0
N_z ~ "g's"
1.0
0
0
10
20
30
40
TIME ~ SEC.
ϕ ~ DEG.
2 RT
0
2
4 LT.
10
20
30
40
TIME ~ SEC.

RT.
LT.
UP
DN
TIME ~ SECONDS
STEP
PROBE FAILURE AT 60 SECONDS
INDICATED MACH NO.

FIGURE 23 G

FIGURE 23h

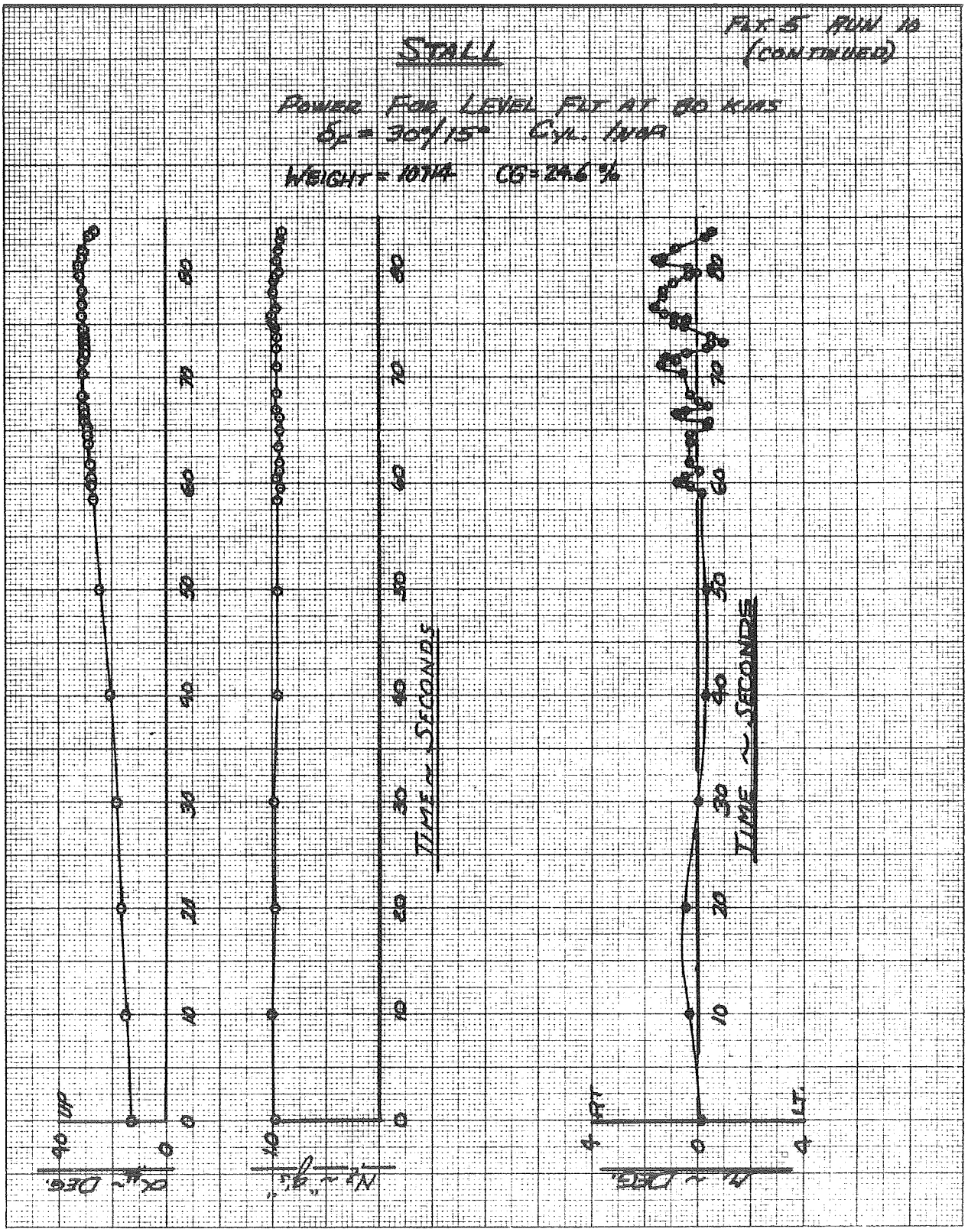
Flt. 5 Run 10
(continued)
STALL
Power For Level Flt at 60 kias
δ_f = 30°/15° Cyl. Lwar
WEIGHT = 1014 CG = 24.6 %
α_w ~ Deg.
N_z ~ "g's"
ϕ ~ Deg.
TIME ~ SECONDS
TIME ~ SECONDS
0
10
20
30
40
50
60
70
80
4 RT
0
4 LT

FIGURE 23c.

FIGURE 23 J

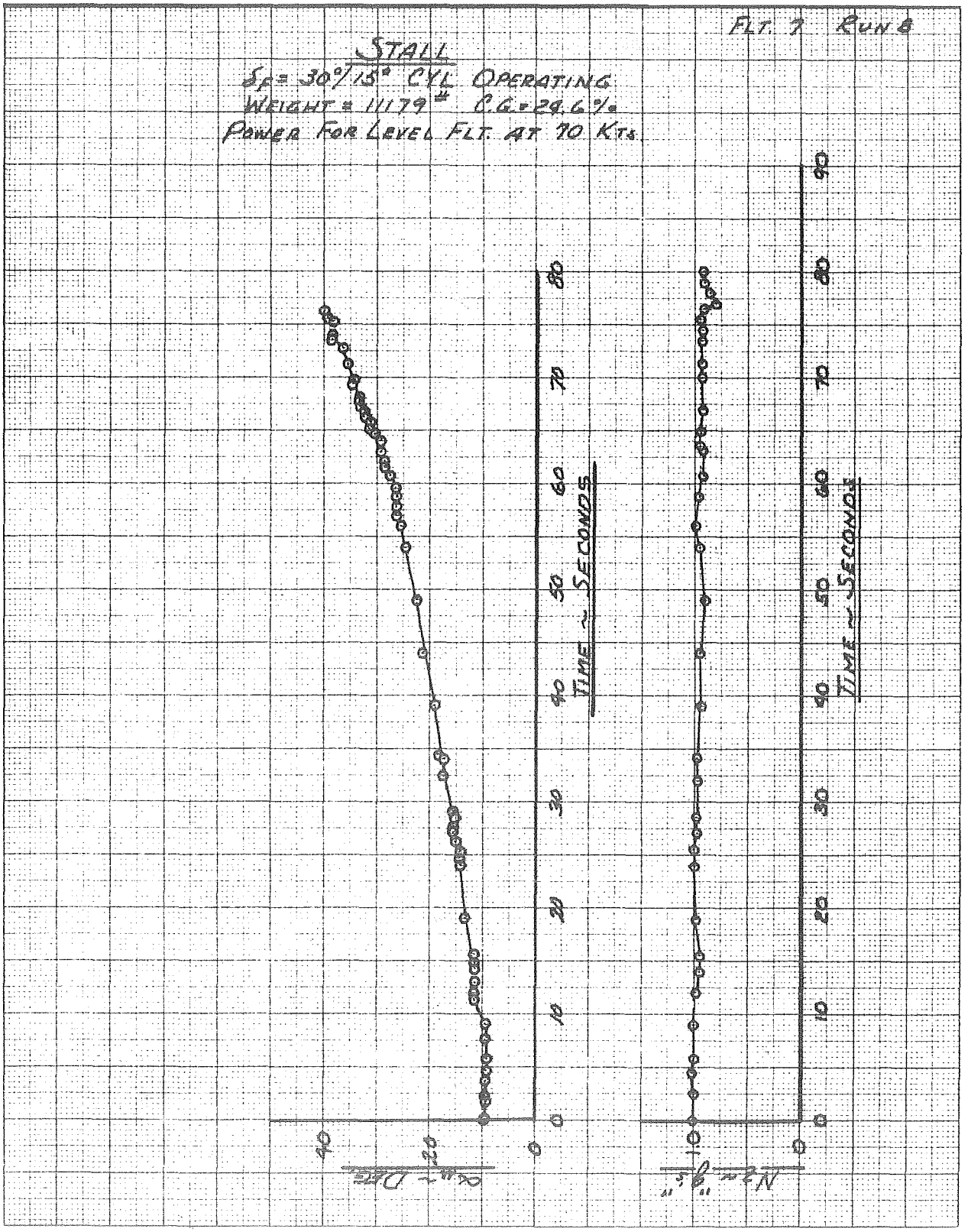
FLT. 7 RUN 6
STALL
δ_F = 30°/15° CYL OPERATING
WEIGHT = 11179 # C.G. = 29.6 %
POWER FOR LEVEL FLT. AT 90 KTS.
TIME ~ SECONDS
TIME ~ SECONDS
0
10
20
30
40
50
60
70
80
90
40
20
0
1.0
0

FIGURE 23H

Stall
C_L = 30% Out Of Trim
Weight = 1120 lbs. C_{D_0} = 2.2%
Flight Time
Fig. 23H

FIGURE 23L

FLT. 7 RUN 9

STALL

δ_F = 30°/15° CYL. OPERATING
WEIGHT = 11129 # C.G. = 29.6%
FLIGHT IDLE

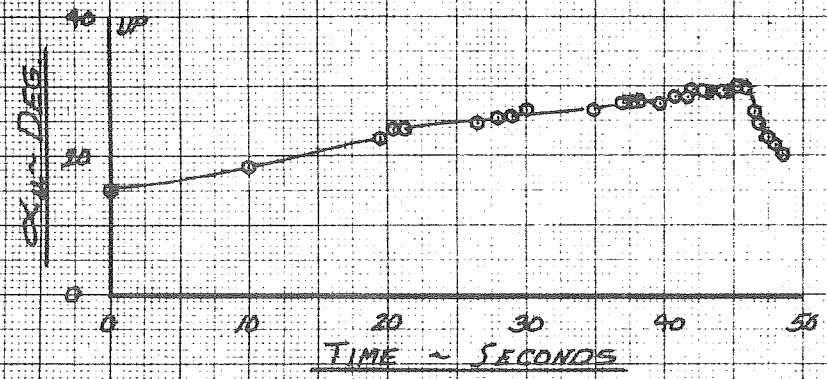

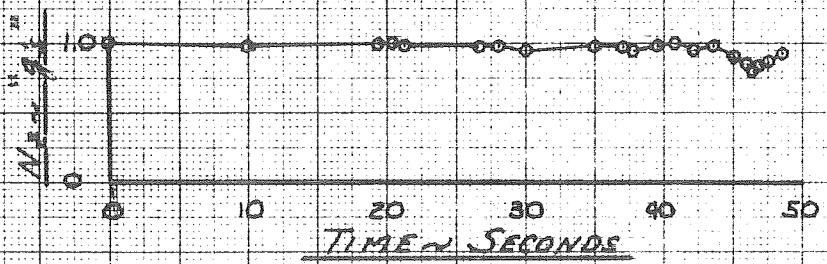

FIGURE 24a

FIGURE 24b

FLT. 10 RUN 5

MINIMUM SPEED INVESTIGATION

δ_F = 40°/20° CYL. OPERATING
WEIGHT = 11351 # C.G. = 25.9%
POWER FOR LEVEL FLT. AT 60 KIAS

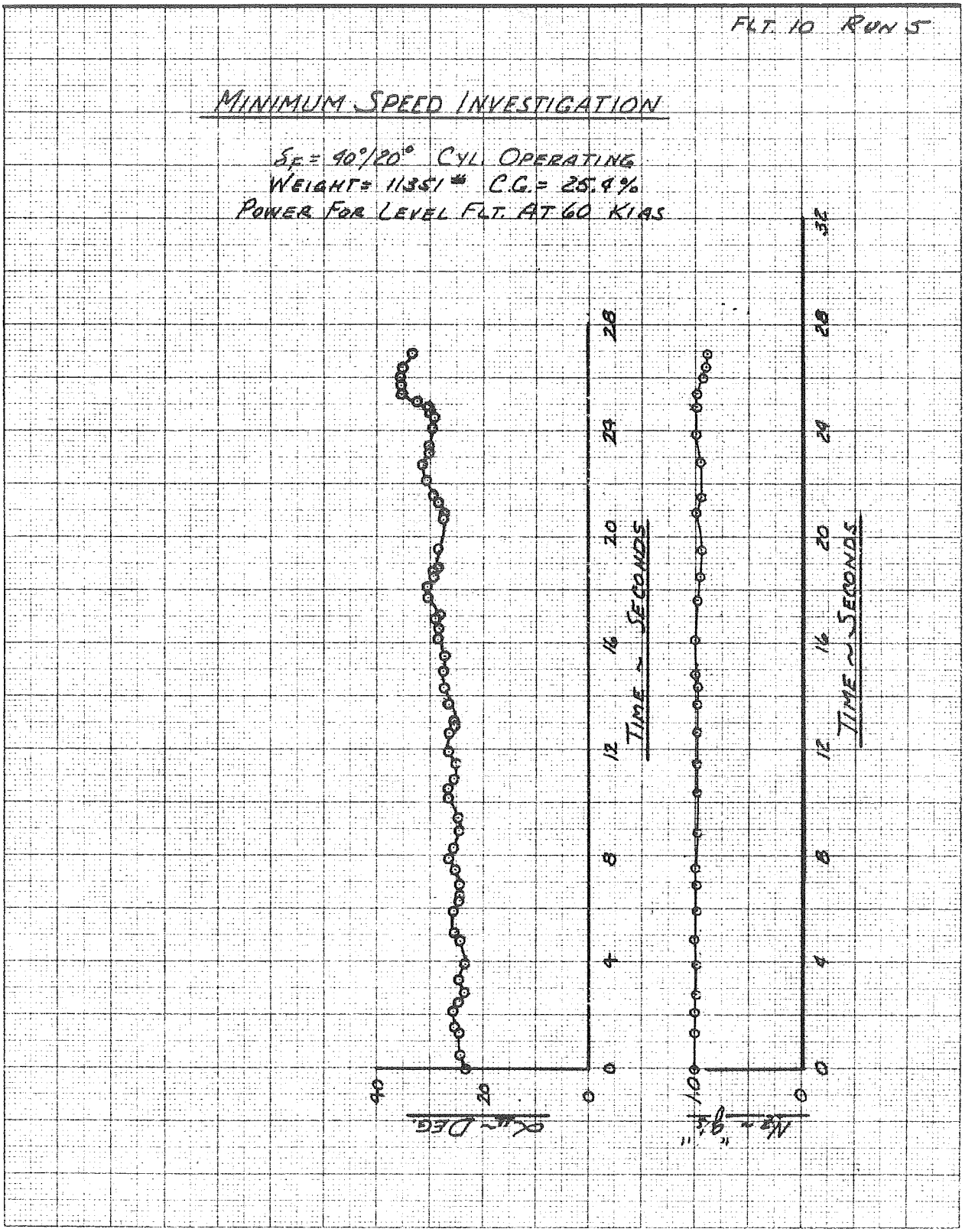

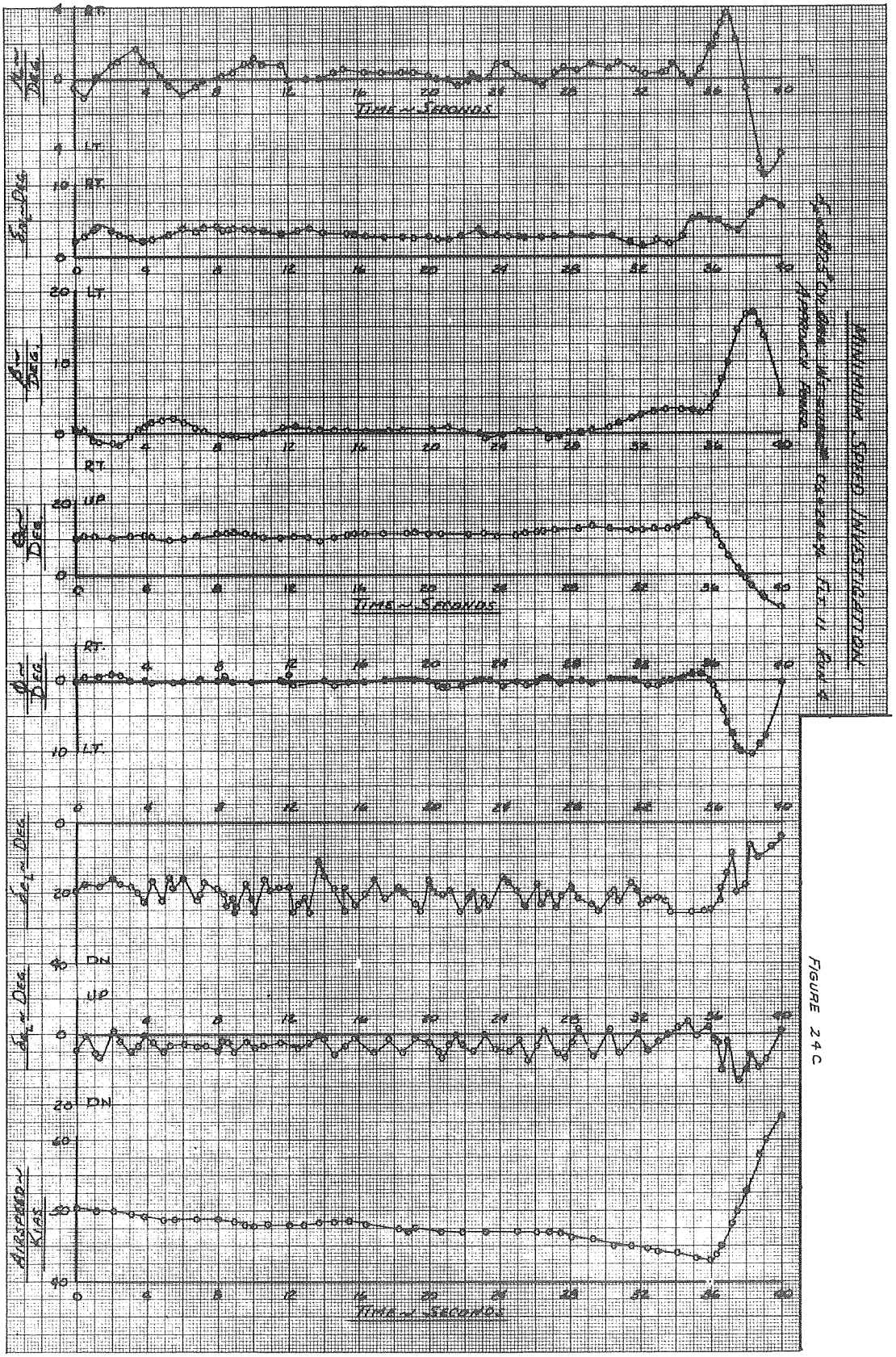
MINIMUM - SPEED INVESTIGATION
APPROACH POWER
Time — Seconds
RT.
LT.
UP
DN
Time — Seconds

FIGURE 24C

FIGURE 24 d

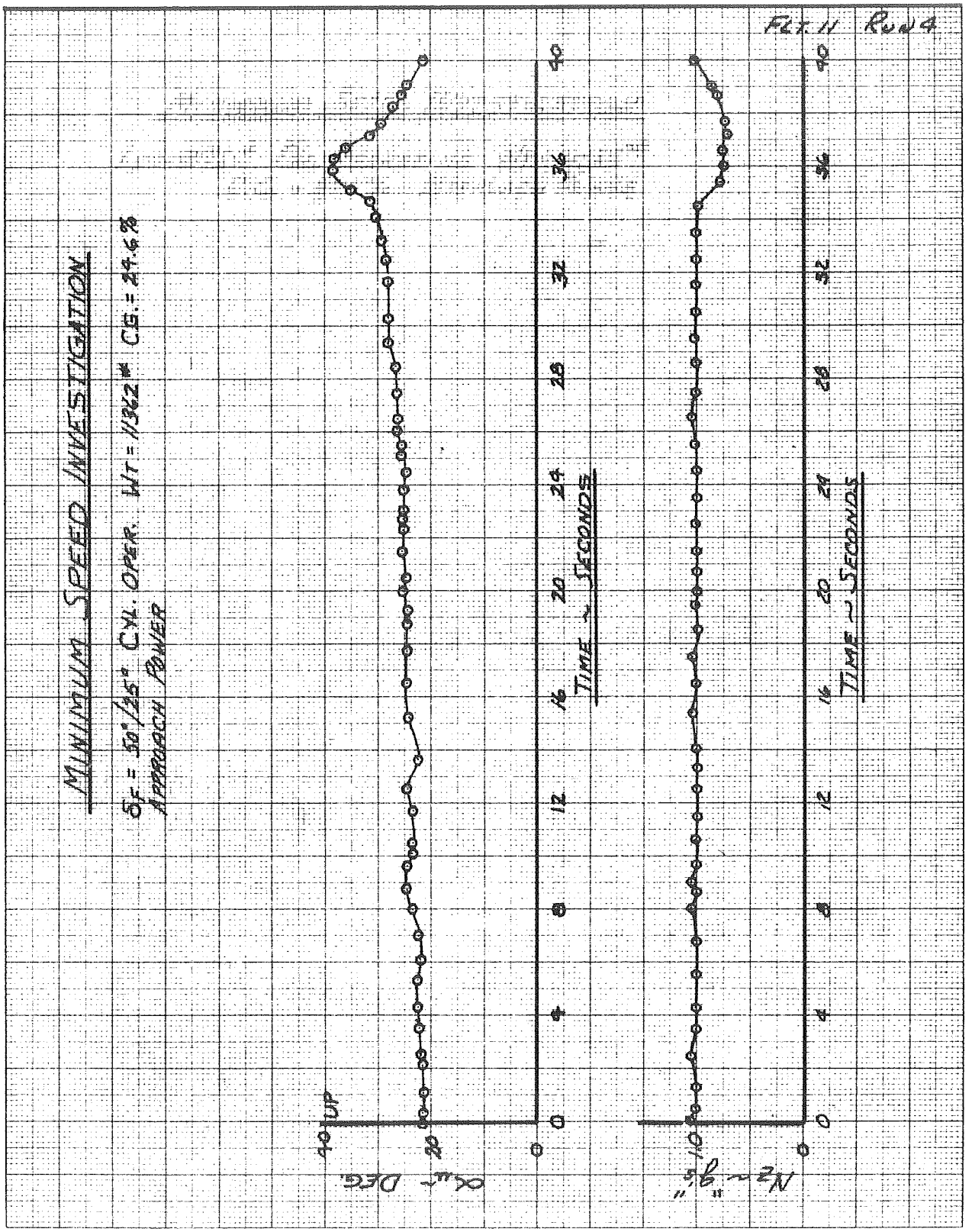
Flt. 11 Run 4
MINIMUM SPEED INVESTIGATION
δF = 50°/25° Cyl. Oper. Wt = 11362 # C.G. = 24.6%
APPROACH POWER
UP
0
4
8
12
16
20
24
28
32
36
40
TIME ~ SECONDS
TIME ~ SECONDS

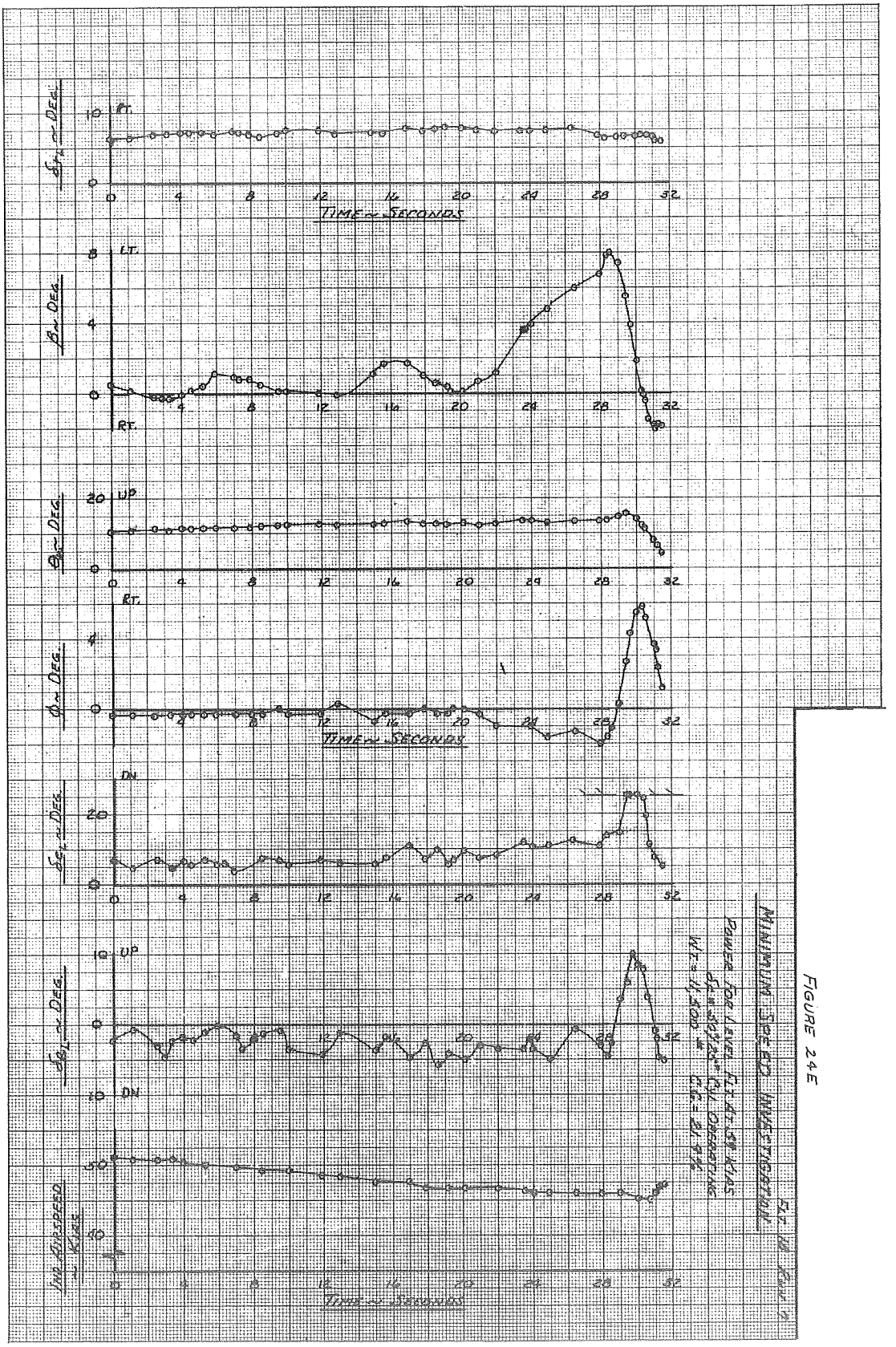

FIGURE 24E

FIGURE 24E

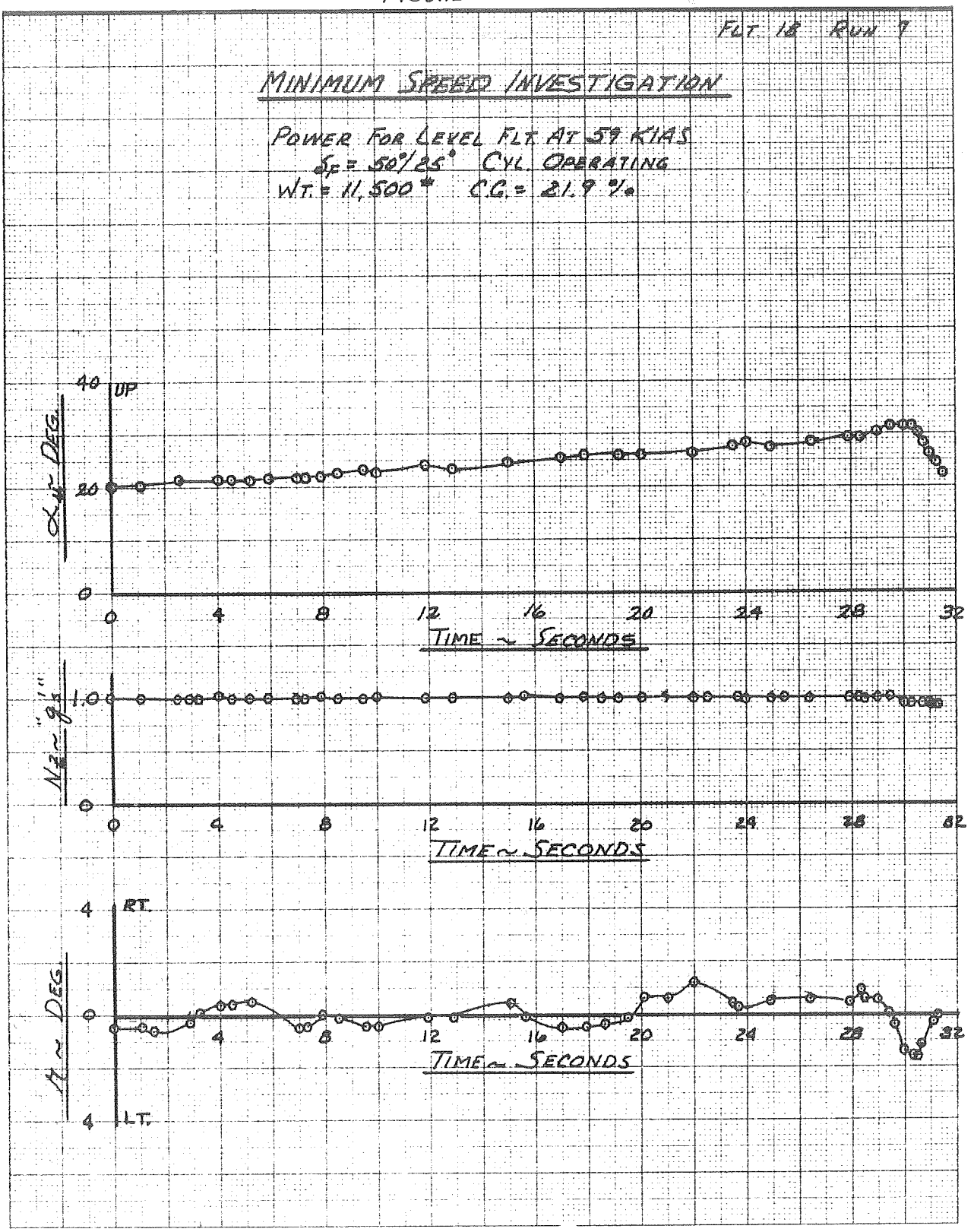
FLT 18 RUN 7
MINIMUM SPEED INVESTIGATION
POWER FOR LEVEL FLT AT 59 KIAS
δ_F = 50°/25° CYL. OPERATING
WT. = 11,500 # C.G. = 21.9 %
40
UP
20
0
α_w ~ DEG.
0 4 8 12 16 20 24 28 32
TIME ~ SECONDS
1.0
0
N_z ~ g's
0 4 8 12 16 20 24 28 32
TIME ~ SECONDS
4
RT.
0
4
LT.
ϕ ~ DEG.
4 8 12 16 20 24 28 32
TIME ~ SECONDS

MINIMUM SPEED INVESTIGATION
GE = 60,130 Cit. Operating
WEIGHT = 1550 # CG = 24.6%
ALTITUDE 10,000
FLT. # 6044
TIME - SECONDS
RT.
UP
DN.
LT.

FIGURE 24 G

FIGURE 24h

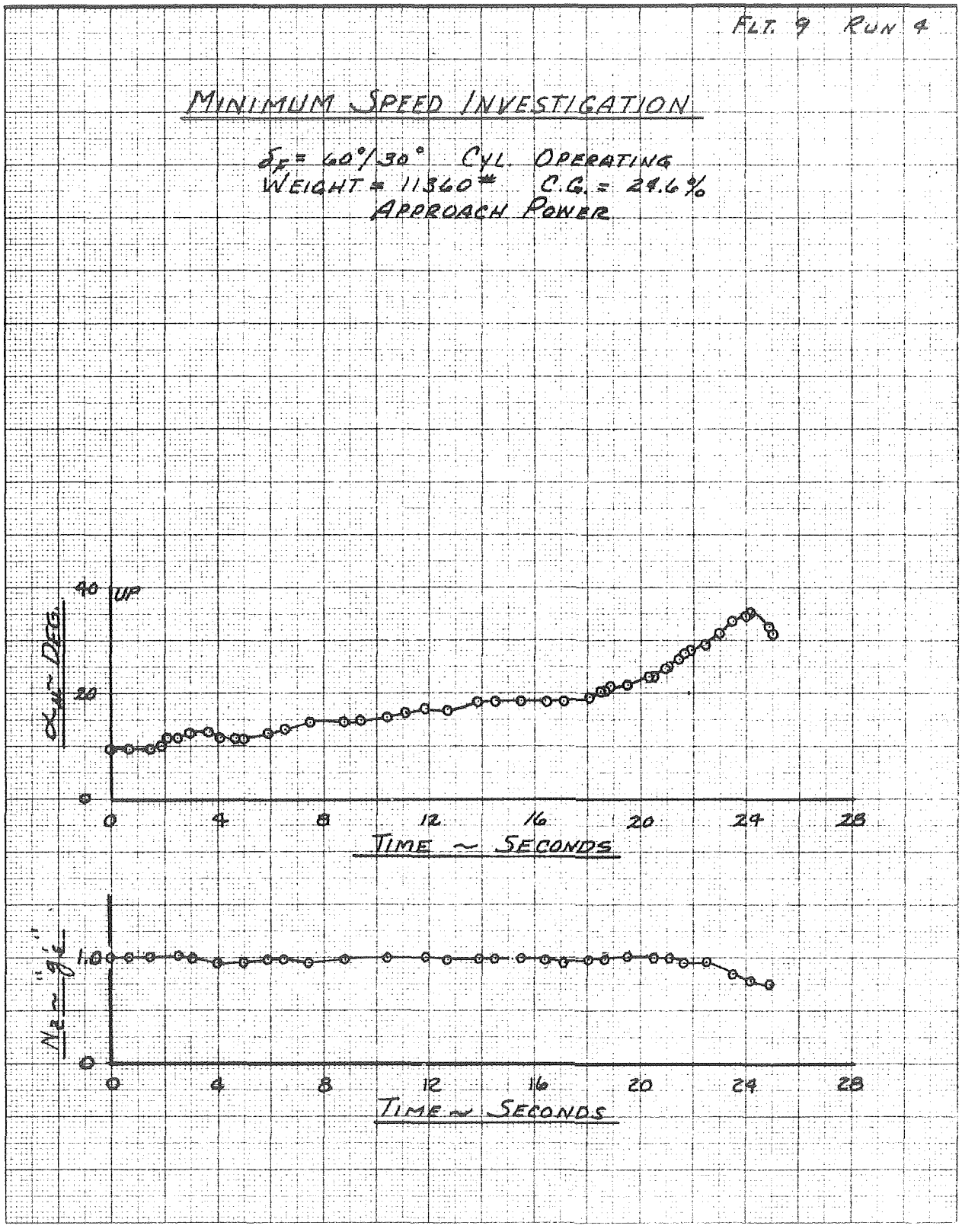
FLT. 9 RUN 4
MINIMUM SPEED INVESTIGATION
δ_F = 60°/30° CYL. OPERATING
WEIGHT = 11360# C.G. = 29.6%
APPROACH POWER
α_{cg} ~ DEG
40
UP
20
0
0
4
8
12
16
20
24
28
TIME ~ SECONDS
N_z ~ g's
1.0
0
0
4
8
12
16
20
24
28
TIME ~ SECONDS

MINIMUM SPEED UNDESIRABLE
POWER FOR LEVEL FLIGHT AT 170 KNOTS
$C_L = \frac{2W}{\rho V^2 S} = \frac{2(3,200)}{(.002378)(170)^2(174)} = .2$
W.T. = 11,200 = 3,200 LB. OVERCAST
R.P.M. = 2,300
FLAPS UP
δ_e = 0 DEG.
δ_a = 0 DEG.
δ_r = 0 DEG.
RT.
LT.
UP
DN.
TIME — SECONDS
0
10
20
30
40
50
60
70

FIGURE 24i

FIGURE 24 j

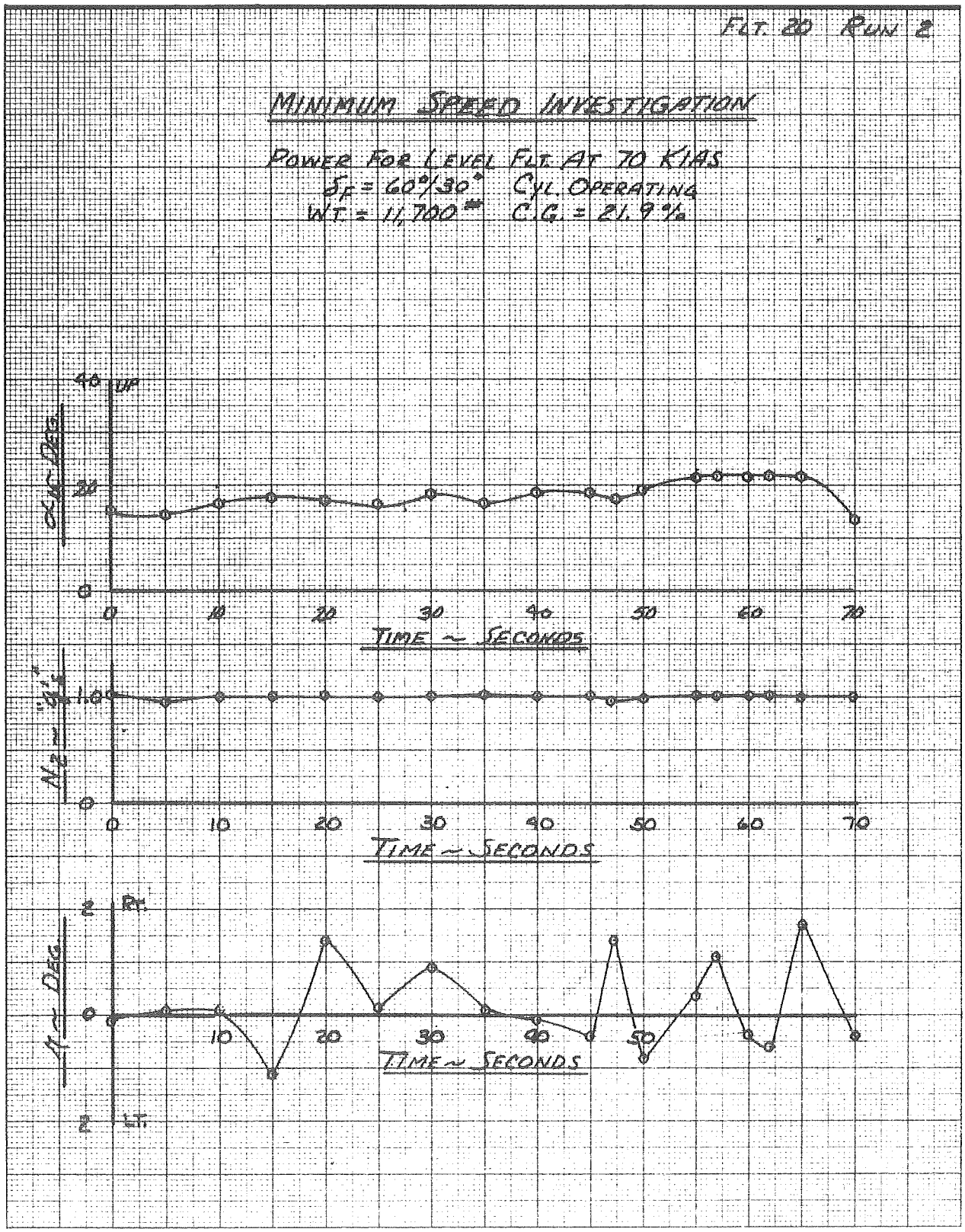
FLT. 20 RUN 2
MINIMUM SPEED INVESTIGATION
POWER FOR LEVEL FLT. AT 70 KIAS
δ_F = 60°/30° CYL. OPERATING
WT. = 11,700 # C.G. = 21.9%
40 UP
20
0
α_w ~ DEG.
0 10 20 30 40 50 60 70
TIME ~ SECONDS
1.0
N_z ~ "g's"
0 10 20 30 40 50 60 70
TIME ~ SECONDS
2 RT.
0
2 LT.
ϕ ~ DEG.
10 20 30 40 50
TIME ~ SECONDS

FIGURE 25a

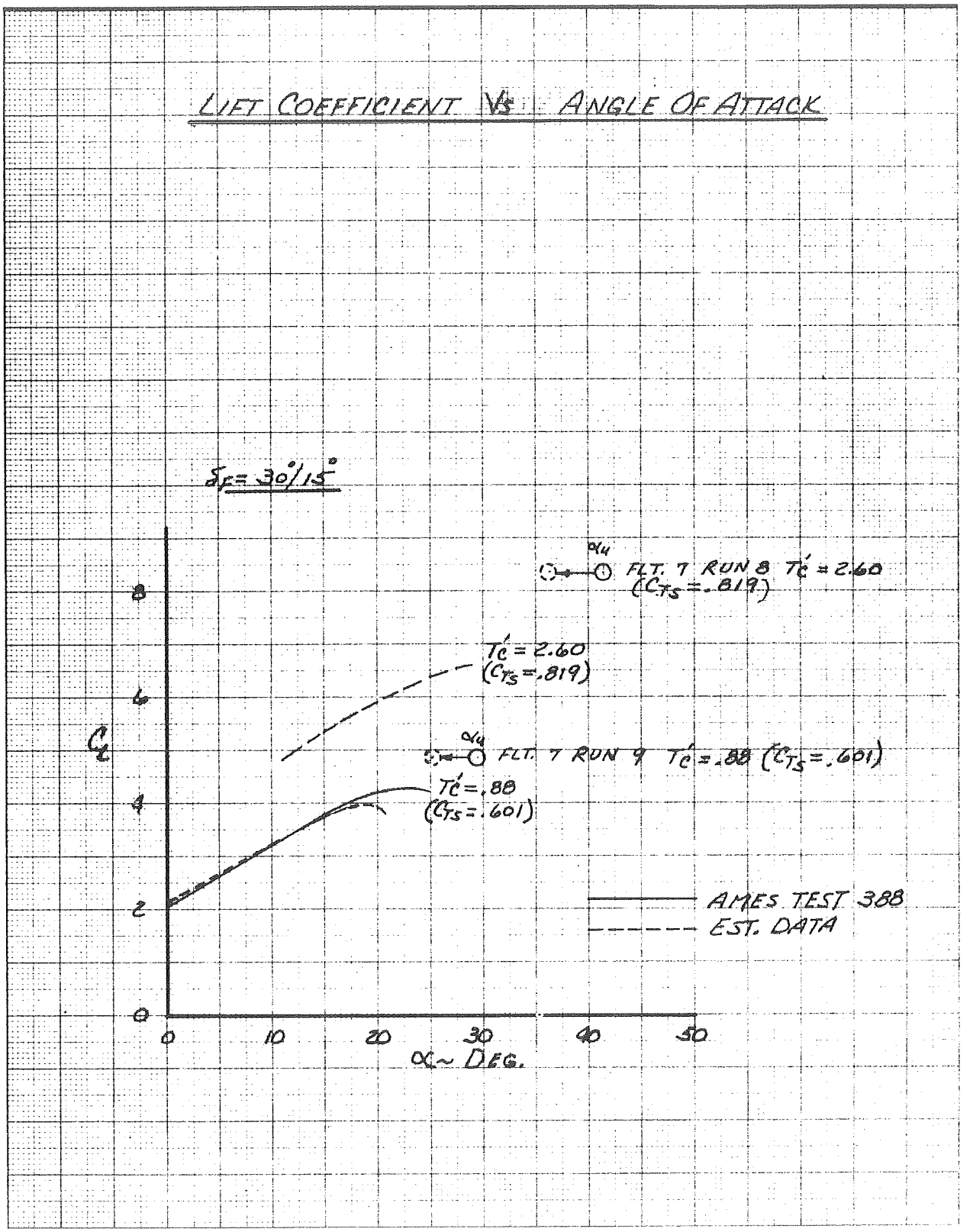
LIFT COEFFICIENT VS ANGLE OF ATTACK
$\delta_F = 30°/15°$
α_4
FLT. 7 RUN 8 $T_C' = 2.60$ ($C_{T_S} = .819$)
$T_C' = 2.60$ ($C_{T_S} = .819$)
α_4
FLT. 7 RUN 9 $T_C' = .88$ ($C_{T_S} = .601$)
$T_C' = .88$ ($C_{T_S} = .601$)
AMES TEST 388
EST. DATA
C_L
8
6
4
2
0
0
10
20
30
40
50
$\alpha \sim$ DEG.

FIGURE 256

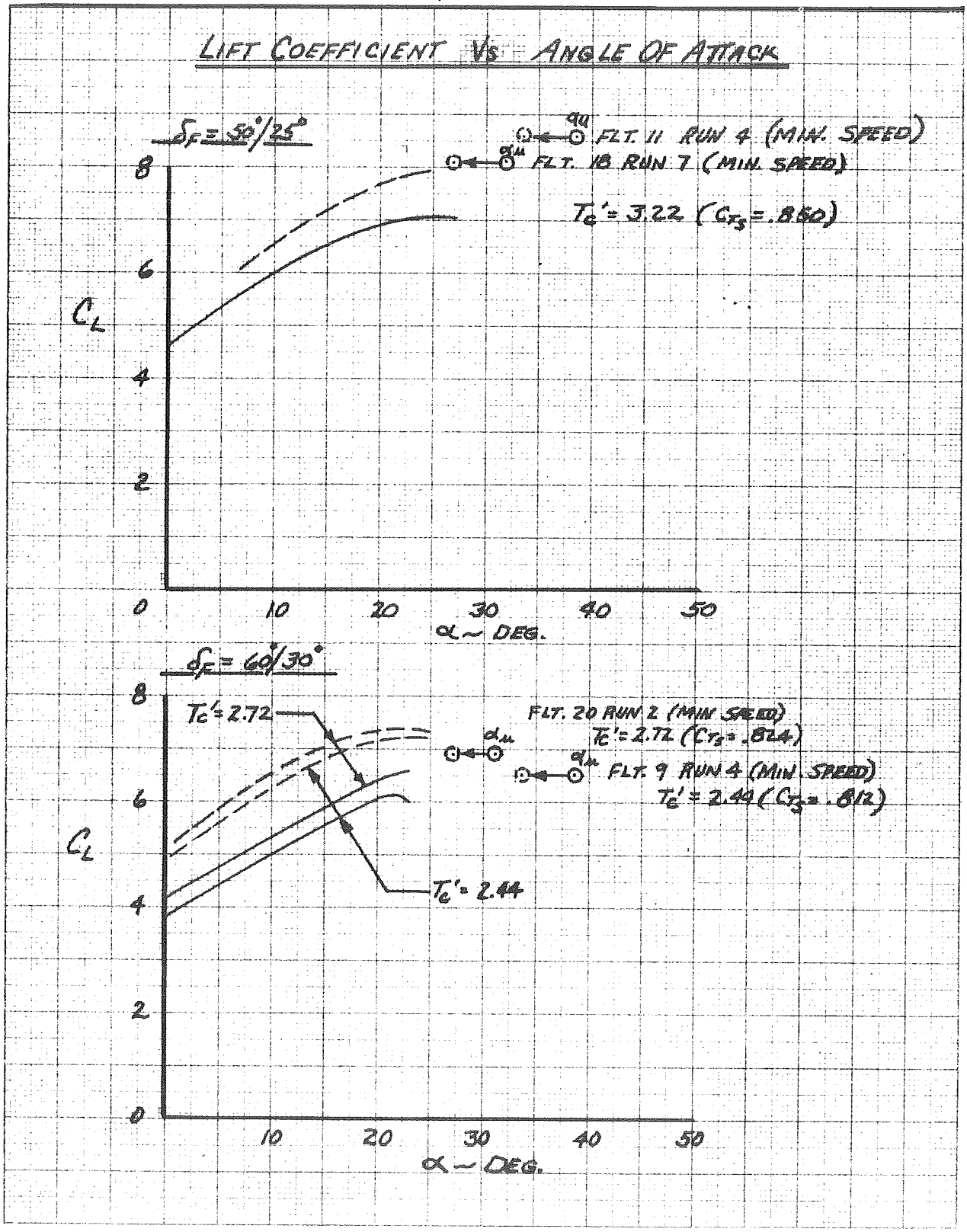
LIFT COEFFICIENT Vs ANGLE OF ATTACK
$\delta_F = 50°/25°$
q_{II} FLT. 11 RUN 4 (MIN. SPEED)
q_{III} FLT. 18 RUN 7 (MIN. SPEED)
$T_c' = 3.22$ ($C_{T_3} = .850$)
C_L
8
6
4
2
0
10
20
30
40
50
α ~ DEG.
$\delta_F = 60°/30°$
$T_c' = 2.72$
FLT. 20 RUN 2 (MIN SPEED)
$T_c' = 2.72$ ($C_{T_3} = .824$)
q_{III}
q_{III} FLT. 9 RUN 4 (MIN. SPEED)
$T_c' = 2.44$ ($C_{T_3} = .812$)
$T_c' = 2.44$
C_L
8
6
4
2
0
10
20
30
40
50
α ~ DEG.

FIGURE 26a

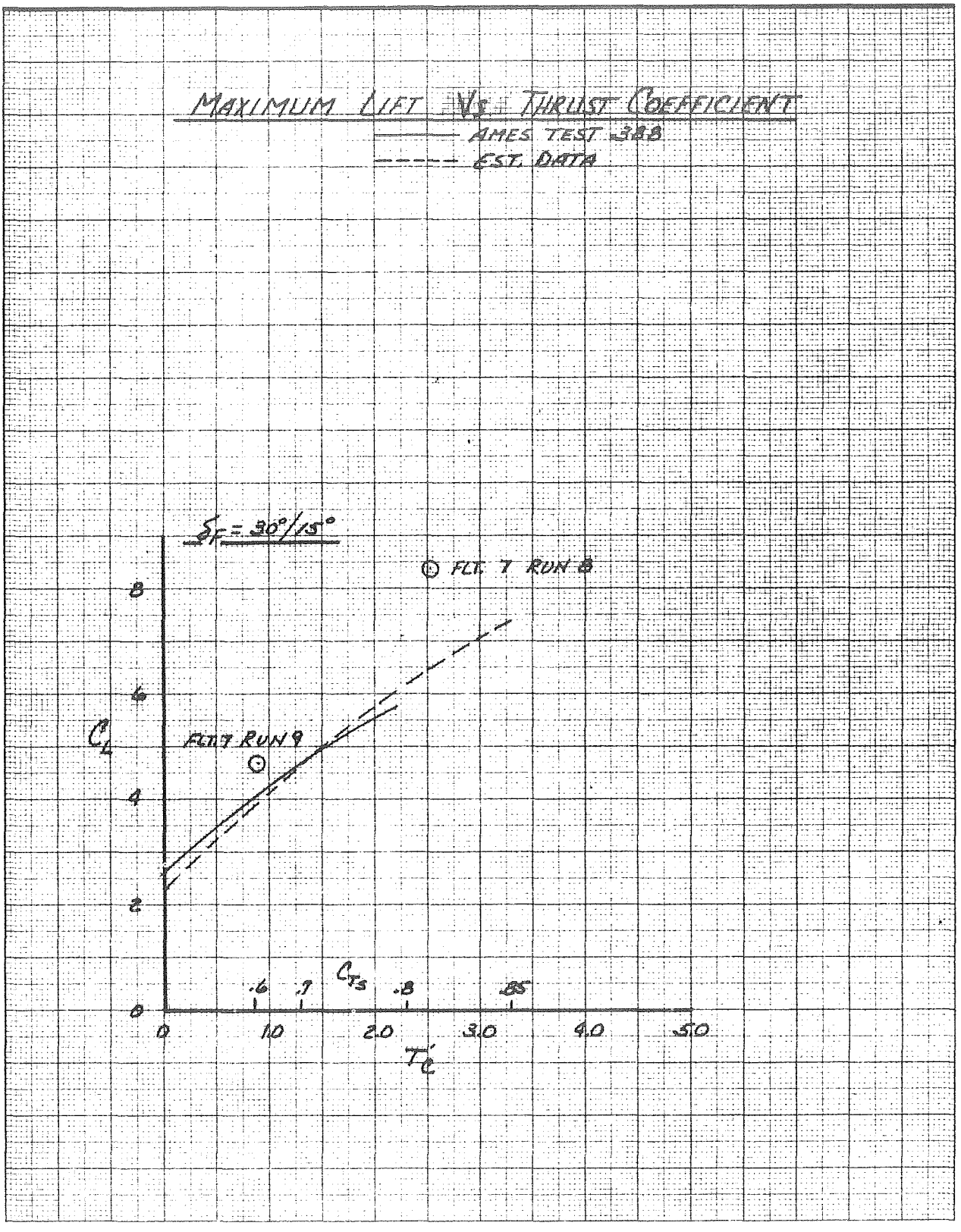
MAXIMUM LIFT Vs THRUST COEFFICIENT
AMES TEST 388
EST. DATA
$\delta_F = 30°/75°$
FLT 7 RUN 8
FLT 7 RUN 9
C_L
8
6
4
2
0
.6
.7
C_{T_S}
.8
.85
0
1.0
2.0
3.0
4.0
5.0
T_C

FIGURE 26b

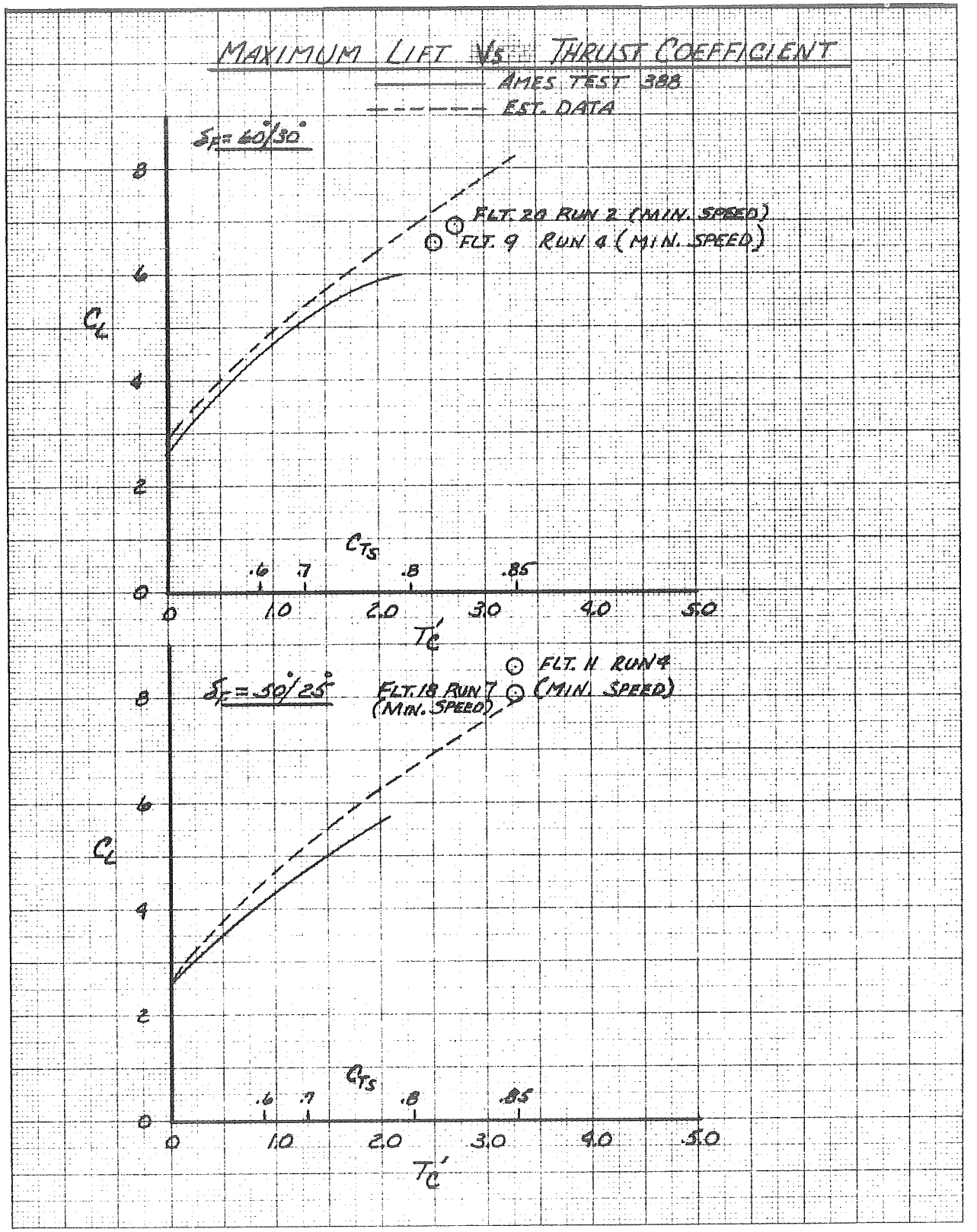
MAXIMUM LIFT Vs THRUST COEFFICIENT
AMES TEST 388
EST. DATA
δ_F = 40°/30°
FLT. 20 RUN 2 (MIN. SPEED)
FLT. 9 RUN 4 (MIN. SPEED)
C_L
C_{TS}
.6
.7
.8
.85
0
1.0
2.0
3.0
4.0
5.0
T_C'
δ_F = 50°/25°
FLT. 18 RUN 7 (MIN. SPEED)
FLT. 11 RUN 4 (MIN. SPEED)

FIGURE 272

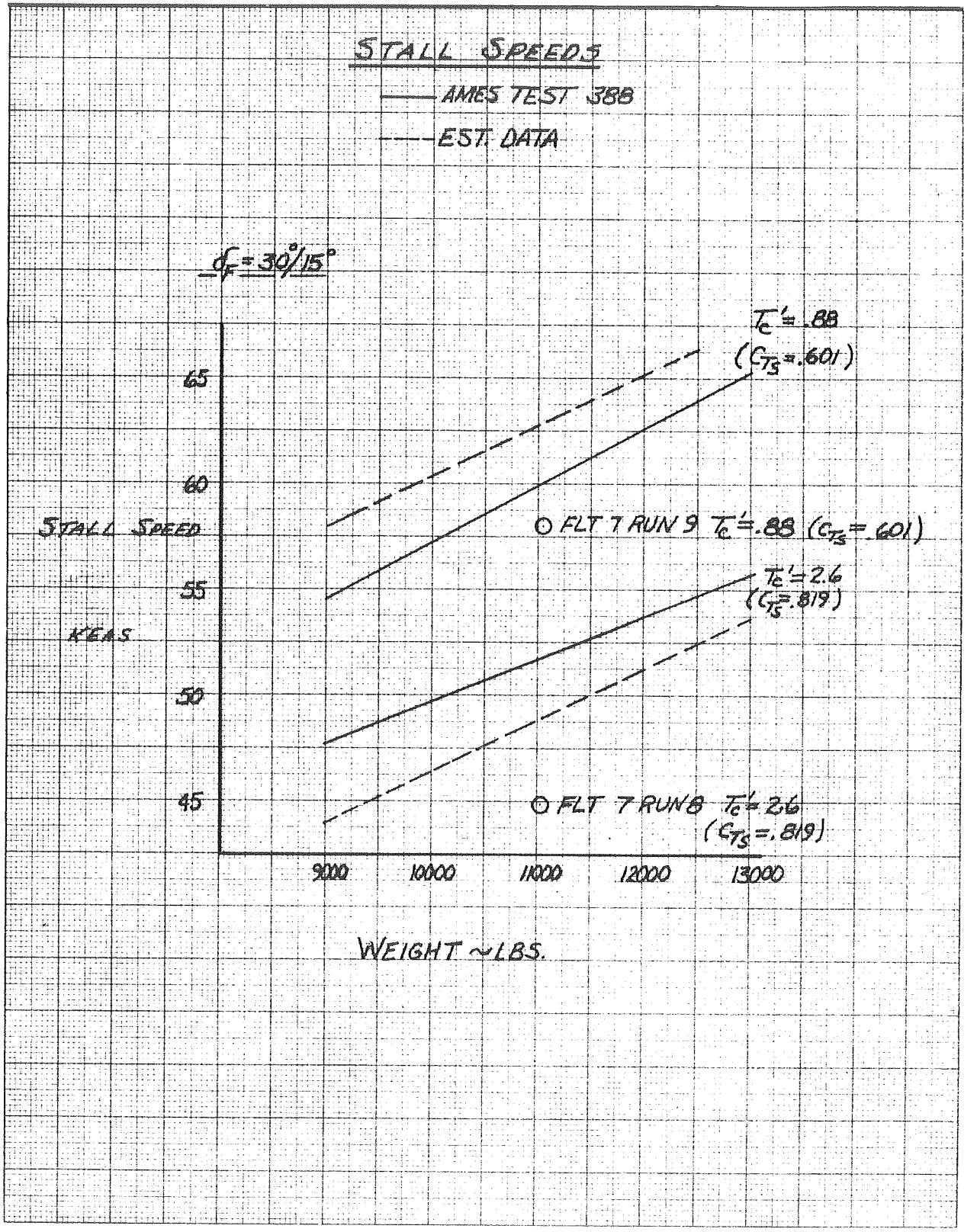
STALL SPEEDS
AMES TEST 388
EST. DATA
$\delta_F = 30°/15°$
$T_c' = .88$
$(C_{TS} = .601)$
65
60
STALL SPEED
55
KEAS
50
45
FLT 7 RUN 9 $T_c' = .88$ $(C_{TS} = .601)$
$T_c' = 2.6$
$(C_{TS} = .819)$
FLT 7 RUN 8 $T_c' = 2.6$
$(C_{TS} = .819)$
9000
10000
11000
12000
13000
WEIGHT ~ LBS.

FIGURE 27b

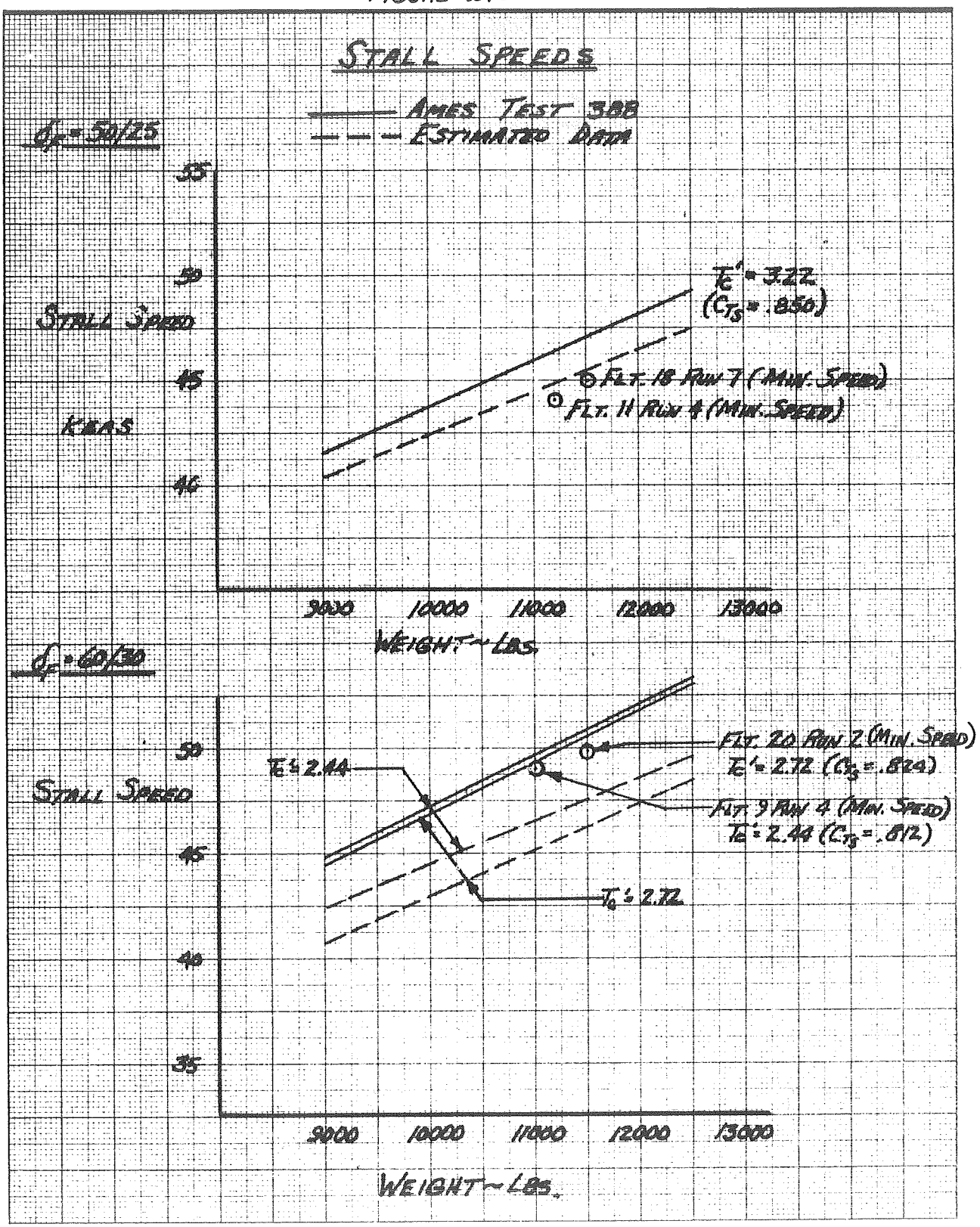
STALL SPEEDS
AMES TEST 388
ESTIMATED DATA
δ_f = 50/25
STALL SPEED
KIAS
35
40
45
50
T_c' = 3.22
(C_{T_S} = .850)
FLT. 18 RUN 7 (MIN. SPEED)
FLT. 11 RUN 4 (MIN. SPEED)
9000
10000
11000
12000
13000
WEIGHT ~ LBS.
δ_f = 60/30
STALL SPEED
35
40
45
50
T_c = 2.44
FLT. 20 RUN 2 (MIN. SPEED)
T_c' = 2.72 (C_{T_S} = .824)
FLT. 9 RUN 4 (MIN. SPEED)
T_c' = 2.44 (C_{T_S} = .812)
T_c = 2.72
9000
10000
11000
12000
13000
WEIGHT ~ LBS.


Time — Seconds
UP
DN
Time — Seconds
UP
DN
Time — Seconds
UP
DN
Time — Seconds
Time — Seconds

FIGURE 28a.

ALTITUDE ~ FT.
800
400
0
0
10
20
30
40
50
TIME ~ SEC.
UP
DOWN
θ ~ DEG.
20
10
0
UP
θ ~ DEG.
8
4
0
TIME ~ SEC.
φ ~ DEG.
10
0
RT
UP
ψ ~ DEG.
10
0
FOR AIRCRAFT ~ KTS
60
20
10
TIME ~ SEC.
TRAJECTORIES
SF = 30% MF* CYL. ORIF.
WT = 10,500 LBS. CG = 24.2%

FIGURE 28 b

TIME — SECONDS
TIME — SECONDS
TIME — SECONDS
TIME — SECONDS
RT.
LT.
UP
DN
UP
DN
MANEUVRING
ALT. 25K FEET

FIGURE 28C

TIME ~ SEC.
ALTITUDE ~ FT.
100
200
300
20 UP
θ ~ DEG.
10
0
0 2 4 6 8 10 12 14
8 UP
φ ~ DEG.
4
0
TIME ~ SEC.
4 RT.
φ ~ DEG.
0
LT.
20 UP
ψ ~ DEG.
0
20 DN
AIRSPEED ~ FPS
50
60
TIME ~ SEC.

FIGURE 29d

FIGURE 28E

Altitude - Ft
Time - Sec
Elev Def
Ail Def
Rud Def
Pitch Rate
Roll Rate
Yaw Rate
Vert Acc
Lat Acc
Long Acc
LANDING
FLT 11 RUN 12

FIGURE 28 F

ALTITUDE ~ FT.
100
0
TD
2
4
6
8
12
TIME ~ SECONDS
ELEV ~ DEG.
UP
10
0
10 DN
AIL ~ DEG.
UP
4
0
4 DN
RUD ~ DEG.
4
RT.
2
0
2
LT.
TIME ~ SECONDS
10
UP
0
10
DN
ROLL ~ DEG.
70
60
50
0
2
4
6
8
10
12
TIME ~ SECONDS
LANDING
FLAPS 50°/25°
INERTIA = 1.0 SLUG-FT²
CG = 25% MAC
ELEV 12
RUDDER 12

FIGURE 28 G

ALTITUDE - FT.
100
0
TD
2
4
6
8
TIME — SECONDS
ELEV. DEG.
20 UP
10
0
DN
TIME — SECONDS
AILER. DEG.
UP
6
4
0
TIME — SECONDS
RT.
2
0
TIME — SECONDS
L.T.
UP
10
5
DN
TIME — SECONDS
ALTITUDE - FT.
50
-50
TIME — SECONDS

FIGURE 28h

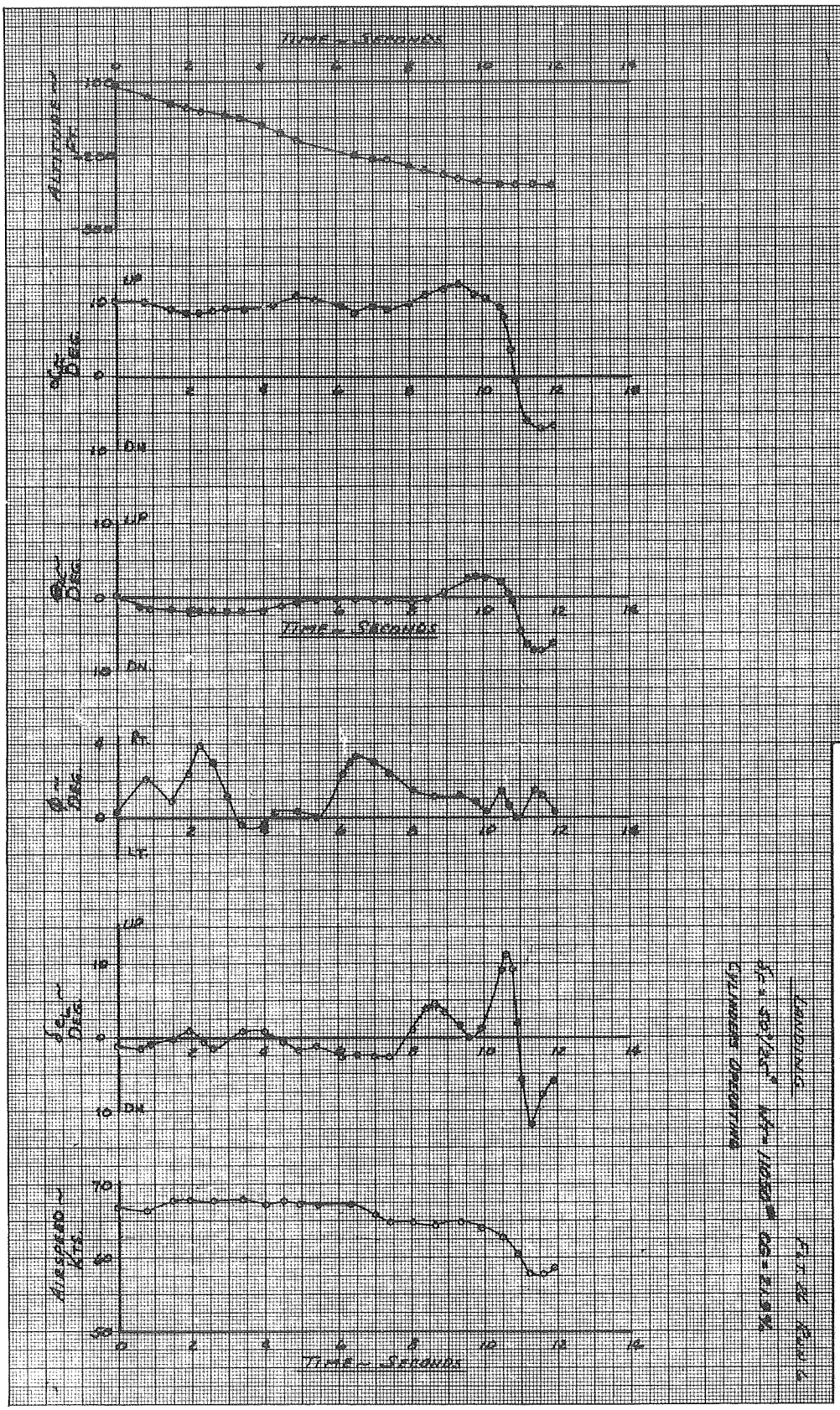
TIME - SECONDS
ALTITUDE - FEET
PITCH ANGLE - DEG
UP
DN
ROLL ANGLE - DEG
RT
LT
YAW ANGLE - DEG
LF
RT
HEADING - DEG

FIGURE 28i

FIGURE 29a

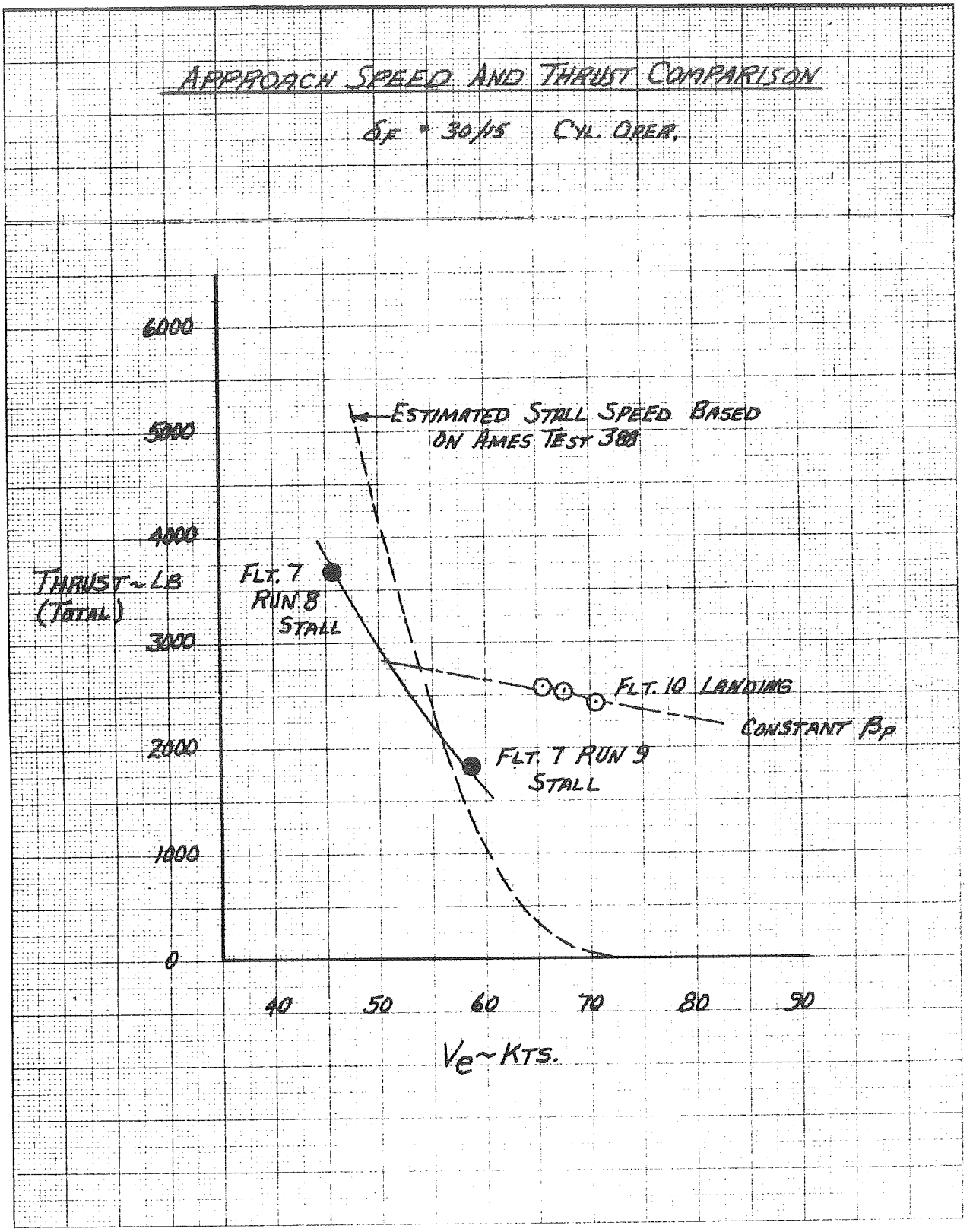
APPROACH SPEED AND THRUST COMPARISON
δ_F = 30/15 CYL. OPER.
6000
5000
4000
3000
2000
1000
0
THRUST ~ LB (TOTAL)
ESTIMATED STALL SPEED BASED ON AMES TEST 388
FLT. 7 RUN 8 STALL
FLT. 10 LANDING
CONSTANT β_p
FLT. 7 RUN 9 STALL
40
50
60
70
80
90
V_e ~ KTS.

FIGURE 296

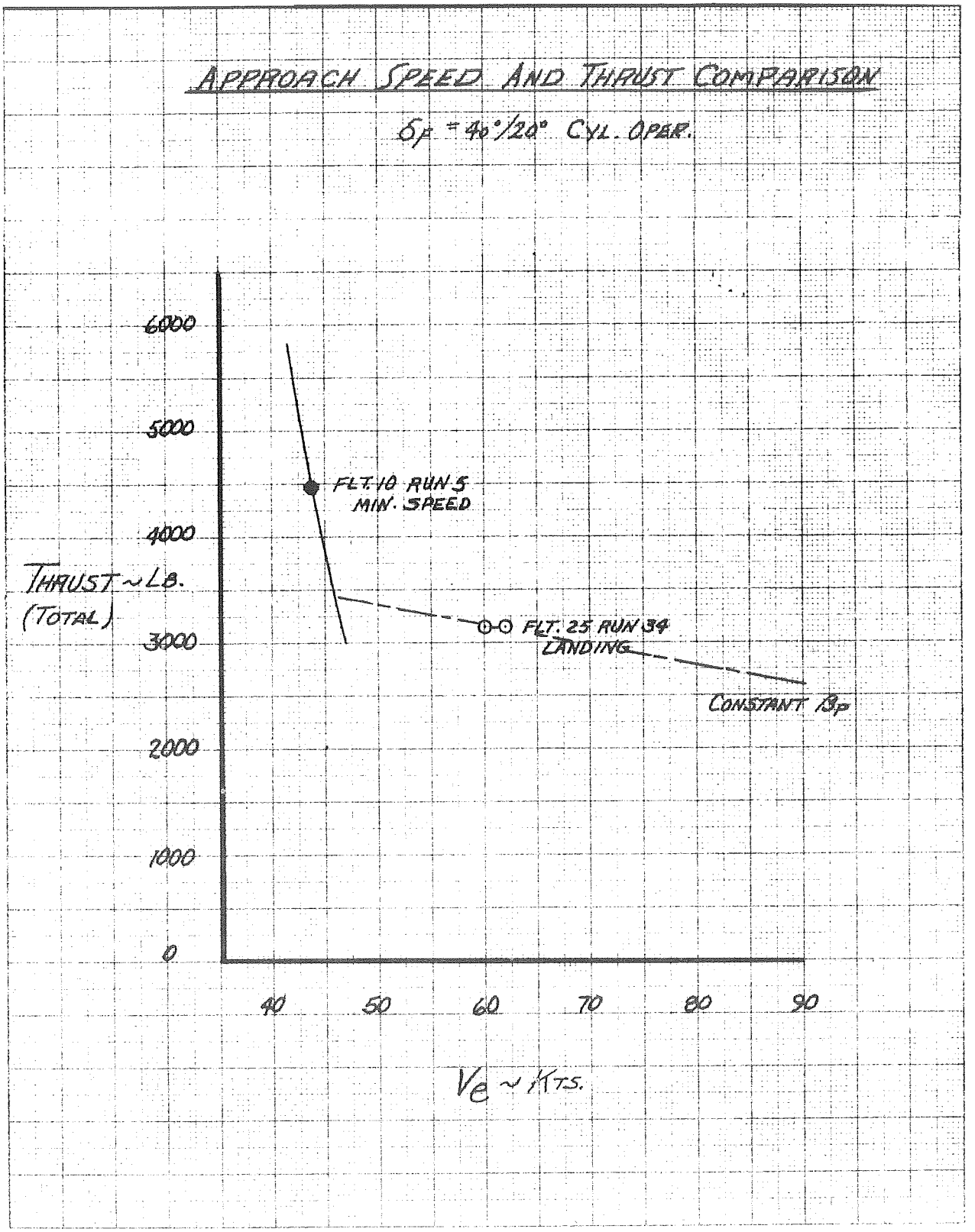
APPROACH SPEED AND THRUST COMPARISON
δ_F = 40°/20° CYL. OPER.
6000
5000
4000
3000
2000
1000
0
THRUST ~ LB. (TOTAL)
FLT. 10 RUN 5 MIN. SPEED
FLT. 25 RUN 34 LANDING
CONSTANT β_P
40
50
60
70
80
90
V_e ~ KTS.

FIGURE 29C

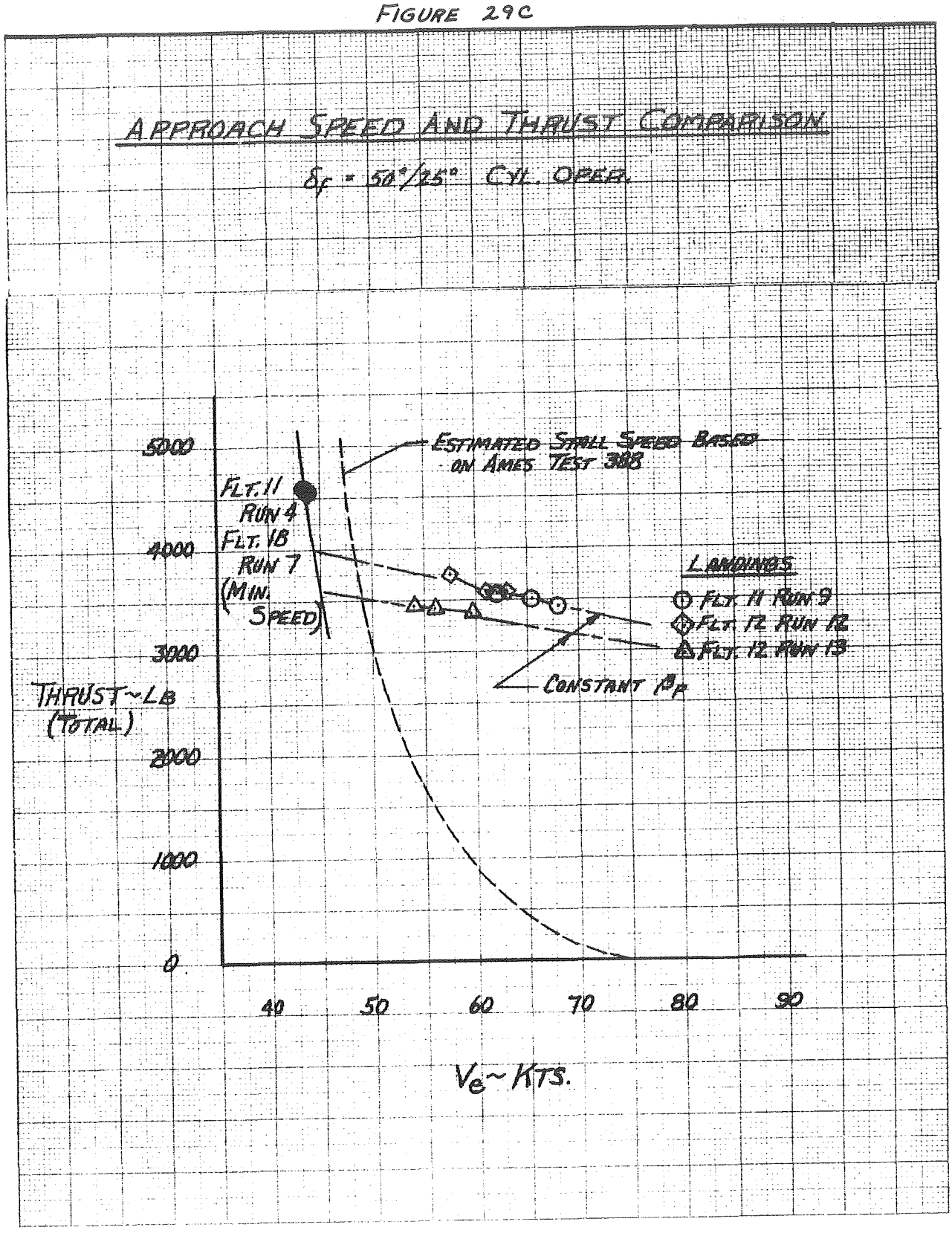
APPROACH SPEED AND THRUST COMPARISON
δ_f = 50°/25° CYL. OPER.
ESTIMATED STALL SPEED BASED ON AMES TEST 388
FLT. 11 RUN 4
FLT. 18 RUN 7 (MIN. SPEED)
LANDINGS
FLT. 11 RUN 9
FLT. 12 RUN 12
FLT. 12 RUN 13
CONSTANT β_p
THRUST ~ LB (TOTAL)
5000
4000
3000
2000
1000
0
40
50
60
70
80
90
V_e ~ KTS.

FIGURE 30a

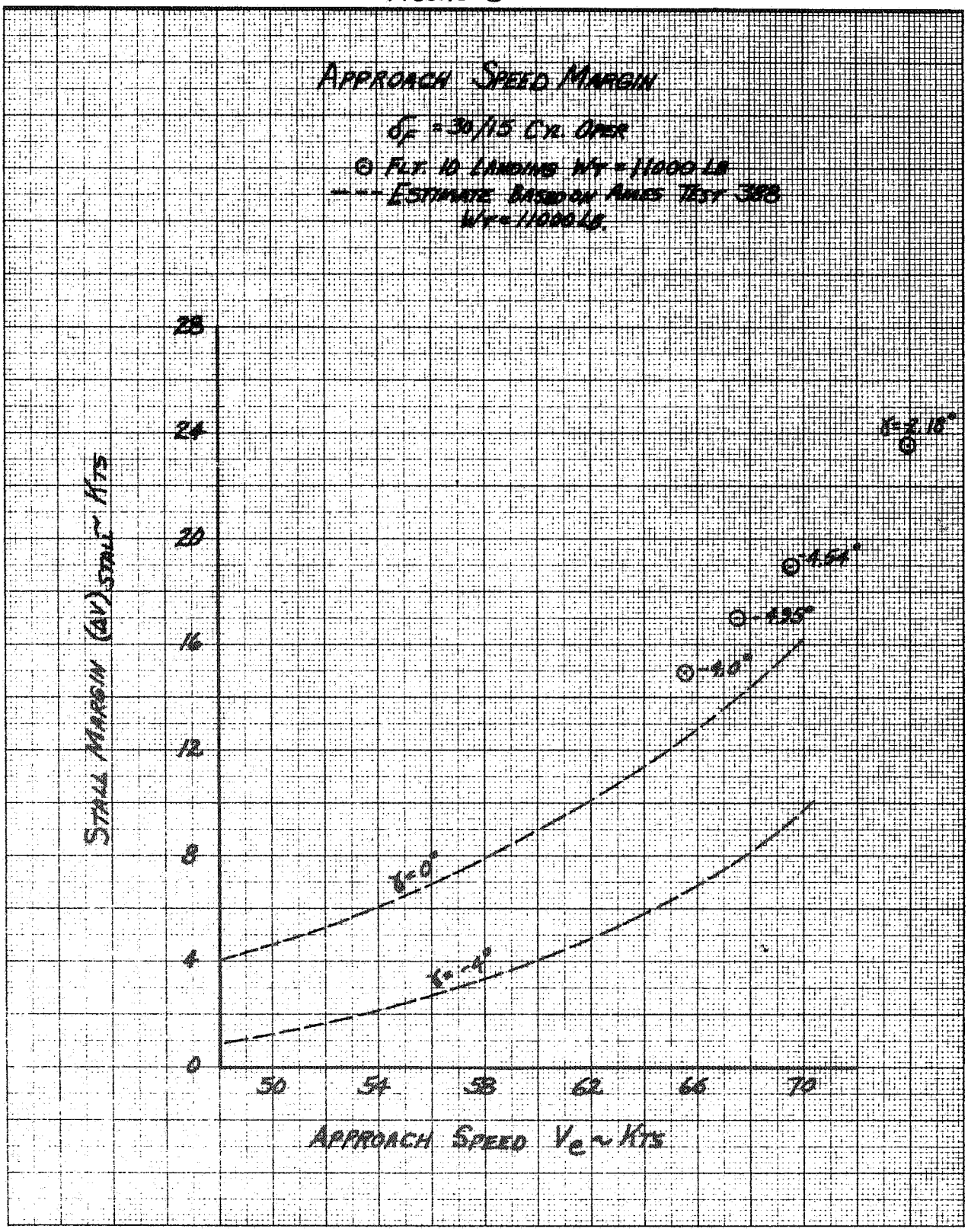
APPROACH SPEED MARGIN
δ_F = 30/15 CFG. OPER.
⊙ FLT. 10 LANDING W/T = 11000 LB
---- ESTIMATE BASED ON ARES TEST 388
W/T = 11000 LB.
28
24
20
16
12
8
4
0
STALL MARGIN (ΔV)STALL ~ KTS
γ = 2.18°
γ = -4.54°
γ = -4.35°
γ = -4.0°
γ = 0°
γ = -4°
50
54
58
62
66
70
APPROACH SPEED V_e ~ KTS

FIGURE 30b

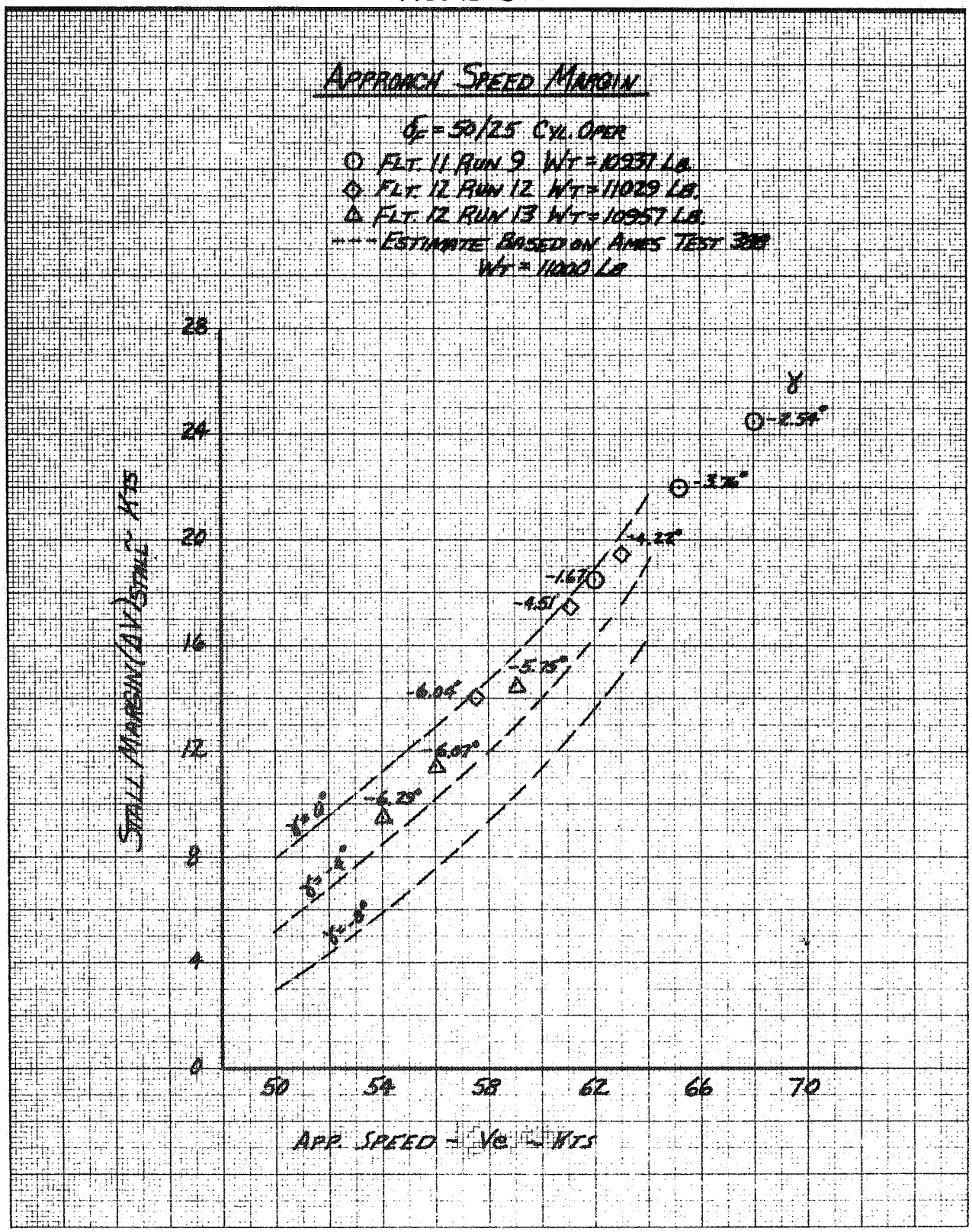
APPROACH SPEED MARGIN
δ_F = 50/25 CYL. OPER
○ FLT. 11 RUN 9 W_T = 10931 LB.
◇ FLT. 12 RUN 12 W_T = 11029 LB.
△ FLT. 12 RUN 13 W_T = 10957 LB.
---- ESTIMATE BASED ON AMES TEST
W_T = 11000 LB
STALL MARGIN (ΔV)STALL - KTS
APP. SPEED - Ve - KTS
γ
-2.54°
-3.76°
-4.22°
-1.67°
-4.51°
-5.75°
-6.04°
-6.07°
-6.28°
γ = 0°
γ = 4°
γ = 8°
0
4
8
12
16
20
24
28
50
54
58
62
66
70

FIGURE 31

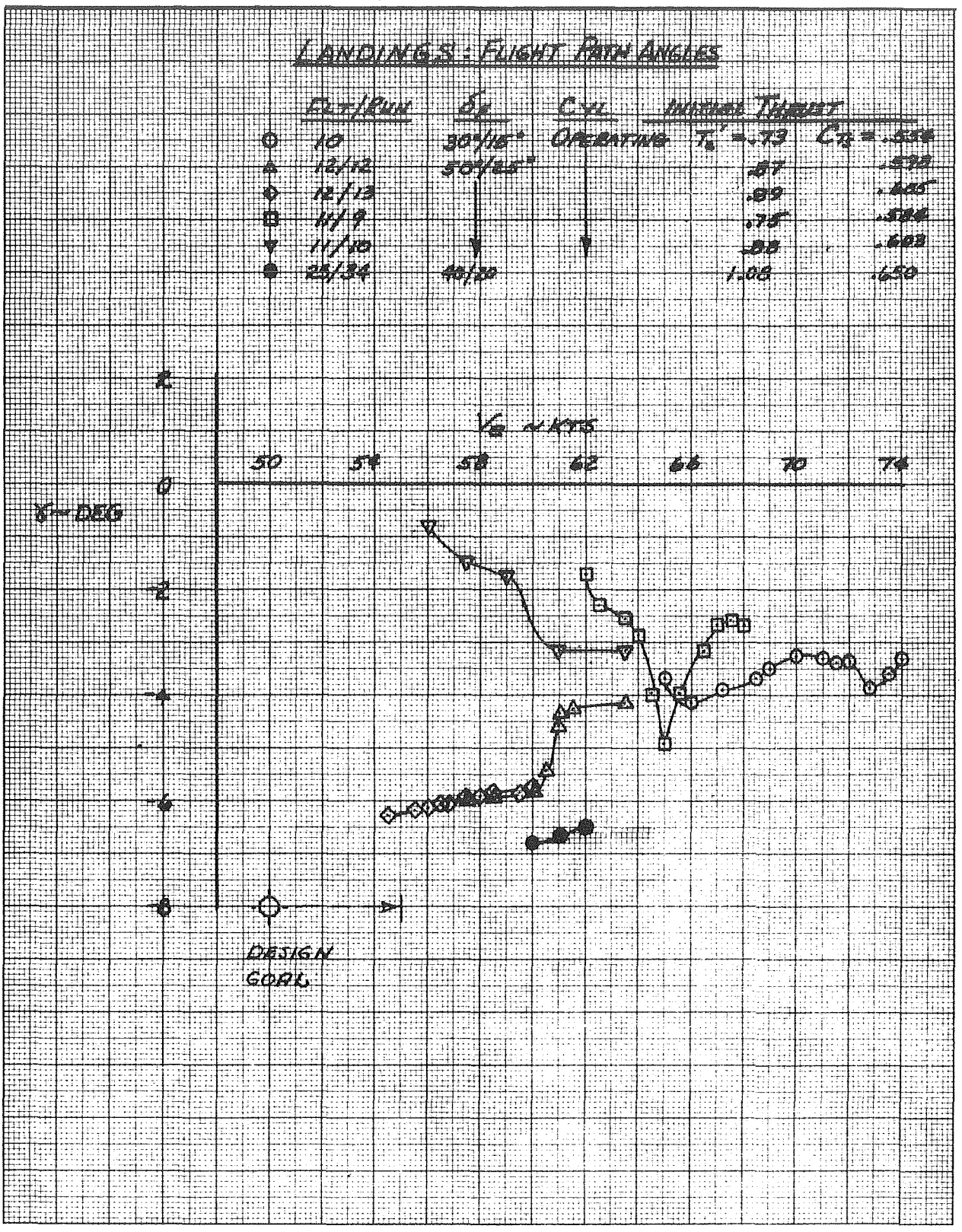
LANDING G.S. : FLIGHT PATH ANGLES
$C_{L_T}/C_{L_{MAX}}$
δ_F
C_{YL}
INDICATED THRUST
OPERATING
$T_c' = .73$
$C_{T_c} = .536$
10
30°/15°
.67
.592
12/12
.89
.625
11/9
.75
.584
11/10
.88
.603
25/24
40/30
1.08
.650
V_{IAS} ~ KTS
50
54
58
62
66
70
74
γ — DEG
0
-2
-4
-6
-8
DESIGN GOAL

FIGURE 32a

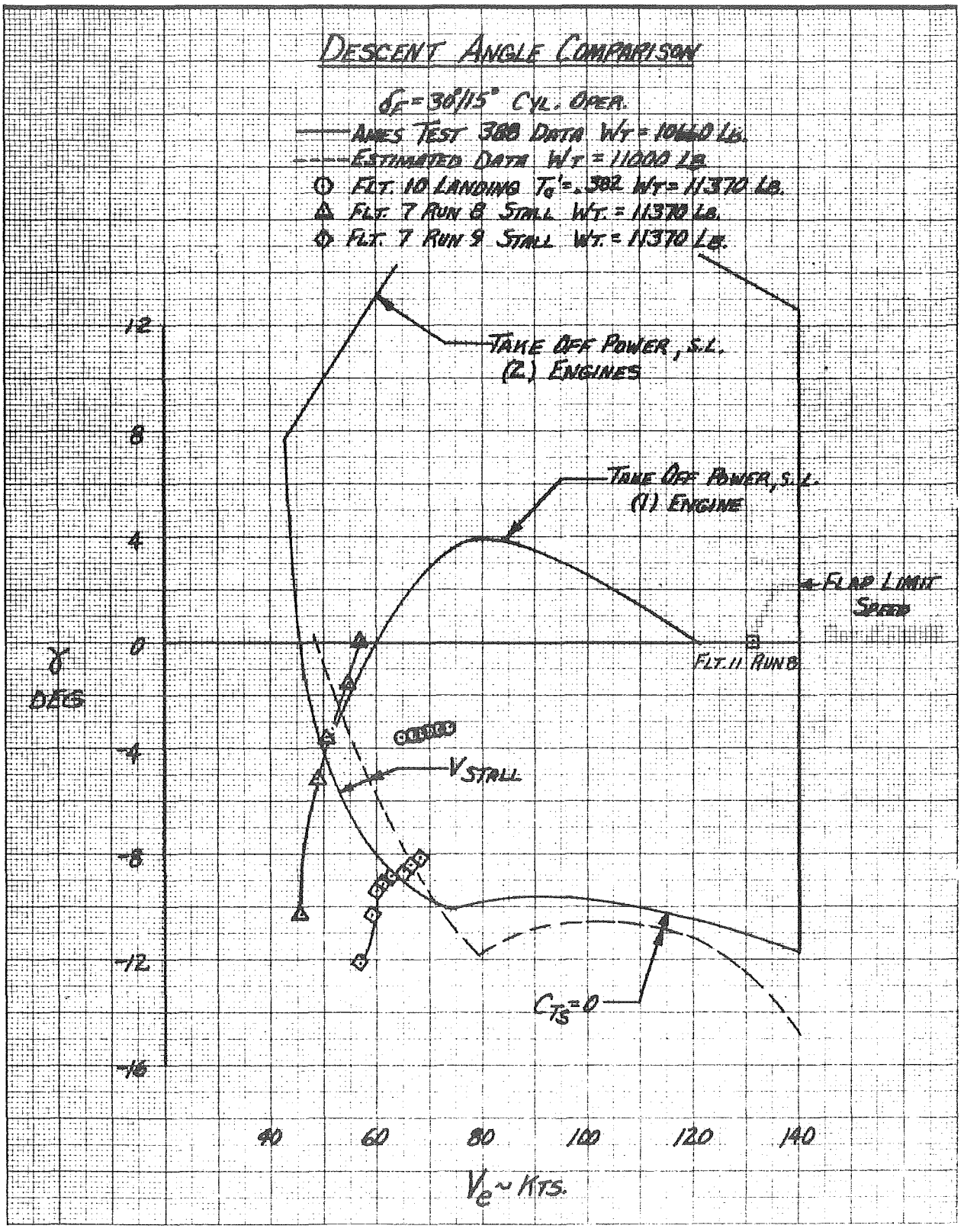
DESCENT ANGLE COMPARISON
$\delta_F = 30°/15°$ CYL. OPER.
AMES TEST 388 DATA WT = 10440 LB.
ESTIMATED DATA WT = 11000 LB.
FLT. 10 LANDING $T_C' = .382$ WT = 11370 LB.
FLT. 7 RUN 8 STALL WT. = 11370 LB.
FLT. 7 RUN 9 STALL WT. = 11370 LB.
TAKE OFF POWER, S.L. (2) ENGINES
TAKE OFF POWER, S.L. (1) ENGINE
FLAP LIMIT SPEED
FLT. 11 RUN 8
V_{STALL}
$C_{TS}=0$
12
8
4
0
-4
-8
-12
-16
γ DEGS
40
60
80
100
120
140
V_e ~ KTS.

FIGURE 32b

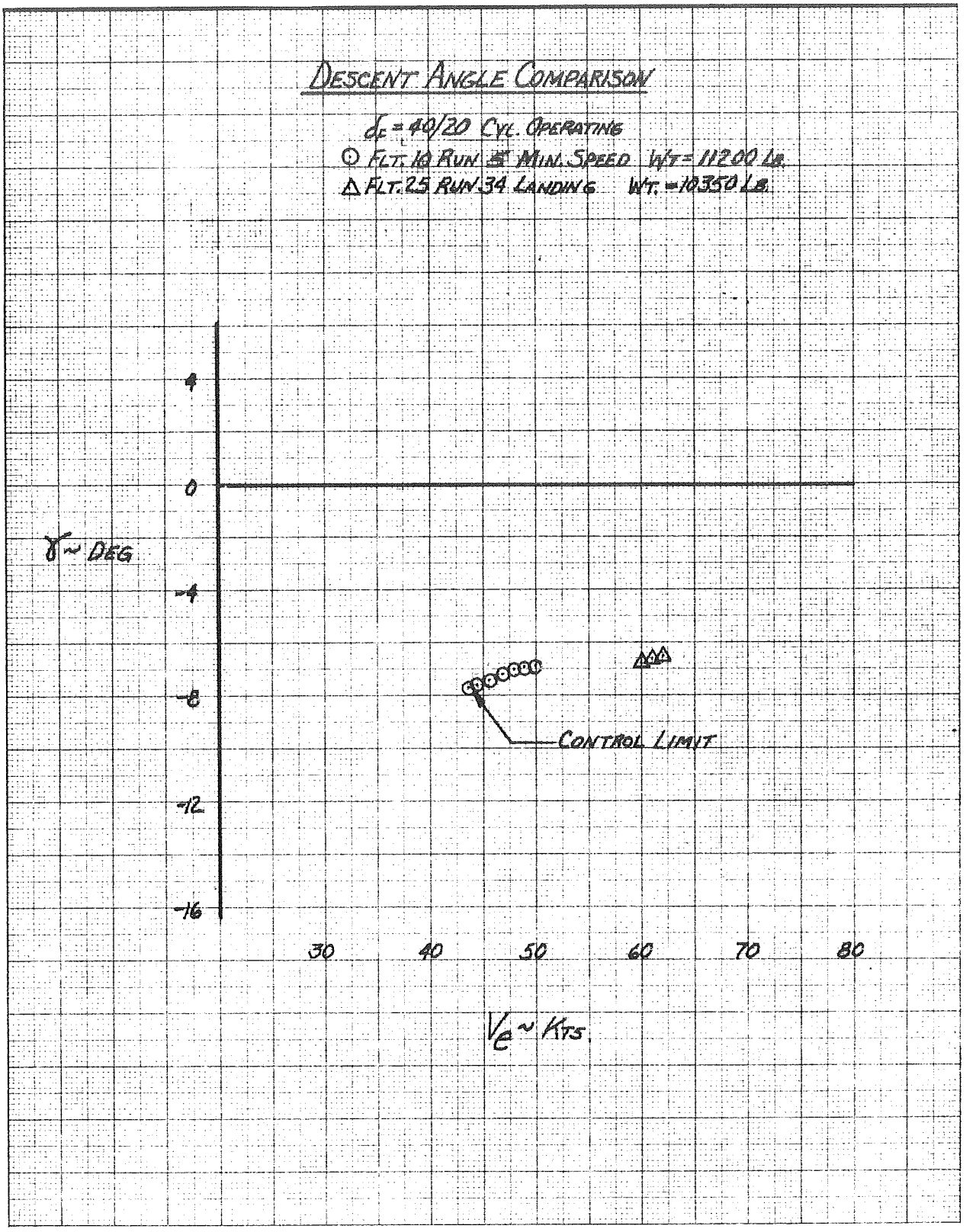
DESCENT ANGLE COMPARISON
δ_c = 40/20 CYL. OPERATING
○ FLT. 10 RUN 3 MIN. SPEED WT = 11200 LB.
△ FLT. 25 RUN 34 LANDING WT. = 10350 LB.
4
0
-4
-8
-12
-16
γ ~ DEG
CONTROL LIMIT
30
40
50
60
70
80
V_e ~ KTS.

FIGURE 32C

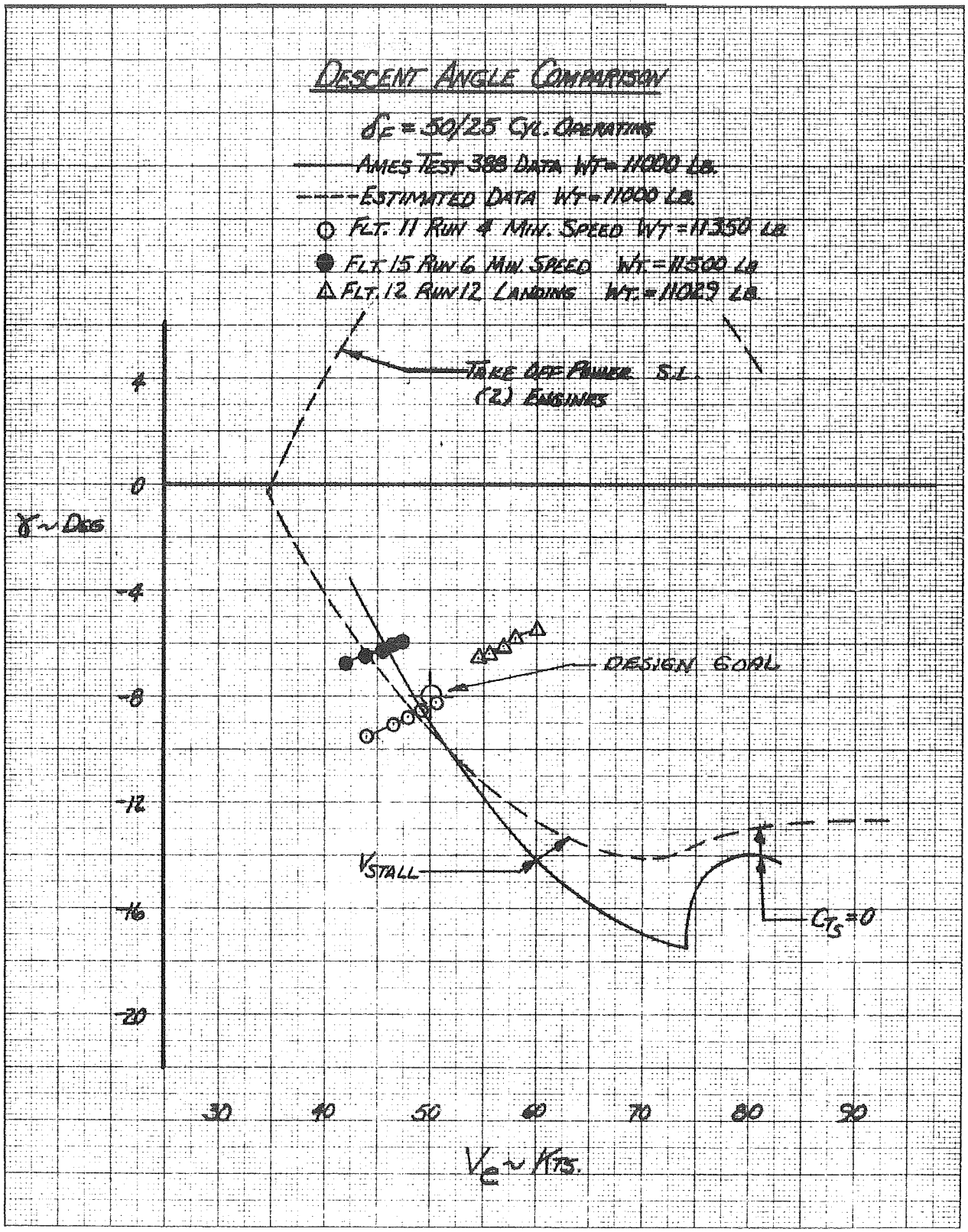
DESCENT ANGLE COMPARISON
δ_E = 50/25 CYL. OPERATING
AMES TEST 388 DATA WT = 11000 LB.
ESTIMATED DATA WT = 11000 LB.
FLT. 11 RUN 4 MIN. SPEED WT = 11350 LB.
FLT. 15 RUN 6 MIN. SPEED WT = 11500 LB.
FLT. 12 RUN 12 LANDING WT. = 11029 LB.
TAKE OFF POWER S.L. (2) ENGINES
DESIGN GOAL
V_{STALL}
C_{T_S} = 0
4
0
-4
-8
-12
-16
-20
γ ~ DEG
30
40
50
60
70
80
90
V_E ~ KTS.

FIGURE 32d

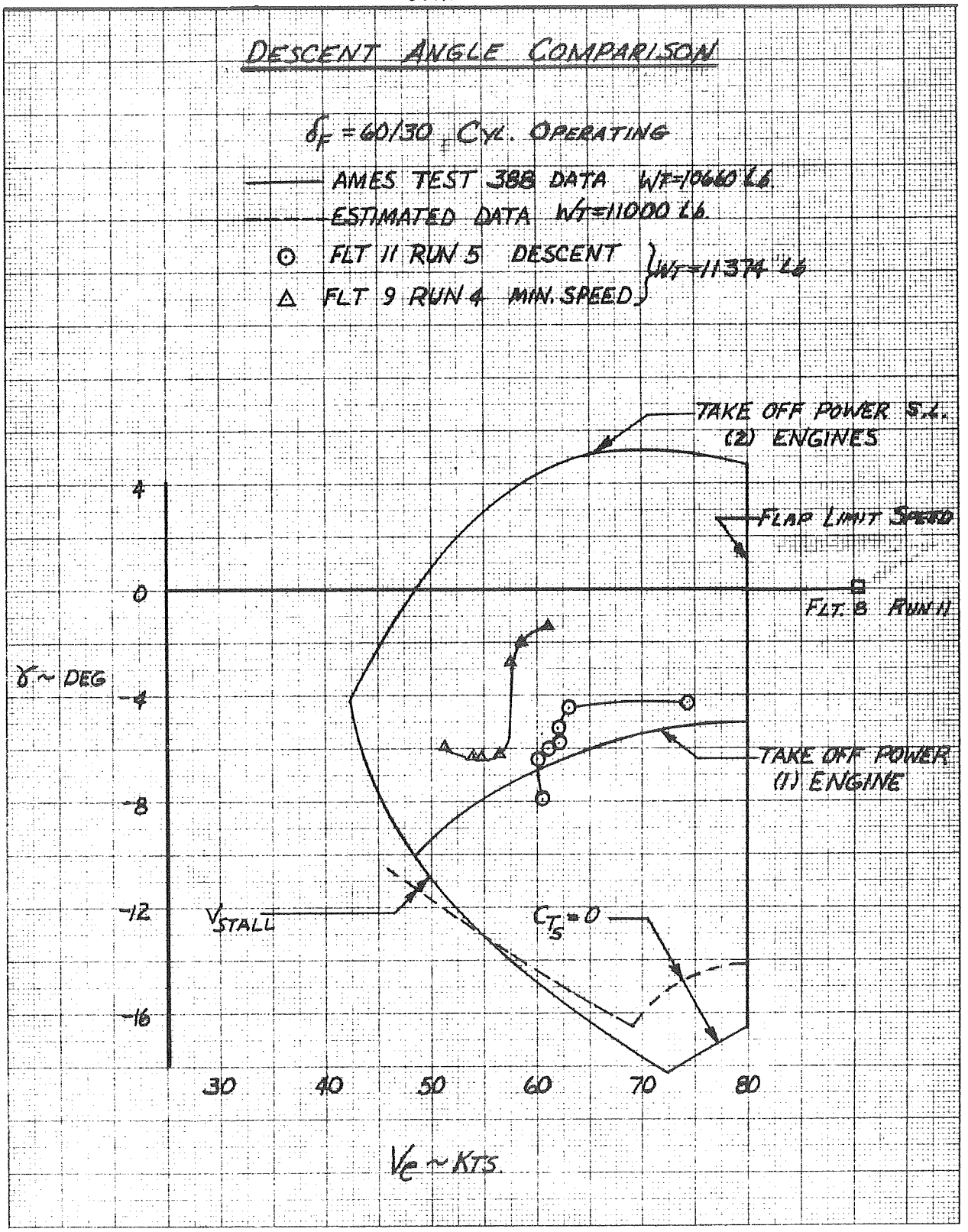
DESCENT ANGLE COMPARISON
δ_F = 60/30 , Cyl. OPERATING
AMES TEST 388 DATA W/T=10660 Lb
ESTIMATED DATA W/T=11000 Lb
FLT 11 RUN 5 DESCENT
FLT 9 RUN 4 MIN. SPEED
W/T=11374 Lb
TAKE OFF POWER S.L. (2) ENGINES
FLAP LIMIT SPEED
FLT. B RUN 11
TAKE OFF POWER (1) ENGINE
C_{T_S} = 0
V_{STALL}
γ ~ DEG
4
0
-4
-8
-12
-16
30
40
50
60
70
80
V_E ~ KTS

FIGURE 33a

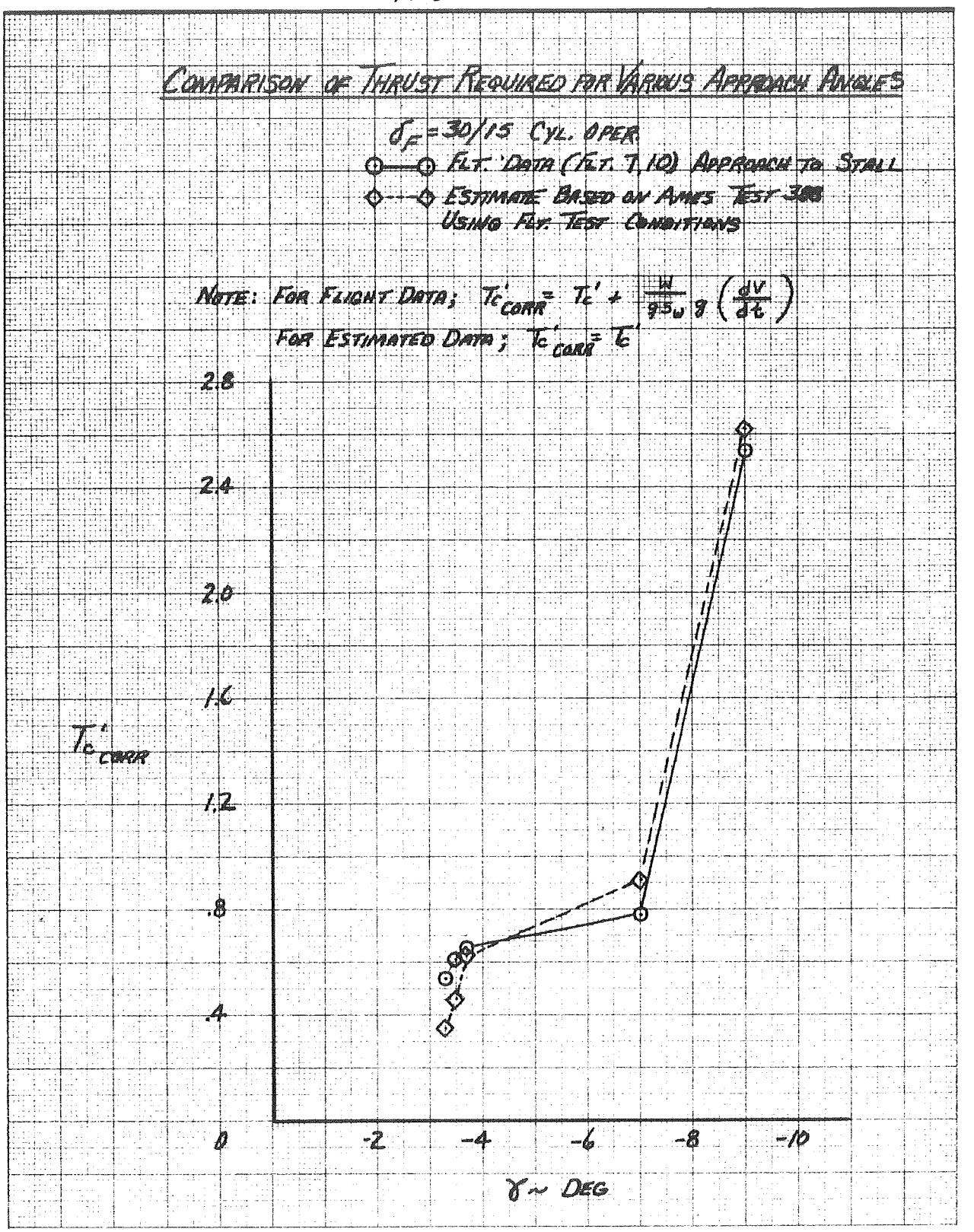
COMPARISON OF THRUST REQUIRED FOR VARIOUS APPROACH ANGLES
δ_F = 30/15 CYL. OPER.
FLT. DATA (FLT. 7, 10) APPROACH TO STALL
ESTIMATE BASED ON AMES TEST 308 USING FLT. TEST CONDITIONS
NOTE: FOR FLIGHT DATA; $T_{c'_{CORR}} = T_{c'} + \frac{W}{95_w} g \left(\frac{dV}{dt}\right)$
FOR ESTIMATED DATA; $T_{c'_{CORR}} = T_{c'}$
$T_{c'_{CORR}}$
2.8
2.4
2.0
1.6
1.2
.8
.4
0
-2
-4
-6
-8
-10
γ ~ DEG

FIGURE 33b

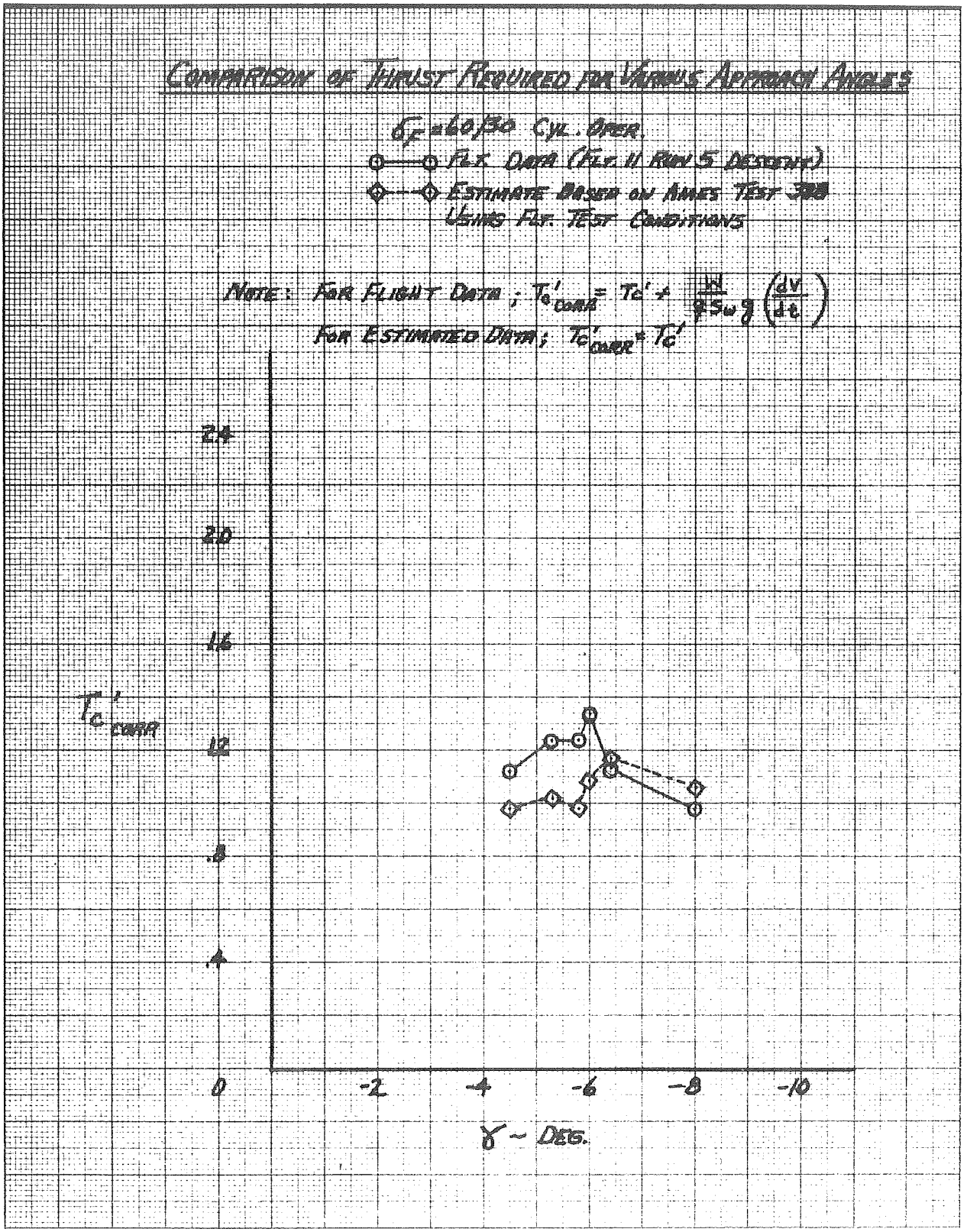
COMPARISON OF THRUST REQUIRED FOR VARIOUS APPROACH ANGLES
δ_F = 60/30 CYL. OPER.
FLT. DATA (FLT. 11 RUN 5 DESCENT)
ESTIMATE BASED ON AMES TEST 308 USING FLT. TEST CONDITIONS
NOTE: FOR FLIGHT DATA; $T_{c'_{CORR}} = T_{c'} + \frac{W}{\rho S w g}\left(\frac{dV}{dt}\right)$
FOR ESTIMATED DATA; $T_{c'_{CORR}} = T_{c'}$
$T_{c'_{CORR}}$
2.4
2.0
1.6
1.2
.8
.4
0
-2
-4
-6
-8
-10
γ ~ DEG.

FIGURE 34a

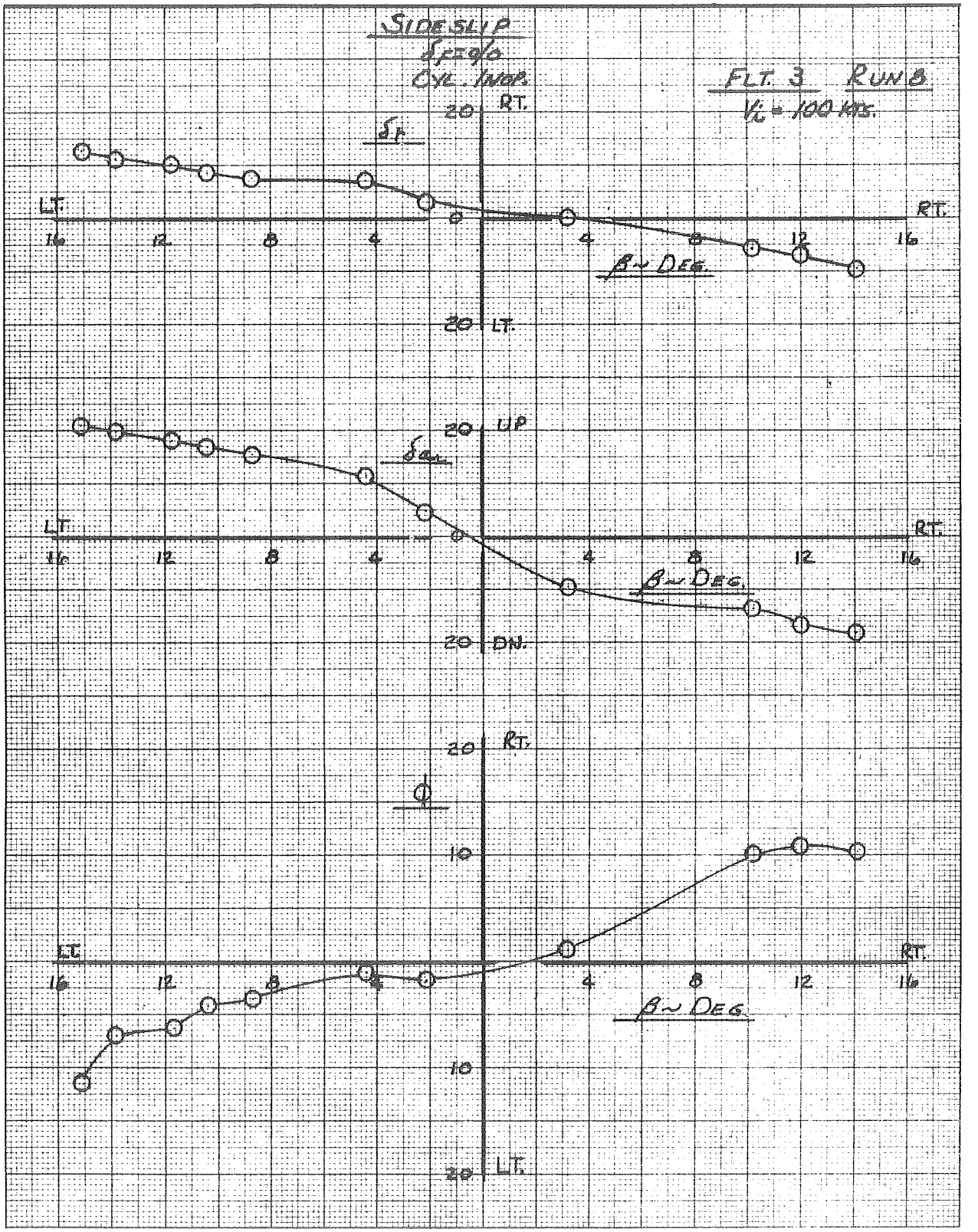
SIDESLIP
δ FREE
CYL. INDIC.
FLT. 3 RUN 8
Vi = 100 KTS.
δr
RT.
LT.
β ~ DEG.
δa
UP
DN.
Q
16
12
8
4
0
20
10

FIGURE 34 b

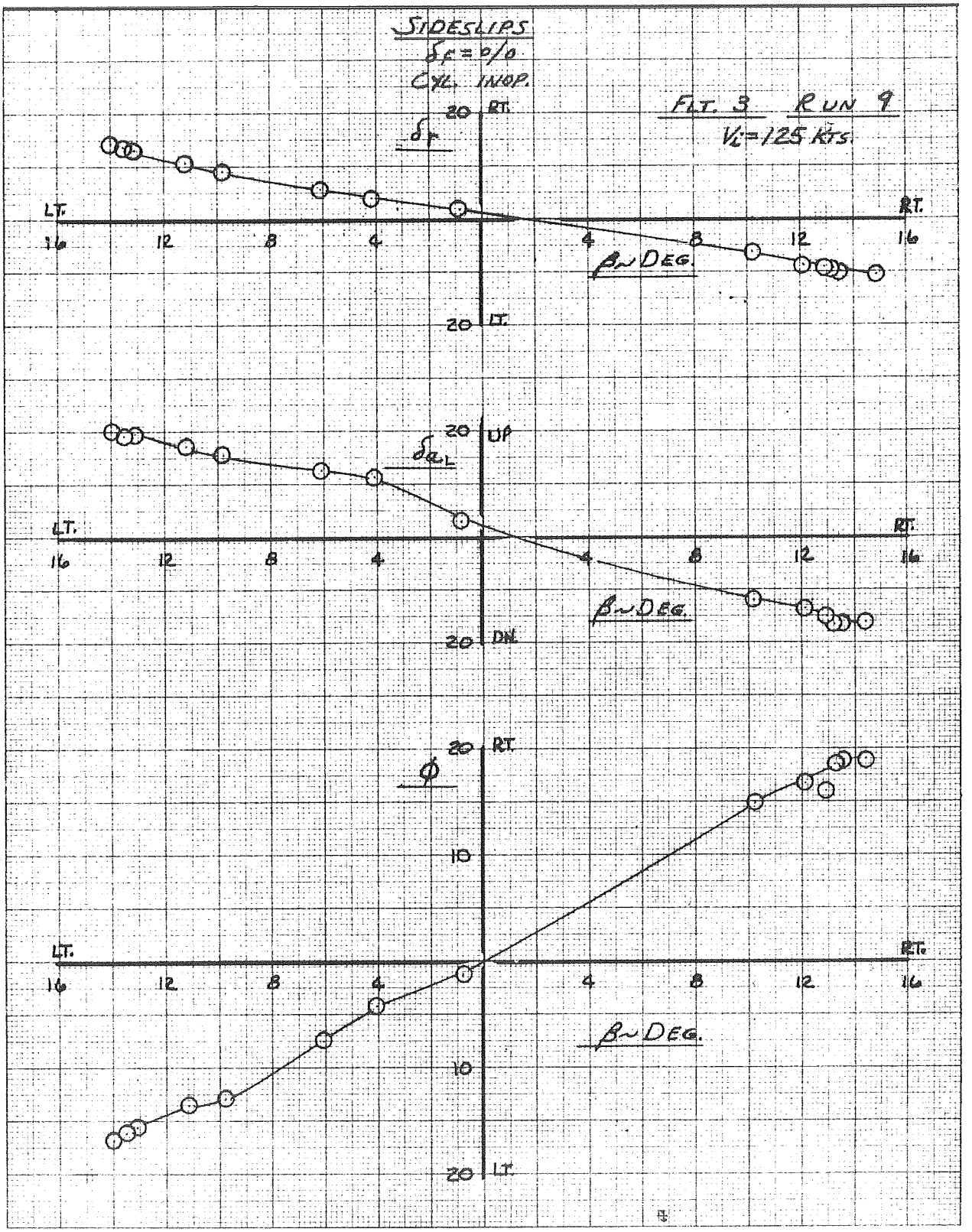
SIDESLIPS
δ_f = 0/0
CYL. INOP.
FLT. 3 RUN 9
V_i = 125 KTS.
δ_r
20 RT.
20 LT.
LT. 16 12 8 4
4 8 12 16 RT.
β ~ DEG.
δ_{a_L}
20 UP
20 DN.
ϕ
20 RT.
10
20 LT.

FIGURE 34C

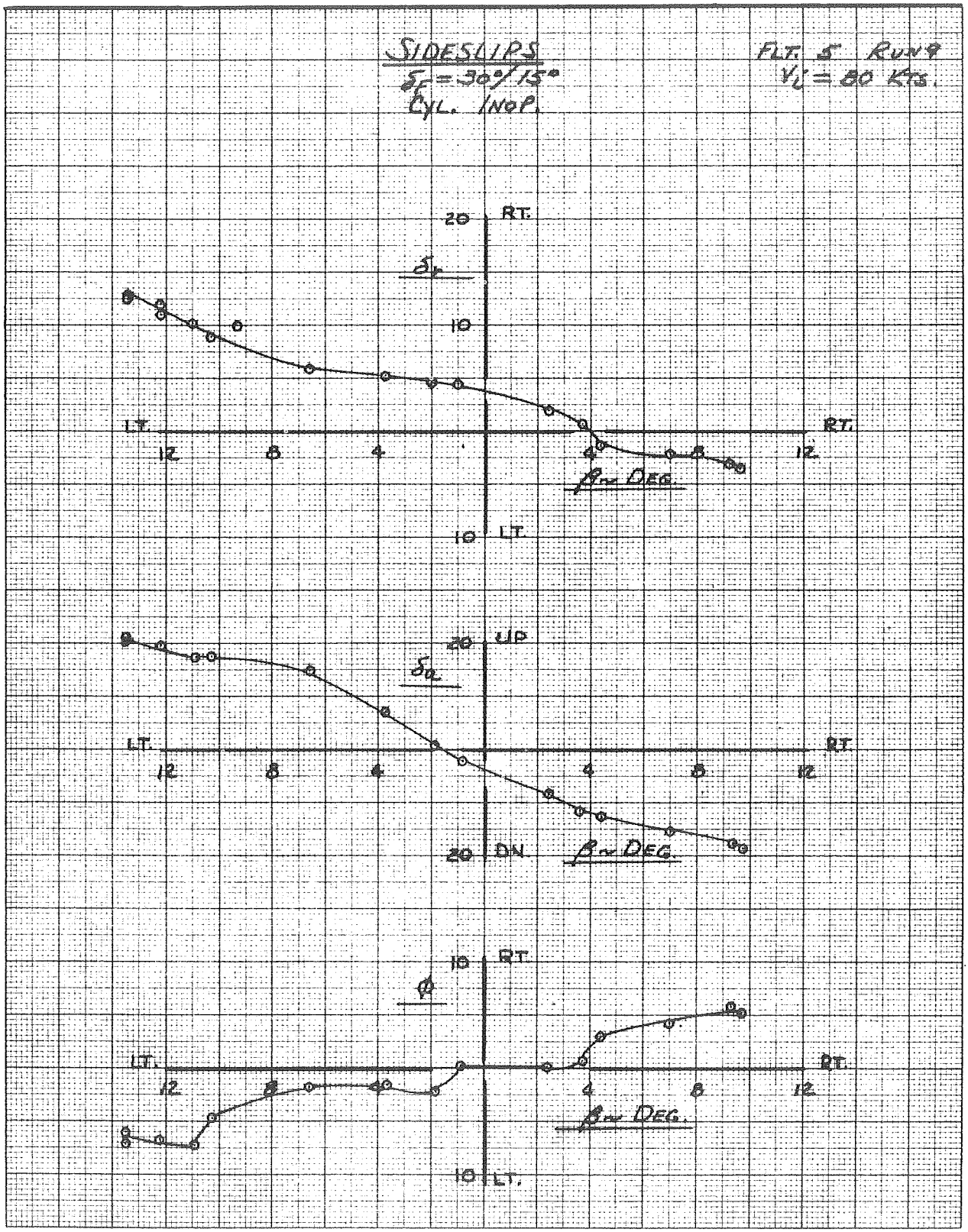
SIDESLIPS
$\delta_F = 30°/15°$
CYL. INOP.
FLT. 5 RUN 9
$V_i = 80$ KTS.
20
RT.
δ_r
10
LT.
12
8
4
4
8
12
β_m DEG.
10
LT.
20
UP
δ_a
20
DN.
β_m DEG.
10
RT.
ϕ
10
LT.
β_m DEG.

FIGURE 34d

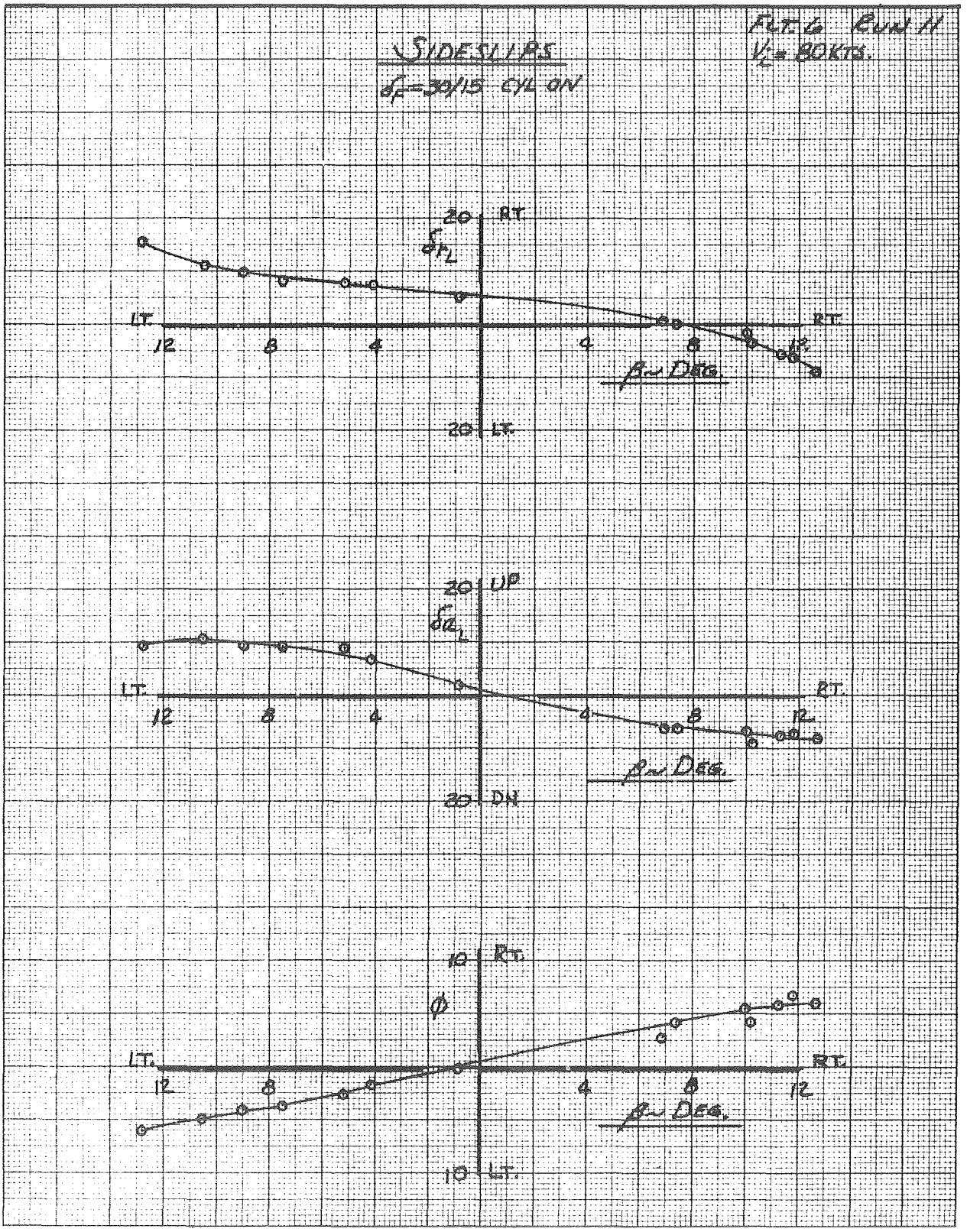
FLT. CONDITION
V_c = 80 KTS.
SIDESLIPS
δ_F = 30/15 CYL ON
20 RT
δ_{r_L}
LT.
RT.
12
8
4
4
8
12
β ~ DEG.
20 LT.
20 UP
δ_{a_L}
LT.
RT.
12
8
4
4
8
12
β ~ DEG.
20 DN
10 RT.
ϕ
LT.
RT.
12
8
4
8
12
β ~ DEG.
10 LT.

FIGURE 34E

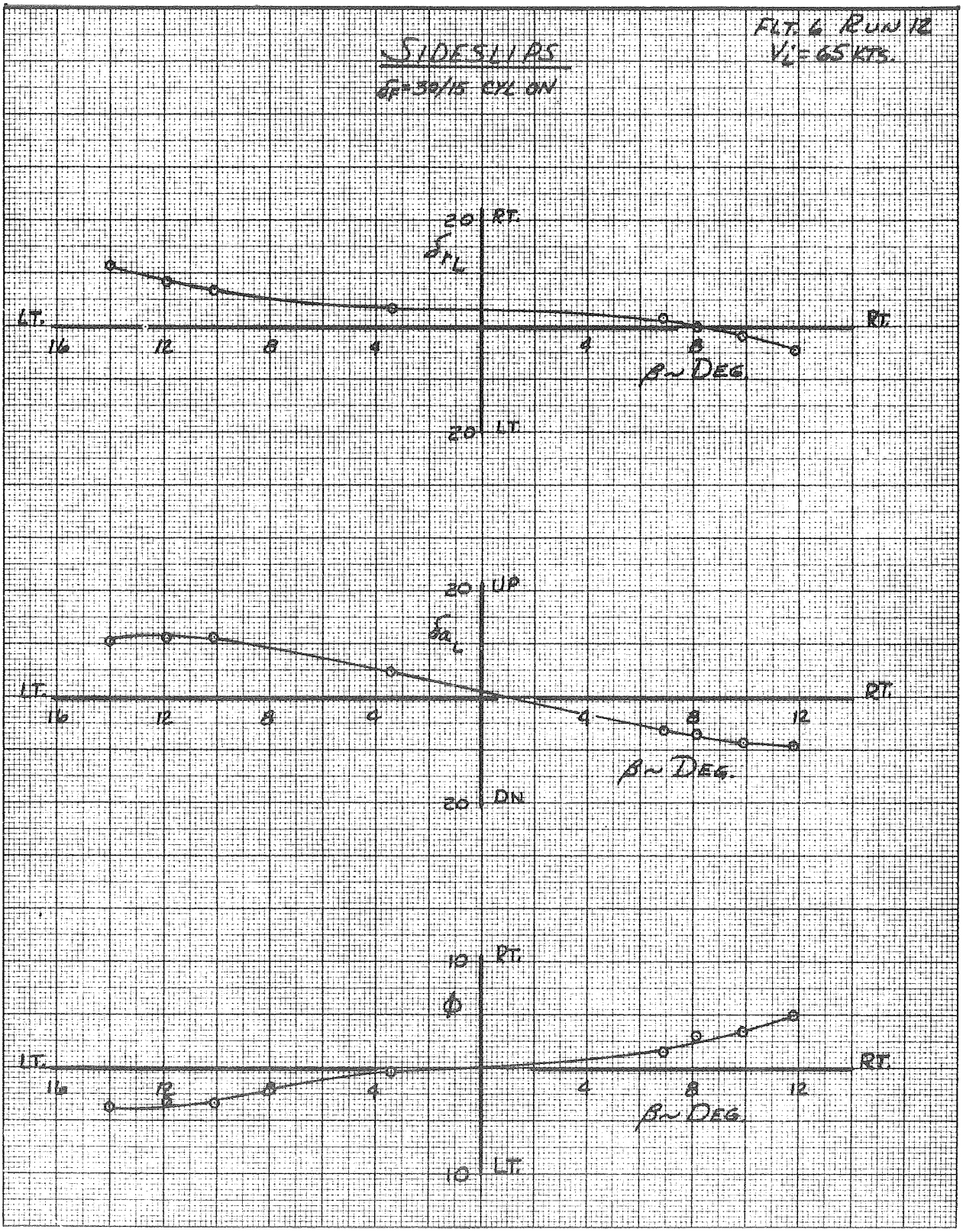
SIDESLIPS
δ_F=30/15 CYL ON
FLT. & RUN 12
V_i=65 KTS.
20 RT.
δ_{RL}
LT.
RT.
16 12 8 4 4 8 12
β~DEG.
20 LT.
20 UP
δ_{AL}
LT.
RT.
16 12 8 4 4 8 12
β~DEG.
20 DN.
10 RT.
ϕ
LT.
RT.
16 12 8 4 4 8 12
β~DEG.
10 LT.

FIGURE 34 f

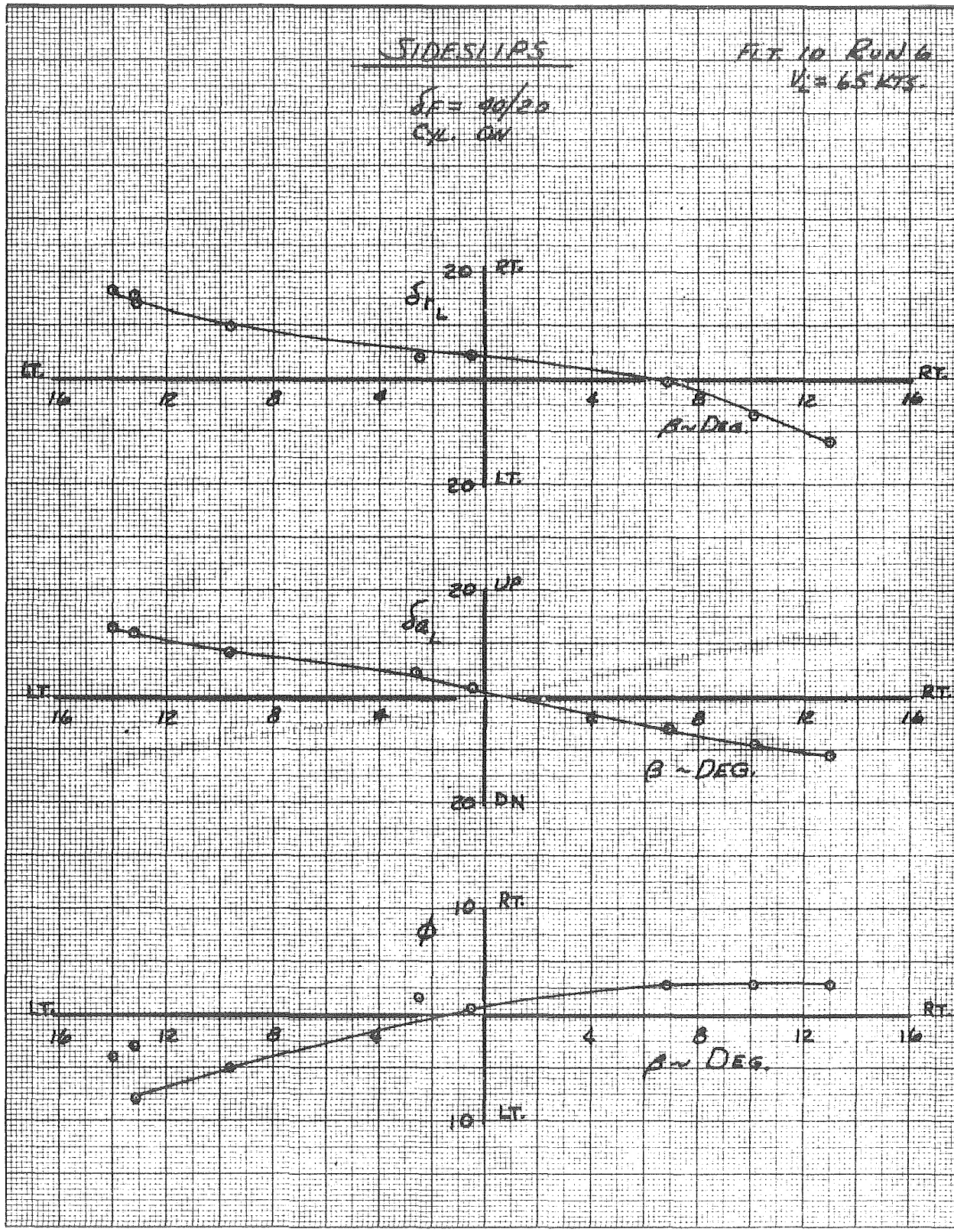
SIDESLIPS
FLT. 10 RUN 6
V_i = 65 KTS.
δ_F = 40/20
CYL. CAM
20 RT.
δ_{r_L}
LT. 16 12 8 4 4 8 12 16 RT.
β ~ DEG.
20 LT.
20 UP
δ_{e_L}
LT. 16 12 8 4 4 8 12 16 RT.
β ~ DEG.
20 DN
10 RT.
ϕ
LT. 16 12 8 4 8 12 16 RT.
β ~ DEG.
10 LT.

FIGURE 34 G

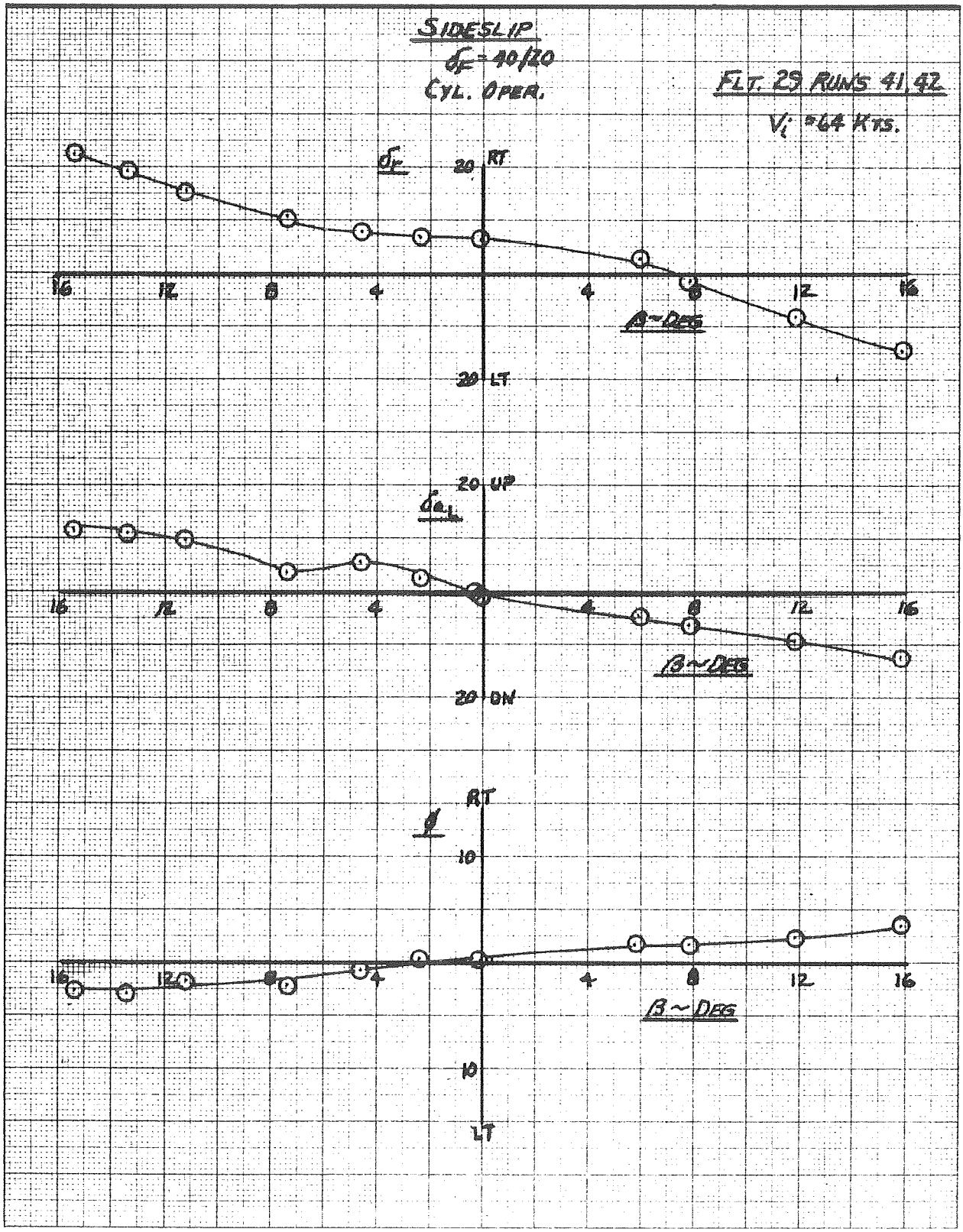
SIDESLIP
δ_F = 40/20
CYL. OPER.
FLT. 29 RUNS 41, 42
V_i = 64 KTS.
δ_r
20 RT
20 LT
16
12
8
4
4
8
12
16
β~DEG
δ_a
20 UP
20 DN
β~DEG
ϕ
RT
10
10
LT
β~DEG

FIGURE 34 h

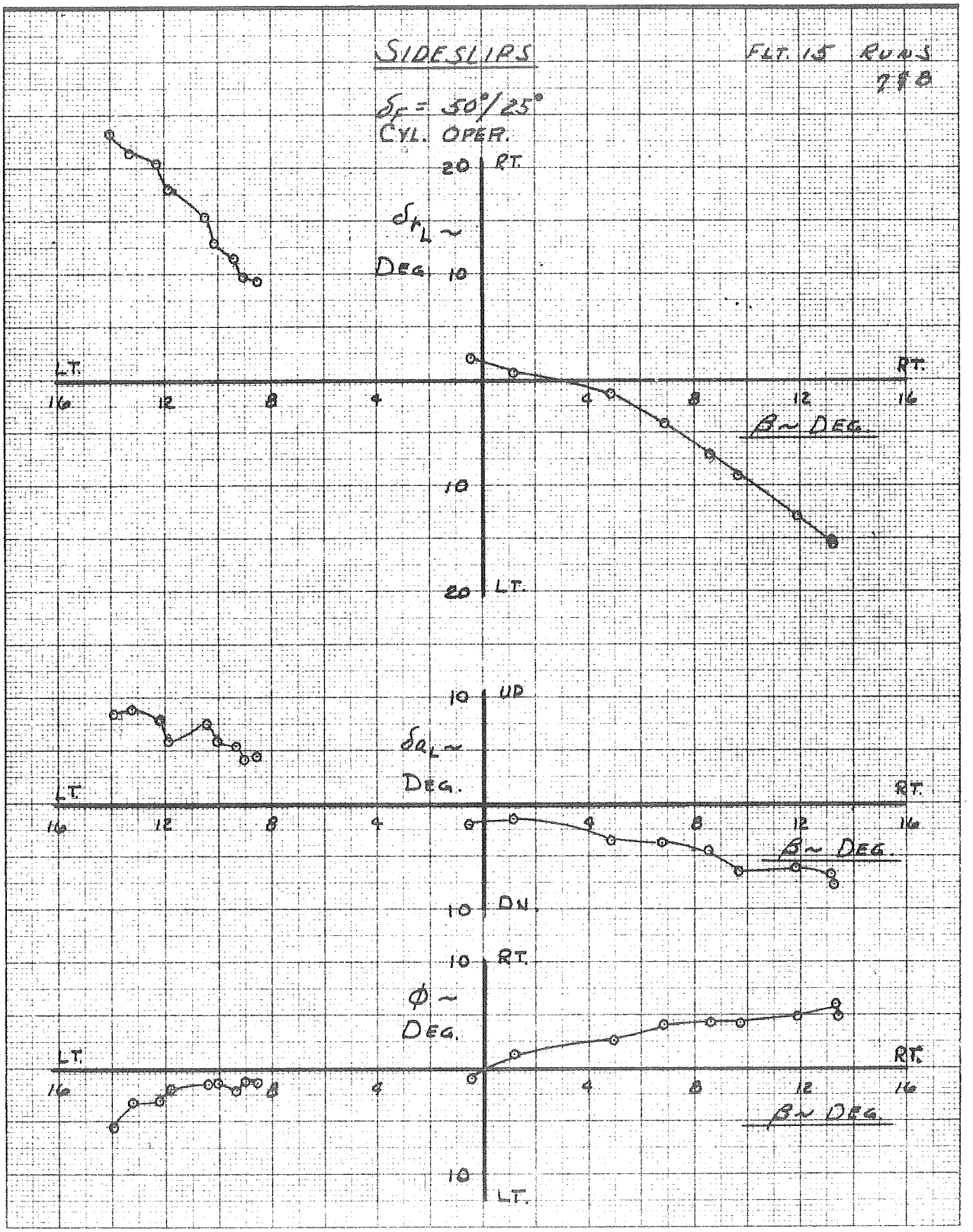
SIDESLIPS
FLT. 15 RUNS 7 & 8
δ_F = 50°/25°
CYL. OPER.
20 RT.
δ_{r_L} ~ DEG.
10
LT.
RT.
16 12 8 4 4 8 12 16
β ~ DEG.
10
20 LT.
10 UP
δ_{a_L} ~ DEG.
LT.
RT.
16 12 8 4 4 8 12 16
β ~ DEG.
10 DN.
10 RT.
ϕ ~ DEG.
LT.
RT.
16 8 4 4 8 12 16
β ~ DEG.
10 LT.

FIGURE 34 i

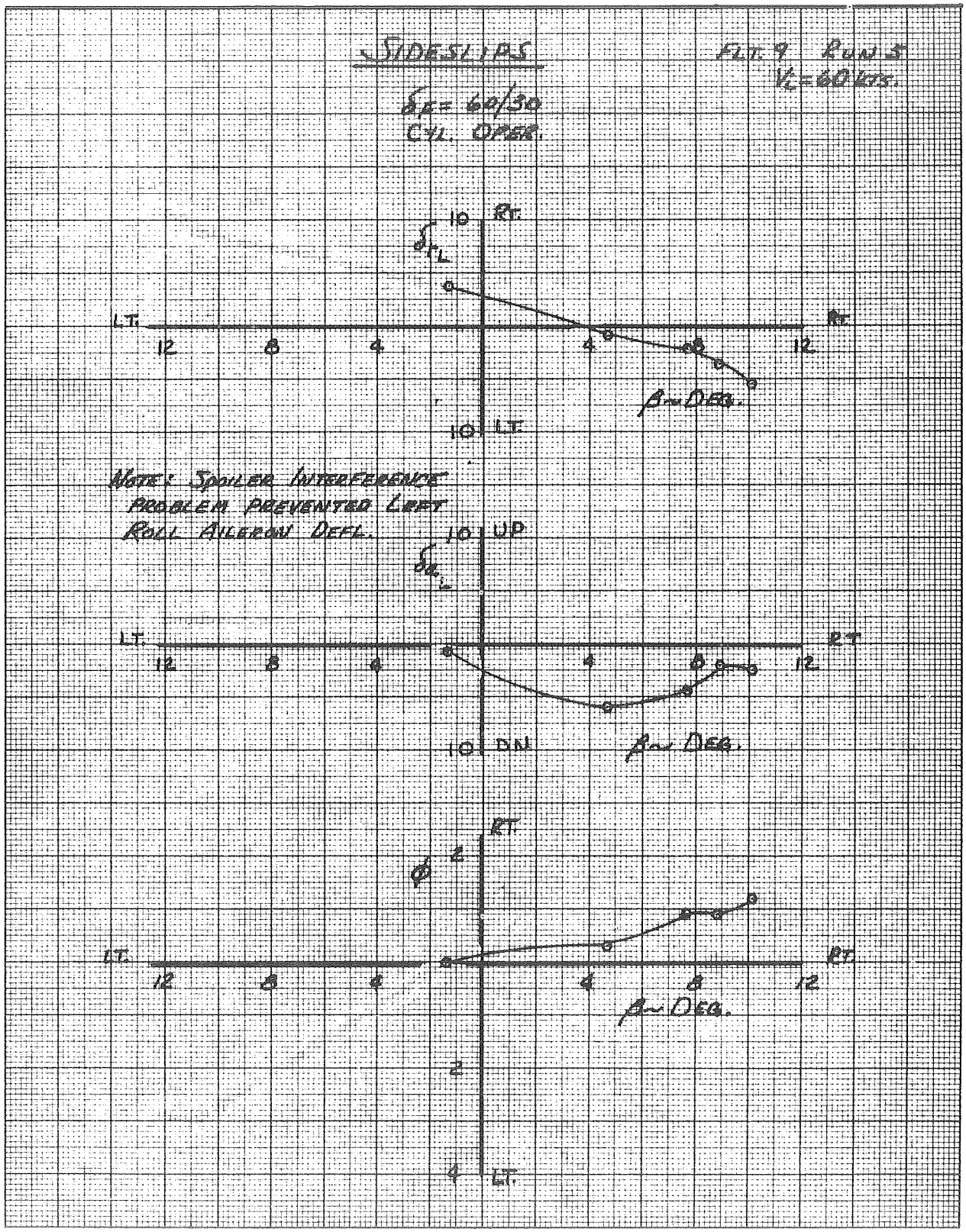
SIDESLIPS
FLT. 9 RUN 5
V_i = 60 KTS.
δ_E = 60/30
CYL. OPER.
10 RT.
δ_{T_L}
LT.
12
8
4
4
8
12
RT.
β ~ DEG.
10 LT.
NOTE: SPOILER INTERFERENCE PROBLEM PREVENTED LEFT ROLL AILERON DEFL.
10 UP
δ_{a_L}
LT.
12
8
4
4
8
12
RT
10 DN
β ~ DEG.
RT.
2
ϕ
LT.
12
8
4
4
8
12
RT.
β ~ DEG.
2
4 LT.

FIGURE 34 j

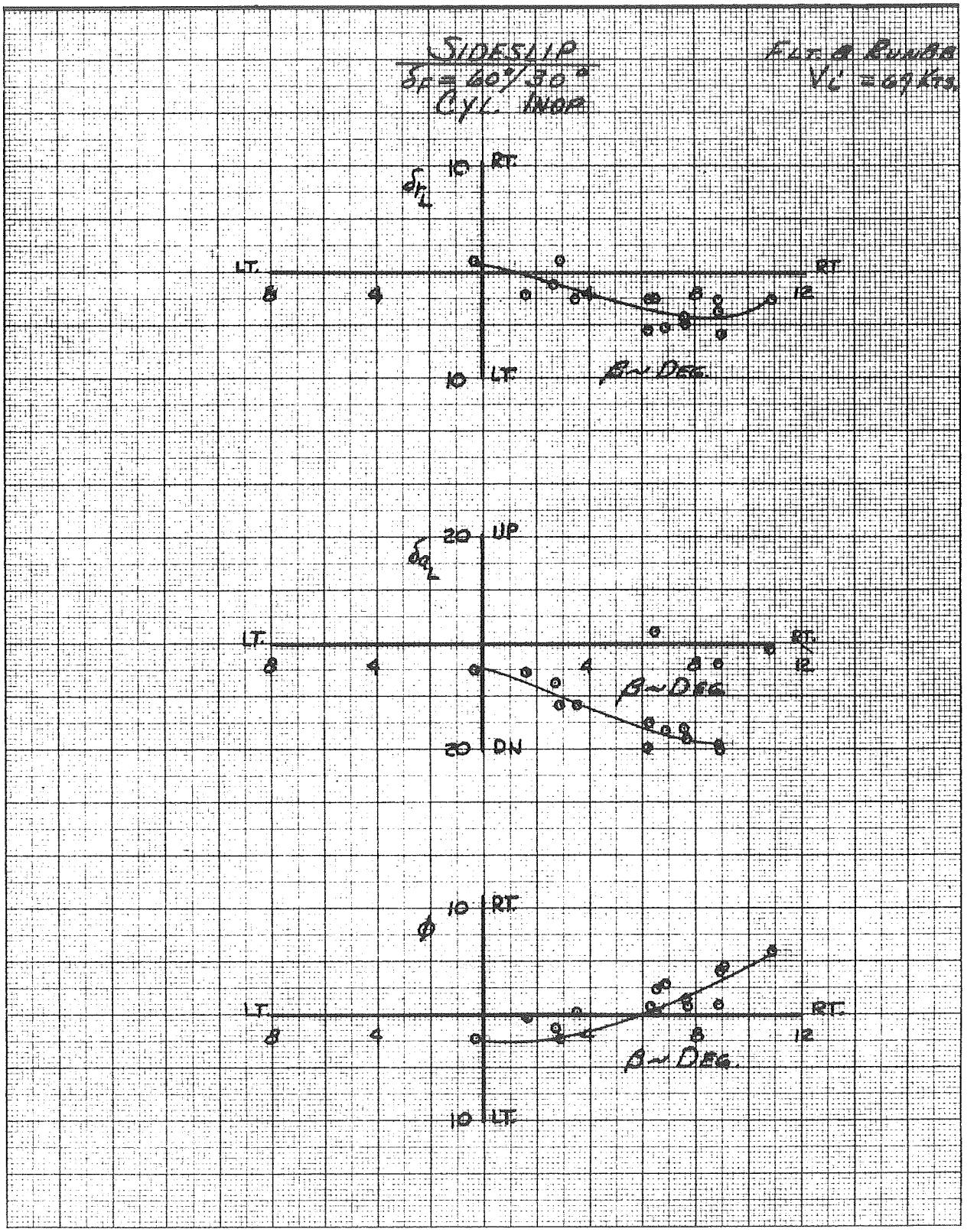
SIDESLIP
δ_F = 40°/30°
CYL. INBD
FLT @ RUNWAY
V_L' = 69 KTS.
δ_{r_L}
10 RT
10 LT
LT.
RT.
8
4
12
β ~ DEG.
δ_{a_L}
20 UP
20 DN
LT.
RT.
8
4
4
8
12
β ~ DEG.
Φ
10 RT
10 LT
LT.
RT.
8
4
8
12
β ~ DEG.

FIGURE 34 K

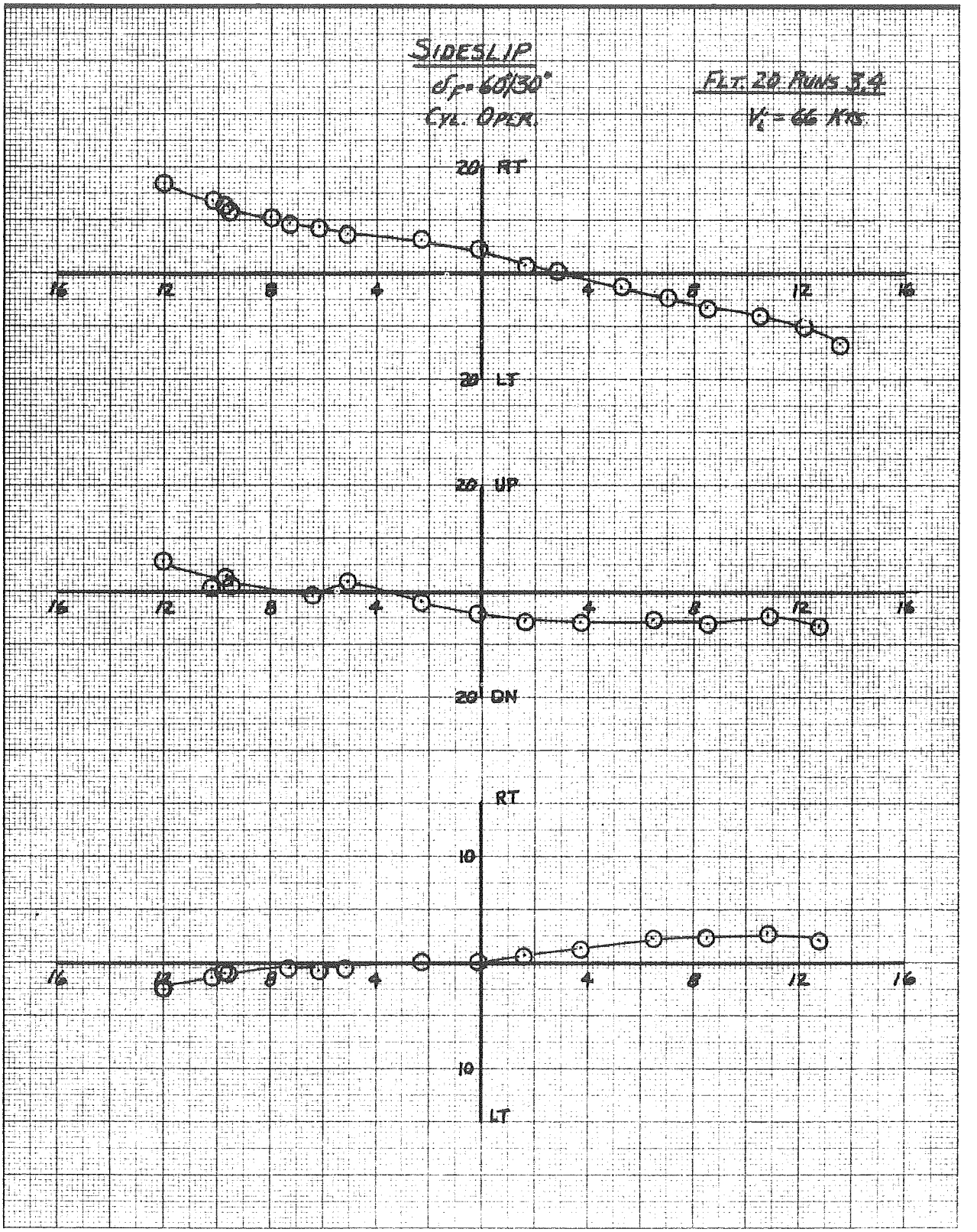
SIDESLIP
δ_f = 60/30°
CYL. OPER.
FLT. 20 RUNS 3,4
V_i = 66 KTS
20 RT
20 LT
20 UP
20 DN
RT
10
10
LT
16
12
8
4
4
8
12
16

FIGURE 35

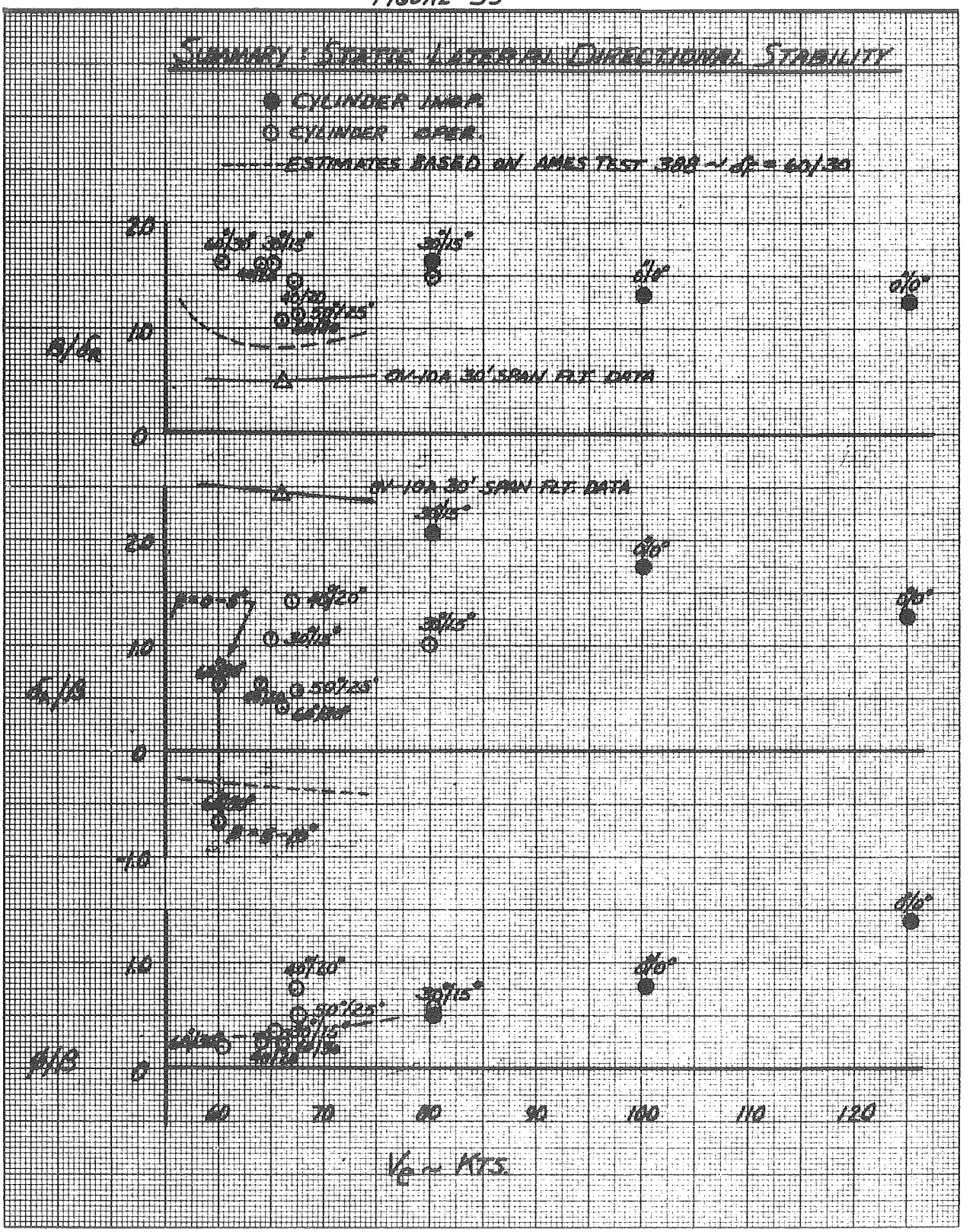
SUMMARY: STATIC LATERAL DIRECTIONAL STABILITY
CYLINDER INBD.
CYLINDER OUTBD.
ESTIMATES BASED ON AMES TEST 388 ~ df = 60/30
20
10
0
-10
Cnβ/CR
Cnβ/CR
Clβ/CR
Clβ/CR
CM-10A 30° SPAN FLT. DATA
CM-10A 30° SPAN FLT. DATA
40/20°
30/15°
50/25°
60/30°
60
70
80
90
100
110
120
Vc ~ KTS.

FIGURE 362

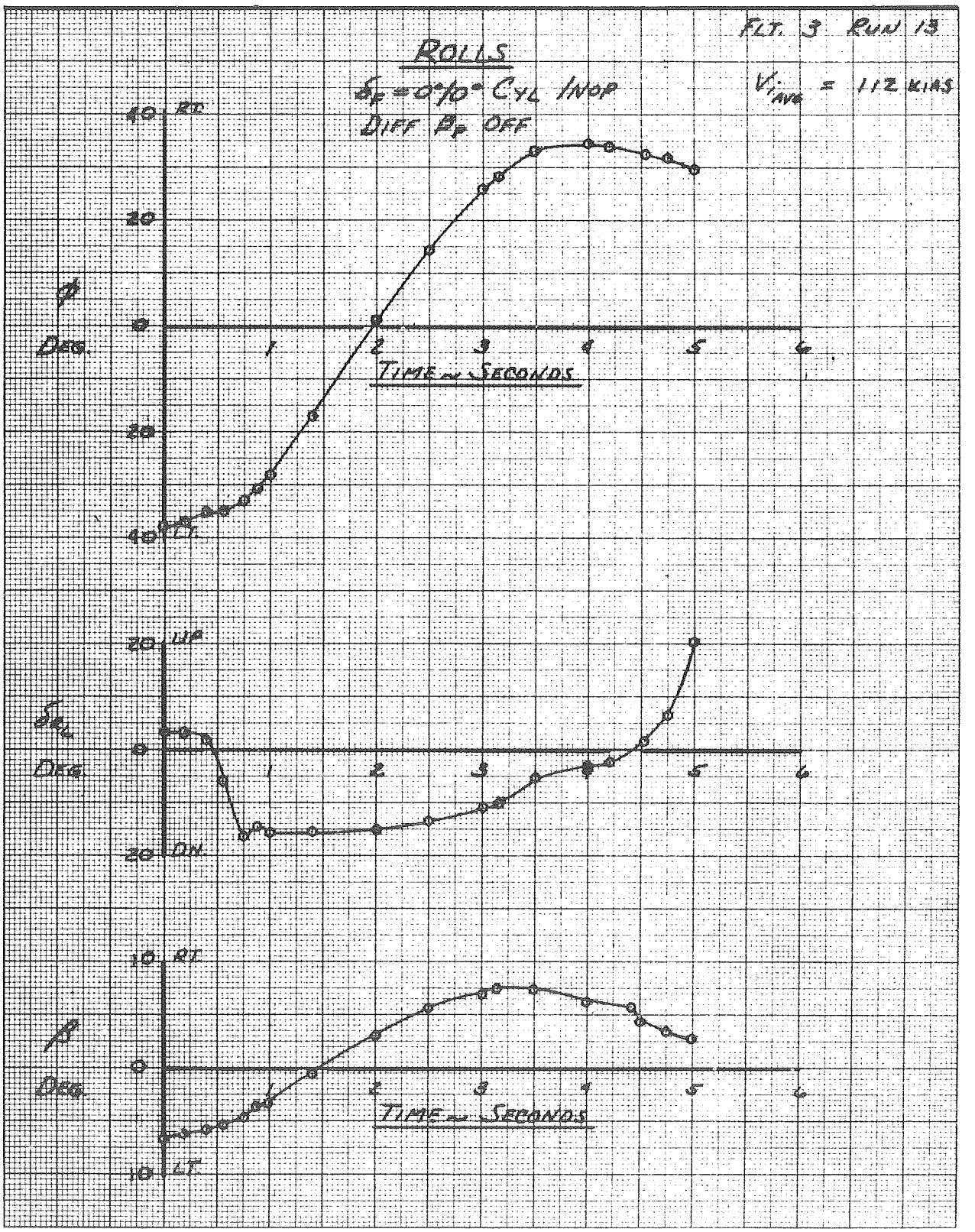
FLT. 3 RUN 13
ROLLS
δ_F = 0°/0° CYL INOP
DIFF β_F OFF
$V_{i_{AVG}}$ = 112 KIAS
40 RT
20
0
20
40 LT.
ϕ
DEG.
1
2
3
4
5
6
TIME — SECONDS
20 UP
0
20 DN.
δ_{R_w}
DEG.
10 RT
0
10 LT.
β
DEG.
TIME — SECONDS

FIGURE 36b

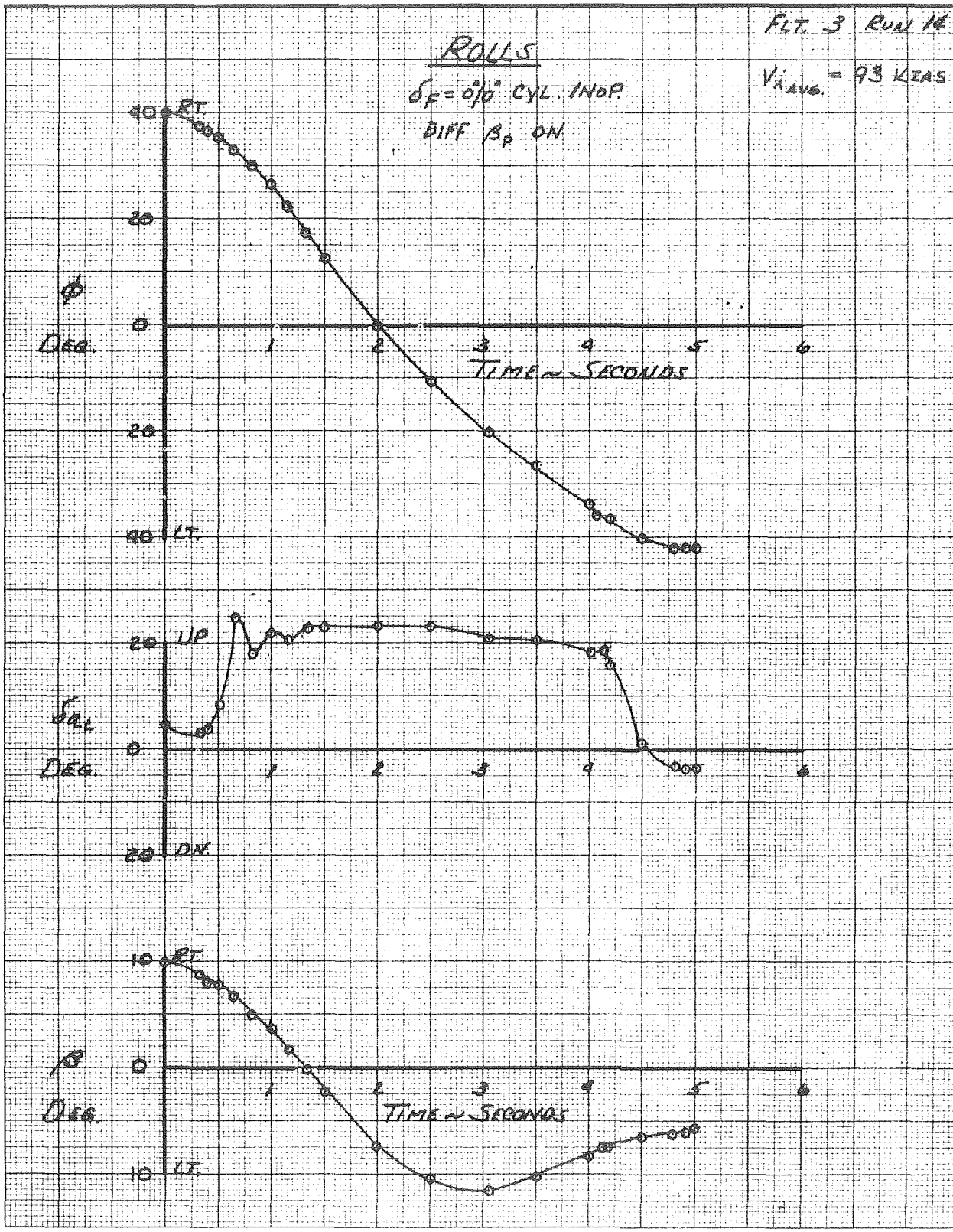
FLT. 3 RUN 16
ROLLS
δ_F = 0°/0° CYL. INOP.
DIFF β_p ON
$V_{i_{AVG.}}$ = 93 KIAS
40 RT.
20
ϕ
0
DEG.
1
2
3
4
5
6
TIME ~ SECONDS
20
40 LT.
20 UP
δ_{AL}
0
DEG.
1
2
3
4
5
6
20 DN.
10 RT.
β
0
DEG.
1
2
3
4
5
6
TIME ~ SECONDS
10 LT.

FIGURE 36C

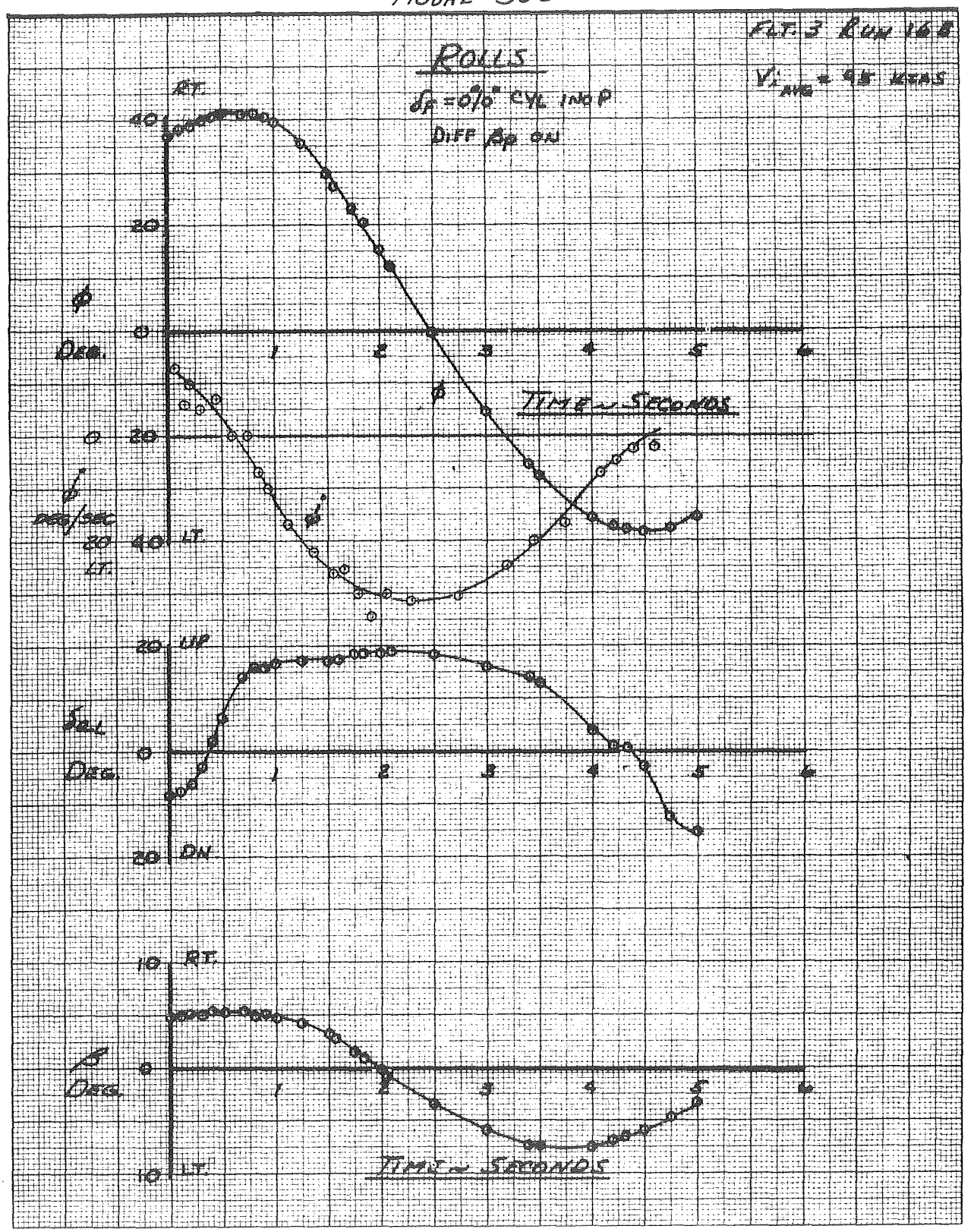
FLT. 3 RUN 16 B
ROLLS
δ_F = 0/0° CYL IND P
DIFF β_P ON
$V_{i_{AVG}}$ = 95 KCAS
RT.
40
20
0
ϕ
DEG.
1
2
3
4
5
6
TIME — SECONDS
ϕ
20
0
$\dot{\phi}$
DEG/SEC
20
40
LT.
20
UP
δ_{a_L}
0
DEG.
20
DN
10
RT.
δ_r
0
DEG.
10
LT.
TIME — SECONDS

FIGURE 36 d

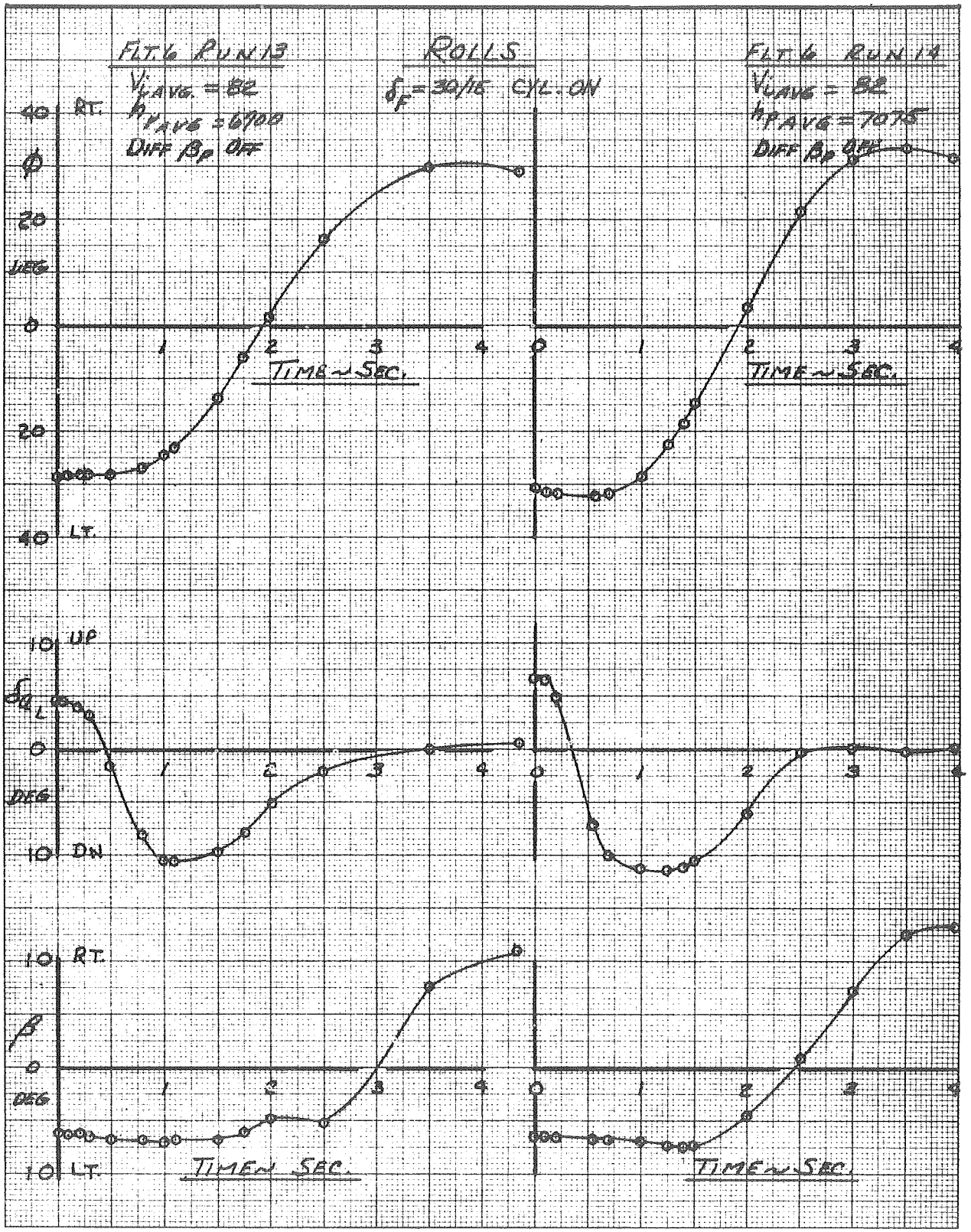
FLT. 6 RUN 13
$V_{t_{AVG.}} = 82$
$h_{P_{AVG}} = 6900$
DIFF β_p OFF
ROLLS
$\delta_F = 30/15$ CYL. ON
FLT. 6 RUN 14
$V_{t_{AVG}} = 82$
$h_{P_{AVG}} = 7075$
DIFF β_p OFF
RT.
LT.
UP
DN
TIME ~ SEC.

FIGURE 36e

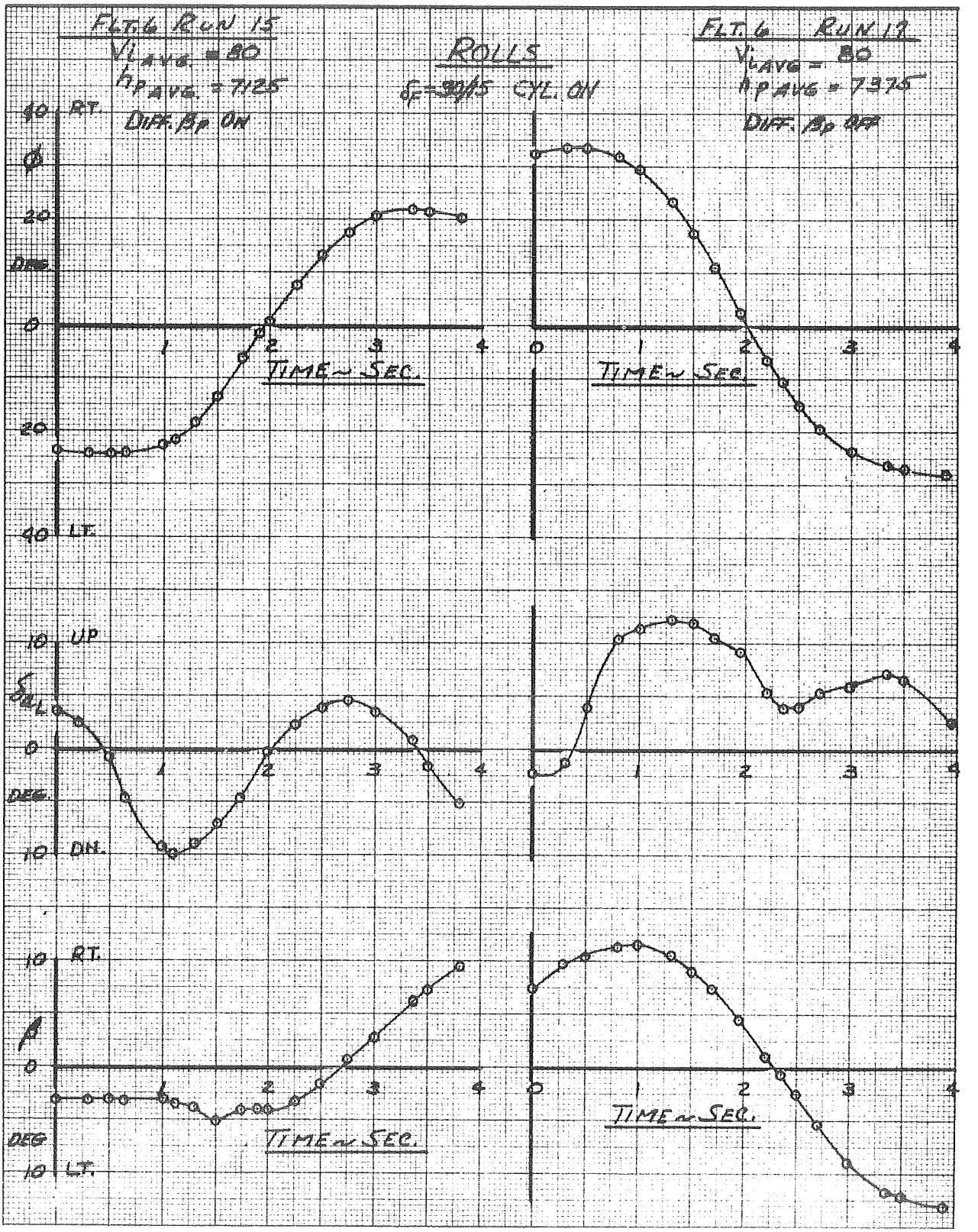
FLT. 6 RUN 15
Vi AVG. = 80
hp AVG. = 7125
DIFF. βp ON
ROLLS
δF = 30/45 CYL. ON
FLT. 6 RUN 12
Vi AVG = 80
hp AVG = 7375
DIFF. βp OFF
40 RT.
Φ
20
DEG
0
20
40 LT.
TIME ~ SEC.
TIME ~ SEC.
10 UP
δAIL
0
DEG.
10 DN.
10 RT.
β
0
DEG
10 LT.
TIME ~ SEC.
TIME ~ SEC.

FIGURE 36F

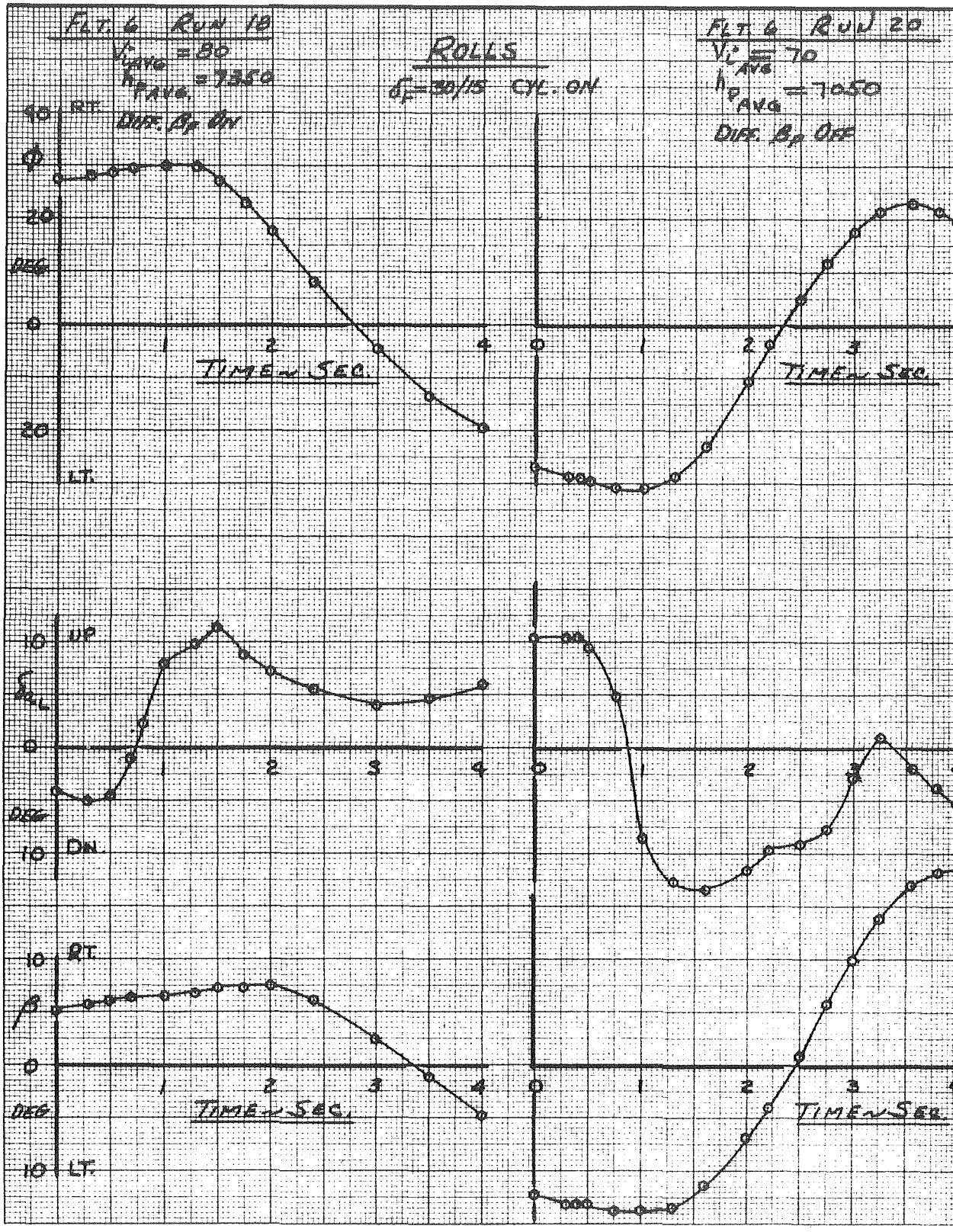
FLT. 6 RUN 18
$V_{t_{AVG}}$ = 80
$h_{p_{AVG}}$ = 7350
ROLLS
δ_F = 30/15 CYL. ON
FLT 6 RUN 20
$V_{t_{AVG}}$ = 70
$h_{p_{AVG}}$ = 7050
DIFF. β_F ON
DIFF. β_F OFF
RT.
LT.
DEG
TIME - SEC.
UP
DN.
ϕ
β

FIGURE 36 G

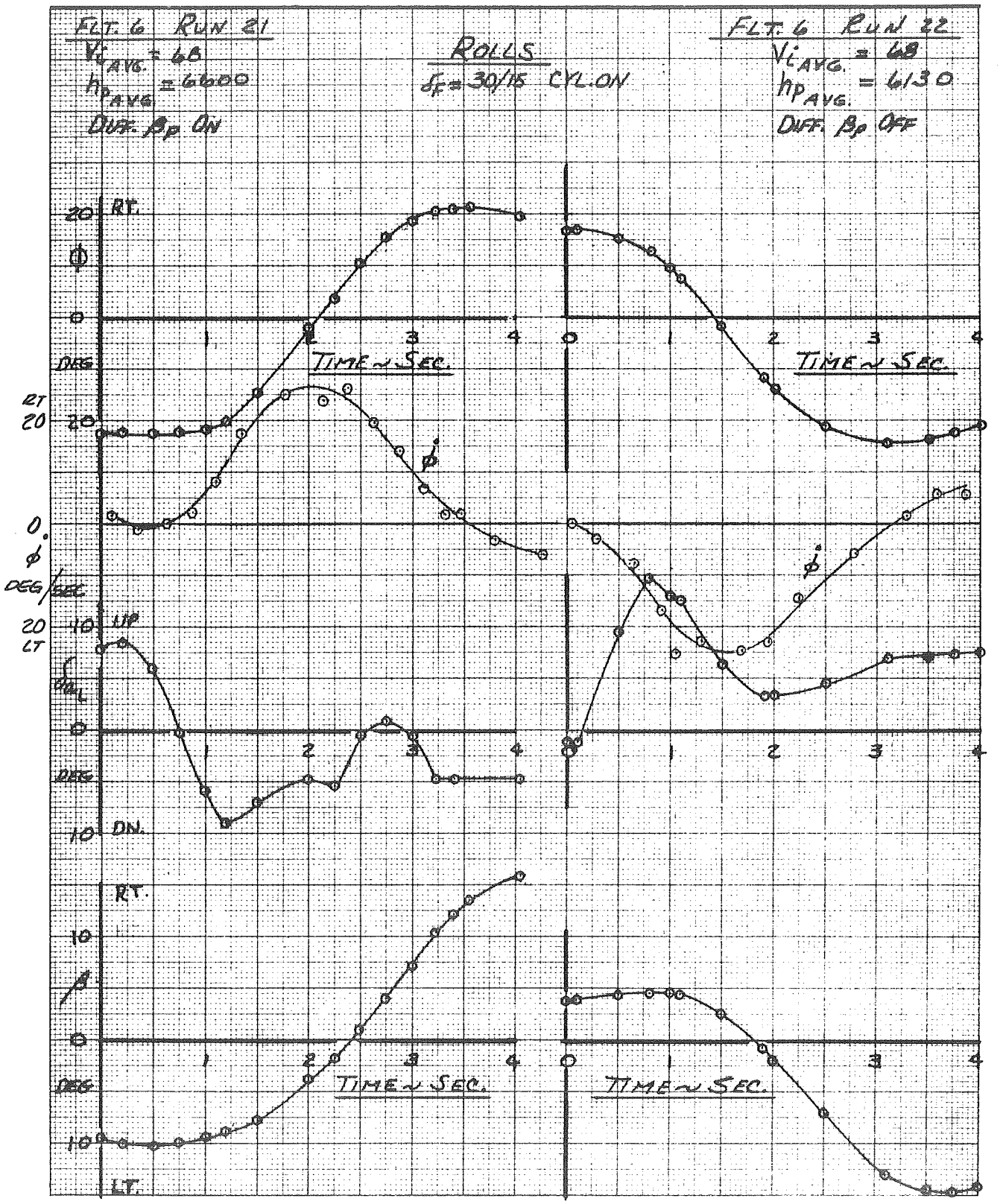
FLT. 6 RUN 21
$V_{t_{AVG.}}$ = 68
$h_{p_{AVG.}}$ = 6600
DUFF. β_p ON
ROLLS
δ_f = 30/15 CYL. ON
FLT. 6 RUN 22
$V_{t_{AVG.}}$ = 68
$h_{p_{AVG.}}$ = 6130
DUFF. β_p OFF
RT.
ϕ
DEG
TIME ~ SEC.
$\dot{\phi}$
DEG/SEC
UP
DN.
β
LT.

FIGURE 36h

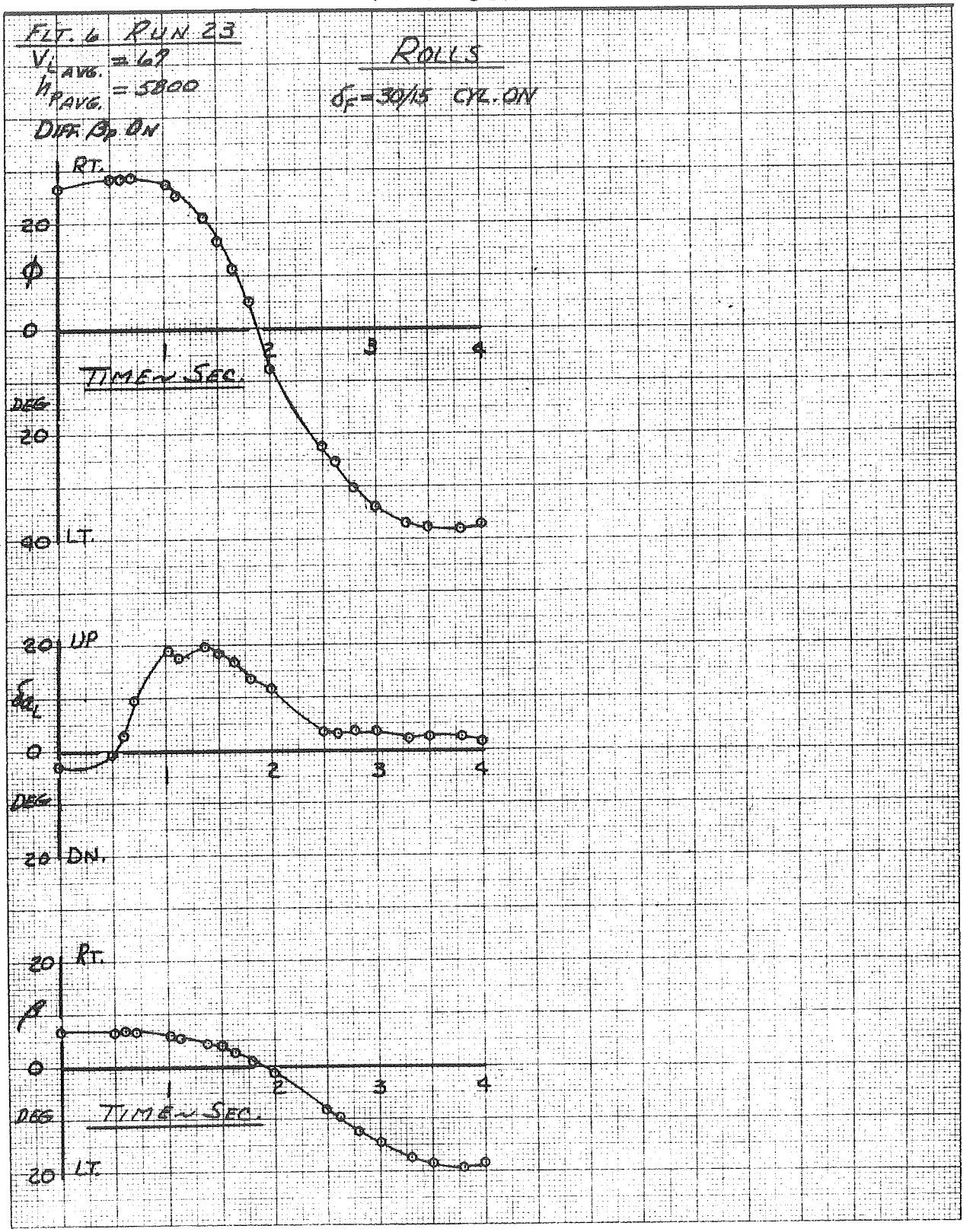
FLT. 6 RUN 23
$V_{t_{AVG.}}$ = 69
$h_{P_{AVG.}}$ = 5800
DIFF. β_p ON
ROLLS
δ_F = 30/15 CYL. ON
RT.
20
ϕ
0
1
2
3
4
TIME ~ SEC.
DEG
20
40 LT.
20 UP
δ_{a_L}
0
1
2
3
4
DEG
20 DN.
20 RT.
β
0
1
2
3
4
DEG
TIME ~ SEC.
20 LT.

FIGURE 36i

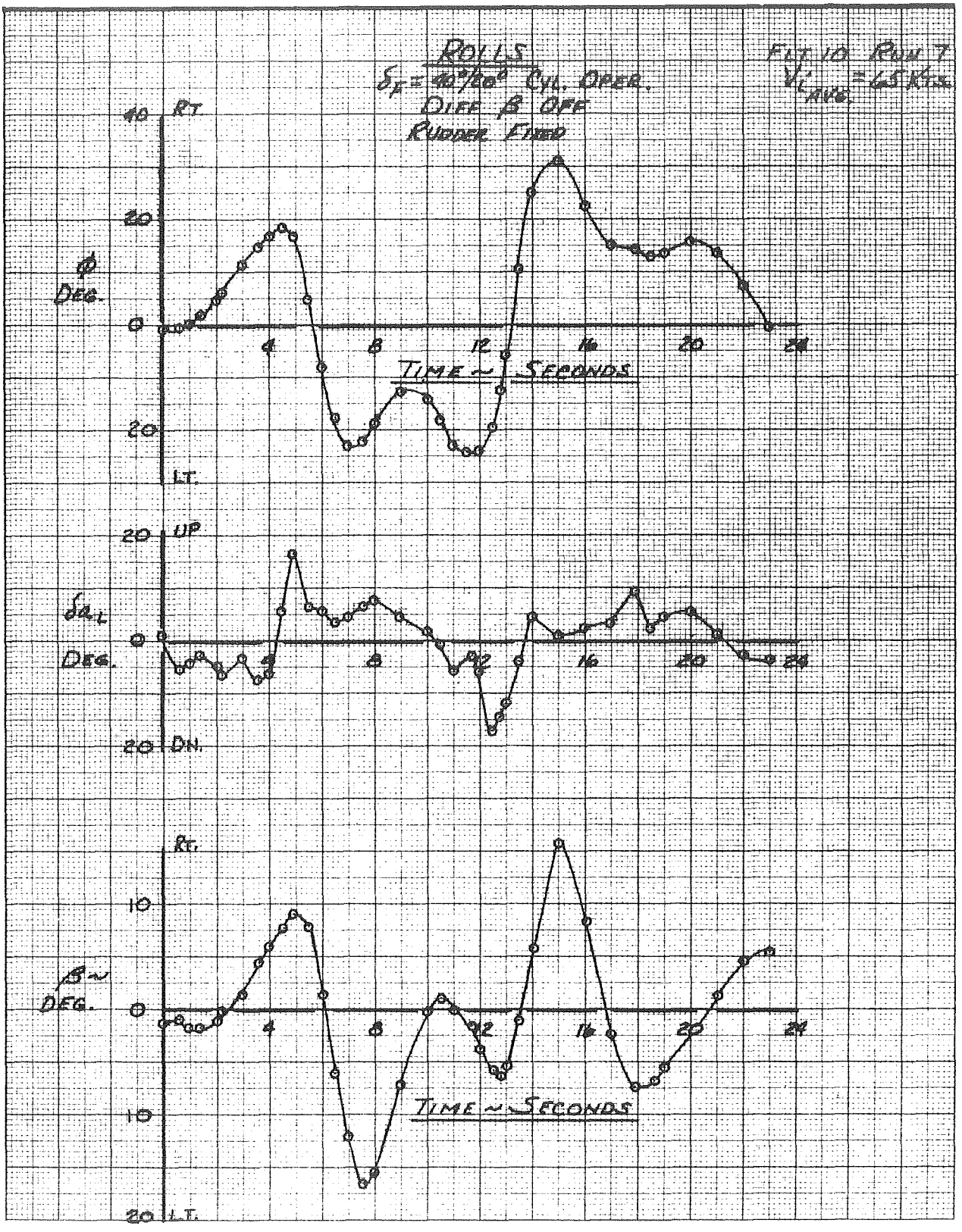
ROLLS
δ_F = 40°/20° CYL. OPER.
DIFF β OFF
RUDDER FIXED
FLT 10 RUN 7
$V_{L_{AVG.}}$ = 65 KTS.
40 RT
20
φ DEG.
0
20 LT.
4
8
12
16
20
24
TIME ~ SECONDS
20 UP
δ_{a_L} DEG.
0
20 DN.
RT.
10
β ~ DEG.
0
10
20 LT.
TIME ~ SECONDS

FIGURE 36 j

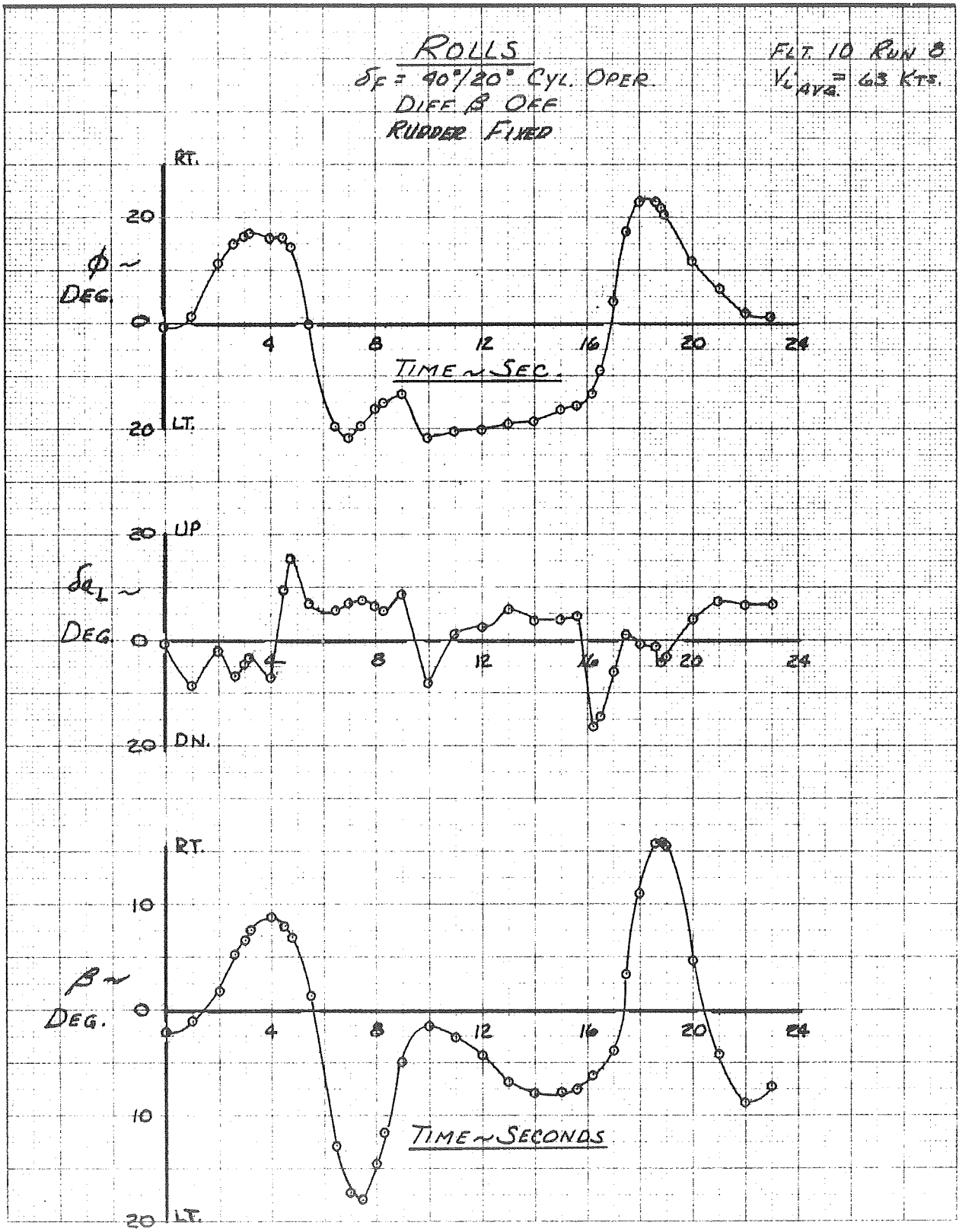
ROLLS
δ_F = 40°/20° CYL. OPER.
DIFF A OFF
RUDDER FIXED
FLT. 10 RUN 8
$V_{L_{AVG.}}$ = 63 KTS.
RT.
20
ϕ ~
DEG.
0
4
8
12
16
20
24
TIME ~ SEC.
20 LT.
20 UP
δa_L ~
DEG.
0
20 DN.
RT.
10
β ~
DEG.
0
10
TIME ~ SECONDS
20 LT.

FIGURE 36 K

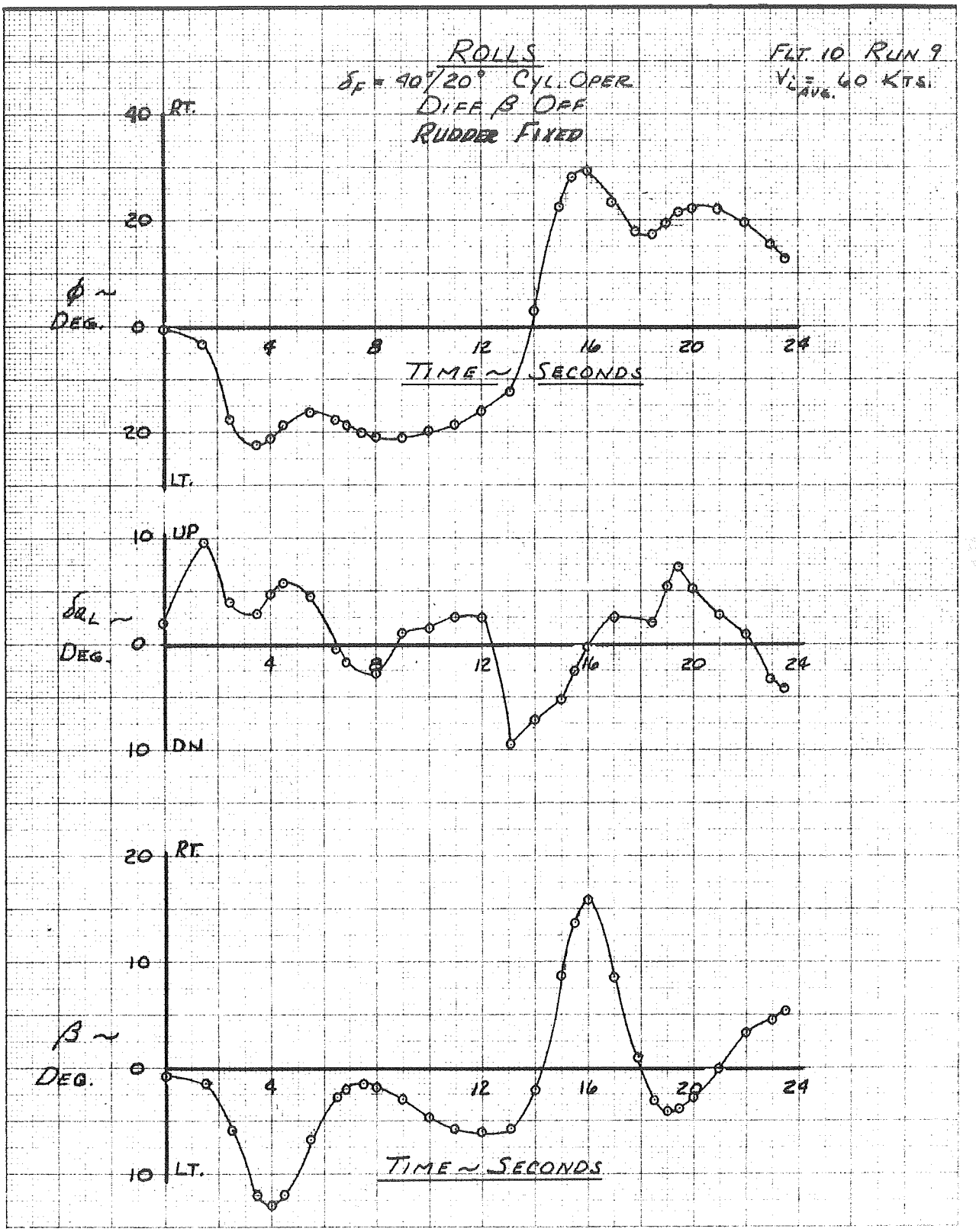
ROLLS
FLT. 10 RUN 9
δ_F = 40°/20° CYL. OPER.
$V_{i_{AVG.}}$ = 60 KTS.
DIFF β OFF
RUDDER FIXED
40 RT.
20
φ ~ DEG.
0
20 LT.
4
8
12
16
20
24
TIME ~ SECONDS
10 UP
δ_{a_L} ~ DEG.
0
10 DN
20 RT.
10
β ~ DEG.
0
10 LT.
TIME ~ SECONDS

FIGURE 36 L

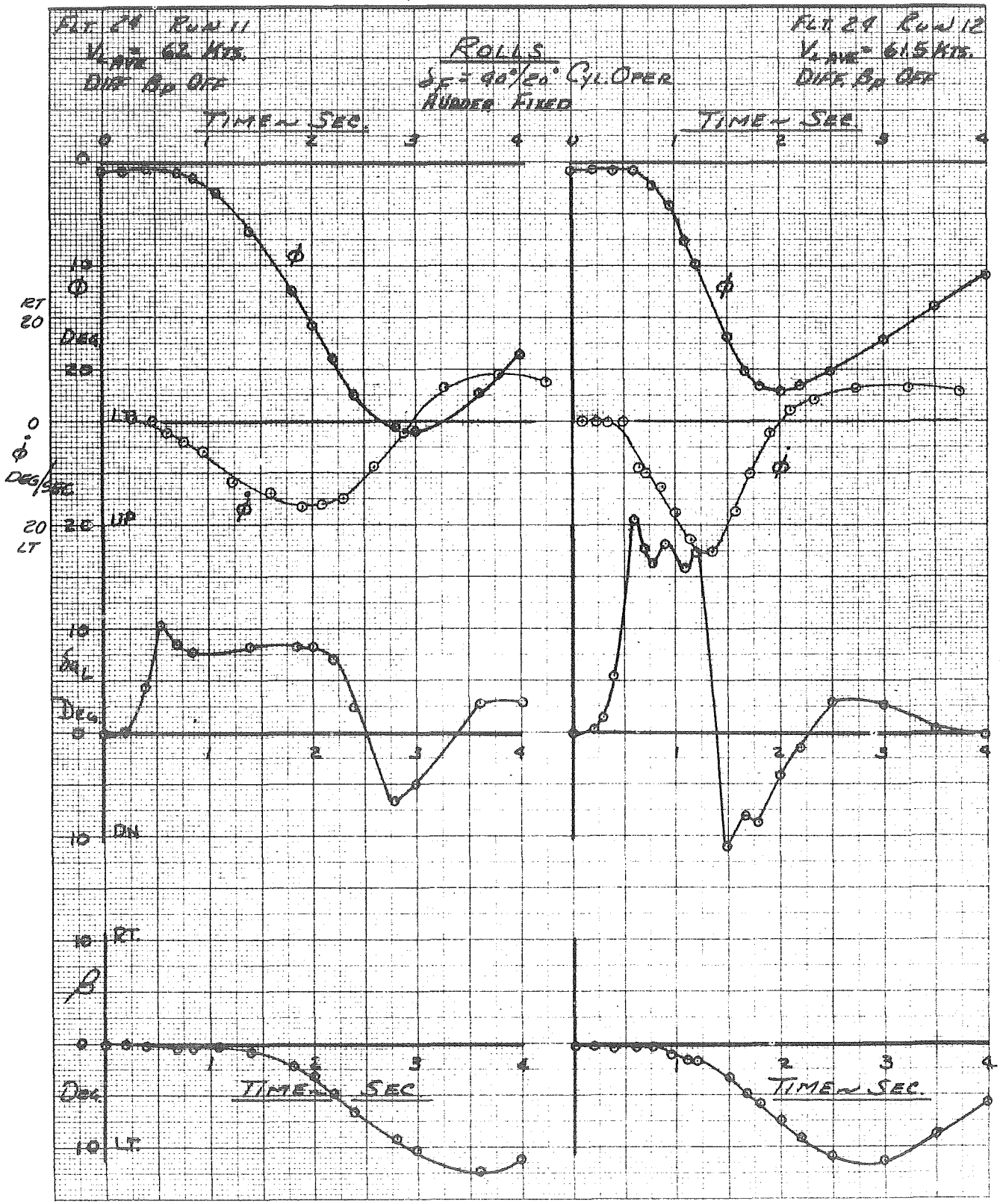
Flt. 24 Run 11
$V_{t\,AVE}$ = 62 Kts.
Diff β_p Off
ROLLS
δ_F = 40°/20° Cyl. Oper
RUDDER FIXED
Flt. 24 Run 12
$V_{t\,AVE}$ = 61.5 Kts.
Diff β_p Off
TIME ~ SEC.
TIME ~ SEC.
RT
LT
UP
DN
RT.
LT.
TIME ~ SEC
TIME ~ SEC.

FIGURE 36 M

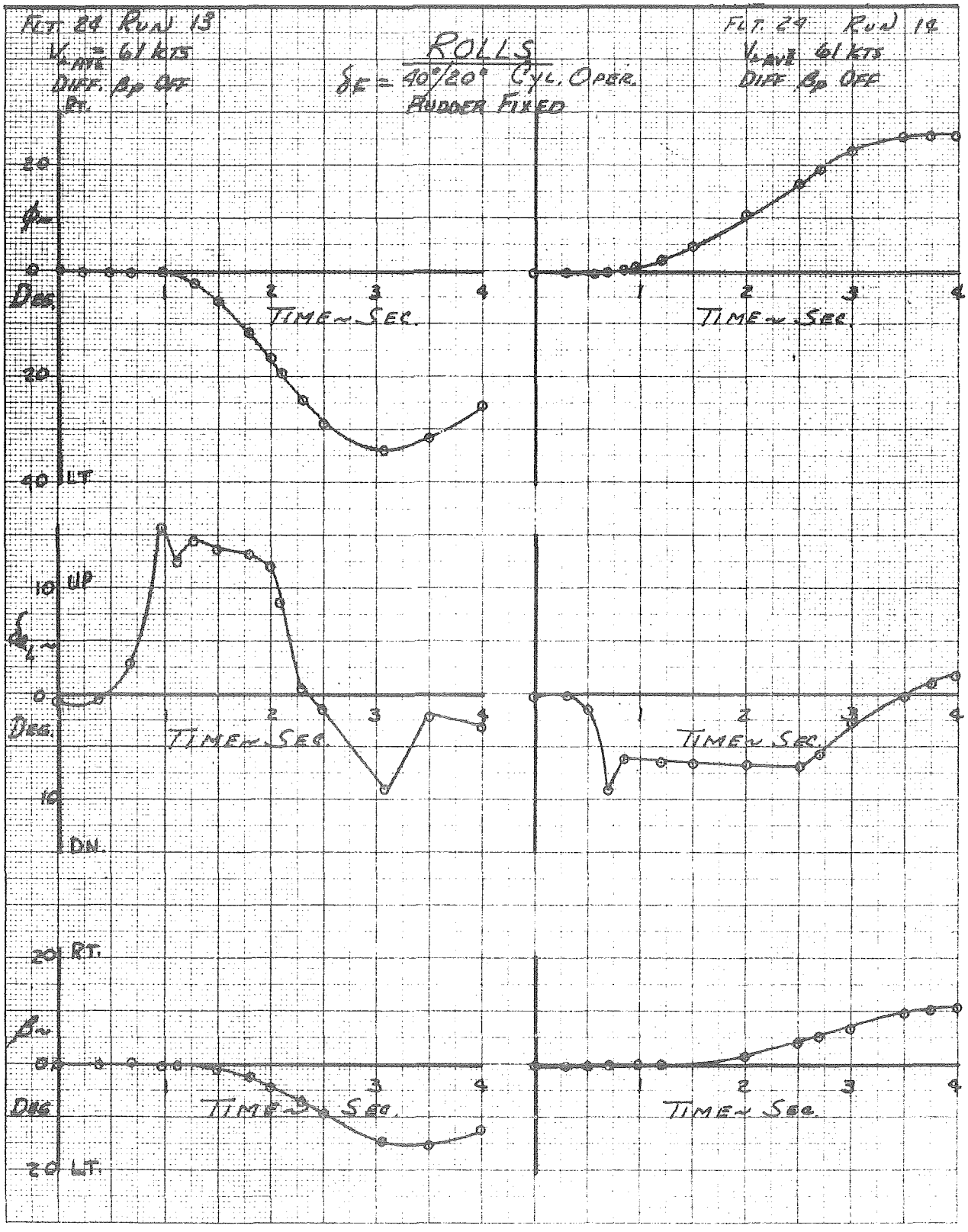
FLT 24 RUN 13
V AVE = 61 KTS
DIFF. Bp OFF
ROLLS
δE = 40°/20° CYL. OPER.
RUDDER FIXED
FLT. 29 RUN 14
V AVE 61 KTS
DIFF. Bp OFF
Φ
DEG.
20
0
20
40 LT
TIME ~ SEC.
ζ
10 UP
0
10
DN.
TIME ~ SEC.
β
20 RT.
0
20 LT.
TIME ~ SEC.

FIGURE 36 N

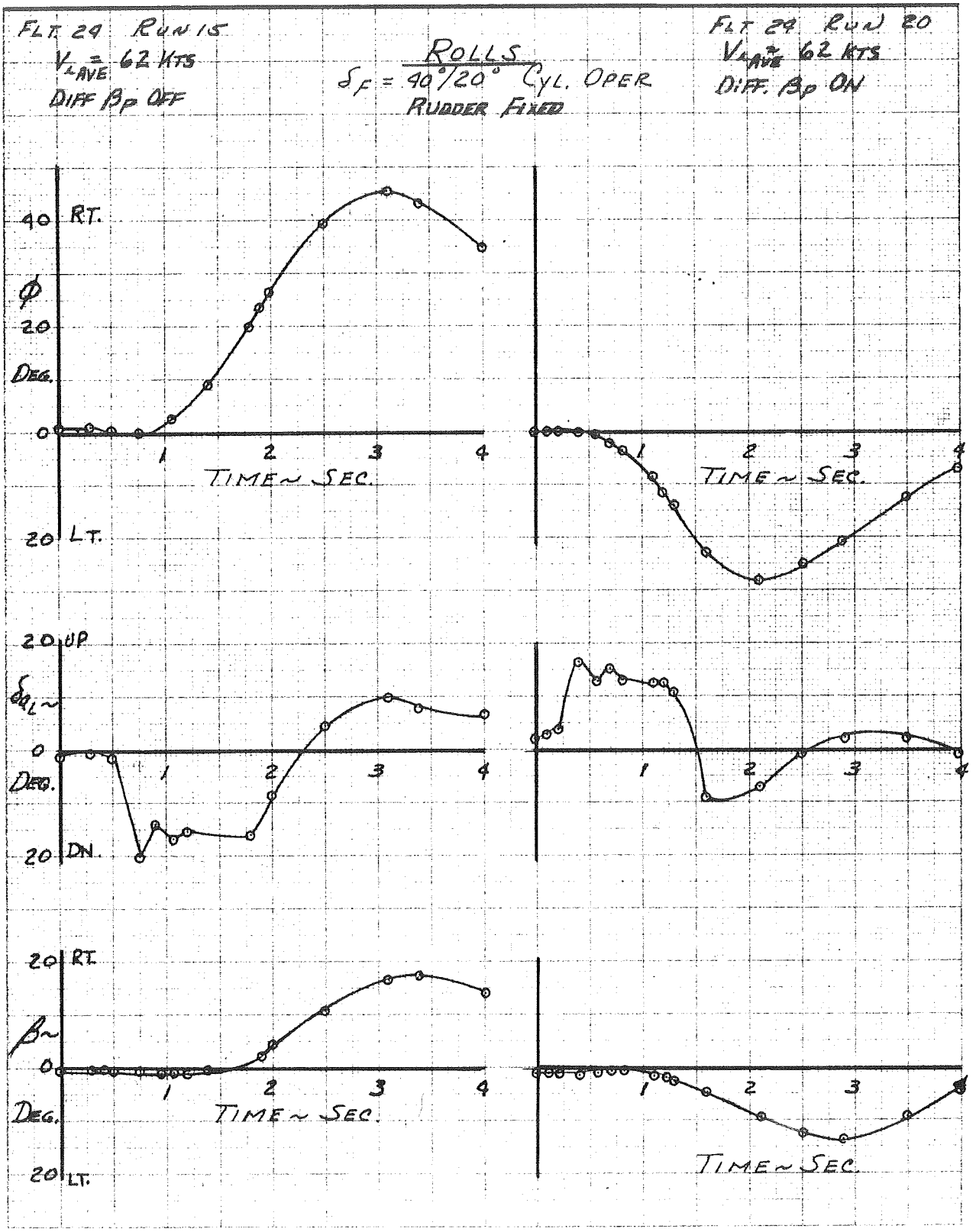
FLT 29 RUN 15
$V_{L_{AVE}}$ = 62 KTS
DIFF β_p OFF
ROLLS
δ_f = 40°/20° CYL. OPER
RUDDER FIXED
FLT 29 RUN 20
$V_{L_{AVE}}$ = 62 KTS
DIFF. β_p ON
40 RT.
ϕ
20
DEG.
0
20 LT.
1 2 3 4
TIME ~ SEC.
20 UP
δ_{a_L} ~
0
DEG.
20 DN.
20 RT.
β ~
0
DEG.
20 LT.

FIGURE 360

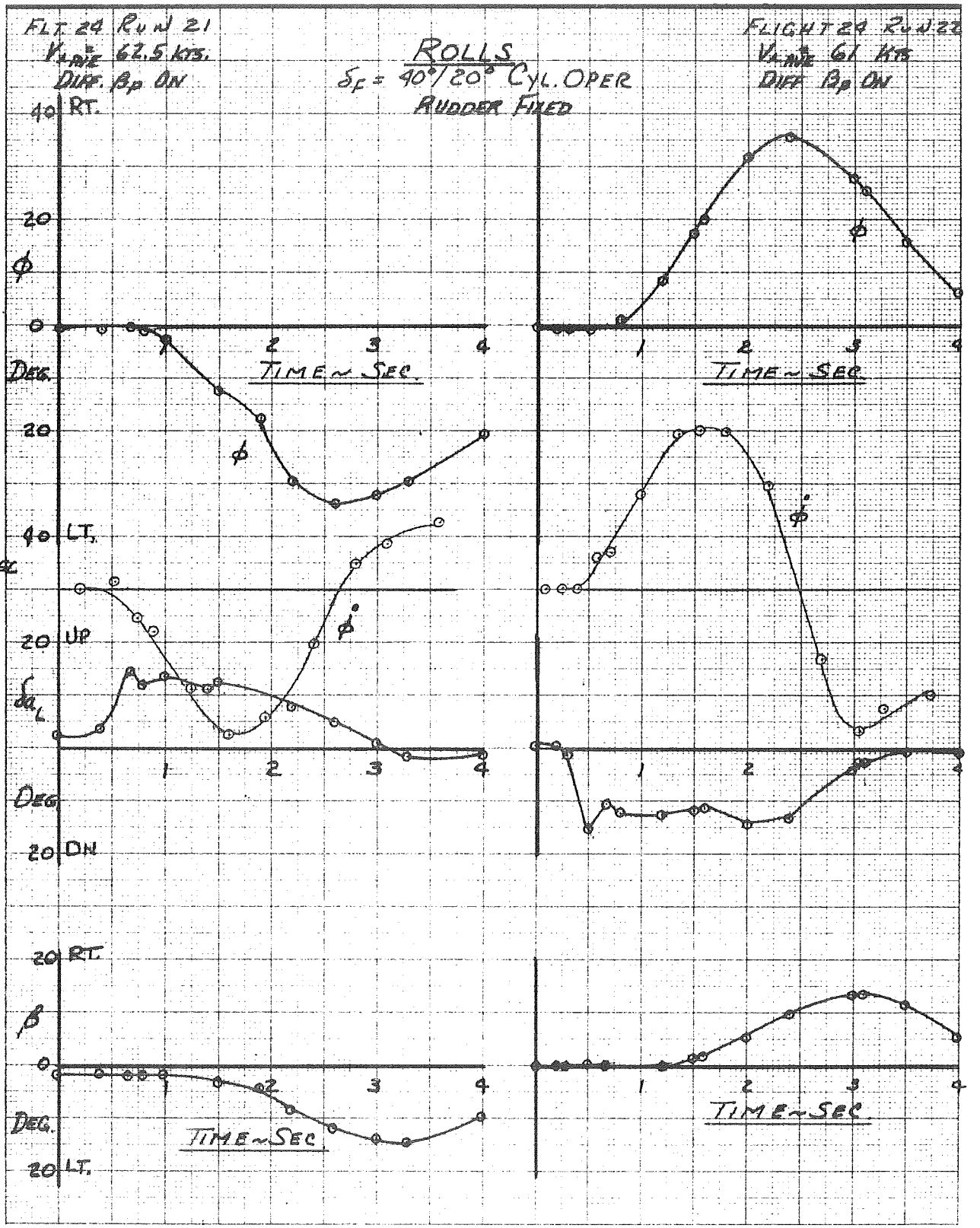
FLT 24 RUN 21
$V_{t_{MIN}}$ 62.5 KTS.
DIFF. β_p ON
ROLLS
δ_F = 40°/20° CYL. OPER
RUDDER FIXED
FLIGHT 24 RUN 22
$V_{t_{MIN}}$ 61 KTS
DIFF β_p ON
40 RT.
20
ϕ
0
DEG.
TIME ~ SEC.
20
RT
20
$\dot{\phi}$
40 LT.
DEG/SEC
0
20 UP
20
δa_L
LT
DEG.
20 DN
20 RT.
β
0
DEG.
20 LT.
TIME ~ SEC.

FIGURE 36 P

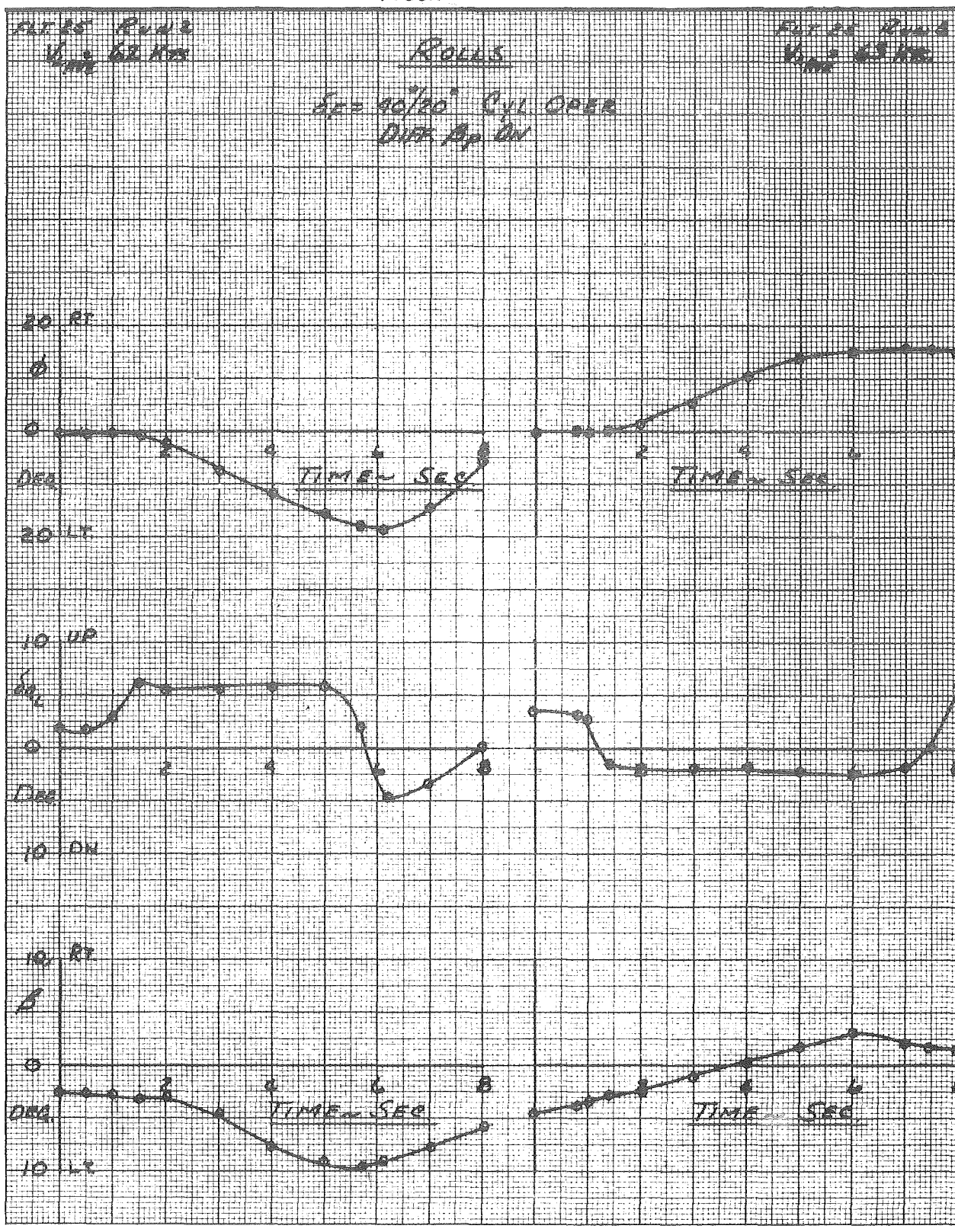
ROLLS
δ_L = 40/20° Cyl Oper
Duct Δp On
20 Rt
0
Deg
20 Lt
10 UP
δ_{HL}
0
Deg
10 DN
10 Rt
β
0
Deg
10 Lt
Time - Sec
Time - Sec
Time - Sec
Time - Sec

FIGURE- 36Q

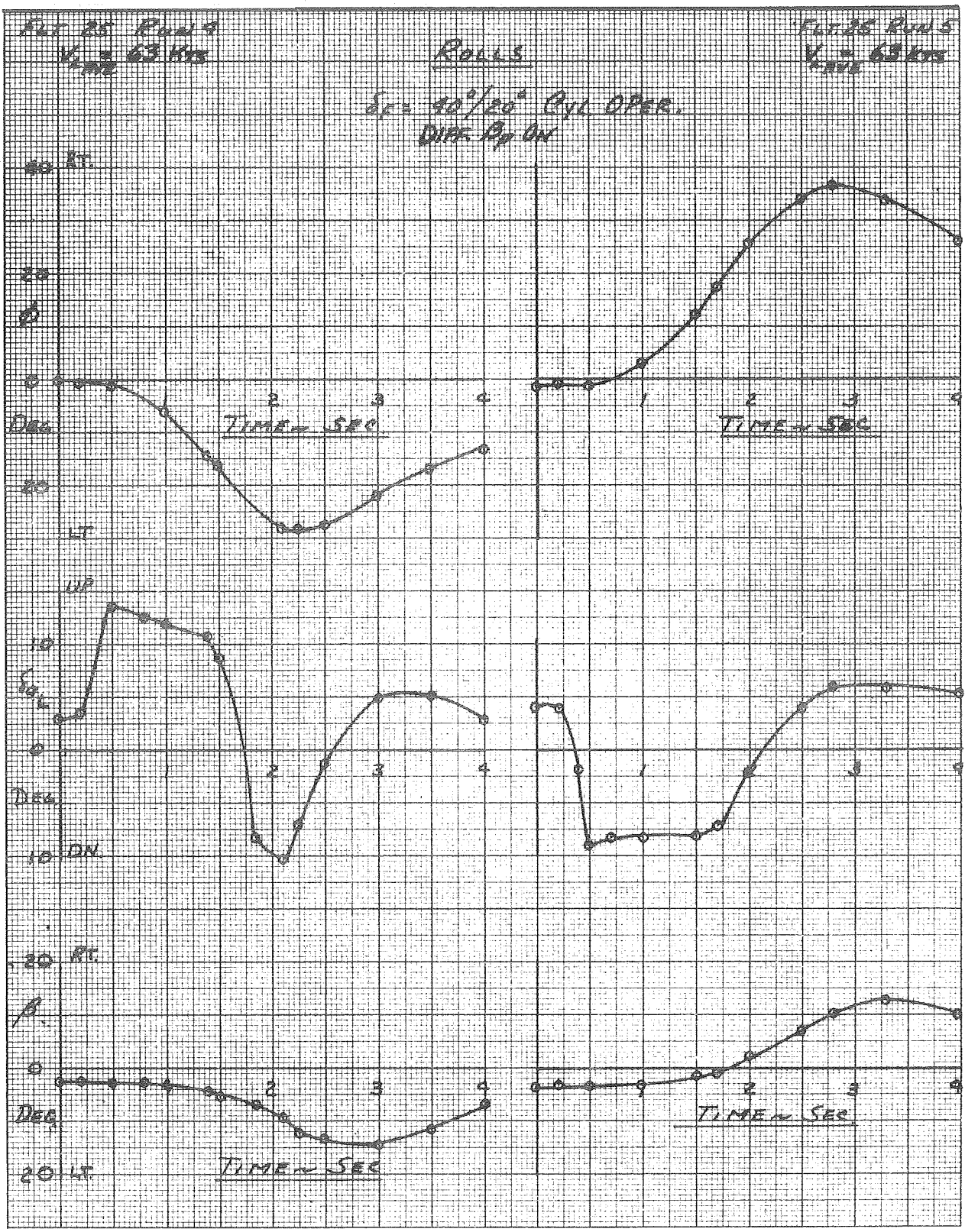
FLT. 25 RUN 4
$V_{K_{AVE}}$ = 63 KTS
ROLLS
δ_c = 40°/20° CYL. OPER.
DIFF. R_F ON
FLT. 25 RUN 5
$V_{K_{AVE}}$ = 63 KTS
40 RT.
20
0
Deg.
20 LT.
TIME - SEC
UP
10
δ_{a_L}
0
Deg.
10 DN.
20 RT.
β
0
Deg.
20 LT.
TIME - SEC

FIGURE 36A

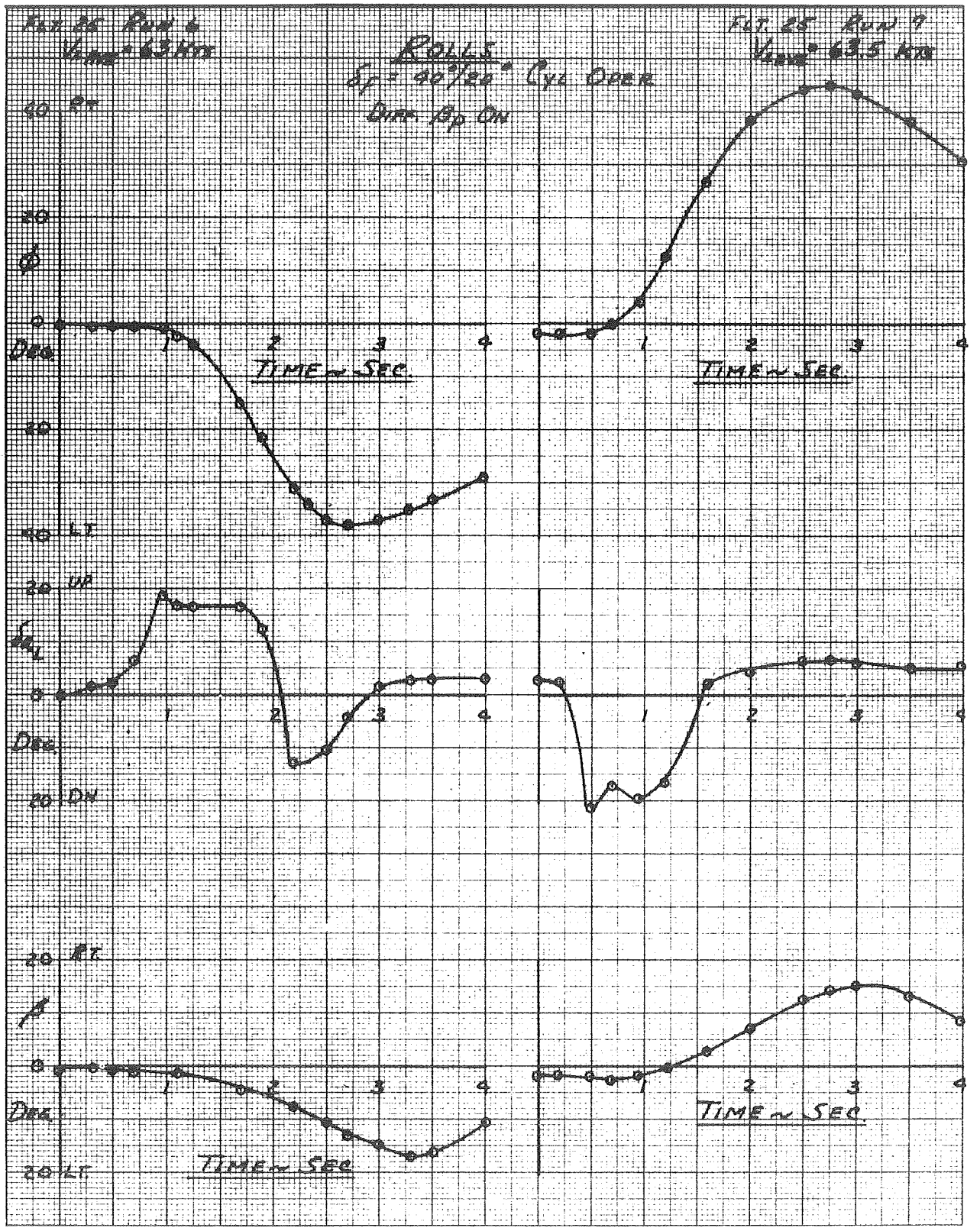
FLT. 25 RUN 6
V_{TRUE} = 63 KTS
ROLLS
δ_F = 40°/20° CYL. ORDER
DIFF. δ_D ON
FLT. 25 RUN 7
V_{TRUE} = 63.5 KTS
40 RT.
20
ϕ
0
DEG.
20
40 LT.
TIME ~ SEC.
TIME ~ SEC.
20 UP
δ_{A_L}
0
DEG.
20 DN
1
2
3
4
20 RT.
β
0
DEG.
20 LT.
TIME ~ SEC.
TIME ~ SEC.

FIGURE 365

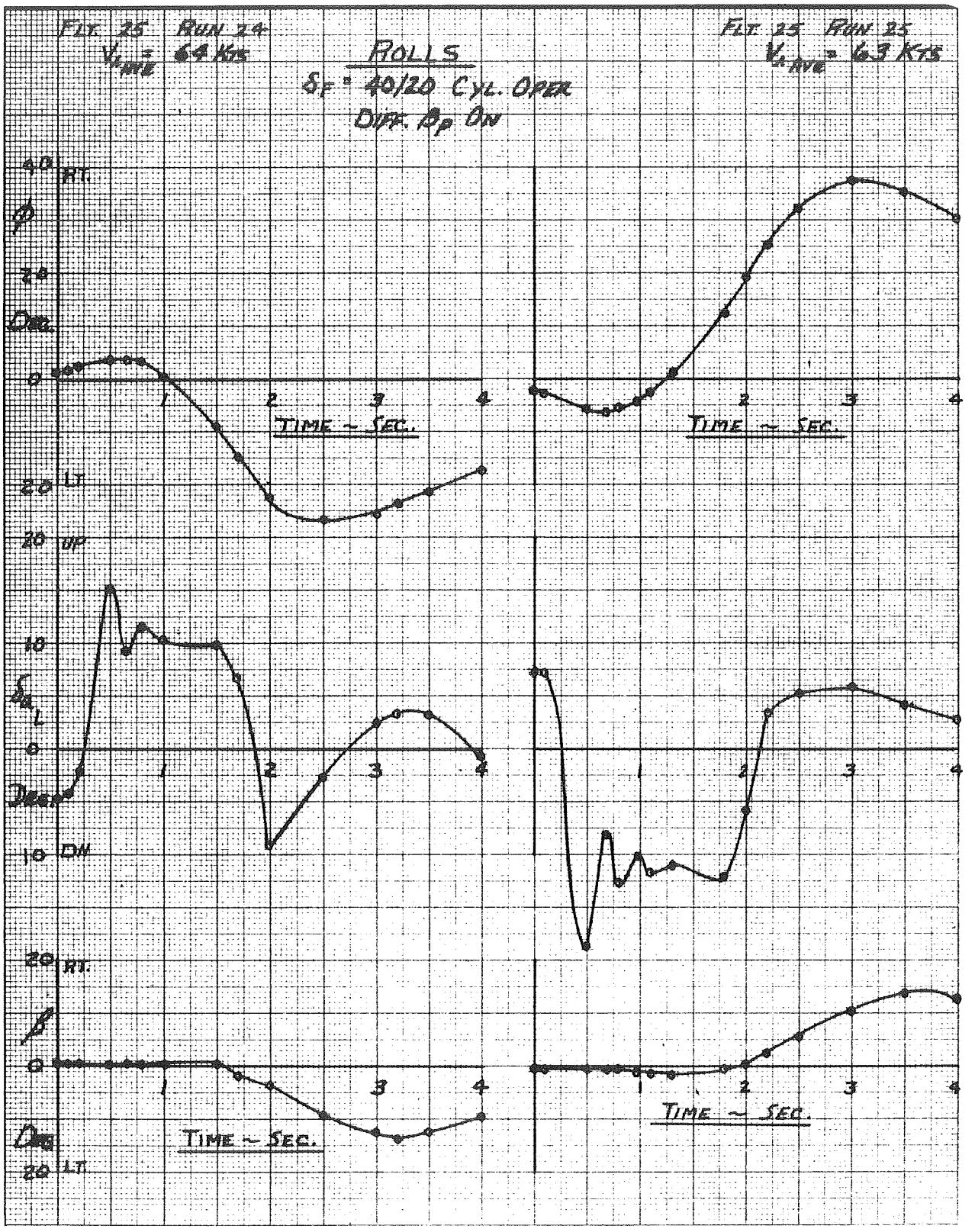
FLT. 25 RUN 24
$V_{L\,AVE}$ = 64 KTS
ROLLS
δ_F = 40/20 CYL. OPER
DIFF. β_p ON
FLT. 25 RUN 25
$V_{L\,AVE}$ = 63 KTS
40 RT.
ϕ
20
Deg.
0
20 LT
TIME ~ SEC.
TIME ~ SEC.
20 UP
10
δ_{R_L}
0
Deg.
10 DN
20 RT.
β
0
Deg.
20 LT
TIME ~ SEC.
TIME ~ SEC.

FIGURE 36 T

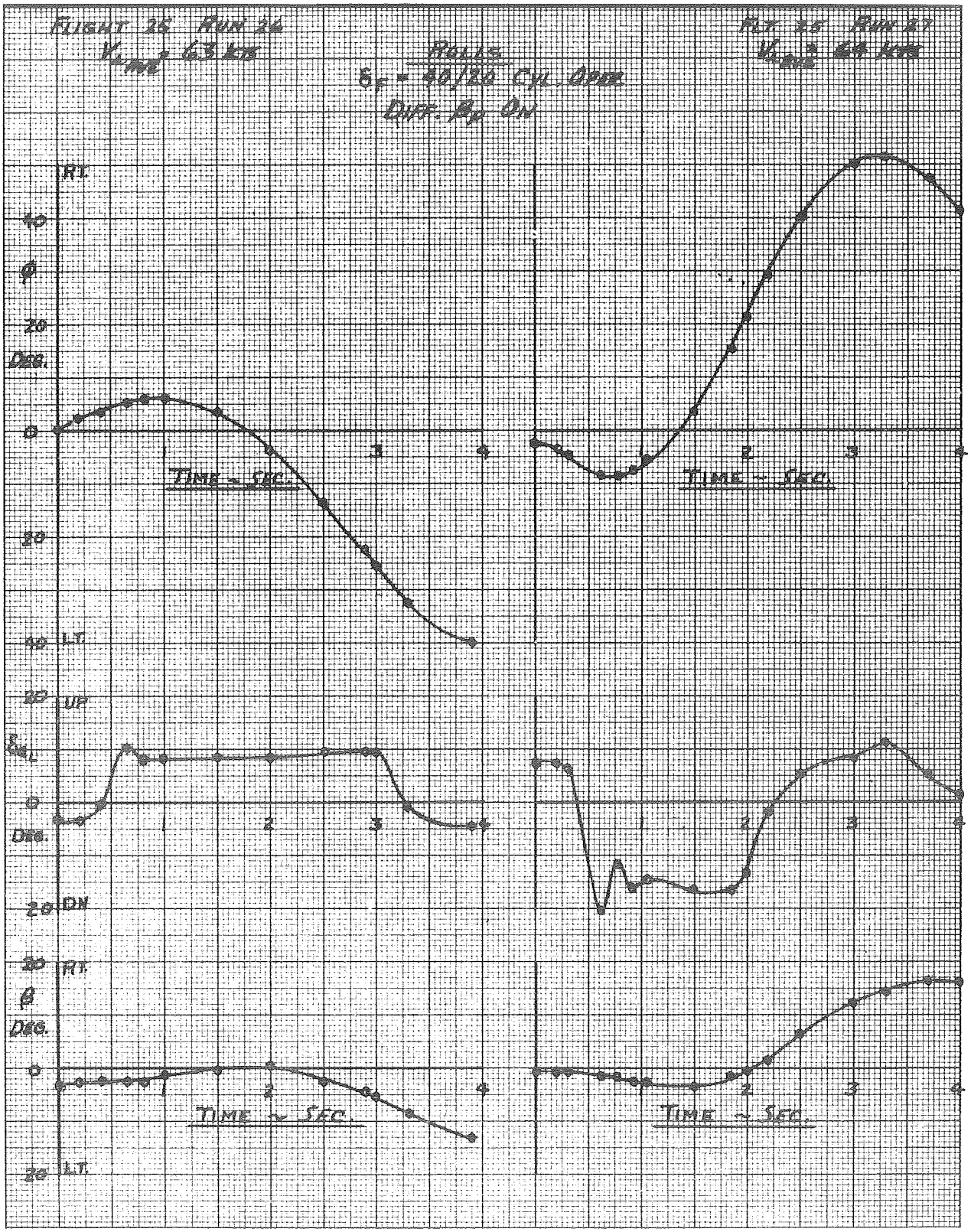
FLIGHT 25 RUN 24
$V_{i_{IND}}$ = 63 KTS
ROLLS
δ_F = 40/20 CYL. OPEN
DIFF. δ_D ON
FLT 25 RUN 27
$V_{i_{IND}}$ = 66 KTS
RT.
LT.
UP
DN
ϕ
β
δ_{AIL}
DEG.
TIME ~ SEC.

FIGURE 37a

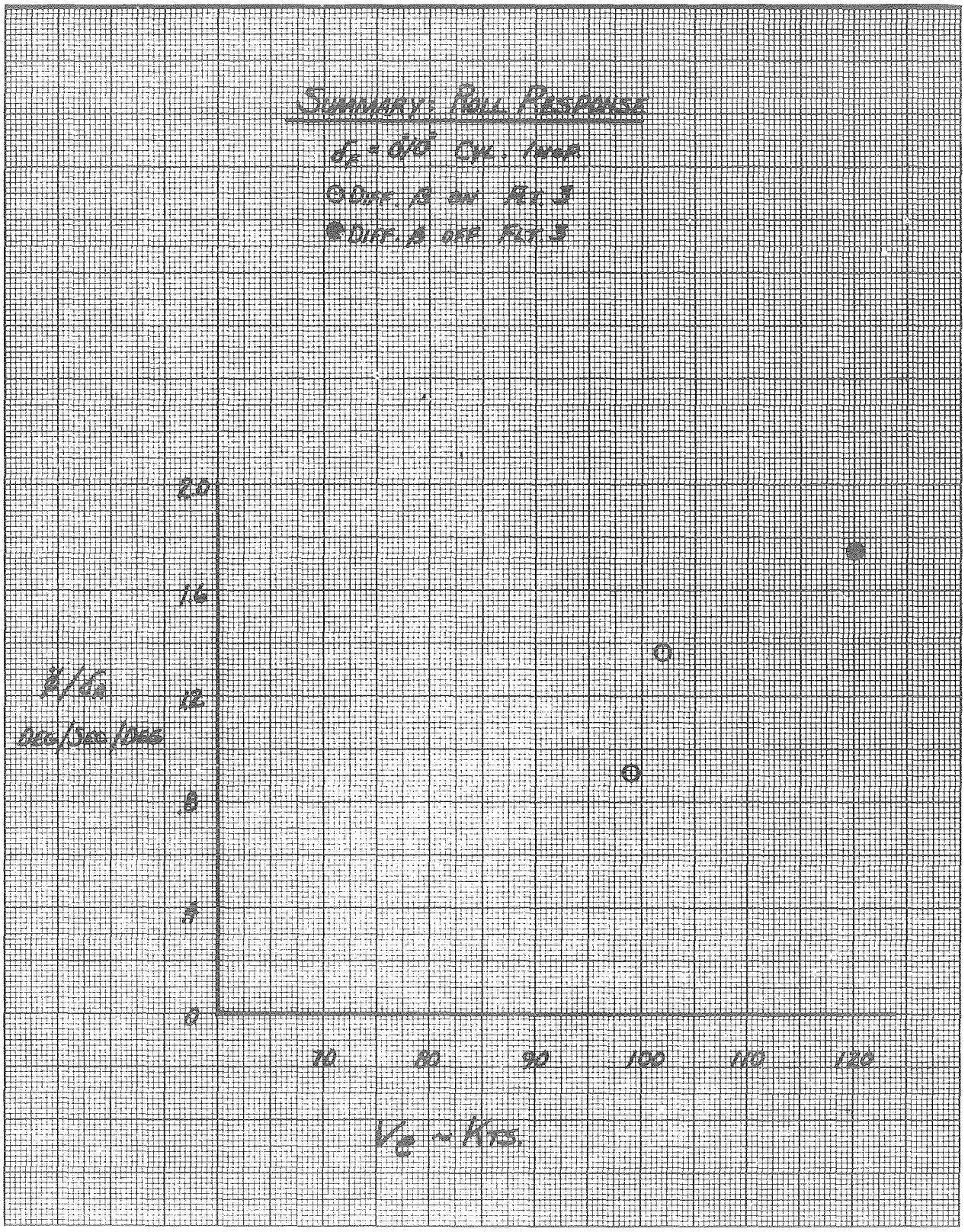
SUMMARY: ROLL RESPONSE
$\delta_E = \delta_A/2$ CYL. FLAPS
⊖ DIFF. δ_R NEU δ_T 5°
● DIFF. δ_R DEF δ_T 5°
2.0
1.6
1.2
.8
.4
0
$\dot{\phi}/\delta_A$
DEG/SEC/DEG
70
80
90
100
110
120
V_c ~ KTS.

FIGURE 376

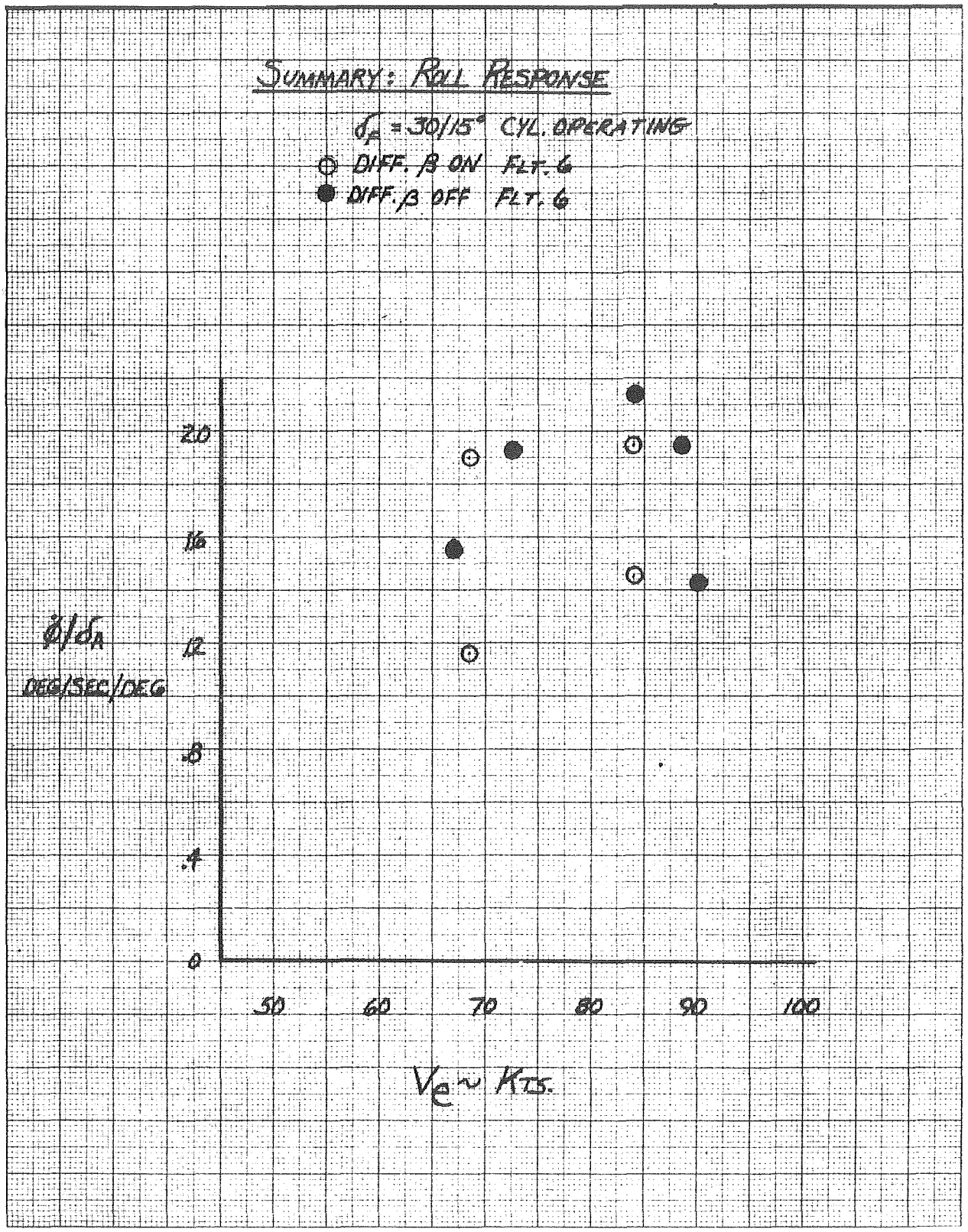
SUMMARY: ROLL RESPONSE
δ_A = 30/15° CYL. OPERATING
DIFF. β ON FLT. 6
DIFF. β OFF FLT. 6
2.0
1.6
1.2
.8
.4
0
ϕ/δ_A
DEG/SEC/DEG
50
60
70
80
90
100
V_e ~ KTS.

FIGURE 37C

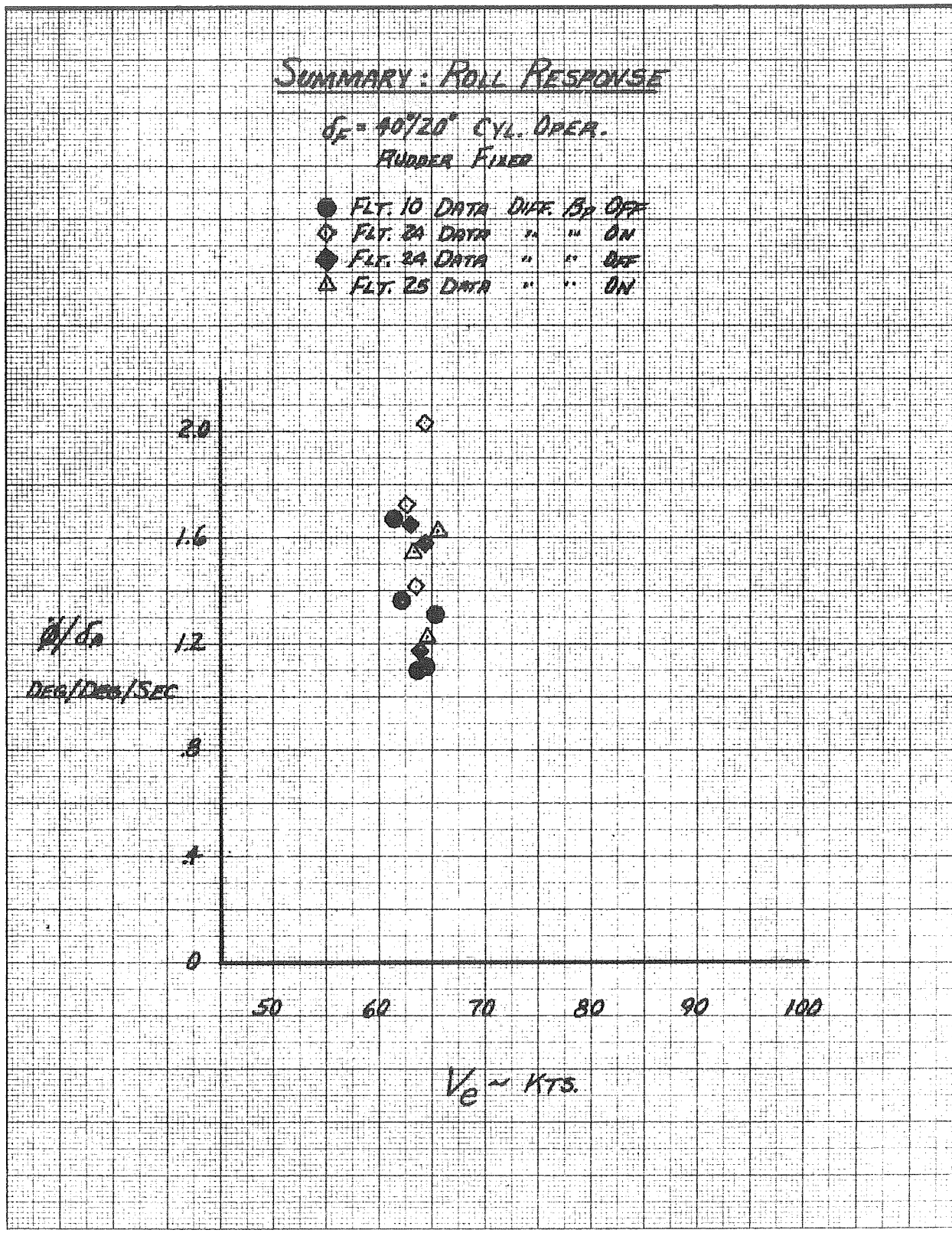
SUMMARY: ROLL RESPONSE
δ_F = 40°/20° CYL. OPER.
RUDDER FIXED
FLT. 10 DATA DIFF. B_A OFF
FLT. 24 DATA " " ON
FLT. 24 DATA " " OFF
FLT. 25 DATA " " ON
$\dot{\phi}/\delta_a$
DEG/DEG/SEC
2.0
1.6
1.2
.8
.4
0
50
60
70
80
90
100
V_e ~ KTS.

FIGURE 382

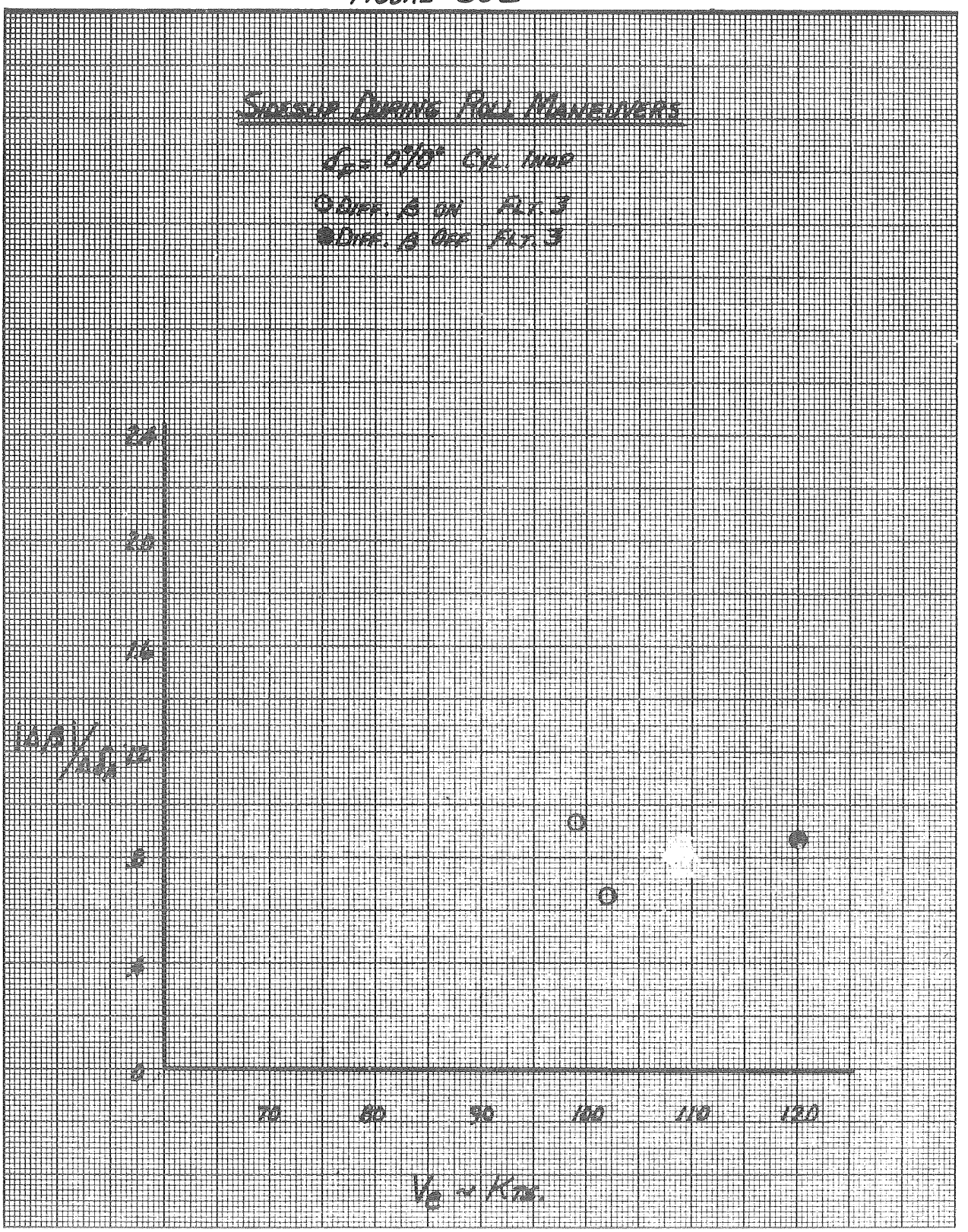
SIDESLIP DURING ROLL MANEUVERS
δ_a = 0 TO 20° CYL. INOP
○ DIFF. β ON FLT. 3
● DIFF. β OFF FLT. 3
24
20
16
12
8
4
0
70
80
90
100
110
120
V_{IA} ~ KTS.

FIGURE 38b

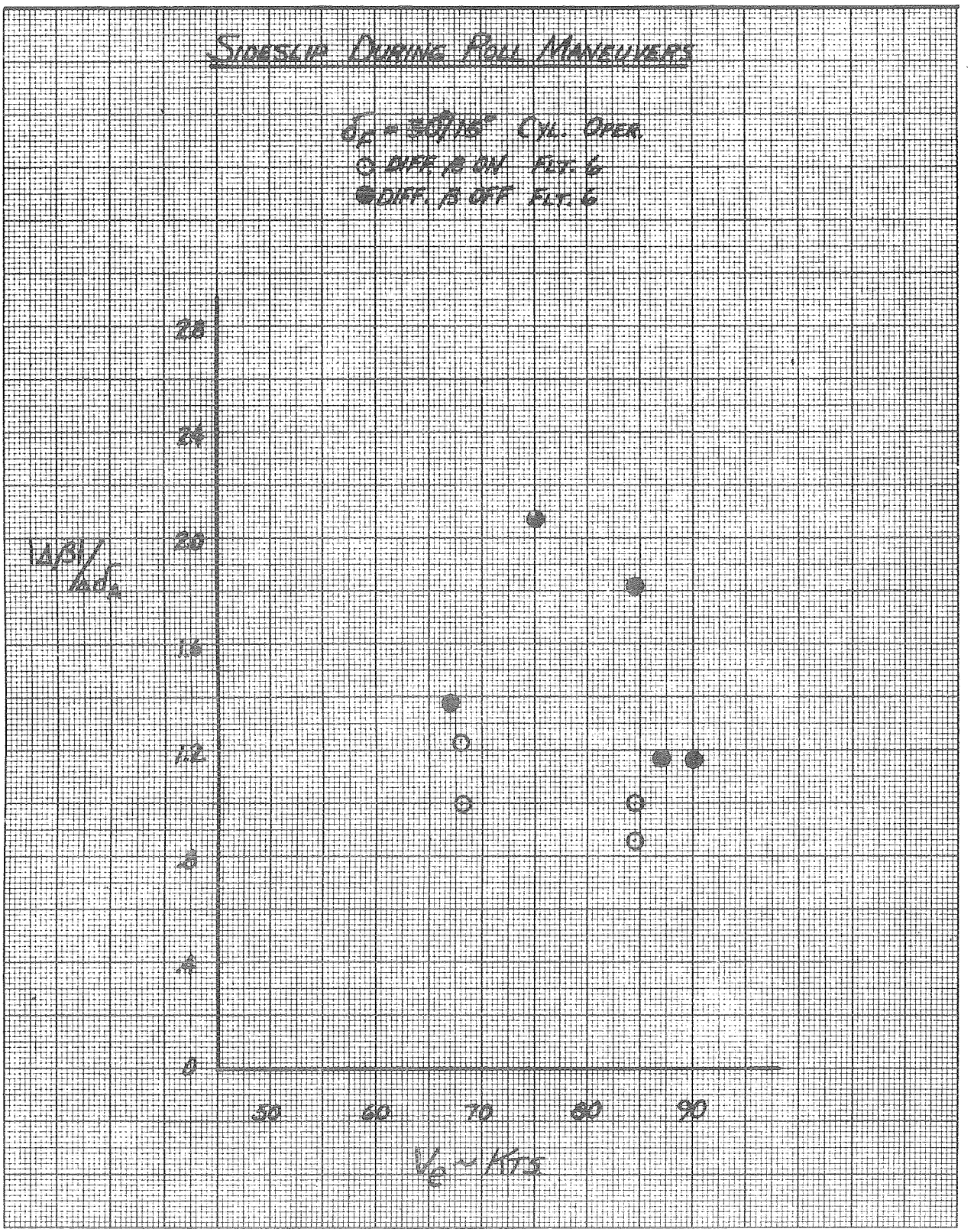
SIDESLIP DURING ROLL MANEUVERS
δ_E = 5 UP TO 15° CYL. OPER.
DIFF. ⍺ ON FLT. 6
DIFF. ⍺ OFF FLT. 6
2.8
2.4
2.0
1.6
1.2
.8
.4
0
$\frac{|\Delta\beta|}{|\Delta\delta_A|}$
50
60
70
80
90
V_E ~ KTS

FIGURE 38 C

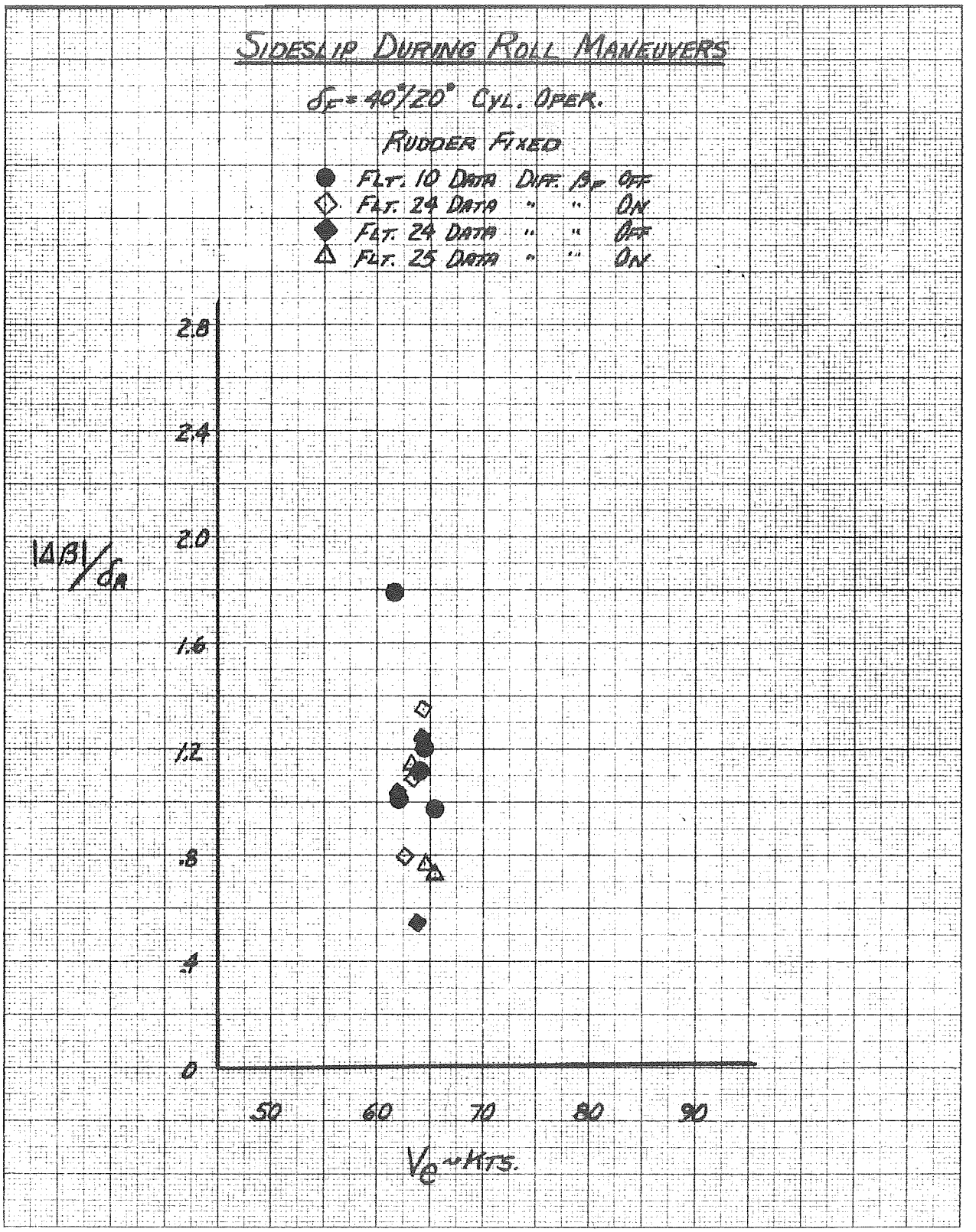
SIDESLIP DURING ROLL MANEUVERS
δ_E = 40°/20° CYL. OPER.
RUDDER FIXED
FLT. 10 DATA DIFF. β_F OFF
FLT. 24 DATA " " ON
FLT. 24 DATA " " OFF
FLT. 25 DATA " " ON
$|\Delta\beta|/\delta_R$
2.8
2.4
2.0
1.6
1.2
.8
.4
0
50
60
70
80
90
V_c ~ KTS.

FIGURE 39

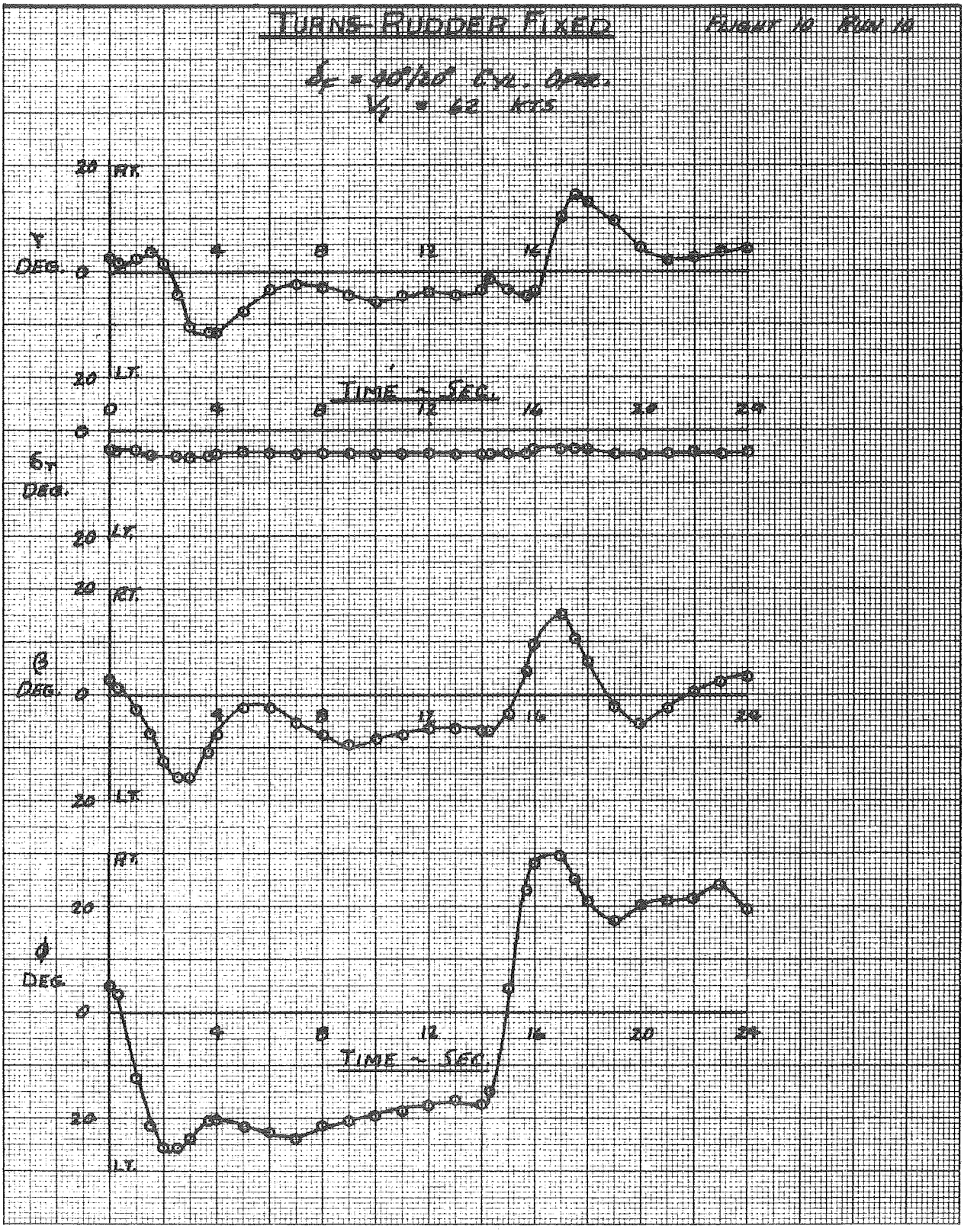
TURNS-RUDDER FIXED
FIGURE 18 RUN 18
δ_r = 40°/80° C.W. OPER.
V_f = 42 KTS
20 RT.
ψ DEG. 0
20 LT.
0 4 8 12 16 20 24
TIME ~ SEC.
δ_T DEG.
20 LT.
20 RT.
β DEG. 0
20 LT.
20 RT.
φ DEG. 0
20 LT.

FIGURE 40

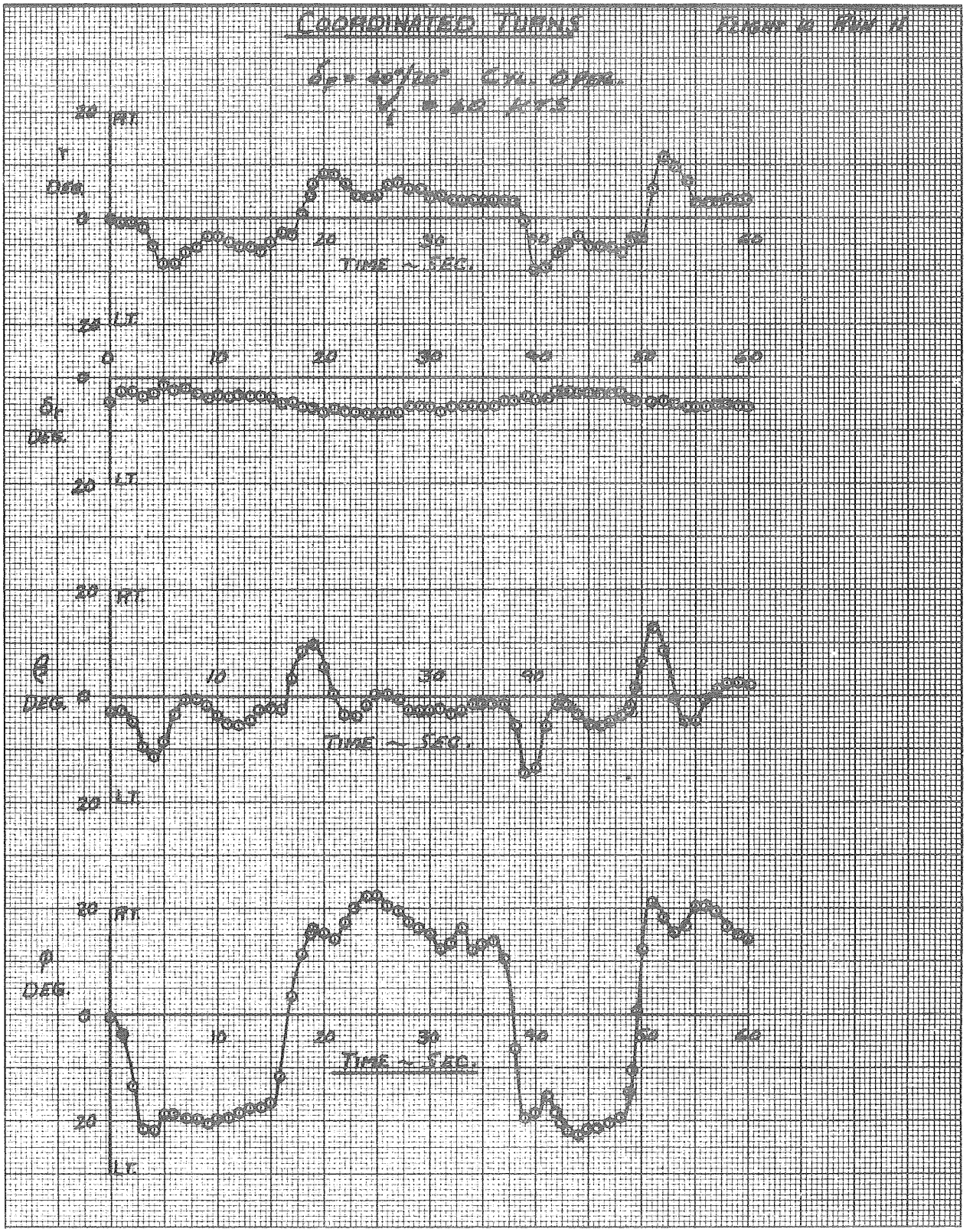
COORDINATED TURNS
Flight 10 Run 11
δ_{ef} = 40°/120° Cm. 0 Pos.
V_t = 440 K.T.S
Y
DEG.
20 RT.
0
20 LT.
TIME ~ SEC.
δ_r
DEG.
ϕ
DEG.
β
DEG.
0
10
20
30
40

FIGURE 41a

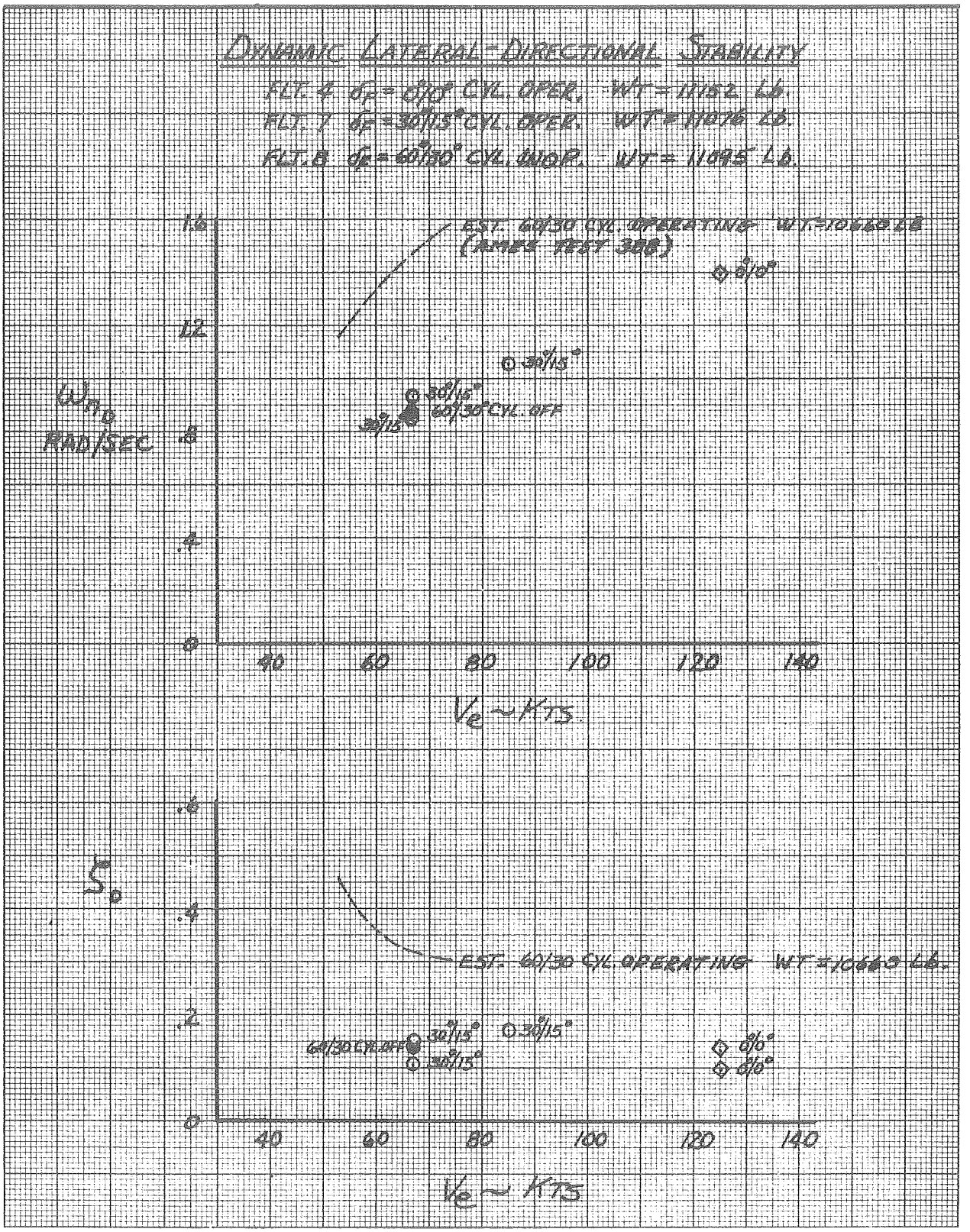
DYNAMIC LATERAL-DIRECTIONAL STABILITY
FLT. 4 δF = 0/0° CYL. OPER. WT = 11152 LB.
FLT. 7 δF = 30/15° CYL. OPER. WT = 11076 LB.
FLT. 8 δF = 60/30° CYL. INOP. WT = 11095 LB.
EST. 60/30 CYL. OPERATING WT=10660 LB
(AMES TEST 328)
0/0°
30/15°
30/15° 60/30° CYL. OFF
30/15°
1.6
1.2
.8
.4
0
ω_{n_0} RAD/SEC
40
60
80
100
120
140
V_e ~ KTS
.6
.4
.2
0
ζ_0
EST. 60/30 CYL. OPERATING WT=10660 LB.
60/30 CYL. OFF
30/15°
30/15°
30/15°
0/0°
0/0°
40
60
80
100
120
140
V_e ~ KTS

FIGURE 416

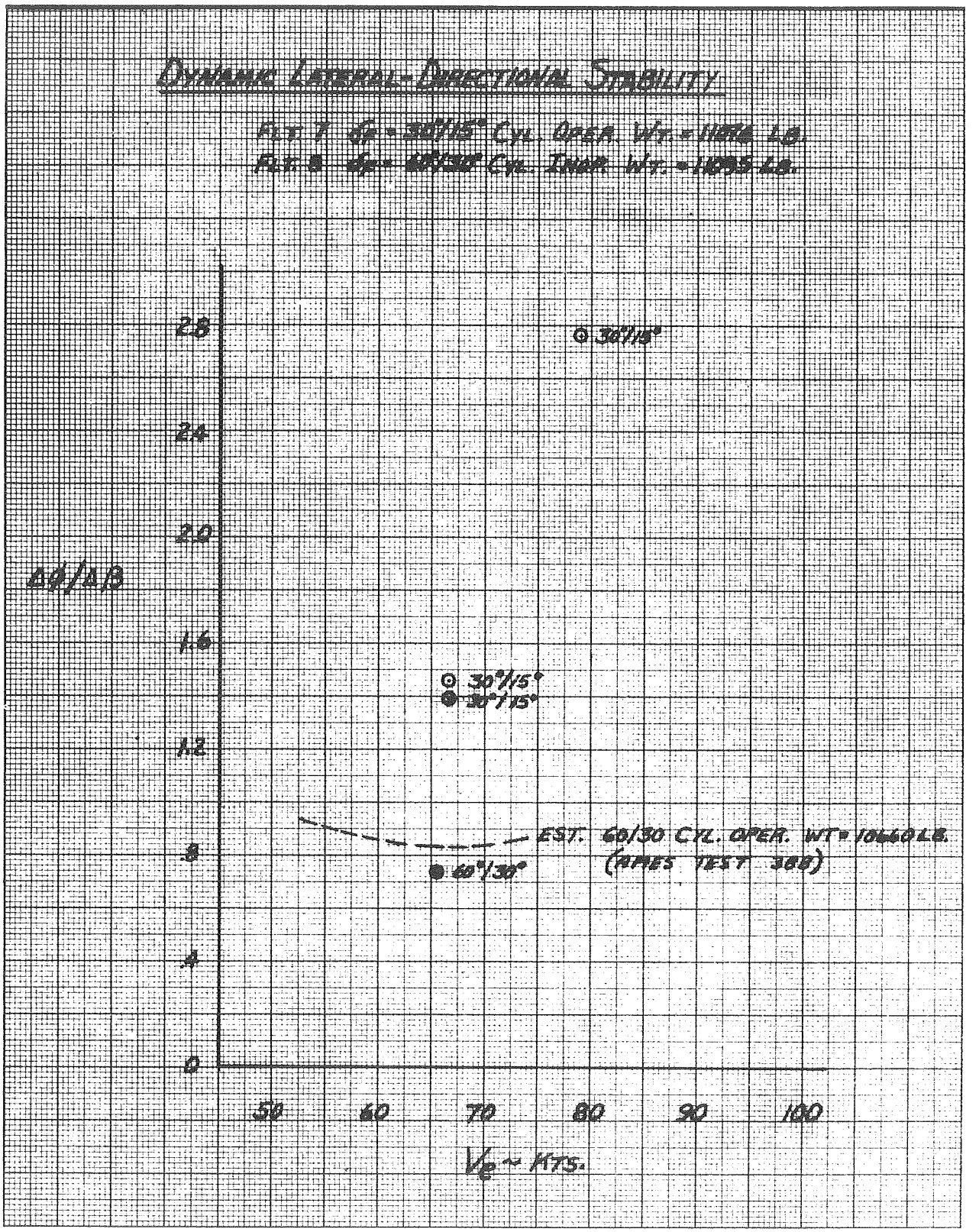
DYNAMIC LATERAL-DIRECTIONAL STABILITY
FLT. 7 df - 30/15° CYL. OPER. WT. = 11616 LB.
FLT. 8 df - 60/30° CYL. INOP. WT. = 11035 LB.
2.8
2.4
2.0
1.6
1.2
.8
.4
0
Δφ/Δβ
30/15°
30/15°
60/30°
EST. 60/30 CYL. OPER. WT = 10660 LB.
(AMES TEST 388)
50
60
70
80
90
100
Ve ~ KTS.

FIGURE 41C

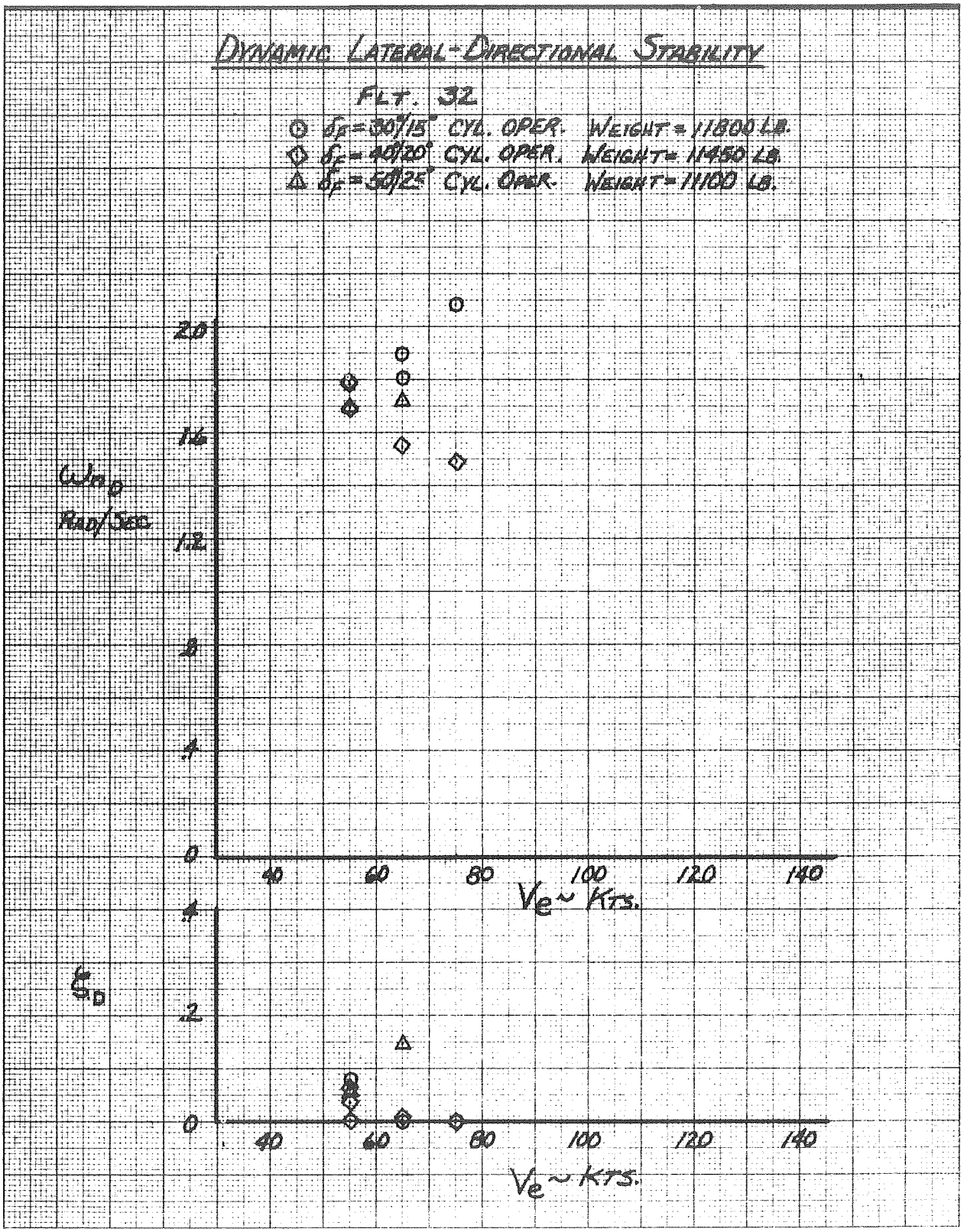
DYNAMIC LATERAL-DIRECTIONAL STABILITY
FLT. 32
δF = 30/15° CYL. OPER. WEIGHT = 11800 LB.
δF = 40/20° CYL. OPER. WEIGHT = 11450 LB.
δF = 50/25° CYL. OPER. WEIGHT = 11100 LB.
ωnD RAD/SEC.
2.0
1.6
1.2
.8
.4
0
40
60
80
100
120
140
Ve ~ KTS.
ζD
.4
.2
0
40
60
80
100
120
140
Ve ~ KTS.

FIGURE 9-11d

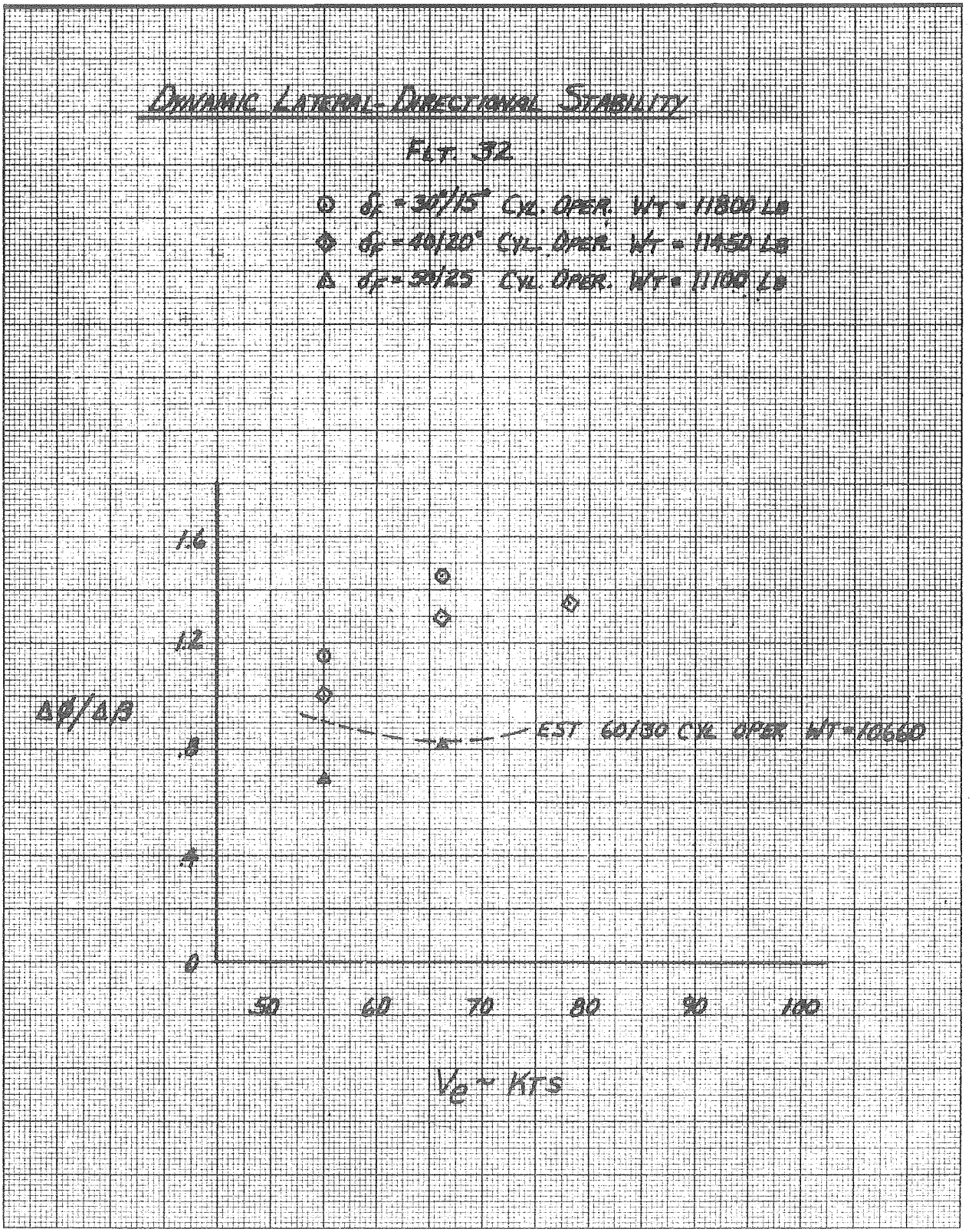
DYNAMIC LATERAL-DIRECTIONAL STABILITY
FLT. 32
⊙ δL = 30/15° CYL. OPER. WT = 11800 LB
◈ δL = 40/20° CYL. OPER. WT = 11450 LB
△ δL = 50/25 CYL. OPER. WT = 11100 LB
EST 60/30 CYL OPER WT = 10660
Δφ/Δβ
1.6
1.2
.8
.4
0
50
60
70
80
90
100
VC ~ KTS

FIGURE 42a

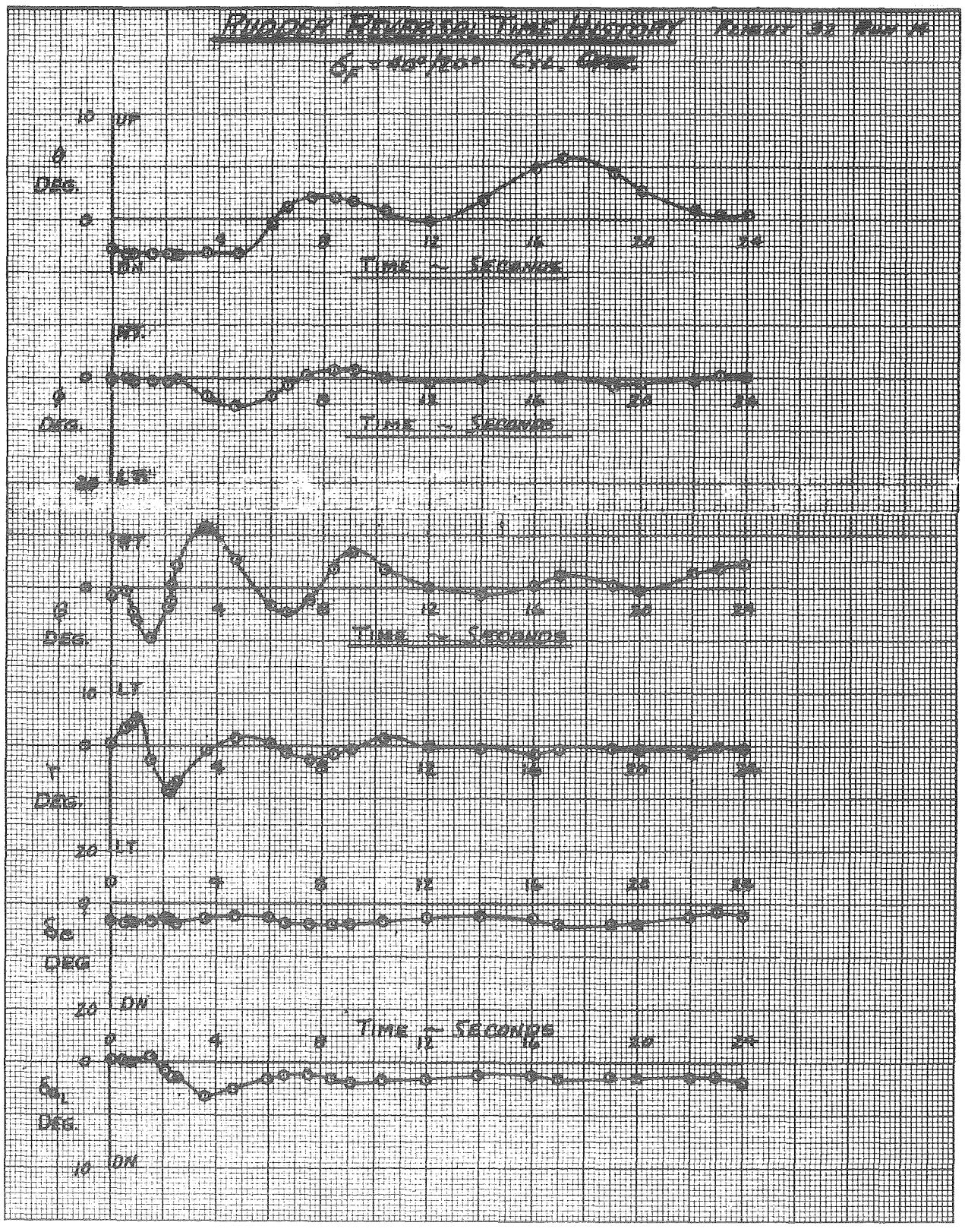
RUDDER REVERSAL TIME HISTORY
θ
DEG.
UP
DN
TIME ~ SECONDS
INT.
LT.
RT.
LT
ON
0
4
8
12
16
20
24

FIGURE 426

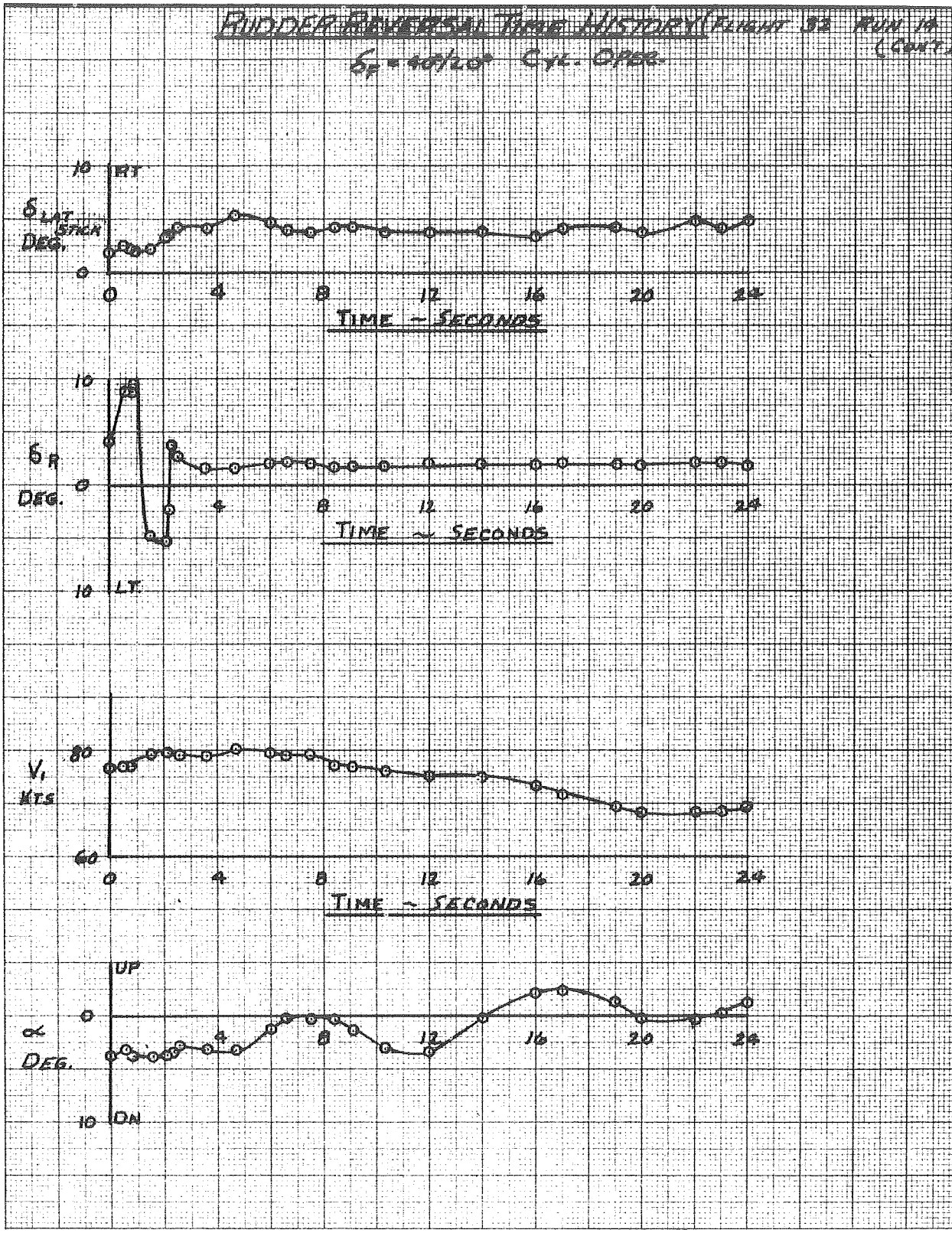
RUDDER REVERSAL TIME HISTORY (FLIGHT 32 RUN 14 (CONT.)
δ_F = 40/20° CYL. OPER.
10
RT
$\delta_{LAT.\ STICK}$
DEG.
0
0
4
8
12
16
20
24
TIME ~ SECONDS
10
δ_R
DEG.
0
10
LT
TIME ~ SECONDS
80
V_i
KTS
60
TIME ~ SECONDS
UP
0
α
DEG.
10
DN

FIGURE 432

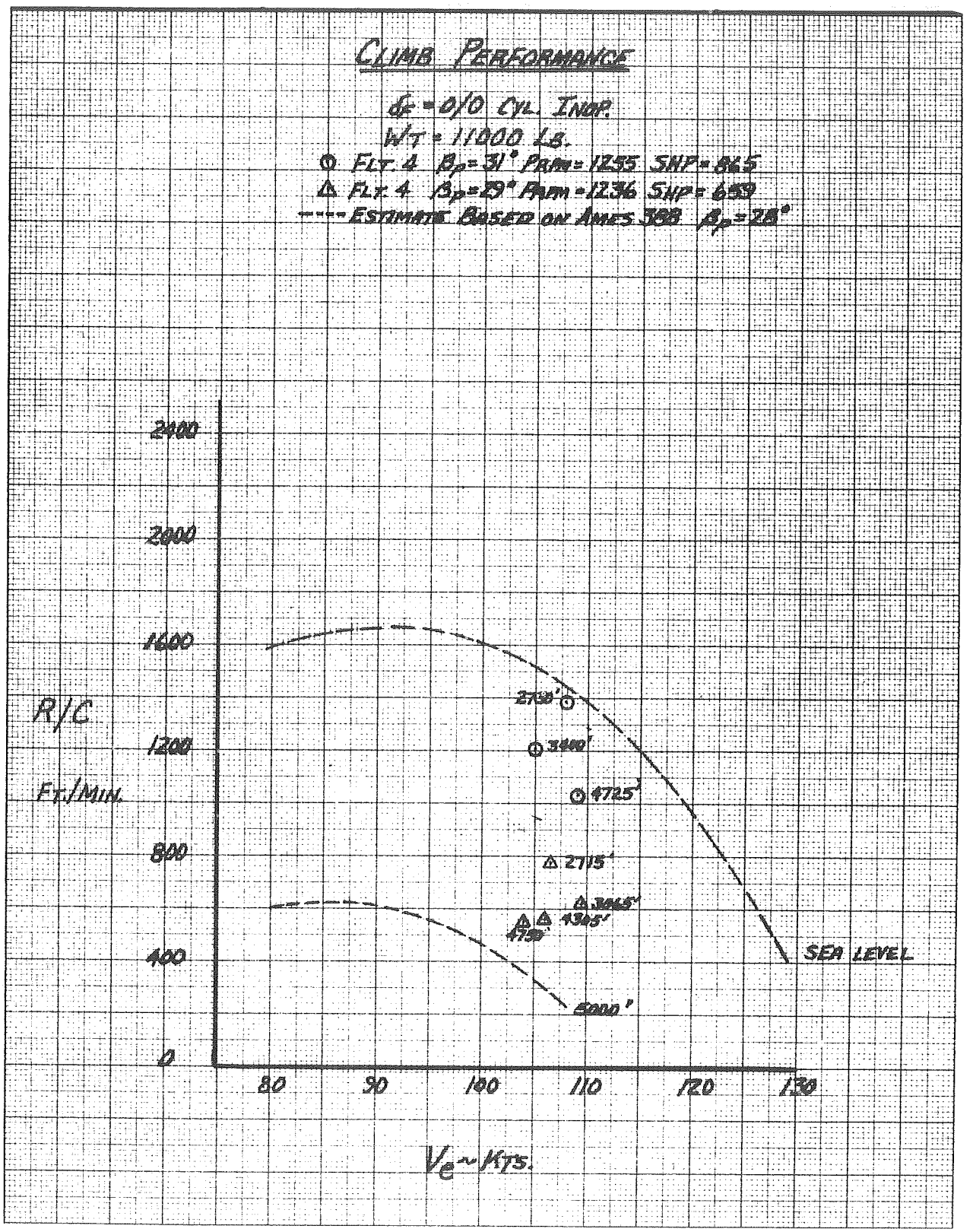
CLIMB PERFORMANCE
δ_F = 0/0 CYL. INOP.
W/T = 11000 LB.
⊙ FLT 4 β_p=31° PRPM=1255 SHP=865
△ FLT 4 β_p=29° PRPM=1236 SHP=659
---- ESTIMATE BASED ON AMES 388 β_p=28°
R/C
FT./MIN.
2400
2000
1600
1200
800
400
0
2730'
3400'
4725'
2715'
3465'
4345'
4139'
SEA LEVEL
8000'
80
90
100
110
120
130
V_e ~ KTS.

FIGURE 436

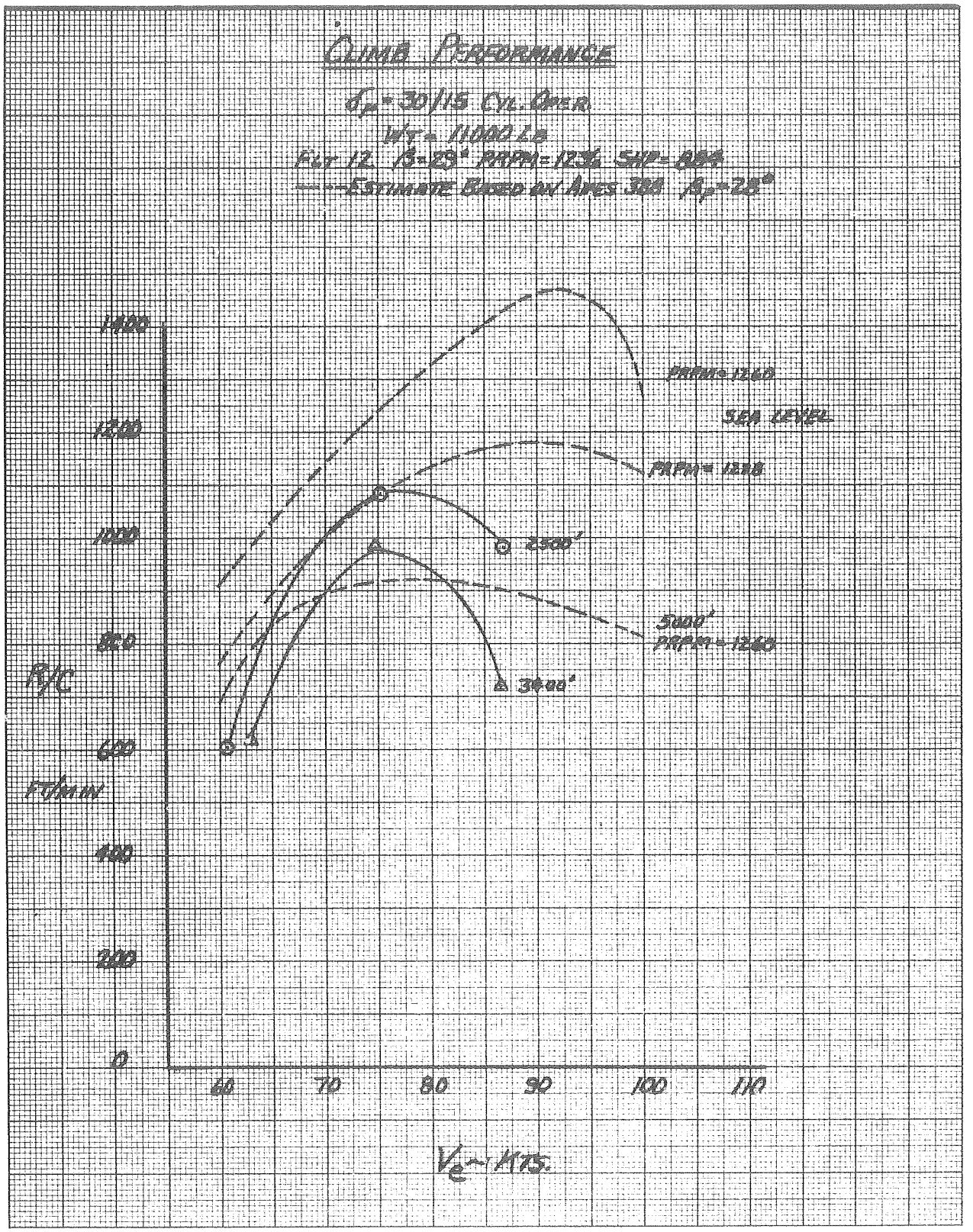
CLIMB PERFORMANCE
σ_p = 30/15 CYL. OPER.
W/T = 11000 LB
FLT 12 β=29° RPM=1230 SHP=824
---ESTIMATE BASED ON APES 384 β_p=28°
1400
1200
1000
800
600
400
200
0
R/C
FT/MIN
PRPM=1260
SEA LEVEL
PRPM=1228
2500'
3000'
PRPM=1240
3400'
60
70
80
90
100
110
V_e ~ KTS.

FIGURE 442

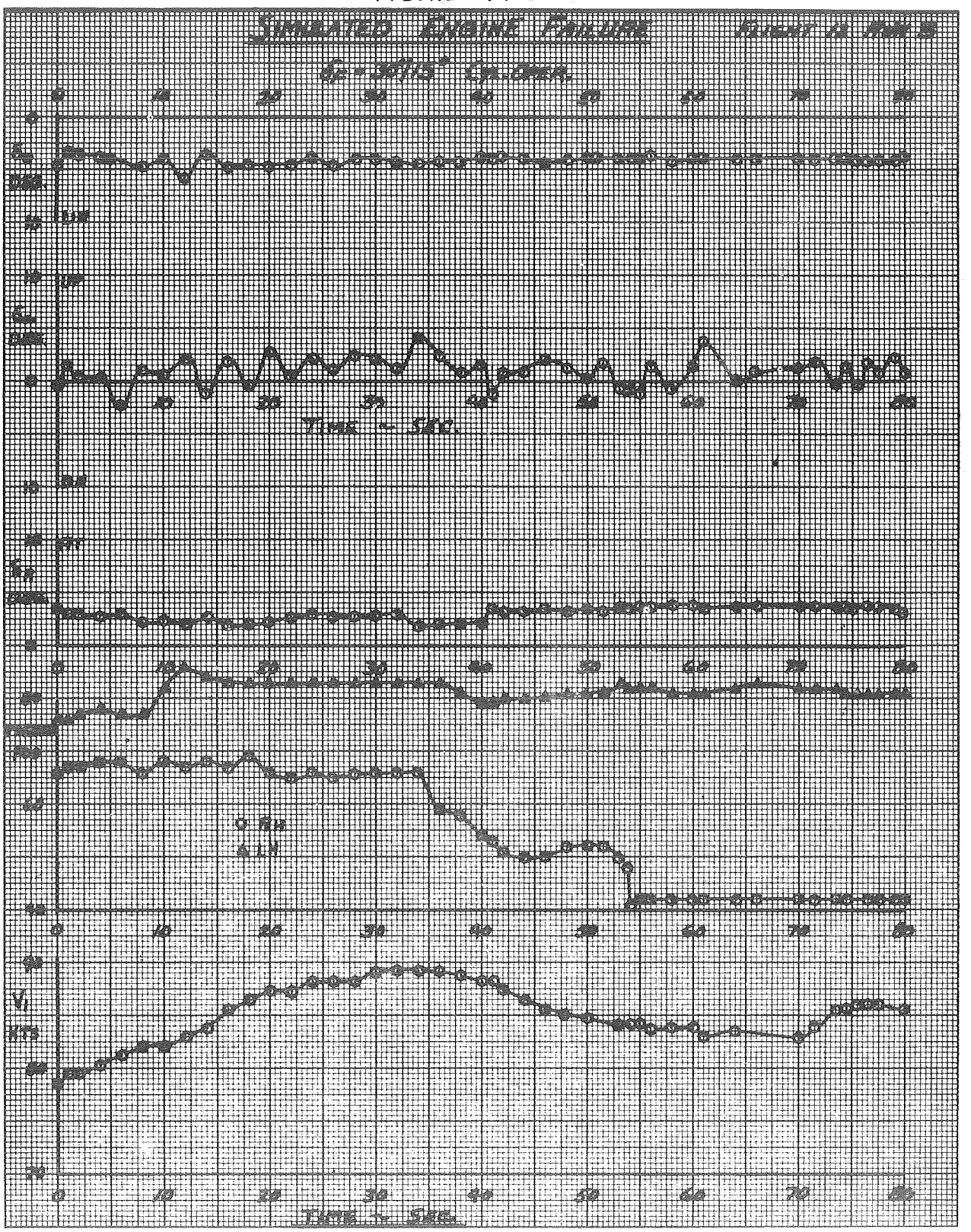
SIMULATED ENGINE FAILURE
FLIGHT 12, RUN 3
δE = 3.5° CPL. DEFL.
TIME ~ SEC.
RH
LH
TIME ~ SEC.

FIGURE 44b

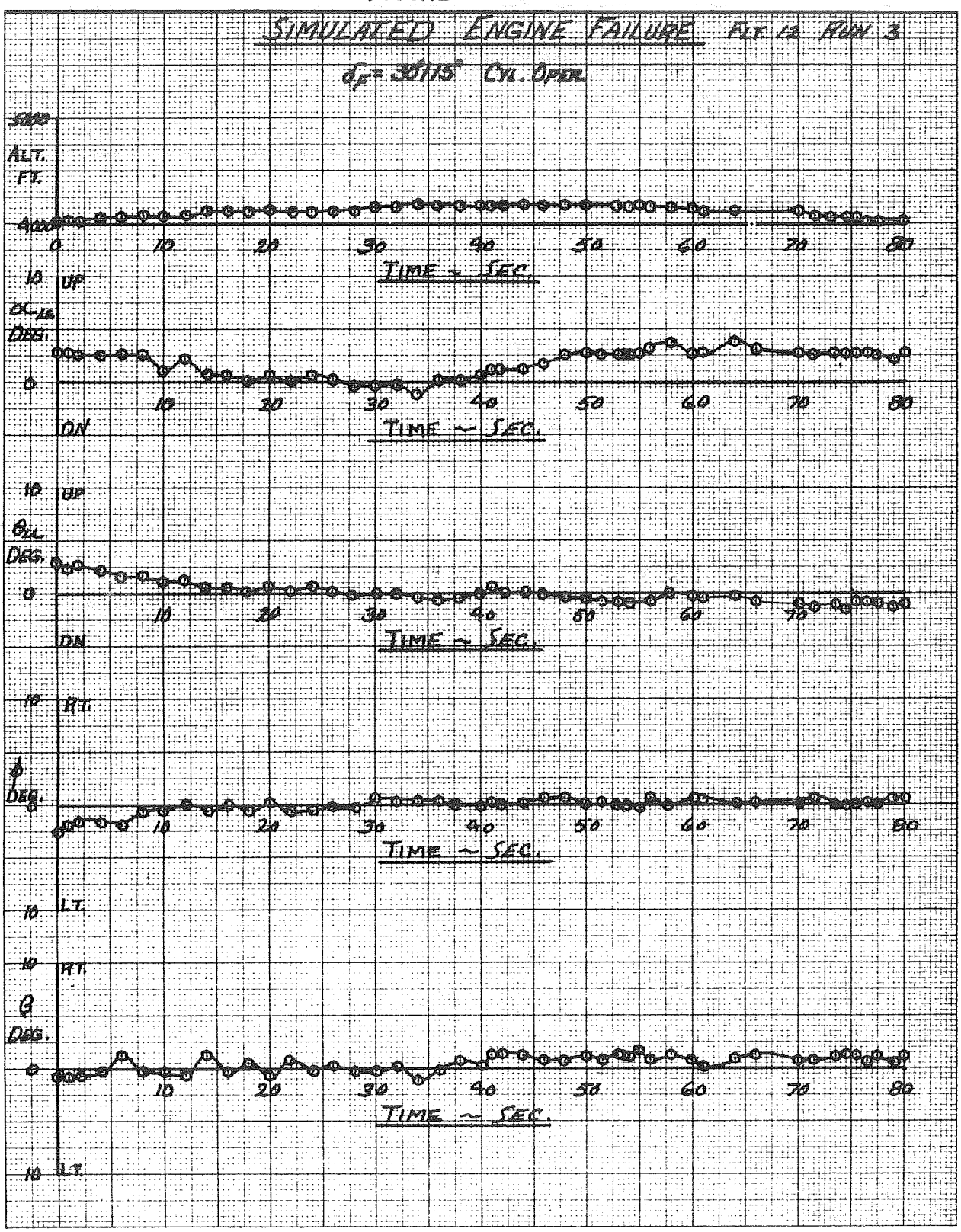
SIMULATED ENGINE FAILURE FLT. 12 RUN 3
δ_F = 30/15° CYL. OPEN.
5000
ALT. FT.
4000
0 10 20 30 40 50 60 70 80
TIME ~ SEC.
10 UP
δ_{EL} DEG.
0
DN
TIME ~ SEC.
θ_{EL} DEG.
TIME ~ SEC.
RT.
ϕ DEG.
LT.
TIME ~ SEC.
θ DEG.
TIME ~ SEC.

FIGURE 452

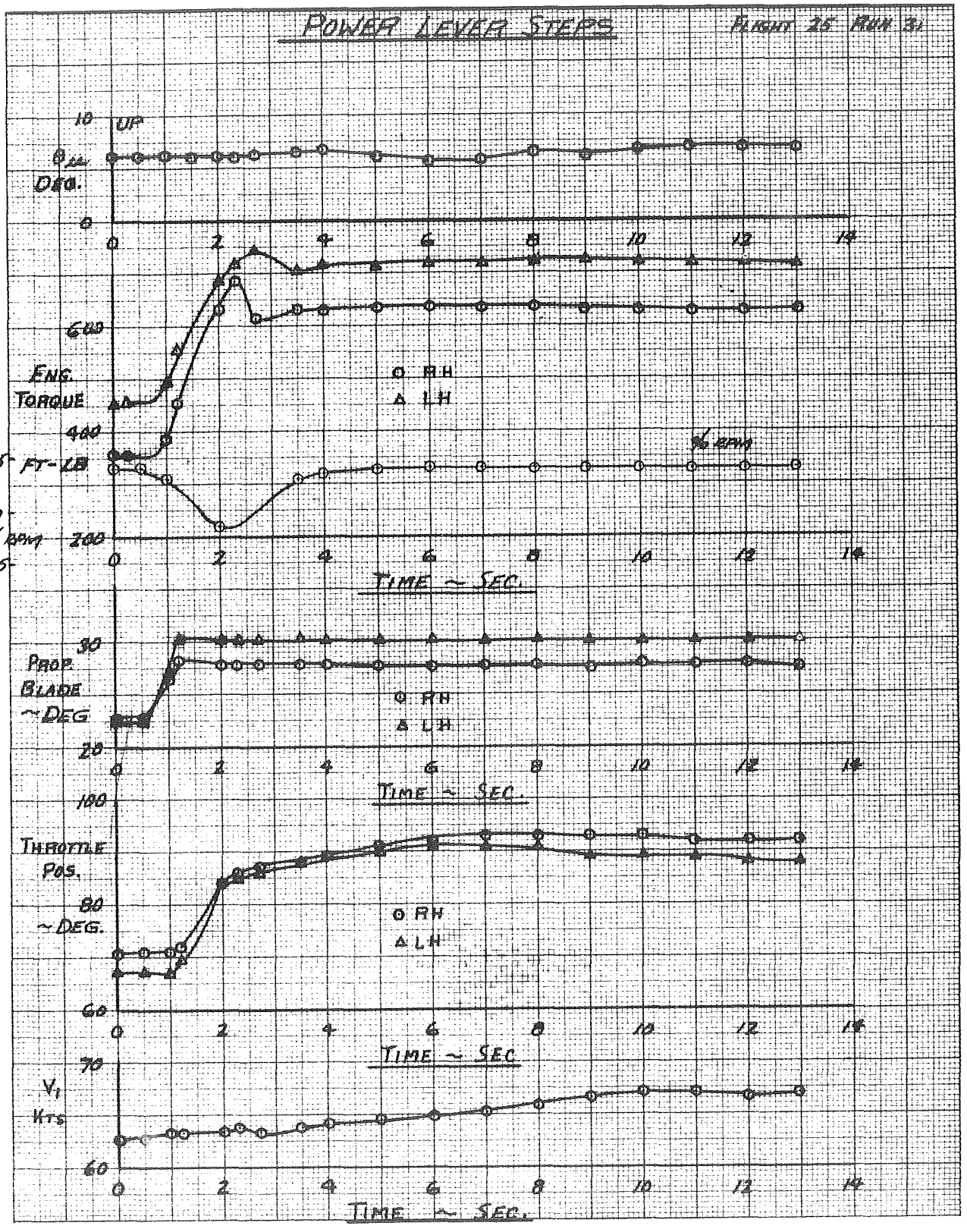
POWER LEVER STEPS
FLIGHT 25 RUN 31
UP
DEG.
ENG. TORQUE
FT-LB
% RPM
RH
LH
TIME ~ SEC.
PROP. BLADE ~ DEG
THROTTLE POS. ~ DEG.
V1 KTS

FIGURE 45b

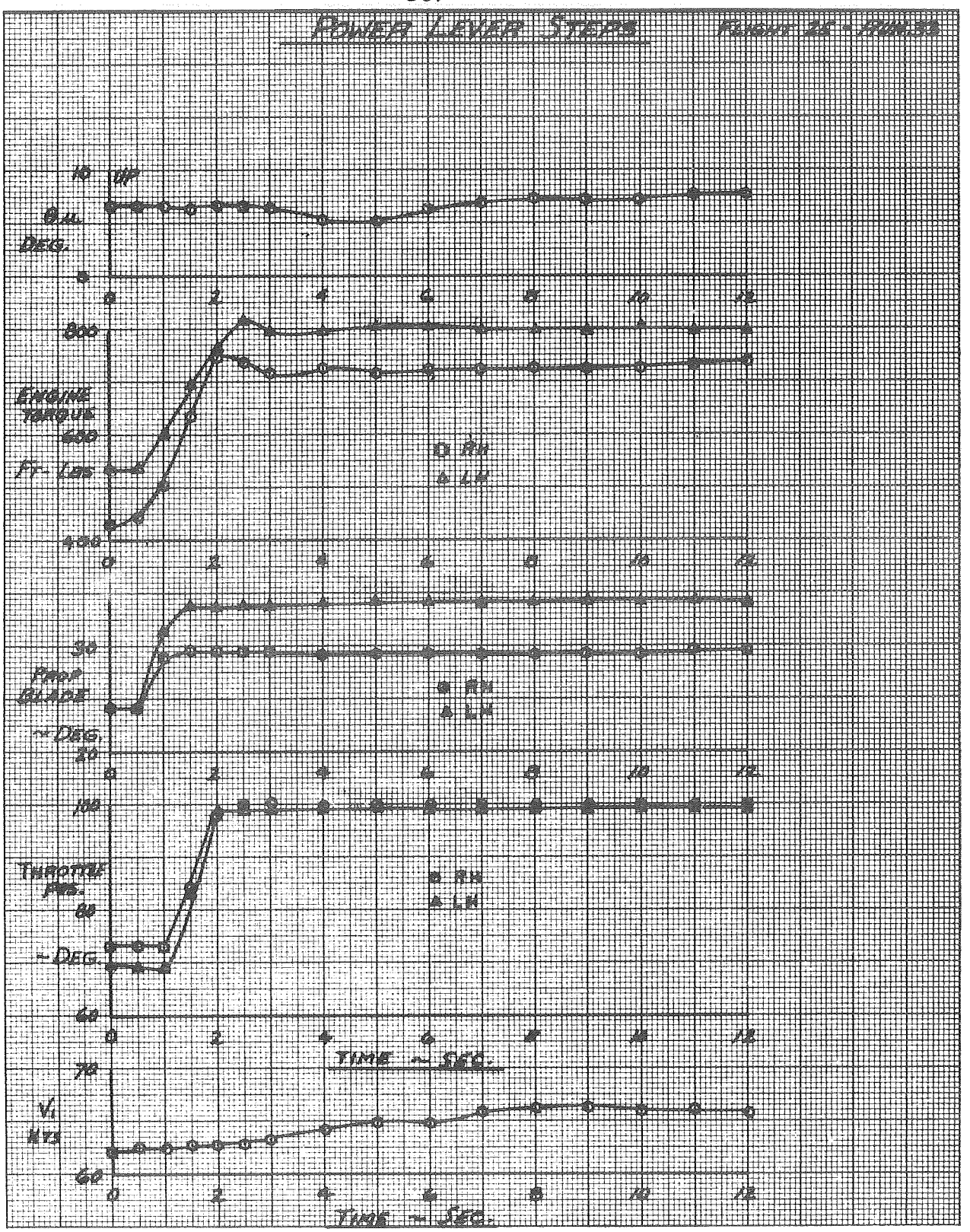
POWER LEVER STEPS
FLIGHT 25 - RUN 38
θ LL DEG.
10
0
-10
0
2
4
6
8
10
12
ENGINE TORQUE FT-LBS
800
600
400
RH
LH
PROP BLADE ~ DEG.
30
20
THROTTLE POS. ~ DEG.
10
0
80
60
TIME ~ SEC.
V_I KTS
70
60
TIME ~ SEC.

FIGURE 45C

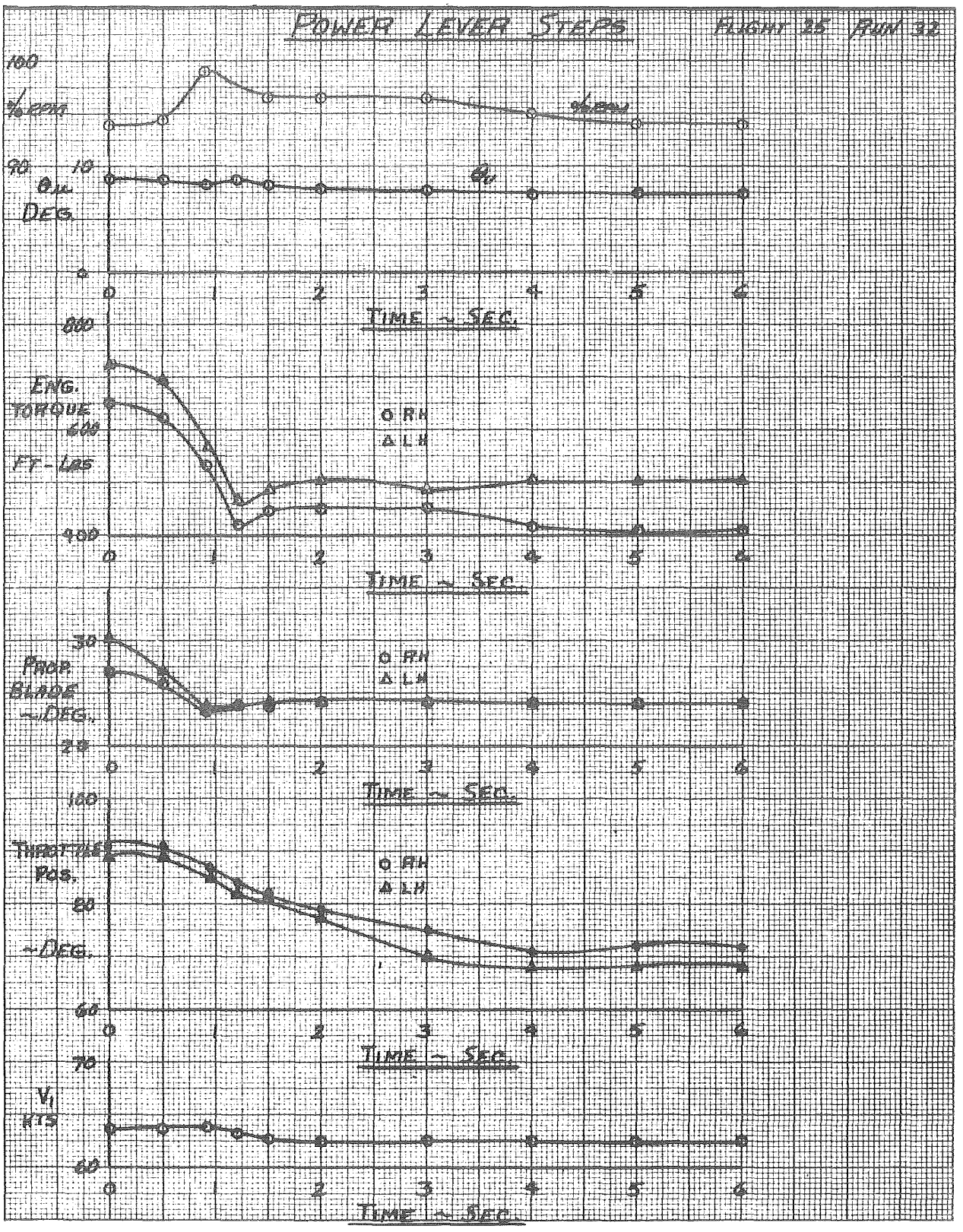
POWER LEVER STEPS
FLIGHT 25 RUN 32
100
% RPM
90
10
θ LL DEG.
0
0 1 2 3 4 5 6
TIME ~ SEC.
800
ENG. TORQUE FT-LBS
600
400
O RH
Δ LH
0 1 2 3 4 5 6
TIME ~ SEC.
30
PROP. BLADE ~ DEG.
25
O RH
Δ LH
0 1 2 3 4 5 6
TIME ~ SEC.
100
THROTTLE POS. ~ DEG.
80
60
O RH
Δ LH
0 1 2 3 4 5 6
TIME ~ SEC.
70
V1 KTS
60
0 1 2 3 4 5 6
TIME ~ SEC.

NATIONAL AERONAUTICS AND SPACE ADMINISTRATION
WASHINGTON, D.C. 20546

OFFICIAL BUSINESS
PENALTY FOR PRIVATE USE $300

FIRST CLASS MAIL

POSTAGE AND FEES PAID
NATIONAL AERONAUTICS AND
SPACE ADMINISTRATION
451

U.S.MAIL

POSTMASTER: If Undeliverable (Section 158 Postal Manual) Do Not Return

"The aeronautical and space activities of the United States shall be conducted so as to contribute . . . to the expansion of human knowledge of phenomena in the atmosphere and space. The Administration shall provide for the widest practicable and appropriate dissemination of information concerning its activities and the results thereof."

—NATIONAL AERONAUTICS AND SPACE ACT OF 1958

NASA SCIENTIFIC AND TECHNICAL PUBLICATIONS

TECHNICAL REPORTS: Scientific and technical information considered important, complete, and a lasting contribution to existing knowledge.

TECHNICAL NOTES: Information less broad in scope but nevertheless of importance as a contribution to existing knowledge.

TECHNICAL MEMORANDUMS: Information receiving limited distribution because of preliminary data, security classification, or other reasons. Also includes conference proceedings with either limited or unlimited distribution.

CONTRACTOR REPORTS: Scientific and technical information generated under a NASA contract or grant and considered an important contribution to existing knowledge.

TECHNICAL TRANSLATIONS: Information published in a foreign language considered to merit NASA distribution in English.

SPECIAL PUBLICATIONS: Information derived from or of value to NASA activities. Publications include final reports of major projects, monographs, data compilations, handbooks, sourcebooks, and special bibliographies.

TECHNOLOGY UTILIZATION PUBLICATIONS: Information on technology used by NASA that may be of particular interest in commercial and other non-aerospace applications. Publications include Tech Briefs, Technology Utilization Reports and Technology Surveys.

Details on the availability of these publications may be obtained from:

SCIENTIFIC AND TECHNICAL INFORMATION OFFICE

NATIONAL AERONAUTICS AND SPACE ADMINISTRATION

Washington, D.C. 20546